Lehrstuhl für Regelungstechnik

Technische Universität München

Total Energy Shaping for Underactuated Mechanical Systems: Dissipation and Nonholonomic Constraints

Sergio Delgado Londoño

Vollständiger Abdruck der von der Fakultät für Maschinenwesen der Technischen Universität München zur Erlangung des akademischen Grades eines

Doktor-Ingenieurs

genehmigten Dissertation.

Vorsitzender:	Prof. Dr.-Ing. Manfred Hajek
Prüfer der Dissertation:	1. Prof. Dr.-Ing. habil. Boris Lohmann
	2. Prof. Dr. phil. Ravi N. Banavar, Indian Institute of Technology Bombay, Mumbai, Indien

Die Dissertation wurde am 30.03.2016 bei der Technischen Universität München eingereicht und durch die Fakultät für Maschinenwesen am 15.06.2016 angenommen.

To my family.

Abstract

This thesis deals with a new systematic design of energy shaping control techniques for underactuated mechanical systems. Thereby, the focus is put on challenges arising from the implementation to practical systems. The first part of the thesis is devoted to dissipation in unactuated coordinates. The second part is devoted to nonholonomic systems.

Kurzfassung

Diese Arbeit behandelt einen neuartigen systematischen Entwurf energiebasierter Regler für unteraktuierte mechanische Systeme. Insbesondere werden Aspekte der praktischen Implementierung berücksichtigt. Der erste Teil der Arbeit befasst sich mit Dämpfung in unaktuierten Koordinaten. Der zweite Teil behandelt nichholonome Systeme.

Preface

This manuscript is the result of years of work at the Institute of Automatic Control of the Technische Universität München. I would like to thank my supervisor Prof. Dr. Boris Lohmann for his support, kindness, and freedom he gave me during the last 5 years. Thanks to my second supervisor, Prof. Ravi Banavar, who gave me the opportunity to join him at IIT Bombay in Mumbai. It was an incredible experience.

Thanks to Nils Pletschen, Johannes Strohm, and Paul Kotyczka, who contributed to improve the layout and readability of the manuscript. I also feel grand gratitude for my colleague Klaus Albert and his students, who not only built the wheeled inverted pendulum *KRT32* and identified its dynamical parameters, but also kindly allowed me to use it for the experiments.

Thanks to my friends and former colleagues, who made every single day at the institute very special. Thanks to every single person, who in one way or another, joined me during this amazing journey.

My greatest hug and deepest gratitude goes to my parents and my brother. Their unconditional love and support throughout the last 30 years brought me to where I am now.

Last, thanks dear reader for reading the first page. I wish you a great journey through this manuscript. And don't give up. I didn't.

July 2016

Sergio Delgado Londoño

Contents

Glossary

Notation

By convention, scalars are denoted by lower and upper case letters in italic type. Vectors are written in lower case letters, in upright boldface type; matrices in upper case letters, in upright boldface type. Sets and manifolds are denoted by upper case letters in calligraphic or blackboard type.

$\alpha,\ b,\ \Pi(\cdot),\ f(\cdot)$	Scalars/ scalar-valued functions
$\boldsymbol{\xi},\ \mathbf{x},\ \boldsymbol{\nu}(\cdot),\ \mathbf{f}(\cdot)$	Vectors/ vector-valued functions
$\mathbf{R},\ \boldsymbol{\Sigma},\ \mathbf{J}(\cdot),\ \mathbf{M}(\cdot)$	Matrices/ matrix-valued functions
$\mathbb{R},\ \mathbb{S}^n,\ \mathbb{D},\ \mathcal{M},\ \mathcal{X}$	Sets, manifolds

According to the standard convention for partial derivatives, the Jacobian is written as $\frac{\partial \mathbf{f}}{\partial \mathbf{x}}$, and, for a scalar function $f(\mathbf{x})$, it represents the row vector of first-order partial derivatives. The ∇-symbol is used to denote the gradient (column vector of first-order partial derivatives) of a scalar function $f(\mathbf{x})$. The Hessian—or second-order derivative—of a function $f(\mathbf{x})$ with respect to its argument $\mathbf{x}$ is represented by $\nabla^2_{\mathbf{x}} f$. The (element-wise) derivative of a matrix function $\mathbf{A}(\mathbf{x})$ with respect to x_i is denoted by $\partial_{x_i}\mathbf{A}$. If obvious from the context, arguments will be dropped for simplicity.

Mathematical accents, subscripts, and superscripts

$\dot{(\cdot)}$	First-order time derivative of the scalar, vector, or matrix $(\cdot)$
$\ddot{(\cdot)}$	Second-order time derivative of the scalar or vector $(\cdot)$
$(\cdot)^{\mathrm{T}}$	Transpose of the vector or matrix $(\cdot)$
$(\cdot)_i$	i-th component of a vector: x_i is i-th component of $\mathbf{x}$
$(\cdot)_{ij}$	Entry of the matrix $(\cdot)$ in row i and column j
$(\cdot)^{-1}$	Inverse of the quadratic matrix $(\cdot)$

$(\cdot)_0$	Initial value of the scalar or vector $(\cdot)$
$(\cdot)^*$	(Desired) equilibrium point
$(\cdot)_*$	Value of the matrix function $(\cdot)$ at the desired equilibrium point: $\mathbf{A}_* = \mathbf{A}(\mathbf{x}^*)$
$\hat{(\cdot)}$	Reference value of the state/configuration/velocity $(\cdot)$
$(\cdot)_\mathrm{e}$	State/configuration/velocity error $(\cdot)_\mathrm{e} = (\cdot) - \hat{(\cdot)}$
$(\cdot)_\mathrm{d}$	Desired (closed-loop) matrix or scalar function $(\cdot)$ in IDA-PBC
$(\cdot)_\mathrm{c}$	Desired (closed-loop) matrix or scalar function $(\cdot)$ in CL
$(\cdot)_\perp$	Full rank left annihilator of the matrix or vector $(\cdot)$

List of frequently used symbols and operators

$\mathbb{R}$	Set of real numbers
$\mathbb{R}_0^+$	Set of non-negative real numbers
$\mathbb{R}^+$	Set of positive real numbers
$\mathbb{R}^n$	Set of real vectors with n components
$\mathbb{R}^{n\times m}$	Set of real $n\times m$ matrices
$\mathbb{S}^n$	n-dimensional unit sphere
$\mathcal{Q}$	Configuration space (manifold)
$\mathcal{Q}_\mathrm{R}$	Reduced (unconstrained) configuration manifold
$\mathcal{Q}_\mathrm{C}$	Subset of the configuration manifold (constrained)
$\mathcal{D}$	Constrained distribution
$\mathbf{0}$	Column vector or matrix with all elements equal to zero
$\mathbf{I}$	Identity matrix
$\mathrm{rank}(\mathbf{A})$	Rank of the matrix (function) $\mathbf{A}$
$\mathrm{sym}(\mathbf{A})$	Symmetric part of the matrix (function) $\mathbf{A}$
$\mathbf{A} > (<)\, \mathbf{0}$	The symmetric matrix $\mathbf{A}$ is positive (negative) definite
$\mathbf{A} \geq (\leq)\, \mathbf{0}$	The symmetric matrix $\mathbf{A}$ is positive (negative) semidefinite
$V > (<)\, 0$	The scalar function V is positive (negative) definite
$V \geq (\leq)\, 0$	The scalar function V is positive (negative) semidefinite

$\lvert x\rvert$	Absolute value of the scalar x
$\lVert\mathbf{x}\rVert$	Euclidean norm of the vector $\mathbf{x}$
$[\mathbf{f}_i, \mathbf{f}_j]$	Lie bracket of the vector fields $\mathbf{f}_i$ and $\mathbf{f}_j$
diag($\mathbf{A}$,...,$\mathbf{Z}$)	Block diagonal matrix with the square matrix blocks $\mathbf{A}, \ldots, \mathbf{Z}$
col($\mathbf{x}, \mathbf{y}$)	Stacked column vector of the vectors $\mathbf{x}$ and $\mathbf{y}$, col($\mathbf{x}, \mathbf{y}$) = $[\mathbf{x}^{\mathrm{T}}\ \mathbf{y}^{\mathrm{T}}]^{\mathrm{T}}$
$\Lambda(\mathbf{A})$	Set of eigenvalues of the square matrix $\mathbf{A}$

Acronyms

CL	(Method of) Controlled Lagrangians
DA	Domain of Attraction
DC	Dissipation Condition
DE	Dynamical Equilibrium
IDA	Interconnection and Damping Assignment
IP	Inverted Pendulum (on a cart)
ISS	Input-to-State Stable/Stability
IWP	Inertia Wheel Pendulum
LLDA	Local Linear Dynamics Assignment
LMI	Linear Matrix Inequality
LQR	Linear Quadratic Regulator
LTI	Linear Time-Invariant
ODE	Ordinary Differential Equation
PBC	Passivity-Based Control
PDE	Partial Differential Equation
PFL	Partial Feedback Linearization
pH	port-Hamiltonian
PVFC	Passive Velocity Field Control
WIP	Wheeled Inverted Pendulum

I

Preliminaries

1 Introduction

Since the emergence of control theory in the last century, a lot of effort has been put into the integration of feedback and feedforward control into mechanical systems to develop manipulators that accurately perform a unique task over and over again. To guarantee the required precision and to eliminate possible disturbances that might affect the performance of the machine, mechanical systems have been built remarkably rigid, and strong and stiff actuators have been employed [141]. That is, for a long time, researchers put the focus on stiff fully actuated solutions. While these systems are comparatively straightforward to control, as they are equipped with motors and sensors at every joint, they lack the efficiency and the speed that underactuated mechanical systems are likely to provide. As fully actuated systems are *forced* to follow a desired motion, considerable joint torque is required to cancel out the natural dynamics of the machine. For instance, as of today, a biped robot uses roughly 20 times more energy than a human to walk [202].

For that reason, people have started to carefully reevaluate the objective of control for mechanical systems, dismissing the paradigm of using feedback to cancel out their natural motion, and focusing on exploiting the plant's intrinsic dynamics to potentially achieve faster and more efficient mechanisms [202].

In a formal way, this trend has lead to a deliberate study of underactuated mechanical systems—systems with more degrees of freedom than actuators. Underactuated systems emerge in different contexts:

Dynamics of the system. Drones (flying robots), underwater vehicles, and other systems that locomote like walking machines are intrinsically underactuated. In particular, animal and human locomotion relies on underactuation to achieve more efficient and faster dynamics.

Design. Mainly to reduce costs, weight and space, for instance, in aerospace applications (e. g. satellite with two thrusters).

Elasticity. When joint (or link) elasticity plays a major role, the rigid model has to be augmented by its elastic properties [7]. Apart from being more efficient and less costly, light and flexible robot manipulators are desirable, as they are intrinsically safe

for humans in future human-machine collaborations.

Actuator failure. Fully actuated systems become underactuated if one of the actuator fails. The analysis of underactuated systems is fundamental to study robustness to actuator failure.

The control of underactuated systems is challenging, since not all degrees of freedom can be independently controlled at every instant in time [196]. Hence, underactuated systems cannot be commanded to follow arbitrary trajectories. To control this class of systems, it is necessary to develop control algorithms that exploit the system's complex potential and inertial couplings. In the last two decades, energy shaping has played a central role in this development [188].

The idea of energy shaping emerges from the notion of viewing dynamical systems as "*energy-transformation devices*" [155]. The control objective can then be understood as shaping the energy, such that this *new* virtual energy—according to which the closed-loop system behaves—has a unique minimum at the desired equilibrium point, and changing the way this new energy is interchanged and dissipated to achieve the desired dynamics.

Example 1.0.1 (Total energy shaping). To illustrate total energy shaping for mechanical systems, let us consider the simple two degree of freedom mechanical system from Figure 1.1 (left), whose dynamics are given by

$$\mathbf{M}\ddot{\mathbf{x}} = \mathbf{G}\mathbf{u} - \nabla_{\mathbf{x}} V, \tag{1.1}$$

with constant inertia matrix $\mathbf{M} = \left[\begin{smallmatrix} m_1 & 0 \\ 0 & m_2 \end{smallmatrix}\right]$, potential energy $V(\mathbf{x}) = \frac{1}{2}k(x_2 - x_1)^2$, and input matrix $\mathbf{G} = \left[\begin{smallmatrix} 1 \\ 0 \end{smallmatrix}\right]$.

What does it mean to *shape* the potential energy through feedback? The idea is to *create* a virtual potential field $V_{\text{vir}}(\mathbf{x})$, such that the resulting closed-loop potential energy $V_{\text{tot}}(\mathbf{x}) = V_{\text{vir}}(\mathbf{x}) + V(\mathbf{x})$ has desired properties (for instance, an isolated minimum at the desired equilibrium $\mathbf{x}^*$). We are, however, not free to choose the function $V_{\text{vir}}(\mathbf{x})$.

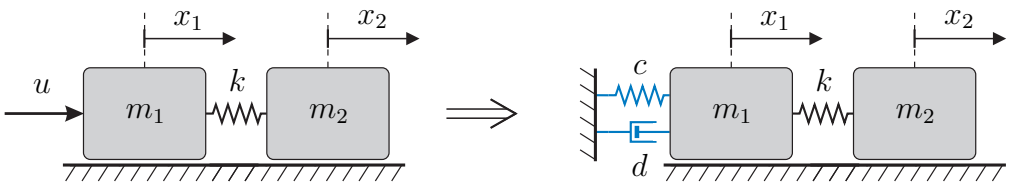

Figure 1.1: Potential energy shaping.

As the system is underactuated, the function $V_{\text{vir}}(\mathbf{x})$ has to satisfy

$$\mathbf{G}_{\perp}\nabla_{\mathbf{x}}V_{\text{vir}}(\mathbf{x}) = 0,$$

which means that the forces arising from the virtual potential $V_{\text{vir}}(\mathbf{x})$ lie in the image of the input matrix—$\mathbf{G}$ is the input matrix, and $\mathbf{G}_{\perp}$ its left annihilator, i. e., $\mathbf{G}_{\perp}\mathbf{G} = 0$—and can be reproduced by the input. In addition to the creation of a new potential, damping is injected for asymptotic stability. Figure 1.1 (right) illustrates the situation. The structure of the system suggests that it is only possible to directly add potential and damping forces to the actuated mass. However, additional virtual dynamic couplings between the bodies can be generated by shaping the kinetic energy. While less interesting for fully actuated systems, this technique is widely used for underatcuated systems for stabilization and performance improvement. □

The outstanding benefit of energy shaping is the physical nature of the approach. The closed-loop system is motivated by the physical properties of mechanical systems, which, in turn, facilitates the controller parametrization. One can hardly overestimate the simplicity that this physical insight is likely to provide [188].

This thesis addresses two practical problems in the implementation of energy shaping to underactuated mechanical systems, which are covered in Part II and Part III. Part II is devoted to the applicability of total energy shaping to systems with physical dissipation in unactuated coordinates. Dissipation is often neglected for mathematical elegance and simplicity. However, it has been shown that damping may impede the passivation of the closed-loop system via energy shaping [74]. How to apply energy shaping in the presence of physical damping nonetheless is the topic of Part II.

Part III is concerned with the application of energy shaping for the stabilization and tracking of underactuated wheeled robots. Manned vehicles, and more recently, wheeled robots and autonomous systems bring many benefits to humans in terms of transportation and human assistance, as working machines, and for leisure and entertainment. While other forms of ground-based locomotion, like walking machines, are still inefficient and require complex control structures, the wheeled locomotion achieves a better performance in terms of energy consumption and speed in even surfaces. In particular, the wheeled inverted pendulum (WIP) has been widely studied for a series of novel applications [128]. For instance, the novel Electric Networked Vehicle, *En-V*, has been developed to address the upcoming challenges of urban mobility [204]. Wheeled mobile robots and vehicles are designed to move from one place to another. In the absence of a pilot in a futuristic scenario, automatic control accounts for the navigation.

1.1 Literature review

The field of energy shaping for stabilization and tracking of both holonomic and nonholonomic systems is evolving at a fast pace. Therefore, it is (probably) impossible to give a complete and comprehensive overview. Nonetheless, to put our work in the right context, in the following we give a short review of the advances in related fields during the last years, and present the state of the art. According to the main contributions of our work, this section focuses on total energy shaping control methods for holonomic and nonholonomic underactuated systems, dissipation related challenges in passivity-based control, and trajectory tracking and path following control using energy arguments.

1.1.1 Total energy shaping for mechanical systems

Energy shaping methods are strongly linked with passivity—a property of dynamical systems that proves to be useful for their stability and robustness analysis. As the name suggests, the basic idea is to *shape* the total energy—consisting of potential and kinetic energy—through feedback. By doing so, these methods provide a closed-loop system that still has mechanical structure, and for which both the specific shape of the energy and the way the energy is interchanged and dissipated within the system's boundaries characterize the behavior. Shaping the energy such that it is bounded from below and injecting damping such that the (closed-loop) energy gets dissipated, ensures passivity of the closed-loop system. There is, therefore, a strong link between passivity-based control (PBC) and total energy shaping [153].

The idea of energy shaping dates back to 1981, the year when Arimoto and Takegaki first presented the idea of shaping the potential energy and adding damping for asymptotic tracking of fully actuated manipulators in their well-known paper [11]. If the system's energy is shaped such that it has an isolated minimum at the desired equilibrium, then it can be used as a Lyapunov function for the closed-loop system. The approach provides in this way a unified framework for the control design and stability analysis of a variety of control systems. The famous PD controller for robotic manipulators (cf. [141, 189]) is a classic example of potential shaping. The proportional (P) gain comprises the virtual forces stemming from the shaped potential energy, the derivative (D) gain constitutes the injected damping to provide asymptotic stability. Potential shaping was put in a geometric framework in [180] for Hamiltonian systems, and has been further developed for diverse applications including the control of flexible joint robots [6, 7], satellite attitude stabilization [19], or attitude control of a quadrotor

helicopter with saturating inputs [64], among many others.

While potential energy shaping (plus damping injection) is enough to stabilize fully actuated mechanical systems, also shaping the kinetic energy might be necessary for the stabilization of some underactuated mechanical systems, or to improve transient performance. Over the last two decades, mainly three approaches to shape both the potential and the kinetic energy simultaneously have been developed: Interconnection and damping assignment passivity-based control (IDA-PBC), Hamiltonian in nature, was first developed for physical (not necessarily mechanical) systems by the beginning of the 21st century [151, 155, 156]. Viewing dynamical systems as *"energy-transformation devices"* [155], one attempts not only to alter the system's energy, but also to change the way the energy gets transformed and dissipated within the system's boundaries. IDA was soon developed for mechanical systems, for which the energy of the closed-loop system is restricted to be the sum of kinetic and potential energy [5, 158]. The Lagrangian counterpart to IDA for mechanical systems is called the method of Controlled Lagrangians (CL). CL in its more general form aims at rendering the closed-loop system mechanical (with desired *controlled* Lagrangian). Generalized gyroscopic forces are additionally introduced as tuning parameters, damping forces for asymptotic stability. Its roots date back to 1992, when Bloch et al. developed stabilizing feedback controllers that artificially altered the mass matrix of rigid bodies, thus, shaping their kinetic energy [26]. This concept was further developed in a series of conference papers [28, 29, 31], and finally formalized in [32]. Originally, the idea was to shape the kinetic energy of underactuated mechanical systems with symmetry[1]. The symmetry condition was relaxed and potential energy shaping was allowed in [25, 30]. The addition of generalized gyroscopic forces finally lead to its most general form, which has been proven to be equivalent to IDA for mechanical systems [22, 47]. Despite potential shaping being significantly more popular, kinetic—and specially total energy shaping approaches—have also found a place in the literature and practical applications, such as the speed regulation of bipedal walking robots [92], smooth trajectory design for a formation of mobile robots [20], and stabilization of underactuated mechanical systems [2, 151]. Less popular, but in essence an energy shaping strategy for port-Hamiltonian systems as well, is another method that relies on time-varying generalized canonical transformations—which preserve the Hamiltonian structure of the closed-loop system—to stabilize mechanical systems [68].

The adaptation of energy shaping to constrained systems came with the work of

[1] A mechanical system is said to exhibit a symmetry if the Lagrangian is independent from a configuration variable. The corresponding variable is known as *cyclic variable*.

Maschke and van der Schaft on the Hamiltonian formulation of nonholonomic systems [185], and their stabilization via potential shaping [134]. As nonholonomic systems are not smoothly stabilizable at a point, for they fail to satisfy Brockett's necessary condition [14], the approach results in the asymptotic stabilization of an invariant set in the state-space. In [21], Blankenstein gives a complete overview of the extension of IDA-PBC to nonholonomic systems. Concerning the Lagrangian framework, an energy-momentum-based technique was developed for the stabilization of constrained systems in [33]. The relation to CL is assumed, but not yet completely understood. The canonical transformations have also been modified for the stabilization of constrained systems [69]. Worth to mention is the work of Fujimoto et al. [66], in which the authors assign non-smooth potential functions for the asymptotic stabilization of fully actuated nonholonomic systems.

For fully actuated systems, energy shaping represents a physically motivated, and intuitive approach, which not only guarantees passivity and stability of the closed-loop system, but has also proven to improve robustness [155]. When dealing with underactuated systems (holonomic and nonholonomic), however, the applicability of energy-shaping is restricted by the solution of nonlinear PDEs, the so-called *matching equations*. Since not every degree of freedom can be controlled independently, when *matching* the system's dynamics with the desired closed-loop dynamics, some conditions—the matching equations[2]—have to be satisfied independent from the control input. The shaping of the potential energy is restricted to the solution of a linear PDE with state dependent coefficients. For kinetic energy shaping, the solution of a nonlinear PDE is necessary.

Despite of large amounts of research, finding a solution for the matching equations is still a very challenging task. Nonetheless, there have been some remarkable advances towards their analytical solution, such as the so-called λ-method—a method used to transform the kinetic energy matching equation into a set of linear PDEs—presented by Auckly and Kapitanski in [15, 16]. For a class of mechanical systems, it is even possible to transform the PDE for the kinetic energy into an ODE as shown in [209]. Viola et al. present in [206] a way of simplifying the projected matching equations via coordinate transformations in the momenta. More recently, the trend goes towards manipulating the equations in order not to require the solution of PDEs. In [4], an approach is pursued to obviate the solution of PDEs for general input-affine systems by designing an approximating integral together with a dynamic extension to replace the PDEs with

[2]The term *matching equations* is sometimes used for the entire matching problem. The conditions that are independent from control are then referred to as *projected* matching equations.

algebraic inequalities. In [58], the structure-preserving requirement for the closed-loop system to be of mechanical structure is obviated. The authors then present a method to shape the total energy of a class of mechanical systems without solving PDEs. In general, these existing methods apply only for a limited number of systems, for very strong assumptions are made. Therefore, finding solutions to the PDEs remains the main obstacle for the wider application of total energy shaping methods. Although it is possible to formulate the matching problem in terms of algebraic equations by fixing the closed-loop energy, this approach has proven difficult to apply [151]. Some approaches exist regarding the algebraic solution in IDA-PBC for general port-Hamiltonian systems (cf. [148]), but to the best of our knowledge, no algebraic solution has been presented for underactuated mechanical systems.

Existing total energy shaping methods also lack transparency regarding the controller parametrization. Despite the approach being physically motivated, the closed-loop system does not always behave as intuitively expected: As shown in [108] (Example 4.2), the (virtual) reduction of the inertia parameters of an electrical machine via energy shaping results, counterintuitively, in slower transient dynamics. On the other hand, although shaping the energy stabilizes underactuated mechanical systems, simulations often show undesired oscillating and slow transient dynamics [1, 167, 173]. Yet, transparency with respect to the parameter tuning can be achieved via local linear dynamics assignment (LLDA), a method that specifies the eigenvalues of the linearized closed-loop system to fix the controller parameters [110]. However, it is not always possible to fix all eigenvalues as desired, which results in the aforementioned strong oscillations and slow convergence.

Finally, systems with a stabilizable linearization cannot always be rendered passive with a storage function that is minimal at the desired equilibrium via IDA, CL, or canonical transformations. In particular, physical dissipation in unactuated desgrees of freedom plays a critical role in their applicability.

1.1.2 Dissipation in passivity-based control

Against the intuition, energy dissipation does not always enhance stability. It has been known for over one-hundred years that the combination of gyroscopic and dissipation forces has unexpected effects on the stability of mechanical systems (cf. theorems of Thompson and Tait [135]). In [221], Ziegler presented the counterintuitive behavior of systems that exhibit stable equilibria (or steady motions) when modeled without friction, but, by introducing small damping, they get destabilized. This is known as

Ziegler's paradox. Since their discovery, dissipation-induced instabilities have awakened the attention of engineers and mathematicians. In their excellent survey article [115], Krechetnikov and Marsden describe the phenomenon of dissipation-induced instabilities with several examples. For instance, the particular behavior of the Tippe-Top can only be fully described if friction is considered. As shown in [37], the Tippe-Top's inversion is a classic example of a dissipation-induced instability, where the static equilibrium gets destabilized by the effect of the dry friction once the top starts to spin.

The importance of dissipation in mechanical control systems has lead researchers to study the effect of physical damping in the application of energy shaping approaches. Most of the work deals with the effect of damping in actuated coordinates, where the dissipation is large compared to the one in unactuated coordinates. Having this damping under control is, therefore, crucial for the performance of mechanical systems. In particular, the studies include the stick-slip effect, which is likely to cause an undesired limit cycle behavior around the desired equilibrium point [43]. For the energy-based modeling and control of dissipation forces in actuated coordinates, the reader is referred to [43, 107, 178].

Soon after the introduction of total energy shaping control methods, researchers began to study dissipation-related issues for underactuated systems. In [73], Gomez-Estern showed the importance of physical damping for the performance of passivity-based control laws. Incidentally, a paradoxical destabilizing effect of the dissipation forces might also occur when the kinetic energy of an underactuated mechanical system is altered through feedback, since damping terms do not necessarily remain dissipative with respect to the closed-loop energy function.

If this phenomenon occurs, and physical dissipation in unactuated coordinates is considered, the closed-loop damping matrix becomes indefinite, which impedes the passivation of the mechanical system through feedback. Thus, the implementation of an IDA-PBC (or CL) controller is hampered by physical dissipation in unactuated degrees of freedom [74]. The so-called *dissipation condition* (DC) determines if required definiteness properties for the closed-loop system can be fulfilled in the presence of dissipation or not. Yet, it is well-known that no stabilizing energy-based controller exists that fulfills the requirements of the DC for a series of mechanical systems [43, 74, 112, 209]. In other words, it is not possible to find a controller that renders the closed-loop system passive with respect to the shaped energy in (simple) mechanical form.

Nonetheless, it is possible to prove asymptotic stability of an equilibrium that has been stabilized via energy shaping for the lossless system, when damping is considered and the DC is not satisfied. The stability verification is based on spectral analysis. One

important contribution can be found in [167, 168, 209], in which the authors show that the presence of (small) damping does not destabilize mechanical systems that have been assumed undamped and stabilized via energy shaping. If the control parameters are appropriately chosen, stability is shown by analyzing the linearized closed-loop system. Yet, by doing so, the domain of attraction is lost. Up to now, no passivity-based methodology exists that accounts for dissipation in unactuated coordinates from the very beginning.

1.1.3 Trajectory tracking and path following for nonholonomic systems

There are roughly two control strategies employed to track the desired motion of mechanical systems: *trajectory tracking* and *path following*. In trajectory tracking, as the name suggests, the mechanical system is controlled to asymptotically converge towards a reference trajectory. The system is commanded to be in a particular position with a defined velocity at a particular time. For fully actuated mechanical systems, the tracking control problem is well understood and can be consulted, for instance, in the textbooks of Bullo and Lewis [42], and Slotine and Li [189].

In path following, the primary goal is to steer the system towards a desired geometric path, and then to move along this path. As the path is usually defined only for the output and not for the entire configuration, path following is also known as output maneuver regulation, in which the *output* approaches and moves along a given geometric curve. For instance, for an industrial paint robot, the path is defined only for the applicator at the tip, and not for the remaining joints. Although, in general, no time dependency is assigned to the path, one may assign a desired velocity profile to specify the dynamics along the path as a secondary goal. Often, the path following problem is solved based on an admissible trajectory, which is assumed to exist and to be known [61, 87].

Trajectory tracking. In the context of energy shaping, the trajectory tracking problem has been tackled by describing the error dynamics as a port-Hamiltonian system, and then stabilizing the origin of the error system via passivity-based control; either by employing generalized canonical transformations [67], or IDA-PBC [114]. This approach has also been used for reference tracking of fully actuated mechanical systems when only position measurements are available [56]. Energy shaping strategies can be used for trajectory tracking of underactuated mechanical systems as well. In [199], the authors combine a feedforward and a feedback controller for the inertia wheel pendulum to track a reference trajectory. In [65], an energy-based trajectory tracking controller is

derived for a quadrotor system, which accounts for input saturation by appropriately designing the required potential fields.

Rather than tracking a reference trajectory, a usual approach is *output trajectory tracking*, where a specific motion of the output is to be exactly followed. This problem has been extensively studied in [118] and [94]. As a desired trajectory of the output is given, dynamic inversion is required to determine the corresponding input, which is a particularly difficult task for systems with unstable zero dynamics [54]. However, this method is extremely useful in the context of differentially flat systems. A dynamical system is said to be differentially flat if its entire state and control signals can be described by means of the output and a finite number of its derivatives [62, 118, 172]. Therefore, any sufficiently smooth output trajectory directly specifies the control input required to precisely track the reference trajectory, and, in addition, automatically provides the time evolution of all remaining state variables. The computed input—which is used as feedforward controller—guarantees exact output tracking in the absence of disturbances. An additional feedback controller is necessary to regulate initial state errors, and to compensate for model uncertainties and external disturbances.

One major drawback in trajectory tracking remains the fact that the reference trajectory has to be admissible, i. e., it has to be compatible with the system's dynamics. For unconstrained and fully actuated mechanical systems, any sufficiently smooth reference trajectory is admissible, as one is able to command arbitrary accelerations in any given direction. However, in general, finding admissible trajectories for underactuated systems is challenging, as not every possible motion between two points is also compatible with the system's dynamics. Note, for instance, that unactuated coordinates can only be steered by exploiting the system's potential and dynamic couplings. In [76], the authors present a numerical method to determine admissible trajectories for underactuated systems with input and output constraints using commercial software tools. In [54], a dynamic inversion procedure for output tracking is presented, which provides bounded input trajectories regardless of unstable zero dynamics.

As far as trajectory tracking for nonholonomic systems is concerned, a useful contribution is the chained form, introduced by Murray and Sastry in 1993 [142]. This special class of systems—which covers flat systems like mobile robot platforms and car-trailer systems—has been in the focus of research for its practical applications. In order to simplify the problem setting, some researchers employ the kinematic model, neglecting the dynamics (cf. [137, 177]). As a consequence, a predefined path can be easily converted to a reference trajectory, as the velocity profile along the path can be arbitrarily designed [57]. Some of the research, nonetheless, considers the dynamic model, and

includes robust backstepping [71, 95] and sliding-mode control [49, 213], among others. However, these approaches assume fully actuated nonholonomic systems.

Path following. Due to the inherent difficulties of trajectory tracking, path following has recently gained more and more attention. Also, for some control applications such as the operation of a welding robot, path following is a more appropriate problem setting. In path following, the geometric path of the output is only required to be continuous, can be time-varying [200], and no dynamic inversion is necessary, as the dynamics along the path are not specified a priori. A well-known method for path following, which relies on potential shaping and which has also been successfully applied to obstacle avoidance in robotic manipulation and navigation of mobile systems, is the introduction of attractive or repulsive potential fields [160, 198]. A further technique is *passive velocity field control* (PVFC), introduced as *velocity field control* by Li and Horowitz in 1993 [123], in which the motion task is encoded in a velocity field, and the closed-loop system interacts in an energetically passive manner with its environment [124]. PVFC was formalized for fully actuated mechanical systems in [125] and [126]. Vector fields methods have proven convenient for path following of mobile robots: In [146], the authors use vector fields that provide the heading commands to force small unmanned vehicles to converge towards a desired path even in the presence of constant disturbances. Once on the path, the velocity field controller guarantees a prescribed forward speed along the path. Further extensions of PVFC for fully actuated mechanical systems have been developed by Duindam and Stramigioli [60], and Fujimoto and Taniguchi [70]. The notion of vector (velocity) fields is similar to that of potential fields in the sense that the control forces are commanded by these fields. However, the vector fields do not necessarily represent the gradient of a scalar function. Rather, the vector fields simply specify the desired direction of motion. From a practical point of view, the vector field strategy can be easily embedded in the energy shaping framework, even though, strictly speaking, no energy is being shaped. Despite the advantages of vector-field-based approaches, the characterization of a vector field that encodes a complex task is difficult, and the description of that vector field often requires a lot of storage memory. A simple technique for path following which bypasses these drawbacks is *waypoint tracking*. The idea is to define discrete equilibrium points along a geometric path. These points are then successively stabilized by a stabilizing controller. Even though the path is only approximated by the discrete set points, very complex maneuvers are possible, as relatively little storage memory is required. Additionally, following waypoints can be computed in real time to improve robustness and performance. Nonetheless, because of the step-wise changes of the desired equilibrium, the time evolution of the state exhibits

a periodic pattern, as the system continuously accelerates and decelerates [138]. How to define the different waypoints, and, if necessary, how to place new waypoints as the system moves, is still topic of research: In [40], the authors employ a Lyapunov-based generator of waypoints for linear systems that accounts for input saturation and guarantees stability. As the strategy uses continuously moving waypoints, the undesired acceleration and deceleration of the plant is avoided. In [55], the authors present an extension of the aforementioned strategy by including nonlinearities via Takagi-Sugeno formulation, and considering multiple inputs.

Because of the flexibility of the problem setting, path following is preferred for nonholonomic underactuated systems, like the wheeled inverted pendulum (WIP)—the paramount example for this class of mobile robots. Although reference tracking has been successfully implemented in the past for the linearized system [78], path following is more common in recent publications: In [216], the authors develop a path following strategy for a wheeled pendulum with inherently stable pitch dynamics, for the pendulum's center of mass lies below the wheel axis; in [138], the authors use waypoint tracking for the WIP, which requires less storage memory, but the path cannot be followed exactly, as the finite number of waypoints only approximate the path. Additionally, the pitch dynamics exhibit an undesired periodic pattern due to the acceleration and deceleration of the WIP.

1.2 Contributions of this thesis

This thesis is devoted to the development of energy shaping control techniques for underactuated mechanical systems. Therein, the focus is set on theoretical developments to tackle implementation problems in practice, and thereby enhance the applicability of the control approach. Whilst Part II deals with the difficulties in the implementation of energy-based controllers that arise from physical dissipation in unactuated coordinates, Part III is devoted to constrained systems, and, in particular, the stabilization, tracking, and path following control for nonholonomic mechanical systems. Thereby, we place emphasis on the wheeled inverted pendulum. The main contributions of our work are summarized in the following:

Chapter 3: Augmented Interconnection and Damping Assignment. In this chapter, we are concerned with the stabilization of mechanical systems via IDA in the presence of dissipation in unactuated coordinates. The so-called dissipation condition (DC) [74] represents an obstacle for the passivation of the closed-loop system.

Therefore, inspired by the analysis of the linear system, we augment the closed-loop Hamiltonian by a non-physical cross term between coordinates and momenta to bypass the DC. By doing so, we are able to develop a passivity-based methodology that accounts for dissipation in unactuated coordinates from the very beginning, retaining the usual benefits from PBC: passivation of the closed-loop system, and simple stability analysis and estimation of the domain of attraction via Lyapunov theory [155]. Additionally, our approach only requires the solution of algebraic equations to satisfy the matching problem rather than the solution of difficult PDEs. Further, the introduction of additional design degrees of freedom by augmenting the closed-loop Hamiltonian allows for performance improvement and facilitates the parametrization via LLDA [109]. The main contributions of Chapter 3 are:

- the development of a passivity-based control technique for underactuated mechanical systems that accounts for physical dissipation in unactuated coordinates from the very beginning,
- the algebraic formulation of the matching problem for underactuated mechanical systems, and
- sufficient conditions for the solution of the algebraic matching equations.

Chapter 4: Controller Design. In this chapter, we address the question of how to use the theory developed in Chapter 3 for a systematic controller design procedure. As we do not require the solution of PDEs for matching, the simultaneous solution to the matching equations and the parametrization of the closed-loop system is based on the solution of one Lyapunov equation. Inspired by LLDA as a parametrization tool for the controller that relies on the assignment of desired local dynamics, we guarantee not only stability, but—locally—also desired transient behavior with the developed controller. A procedure comprising five simple steps summarizes the controller design. The contributions of Chapter 4 are:

- the derivation of a systematic procedure for the controller design for a class of underactuated mechanical systems that guarantees desired local behavior in terms of the eigenvalues of the closed-loop system by solving one Lyapunov equation, and
- the characterization of the class of systems, for which the procedure can be systematically applied.

Chapter 5: Applications. In this chapter, we illustrate the application of the augmented IDA approach step by step as developed in Chapter 3 and Chapter 4, and demonstrate its effectiveness on a number of benchmark examples. We consider the stabilization of the three underactuted mechanical systems acrobot, inertia wheel pendulum, and inverted pendulum on a cart. Not only a series of simulations illustrates the performance compared to other controllers, but also experiments conducted on the inverted pendulum on a cart show its practical applicability. The main contribution of Chapter 5 is:

- the demonstration of the applicability and performance of the augmented IDA technique for the control of mechanical systems with dissipation in unactuated coordinates.

Chapter 6: Total Energy Shaping for Nonholonomic Systems. This chapter deals with the position and velocity stabilization of a class of nonholonomic mechanical systems via total energy shaping. Thereby, we assume that the DC is satisfied, such that no augmentation of the desired energy is required to render the closed-loop system passive with respect to the closed-loop energy function. Specifically, we design smooth control laws for the position stabilization in a reduced (unconstrained) configuration space $\mathcal{Q}_\mathrm{R}$, and show that, for a class of systems, the solution to the matching problem in reduced coordinates automatically provides the solution to the matching problem in configuration space $\mathcal{Q}$ (or a subset $\mathcal{Q}_\mathrm{C}$ thereof). In this case, nonetheless, the energy shaping approach asymptotically stabilizes an invariant set. If some (minor) conditions are satisfied, then the results can be directly applied for velocity stabilization as well. In addition to the design of stabilizing control laws, we consider in this chapter two aspects of practical relevance: the robustness properties of the controllers by means of input-to-state stability (ISS), and the incorporation of actuator dynamics into the controller design. As far as we are aware, there is no unified framework that uses the structural advantages of energy shaping for the position stabilization and speed control of underactuated nonholonomic systems, which, at the same time, takes into account the robustness of the control system, and also includes actuator dynamics. The contributions of Chapter 6 are:

- the application of the same unifying framework for the position and velocity control design for underactuated nonholonomic systems in reduced space $\mathcal{Q}_\mathrm{R}$,
- the derivation of conditions, under which the result can be directly transfered to a constrained subset of the configuration space $\mathcal{Q}_\mathrm{C} \subseteq \mathcal{Q}$ for the asymptotic stabilization of an invariant set

- the estimation of the magnitude of the disturbance tolerated by the controllers by means of an ISS analysis, and

- the incorporation of actuator dynamics in the energy shaping controller design via backstepping.

Chapter 7: Trajectory Tracking and Path Following. In this chapter, we are concerned with trajectory tracking and path following for nonholonomic underactuated mechanical systems via energy shaping. Due to the difficulty in finding admissible trajectories, [87], especially for systems with unstable zero-dynamics (cf. [54, 76]), we consider in this chapter non-admissible trajectories, and study the boundedness of the closed-loop signals and the stability of the system with respect to the tracking error, that is, as trajectories that are not compatible with the system's dynamics can only be approximately tracked, we show that the tracking error remains bounded and converges towards the origin if the reference trajectory is admissible. In that context, we also develop a stabilizing hybrid position and velocity controller for nonholonomic systems.

In reference tracking, large discrepancies of the initial state with respect to the reference might result in large input torques or saturation. Partially because of that, and in order to bypass the computation of admissible trajectories, path following strategies emerged. They also better describe a number of practical tasks like automatic welding and painting with robotic arms. In this chapter, we incorporate into the energy shaping approach a unified path following strategy that can be applied to track arbitrary geometric paths. Further, we analyze the system's convergence to the path, and the stability of the closed-loop system by means of ISS.

To the best of our knowledge, the structural properties of energy shaping have not been yet exploited to develop control laws for unstable, underactuated nonholonomic systems to (approximately) track non-admissible trajectories or geometric paths. The contributions of Chapter 7 are:

- the stability analysis of the closed-loop system with respect to non-admissible trajectories, i. e., the analysis of the boundedness of the tracking error

- the derivation of a stabilizing hybrid position and velocity controller, and

- the incorporation of path following strategies in the energy shaping controller design, and their stability analysis.

Chapter 8: The Wheeled Inverted Pendulum. In this chapter, we apply the theory developed in Chapter 6 and Chapter 7 to the wheeled inverted pendulum system, which is a mobile robot subject to nonholonomic constraints, and with unstable pitch dynamics. We show an elegant solution to the matching problem for the WIP, and present a procedure to fix the closed-loop parameters to guarantee desired local dynamics by means of the eigenvalues of the linearized system. The applicability of the stabilization, trajectory tracking, and path following controllers is demonstrated by a series of simulations and, in particular, experiments conducted on a small scale WIP, which has been developed at the Institute of Automatic Control of the Technische Universität München. Furthermore, we show in this chapter how the results of Chapter 6 and Chapter 7 can be combined, for instance, for the stabilization of a specific point on the horizontal plane, or for the application of path following strategies with a given velocity profile along the path.

In conclusion, this chapter studies the systematic and integrated design of stabilizing and tracking controllers for the wheeled inverted pendulum system in a single, energy-based framework. An emphasis is put on the structural advantages of the approach and the experimental validation of the control laws. The main contributions of Chapter 8 are:

- the solution to the matching equations for the WIP and the transparent parametrization of the closed-loop system
- the demonstration of the viability and performance of the stabilizing and tracking approaches proposed in Chapter 6 and Chapter 7 and adaptations thereof with the aid of a series of simulations, and, in particular,
- experimental results on a small scale WIP.

1.3 Outline of the thesis

The remainder of the thesis is organized as follows: Chapter 2 gives an overview of the theoretical background required for all upcoming chapters. It includes an introduction of basic notions of geometry and mechanical systems, a review of existing results from stability analysis and passivity for nonlinear systems, and a brief presentation of the two most popular energy shaping methods—Interconnection and Damping Assignment (IDA) and the method of Controlled Lagrangians (CL)—from a passivity-based control (PBC) perspective.

The scientific contributions of the thesis are clustered in two parts: Part II covers Chapters 3, 4 and 5, and deals with the difficulties in the implementation of total energy shaping controllers that occur when physical dissipation is considered in unactuated coordinates. In Chapter 3, the so-called dissipation condition (DC) is presented, and a method that considers physical dissipation in the controller design from the very beginning is developed via IDA-PBC by breaking the mechanical structure of the closed-loop system. Chapter 4 presents the controller design in a series of steps; simulations and experiments for the validation of the proposed method are shown in Chapter 5.

Part III covers Chapters 6, 7 and 8, and deals with energy shaping methods for stabilization, path following, and reference tracking for underactuated nonholonomic systems. Thereby, the DC is assumed to be satisfied, and the conventional total energy shaping approach is applied. Chapter 6 presents the main position and speed stabilization results for underactuated nonholonomic systems using total energy shaping in reduced space. In Chapter 7, methods for path following and trajectory tracking are developed for the considered systems. The energy-based controllers are validated with a series of simulations and experiments using a small scale wheeled inverted pendulum (WIP) in Chapter 8.

The thesis concludes with a short summary and ideas for future work in Chapter 9. An appendix is included to present the proofs of some theorems as well as the dynamical model of the WIP that is used for the controller design and the simulations.

2 Theoretical Fundamentals

This chapter presents the theoretical basis, which this thesis is built on. After some brief mathematical preliminaries in Section 2.1, where we introduce non-euclidean configuration manifolds and some geometric concepts, we discuss simple mechanical systems in both Lagrangian and Hamiltonian representation in Section 2.1.2 and Section 2.1.3, respectively. In particular, when considering nonholonomic constraints, geometric mechanics become indispensable for the understanding of the behavior of the system. Nonholonomic systems are briefly discussed in Section 2.1.4. As this thesis places emphasis on the stabilization of mechanical systems, we then recall some notions of stability in Section 2.2, and present a number of theorems that will be used throughout the manuscript. We close this preliminary chapter by introducing the passivity-based control theory in Section 2.3. Beginning with the passivity property of dynamical systems, we then move on to the class of port-Hamiltonian (pH) systems, and finally present two energy-shaping control approaches that rely on passivity for the stabilization of mechanical systems.

2.1 Simple mechanical systems

The word *simple* does not imply that the class of systems we consider is easy to deal with. A mechanical system is called *simple* if its Lagrangian function is defined as its kinetic minus its potential energy. A large number of mechanical systems belongs to this category, and many of them are highly complex. Throughout this thesis, the word *simple* will often be dropped, and we will refer to this class simply as mechanical systems.

This thesis is devoted to underactuated simple mechanical systems. As the name suggests, this class of systems is characterized by having less actuators than degrees of freedom, and includes robot manipulators with flexible links and/or joints, flying robots, underwater vehicles, and other systems that locomote like mobile robots and walking machines, among others. While fully actuated systems can be controlled with classical control methods like feedback linearization [141], underactuated systems require more sophisticated control techniques that take into account the complex internal

dynamics for stabilization and tracking. Unlike fully actuated systems—which are rigid and bulky, in general, and, thus, lack flexibility and speed—underactuated mechanical systems benefit from their *natural* dynamics, which leads to an increase in the performance in terms of speed, efficiency and robustness [202]. Therefore, this class of systems has moved to the focus of researchers in an attempt to enhance the performance, while lowering the production costs and energy consumption. However, the control of underactuated systems is challenging, as the degrees of freedom cannot be controlled independently, and, for that reason, complex internal potential and inertial couplings need to be exploited for the design of control systems [196].

We will differentiate between holonomic and nonholonomic systems. In 1894, Heinrich Hertz defined holonomic systems as *"systems between whose possible positions all conceivable continuous motions are also possible motions"* [86]. For nonholonomic systems, on the contrary, not every *"conceivable continuous motion"* between two positions is also possible: Nonholonomic constraints restrict the motion direction at any given configuration. For that reason, control theorists face additional challenges designing techniques to control nonholonomic systems.

In the following, we introduce some geometric concepts that are necessary to understand the behavior of mechanical systems, and in particular, of nonholonomic systems. Thereafter, we present the equations of motion of mechanical systems in both the Lagrangian and Hamiltonian framework, and introduce nonholonomic constraints.

2.1.1 Geometric preliminaries

As an engineer, we are familiar with the concepts of differential and integral calculus in the n-dimensional Euclidean space $\mathbb{R}^n$. Dynamical systems—and in particular mechanical systems—often evolve on a manifold $\mathcal{Q}$, which may or may not be Euclidean. The configuration manifold $\mathcal{Q}$ represents the set of all possible configurations and is locally homeomorphic to, e. i., looks like, an Euclidean space of the same dimension. Globally, however, they might differ. Generally, we will work with a local set of coordinates, say $\mathbf{x}_i$, and assume that the configuration manifold is $\mathbb{R}^n$. Nonetheless, we have to keep in mind that $\mathcal{Q}$ is, in general, non-Euclidean. It is important to make the distinction, since $\mathcal{Q}$ does often not accept globally stabilizing smooth control laws[1] [42].

We do not aim at giving a comprehensive introduction to differential geometry. Rather, our intention is to intuitively introduce the geometric concepts that will be used throughout the manuscript. To a great extent, this section is based on the text-

[1] For instance, no global stabilizing smooth control law exists for the unit circle $\mathbb{S}^1$.

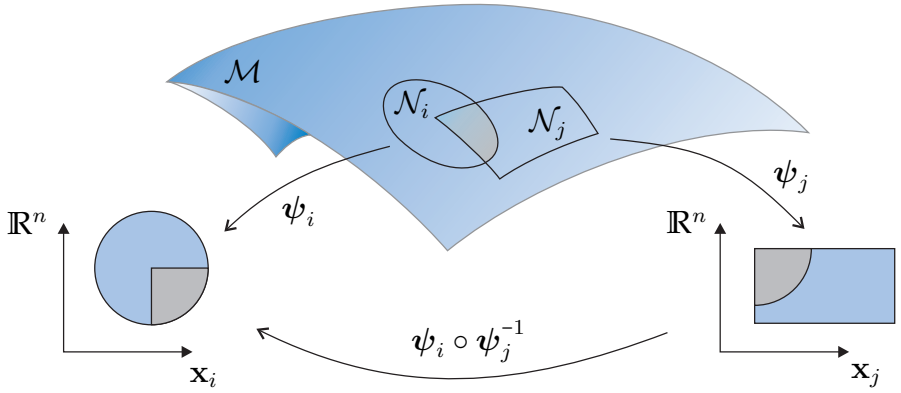

Figure 2.1: Smooth manifold $\mathcal{M}$ with compatible coordinate charts $\mathcal{N}_i$ and $\mathcal{N}_j$. We will normally work with a set of local coordinates, e. g., $\mathbf{x}_i$, and pretend to be dealing with an open subset of $\mathbb{R}^n$.

books [24, 63, 116]. For a general introduction to smooth manifolds and differential geometry, the reader is referred to the excellent textbooks of Lee [116] and Spivak [193]. For a treatment in application to physics and mechanical systems, the books of Frankel [63], Bullo and Lewis [42], Marsden [132], Marsden and Ratiu [133], or Bloch [24] can be consulted. For manifolds in the context of control, we refer to the textbooks of Lévine [118], Nijmeijer and van der Schaft [147], and Isidori [94].

Definition 2.1 (Smooth manifold [24])**.** An n-dimensional smooth manifold $\mathcal{M}$ is a set of points together with a finite or countably infinite set of subsets $\mathcal{N}_i \subset \mathcal{M}$ and smooth diffeomorphisms[2] $\boldsymbol{\psi}_i : \mathcal{N}_i \to \mathbb{R}^n$ such that

1. $\bigcup_i \mathcal{N}_i = \mathcal{M}$

2. For each non-empty intersection $\mathcal{N}_i \cap \mathcal{N}_j$, the set $\boldsymbol{\psi}_i(\mathcal{N}_i \cap \mathcal{N}_j)$ is an open subset of $\mathbb{R}^n$, and the smooth function $\boldsymbol{\psi}_i \circ \boldsymbol{\psi}_j^{-1} : \boldsymbol{\psi}_j(\mathcal{N}_i \cap \mathcal{N}_j) \to \boldsymbol{\psi}_i(\mathcal{N}_i \cap \mathcal{N}_j)$ is 1-to-1 and onto.

Essentially, a manifold is a set that can be locally parametrized by $\mathbb{R}^n$, and different parametrizations need to be compatible with one another. Figure 2.1 explains the situation. The charts $\mathcal{N}_i$ and $\mathcal{N}_j$ are compatible with one another in the sense that in the region, where both charts overlap (gray area), a smooth bijective map that transforms the elements of $\mathcal{N}_i$ into $\mathcal{N}_j$ (and back) exists.

We will normally work with a specific parametrization, and assume to be dealing with an open subset of $\mathbb{R}^n$ with *local coordinates* $\mathbf{x}_i$. We need to take into account, however,

[2] A smooth diffeomorphism is a smooth 1-to-1 mapping.

that our results are only locally valid, since a single *chart* $\mathcal{N}_i$ might not be sufficient to cover the whole manifold $\mathcal{M}$.

A typical and important way, in which manifolds arise is as level sets in $\mathbb{R}^n$: Let $\phi_1, \dots, \phi_m \colon \mathbb{R}^n \to \mathbb{R}$. The level set

$$\mathcal{M} = \{\mathbf{x} \in \mathbb{R}^n | \ \boldsymbol{\phi}(\mathbf{x}) = \mathbf{0}\}$$

is a differentiable manifold of dimension n–m if

$$\operatorname{rank}\left(\left[\frac{\partial \boldsymbol{\phi}}{\partial \mathbf{x}}\right]\right) = m, \qquad \forall\, \mathbf{x} \in \mathcal{M}.$$

We say that the level set is a submanifold of $\mathbb{R}^n$.

Definition 2.2 (Tangent space)**.** Let $\mathcal{M}$ be a smooth manifold of dimension n, then, to every point $\mathbf{x} \in \mathcal{M}$, there exists one *tangent space* $\mathsf{T}_{\mathbf{x}}\mathcal{M}$. The tangent space at $\mathbf{x}$ is an n-dimensional vector space.

Let $\boldsymbol{\gamma} : \mathcal{I} \to \mathcal{M}$ be a smooth curve on $\mathcal{M}$, where $\mathcal{I} \subset \mathbb{R}$ is an interval. The notion of the tangent space naturally leads to an interpretation of the tangent vectors to a curve $\boldsymbol{\gamma}(t)$ on a manifold $\mathcal{M}$. Let $\mathbf{x}_0 = \boldsymbol{\gamma}(t_0)$. The derivative $\boldsymbol{\gamma}'(t_0)$ lives in $\mathsf{T}_{\mathbf{x}_0}\mathcal{M}$ and defines the tangent vector to the curve $\boldsymbol{\gamma}(t)$ at $\mathbf{x}_0$. If the parameter $t \in \mathcal{I}$ represents the time, then the tangent vector is nothing but the velocity vector $\dot{\boldsymbol{\gamma}}(t_0)$. Therefore, the tangent space can be understood as the set of possible velocities at any point $\mathbf{x} \in \mathcal{M}$ (cf. Figure 2.2). For any smooth manifold $\mathcal{M}$, we define the tangent bundle of $\mathcal{M}$, denoted by

$$\mathsf{T}\mathcal{M} = \bigsqcup_{\mathbf{x} \in \mathcal{M}} \mathsf{T}_{\mathbf{x}}\mathcal{M},$$

to be the disjoint union of the tangent spaces at all points $\mathbf{x} \in \mathcal{M}$. The tangent bundle describes, hence, the set of all possible configurations and velocities and is a smooth manifold of dimension $2n$. With some slight abuse of notation, we write $(\mathbf{x}, \dot{\mathbf{x}}) \in \mathsf{T}\mathcal{M}$. In the context of mechanical systems, the configuration manifold $\mathcal{Q}$ represents the set of all possible configurations, the tangent space $\mathsf{T}_{\mathbf{q}}\mathcal{Q}$ is the set of the possible velocities at a given configuration $\mathbf{q} \in \mathcal{Q}$, and the tangent bundle $\mathsf{T}\mathcal{Q}$ is a $2n$-dimensional manifold that characterizes the *state*, which consists of all configurations and velocities $(\mathbf{q}, \dot{\mathbf{q}}) \in \mathsf{T}\mathcal{Q}$.

Definition 2.3 (Vector field)**.** A vector field $\mathbf{f}$ on a manifold $\mathcal{M}$ is a map $\mathbf{f} \colon \mathcal{M} \to \mathsf{T}\mathcal{M}$ that assigns to each point $\mathbf{x} \in \mathcal{M}$ a tangent vector $\mathbf{f}_{\mathbf{x}} = \mathbf{f}(\mathbf{x})$, i. e., an element of the tangent space $\mathsf{T}_{\mathbf{x}}\mathcal{M}$. The vector field is said to be *smooth* if it varies smoothly with $\mathbf{x}$.

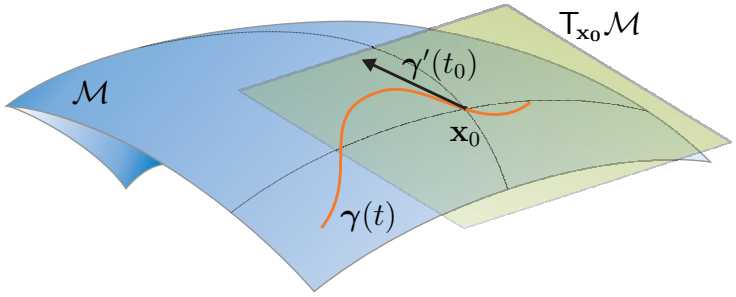

Figure 2.2: Tangent space and curve on manifold. The vector tangent to the curve $\boldsymbol{\gamma}(t)$ at $\mathbf{x}_0$ lives in the tangent space $\mathsf{T}_{\mathbf{x}_0}\mathcal{M}$. The curve $\boldsymbol{\gamma}(t)$ is an integral curve if there exists a vector field $\mathbf{f}$ on the manifold $\mathcal{M}$, such that $\boldsymbol{\gamma}'(t) = \mathbf{f}(\boldsymbol{\gamma}(t))$ is satisfied for all $t \in \mathcal{I}$.

Definition 2.4 (Integral curve)**.** An integral curve of $\mathbf{f}$ with initial condition $\mathbf{x}_0$ at t_0 is a differential map $\boldsymbol{\gamma} : \mathcal{I} \to \mathcal{M}$, such that $\mathcal{I}$ is an open interval containing t_0, $\boldsymbol{\gamma}(t_0) = \mathbf{x}_0$, and

$$\boldsymbol{\gamma}'(t) = \mathbf{f}(\boldsymbol{\gamma}(t)), \qquad \forall\, t \in \mathcal{I}.$$

We will assume—unless explicitly stated otherwise—that $t_0 = 0$, and $\mathcal{I} = [0, \infty[$. If the vector field $\mathbf{f}$ is locally Lipschitz, then there exists a unique *flow* for small times $t \in \mathcal{I}$.

Definition 2.5 (Flow of a vector field)**.** The flow of the vector field $\mathbf{f}$ is the collection of maps

$$\boldsymbol{\gamma}(t) : \mathcal{M} \to \mathcal{M},$$

such that $t \mapsto \boldsymbol{\gamma}_{\mathbf{x}}(t)$ is the integral curve of $\mathbf{f}$ with initial condition $\mathbf{x}$.

The flow describes, therefore, the set of solutions of the ordinary differential equation (ODE)

$$\dot{\mathbf{x}} = \mathbf{f}(\mathbf{x}), \qquad \mathbf{x} \in \mathcal{M}.$$

Definition 2.6 (Lie bracket in coordinates)**.** Let $\mathbf{x} = (x_1, \ldots, x_n)$ be a set of local coordinates for $\mathcal{M}$. The Lie bracket of two vector fields $\mathbf{f}$ and $\mathbf{g}$ is a third vector field defined as

$$[\mathbf{f}, \mathbf{g}] = \frac{\partial \mathbf{g}}{\partial \mathbf{x}}\mathbf{f} - \frac{\partial \mathbf{f}}{\partial \mathbf{x}}\mathbf{g}. \tag{2.1}$$

Geometrically speaking, the Lie bracket characterizes the rate of change of one vector field along the second vector field. The vector fields are said to commute if their Lie bracket vanishes. Figure 2.3 illustrates the Lie bracket in case of non-commuting vector fields.

Definition 2.7 (Smooth distribution)**.** A smooth distribution $\mathbb{D}$ on a manifold $\mathcal{M}$ is the assignment of a subspace of the tangent space to each point $\mathbf{x} \in \mathcal{M}$.

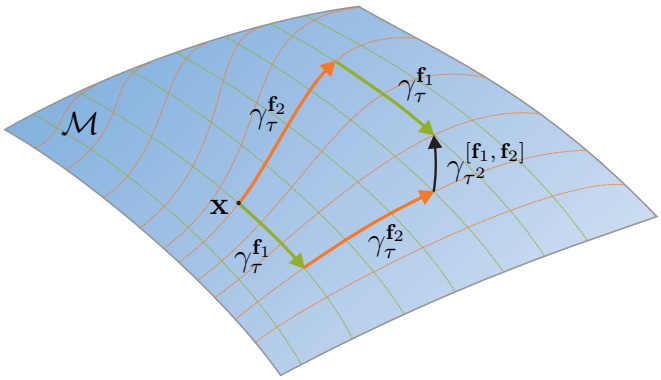

Figure 2.3: Lie bracket of two vector fields $\mathbf{f}_1$ and $\mathbf{f}_2$. Suppose that we start at $\mathbf{x}$ and move along the first vector field $\mathbf{f}_1$ for a given time τ; then move along $\mathbf{f}_2$ for the same time. Let us then repeat the procedure, this time inverting the order, i. e., first moving along $\mathbf{f}_2$, and then along $\mathbf{f}_1$. For non-commuting vector fields, $\gamma_\tau^{\mathbf{f}_1} \circ \gamma_\tau^{\mathbf{f}_2}(\mathbf{x}) \neq \gamma_\tau^{\mathbf{f}_2} \circ \gamma_\tau^{\mathbf{f}_1}(\mathbf{x})$ holds. Geometrically, the vector field $[\mathbf{f}, \mathbf{g}]$ represents this discrepancy.

A distribution $\mathbb{D}$ is said to be *involutive* if for any two vector fields $\mathbf{f}_1$ and $\mathbf{f}_2$ on $\mathcal{M}$ with values in $\mathbb{D}$, $[\mathbf{f}_1, \mathbf{f}_2]$ is also a vector field with values in $\mathbb{D}$. In other words, the distribution is involutive if it is *closed under brackets*[3] [63]

$$\mathbf{f}_1, \mathbf{f}_2 \in \mathbb{D} \Rightarrow [\mathbf{f}_1, \mathbf{f}_2] \in \mathbb{D}. \tag{2.2}$$

Given a set of vector fields $\mathbf{f}_1, \ldots, \mathbf{f}_k$ in $\mathcal{M}$, we denote the distribution given by their span as

$$\mathbb{D} = \operatorname{span}\{\mathbf{f}_1, \ldots, \mathbf{f}_k\}.$$

The distribution at any point $\mathbf{x} \in \mathcal{M}$ is given by $\mathbb{D}_\mathbf{x}$. A distribution is said to be regular if it is of constant rank: There exists a constant d, such that

$$\operatorname{rank}(\mathbb{D}_\mathbf{x}) = d, \qquad \forall\, \mathbf{x} \in \mathcal{M}.$$

Throughout the thesis, regularity of smooth distributions is assumed.

We are now ready to formulate one basic result of differential geometry that plays an important role in both nonlinear control theory and the theory of nonholonomic systems.

Theorem 2.1 (Frobenius)**.** *A regular smooth distribution* $\mathbb{D}$ *is integrable if and only if it is involutive.*

If the distribution $\mathbb{D}$ is the differential of a function $\phi(\mathbf{x})$ on $\mathcal{M}$, then, the distribution

[3] A distribution of commuting vector fields is always involutive.

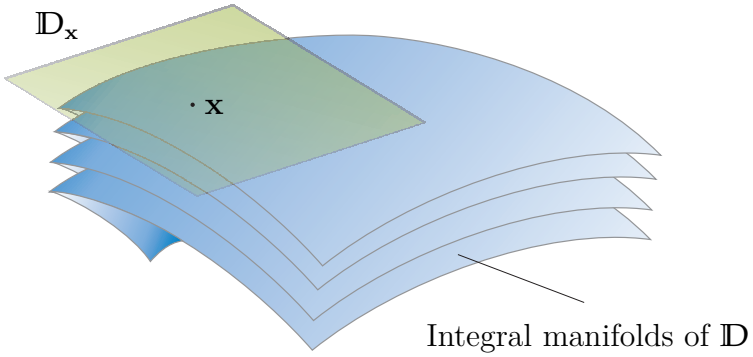

Figure 2.4: The integral manifolds $\mathcal{M}_\mathbb{D}$ of a distribution $\mathbb{D}$. The collection of all $\mathcal{M}_\mathbb{D}$ through all points of $\mathcal{M}$ forms a foliation.

is integrable and

$$\mathcal{M}_\mathbb{D} = \{\mathbf{x} \in \mathbb{R}^n |\ \boldsymbol{\phi}(\mathbf{x}) = c\} \tag{2.3}$$

represents an immersed manifold of $\mathcal{M}$ for any constant c. As a result, $\mathbb{D}$ is the tangent bundle of $\mathcal{M}_\mathbb{D}$. The collection of all integral manifolds (2.3) through all points of $\mathcal{M}$ forms a foliation (cf. Figure 2.4).

Example 2.1.1 (Foliations of $\mathbb{R}^2$). The set of lines parallel to the x-axis ($y = c$, for constant $c \in \mathbb{R}$) is a foliation of $\mathbb{R}^2$. The set of circles with radius $r = c$, for $c \in \mathbb{R}^+$ is a foliation of $\mathbb{R}^2 \backslash \{\mathbf{0}\}$. Each line (or circle) is itself an embedded manifold in $\mathbb{R}^2$. □

Definition 2.8 (Involutive closure)**.** The involutive closure $\overline{\mathbb{D}}$ of a smooth distribution $\mathbb{D}$ is the smallest involutive distribution containing $\mathbb{D}$.

The dual space to the tangent space $\mathsf{T}_\mathbf{x}\mathcal{M}$ is called cotangent space and is denoted by $\mathsf{T}^*_\mathbf{x}\mathcal{M}$. The cotangent space $\mathsf{T}^*_\mathbf{x}\mathcal{M}$ is the set of $\mathbb{R}$-valued real maps on $\mathsf{T}_\mathbf{x}\mathcal{M}$, i. e., the result of the action of the elements of $\mathsf{T}^*_\mathbf{x}\mathcal{M}$ on elements of $\mathsf{T}_\mathbf{x}\mathcal{M}$ lives in $\mathbb{R}$. In the geometric framework of mechanics, forces take values in the cotangent space $\mathsf{T}^*_\mathbf{x}\mathcal{M}$: Force times velocity equals to power, which is a scalar quantity. The cotangent bundle

$$\mathsf{T}^*\mathcal{M} = \bigsqcup_{\mathbf{x} \in \mathcal{M}} \mathsf{T}^*_\mathbf{x}\mathcal{M}$$

is the disjoint union of the cotangent spaces at all points $\mathbf{x} \in \mathcal{M}$.

2.1.2 Lagrangian mechanics

Lagrangian mechanics describes the time evolution of a Lagrangian system in its configuration space $\mathcal{Q}$. In a *simple* mechanical system, the configuration space $\mathcal{Q}$ is an

n-dimensional manifold. The tangent bundle $\mathsf{T}\mathcal{Q}$ represents the *velocity phase space*. The Lagrangian L is a smooth map $L\colon \mathsf{T}\mathcal{Q} \to \mathbb{R}$ and is defined as the kinetic minus the potential energy $L = T - V$ of the system. The motion of a forced mechanical system coincides with the Euler-Lagrange equations

$$\frac{\mathrm{d}}{\mathrm{d}t}\left(\frac{\partial L}{\partial \dot{\mathbf{q}}}\right)^{\mathrm{T}} - \left(\frac{\partial L}{\partial \mathbf{q}}\right)^{\mathrm{T}} = \mathbf{F}_{\mathrm{ext}}, \tag{2.4}$$

where $\mathbf{F}_{\mathrm{ext}}$ represents all non-potential forces, and includes—among others—the control input and friction terms. These equations can be derived from variational principles such as Hamilton's principle of least action or—in the presence of external forces—the Lagrange-d'Alembert principle. The reader is referred to standard textbooks, e. g., [12, 24, 42, 133, 198], for details. It is common to write (2.4) in matrix form as

$$\mathbf{M}\ddot{\mathbf{q}} + \mathbf{C}\dot{\mathbf{q}} + \nabla_{\mathbf{q}} V = \mathbf{F}_{\mathrm{ext}}, \tag{2.5}$$

where $\mathbf{M}(\mathbf{q})$ is the symmetric and positive definite inertia matrix. Moreover, $\mathbf{C}(\mathbf{q}, \dot{\mathbf{q}})$ is the matrix corresponding to the Coriolis and centrifugal forces, which elements c_{kj} are determined by the Christoffel symbols (of the first kind) corresponding to the matrix $\mathbf{M}(\mathbf{q})$. Consequently, the expression $\mathbf{C}(\mathbf{q}, \dot{\mathbf{q}})$ is solely defined by the inertia matrix[4]. The matrices $\mathbf{M}$ and $\mathbf{C}$ are not to be separated, since only together they have an actual meaning[5] (cf. [42]). However, it is of practical convenience to write them detached in the matrix form (2.5), as we will exploit the following property for control in later chapters.

Proposition 2.1. *For a given mechanical system with inertia matrix* $\mathbf{M}$ *it holds true that* $\dot{\mathbf{M}} = \mathbf{C} + \mathbf{C}^{\mathrm{T}}$*, and, as a consequence, the matrix* $(\dot{\mathbf{M}} - 2\mathbf{C})$ *is skew-symmetric.*

Proposition 2.1 is a standard result and its proof can be found, e. g., in [141, 198].

If the Lagrangian is independent from a configuration variable, say q_j, then we say that q_j is a cyclic variable and the Lagrangian exhibits a symmetry. Symmetries can be exploited to express the equations of motion in a reduced form, e. g., the Euler-Poincaré or Routh's equation [12, 133]. Cyclic variables also play an important role when defining *dynamic equilibria*, as we shall see in Chapter 7.

[4] The matrix $\mathbf{C}(\mathbf{q}, \dot{\mathbf{q}})$ may not be unique. However, we assume that it is defined by the Christoffel symbols (see [101, 198]) for the properties in Proposition 2.1 to hold.

[5] Together, the terms containing $\mathbf{M}$ and $\mathbf{C}$ are related to the covariant derivative in the Riemannian geometric point of view.

2.1.3 Hamiltonian mechanics

As stated before, Lagrangian mechanics describes the equations of motion of simple mechanical systems by means of the configuration manifold. Hamiltonian mechanics, as an equivalent formulation, describes the time evolution of the system in an even-dimensional manifold called the *phase space* [12]. This phase space in simple mechanical systems is nothing but the cotangent bundle $\mathsf{T}^*\mathcal{Q}$ of the configuration manifold, and its local coordinates are composed of the configuration $\mathbf{q}$ and the *canonical momenta* $\mathbf{p}$. The Hamiltonian representation of the dynamics can be directly derived from (2.4) and is given as [90]

$$\begin{bmatrix} \dot{\mathbf{q}} \\ \dot{\mathbf{p}} \end{bmatrix} = \begin{bmatrix} \mathbf{0} & \mathbf{I} \\ -\mathbf{I} & \mathbf{0} \end{bmatrix} \begin{bmatrix} \nabla_{\mathbf{q}} H \\ \nabla_{\mathbf{p}} H \end{bmatrix} + \begin{bmatrix} \mathbf{0} \\ \mathbf{F}_{\text{ext}} \end{bmatrix}, \tag{2.6}$$

where the Hamiltonian function H is the *Legendre transform* of the Lagrangian function, i. e.,

$$H(\mathbf{q}, \mathbf{p}) = \mathbf{p}^{\mathrm{T}} \dot{\mathbf{q}} - L(\mathbf{q}, \dot{\mathbf{q}}), \tag{2.7}$$

and the generalized momenta are defined as

$$\mathbf{p} = \left(\frac{\partial L}{\partial \dot{\mathbf{q}}} \right)^{\mathrm{T}} = \mathbf{M} \dot{\mathbf{q}}. \tag{2.8}$$

The Hamilton canonical equations (2.6) constitute a special case of the so-called port-Hamiltonian (pH) systems introduced in Section 2.3.2.

2.1.4 Nonholonomic constraints

A simple mechanical system as described above by the Euler-Lagrange or the Hamiltonian equations is called *holonomic*. Holonomic constraints restrict the possible configuration of a mechanical system. Examples are the restriction of a rigid body to have constant distances between two points, or the restriction of the motion thorough a joint between two links. The choice of so-called *generalized coordinates* allows us to locally describe the motion of holonomic systems with a minimum number of independent variables $\mathbf{q} \in \mathcal{Q}$. Nonholonomic systems represent a special class of mechanical systems, which does not fit in the latter description, and usually arise from constraints given at velocity level that cannot be integrated to the configuration level[6]. For an extensive discussion on the topic, the reader is referred to the textbooks by Bloch [24] and Holm

[6] Every constraint that is non-holonomic is nonholonomic. Nonholonomic constraints are therefore also given, for instance, by inequalities.

[91]. In this thesis, we will focus on the relevant type of non-integrable constraints linear in velocity, which can be written as

$$\mathbf{A}^{\mathrm{T}}(\mathbf{q})\dot{\mathbf{q}} = \mathbf{0}. \tag{2.9}$$

These constraints do not restrict the configuration manifold on which the dynamics evolve, but they restrict the admissible motion direction at a given point [24]. The nonholonomic constraints are given by a non-integrable, smooth distribution $\mathcal{D} \subset \mathsf{T}_{\mathbf{q}}\mathcal{Q}$ known as *constraint distribution*. In a mechanical system with k nonholonomic constraints, the admissible velocities at a configuration $\mathbf{q}$ are, thus, restricted to a $(n\text{–}k)$-dimensional subset ($\mathcal{D}_{\mathbf{q}} \cong \mathbb{R}^{n-k}$) of the tangent space $\mathsf{T}_{\mathbf{q}}\mathcal{Q}$.

Example 2.1.2 (Rolling Coin). The configuration space of a vertical coin rolling on a plain is given by $\mathcal{Q} = \mathbb{R}^2 \times \mathbb{S}^1 \times \mathbb{S}^1$. We can describe the configuration with (generalized) coordinates (x, y, θ, ϕ), where the coordinates of the contact point C are given by (x, y), and θ and ϕ denote the orientation and absolute rotation angle, respectively (cf. Figure 2.5). If r is the radius of the coin, the rolling-without-slipping constraints in the form (2.9) are given as

$$\begin{aligned} \dot{x} - r\dot{\phi}\cos\theta &= 0 \\ \dot{y} - r\dot{\phi}\sin\theta &= 0. \end{aligned}$$

These two constraints restrict the velocity space at any given point to a two-dimensional subspace $\mathcal{D}_{\mathbf{q}} \subset \mathsf{T}_{\mathbf{q}}\mathcal{Q}$. The configuration space, however, remains four-dimensional, as the distribution $\mathcal{D}$ is non-integrable. From our personal experience, *we know* that it is possible to reach any given configuration by rolling the coin back and forth and rotating it to change its orientation[7].

Let us consider the kinematic rolling coin, whose equations of motion are given as

$$\begin{bmatrix} \dot{x} \\ \dot{y} \\ \dot{\theta} \\ \dot{\phi} \end{bmatrix} = \begin{bmatrix} r\cos\theta \\ r\sin\theta \\ 0 \\ 1 \end{bmatrix} u_1 + \begin{bmatrix} 0 \\ 0 \\ 1 \\ 0 \end{bmatrix} u_2 = \mathbf{f}_1 u_1 + \mathbf{f}_2 u_2, \tag{2.10}$$

[7] Independently from the initial and desired configurations, we can *always* steer the coin towards the desired equilibrium $\boldsymbol{\xi}^*$: First, change the orientation to face the desired position $\mathbf{p}^* = [x^* \; y^*]^{\mathrm{T}}$ on the plane, then, move towards the desired position and once there, rotate to the desired orientation θ^*. If the rolling angle $\phi \neq \phi^*$, then make a circular loop of appropriate radius and come back. Theoretically, this can be done arbitrarily fast.

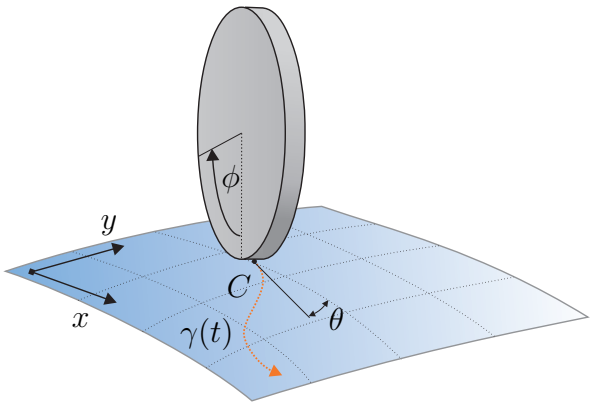

Figure 2.5: The vertical rolling coin.

where we assume to directly command angular velocities $u_1 = \dot{\phi}$ and $u_2 = \dot{\theta}$. The proof of controllability is provided by Chow's Theorem (cf. [85]), which basically states that if the involutive closure (the closure under Lie bracketing) of the constraint distribution $\mathcal{D}$ has full rank n, then the system is controllable. As the constraint distribution $\mathcal{D}$ of the rolling coin is not involutive, Lie bracketing the vector fields associated with the inputs u_1 and u_2 provides directions that are not contained in $\mathcal{D}$. Since the involutive closure

$$\bar{\mathcal{D}} = \operatorname{span}\{\mathbf{f}_1,\, \mathbf{f}_2,\, [\mathbf{f}_1, \mathbf{f}_2],\, [[\mathbf{f}_1, \mathbf{f}_2], \mathbf{f}_2]\} \tag{2.11}$$

has rank four $(= n)$, it is possible to steer the system in any direction by alternating u_1 and u_2, and, thus, to reach any $\mathbf{q} \in \mathcal{Q}$ arbitrarily fast. However, even though the system is controllable in the sense that there exist appropriate—usually discontinuous or time-varying—inputs that drive the system from any initial configuration $\mathbf{q}_0 \in \mathcal{Q}$ to any other configuration $\mathbf{q}_1 \in \mathcal{Q}$ in finite time, no continuous differentiable control law exists that makes $\mathbf{q}_1 \in \mathcal{Q}$ asymptotically stable [39]. In fact, a desired equilibrium cannot be asymptotically stabilized using continuous control laws [217]. □

The distinctive features of nonholonomic systems rely on the fact that the velocity space—which is given by the constraint distribution $\mathcal{D}$—is of a lower dimension than the configuration manifold $\mathcal{Q}$. This particular property has some important consequences for control as we will see in Chapter 6.

The dynamics of systems subject to nonholonomic constraints can be modeled using diverse methods in both Lagrangian and Hamiltonian representation [24, 27, 159, 185]. In particular, the Lagrange-d'Alembert equations [24]

$$\frac{\mathrm{d}}{\mathrm{d}t}\left(\frac{\partial L}{\partial \dot{\mathbf{q}}}\right)^{\mathrm{T}} - \left(\frac{\partial L}{\partial \mathbf{q}}\right)^{\mathrm{T}} = \mathbf{F}_{\mathrm{ext}} + \mathbf{A}\boldsymbol{\lambda} \tag{2.12}$$

have become prevalent for their similarity to the Euler-Lagrange equations (2.4). They differ in the constraints, which are adjoined to the system in (2.12) via Lagrange multipliers $\boldsymbol{\lambda} \in \mathbb{R}^k$ that represent the constraint forces. These forces oblige the system to satisfy the constraints, and are defined such that they do no work, e. i.,

$$W_{\text{constr}} = \int \dot{\mathbf{q}}^{\mathrm{T}} \mathbf{A} \boldsymbol{\lambda} \, \mathrm{d}t = \int \boldsymbol{\lambda}^{\mathrm{T}} \mathbf{A}^{\mathrm{T}} \dot{\mathbf{q}} \, \mathrm{d}t = 0. \tag{2.13}$$

The constraint forces can be eliminated *after* the evaluation of (2.12) by projecting the equations of motion on the admissible space. An analogous Hamiltonian formulation can be constructed via the Legendre transform as shown in [185]. The modeling and control of nonholonomic systems is the focus of Chapter 6.

2.2 Stability of nonlinear systems

This thesis is mainly devoted to the stabilization of mechanical systems. In this section, we formalize the notion of stability in the sense of Lyapunov, and introduce necessary conditions for stability of dynamical systems and equilibrium points. When speaking of asymptotic stability, we also want to know *how far* we can start from the equilibrium point and still converge towards it as time goes to infinity. It gives rise to the domain of attraction, or stability region, which, undoubtedly, also constitutes an important design objective in control. Finally, we introduce the notion of input-to-state stability, which naturally expands the concept of stability to systems with inputs. The material of this section is essentially borrowed from the books [102, 179, 189], where also the proofs of the theorems can be found.

2.2.1 Time-invariant systems

We consider nonlinear systems whose dynamics evolve on $\mathcal{X} \subset \mathbb{R}^n$

$$\dot{\mathbf{x}} = \mathbf{f}(\mathbf{x}), \qquad \mathbf{x}_0 = \mathbf{x}(t_0), \tag{2.14}$$

where the vector field $\mathbf{f} : \mathcal{X} \to \mathbb{R}^n$ is locally Lipschitz. Let $\boldsymbol{\gamma}(t, t_0, \mathbf{x}_0)$ be the solution of (2.14) that starts at initial state $\mathbf{x}_0$ at time t_0, and let it be defined for all $t \geq t_0$. Time-invariant systems satisfy $\boldsymbol{\gamma}(t+T, t_0+T, \mathbf{x}(t_0+T)) = \boldsymbol{\gamma}(t, t_0, \mathbf{x}(t_0))$ for any $T \in \mathbb{R}$. Without loss of generality, we, thus, set $t_0 = 0$, and write $\boldsymbol{\gamma}_{\mathbf{x}_0}(t)$ instead of $\boldsymbol{\gamma}(t, t_0, \mathbf{x}_0)$. A point $\mathbf{x}^*$ is an equilibrium point of (2.14) if $\mathbf{f}(\mathbf{x}^*) = \mathbf{0}$.

Definition 2.9 (Lyapunov stability)**.** The equilibrium point $\mathbf{x}^*$ of (2.14) is

- stable if, for each $\epsilon > 0$, there exists a $\delta = \delta(\epsilon) > 0$, such that

$$\|\mathbf{x}_0 - \mathbf{x}^*\| < \delta \implies \|\boldsymbol{\gamma}_{\mathbf{x}_0}(t) - \mathbf{x}^*\| < \epsilon, \qquad \forall\, t \geq 0, \tag{2.15}$$

  where $\|\cdot\|$ is the Euclidean norm.

- asymptotically stable if it is stable, and δ can be chosen such that

$$\|\mathbf{x}_0 - \mathbf{x}^*\| < \delta \implies \lim_{t\to\infty} \boldsymbol{\gamma}_{\mathbf{x}_0}(t) = \mathbf{x}^*. \tag{2.16}$$

- unstable if it is not stable.

If the equilibrium $\mathbf{x}^*$ is obvious from the context, we will say, with some abuse of terminology, that the system (2.14) is stable (unstable), meaning that $\mathbf{x}^*$ is a stable (unstable) equilibrium of (2.14).

Theorem 2.2 (Lyapunov's indirect method)**.** *Assume that $\mathbf{x}^*$ is an equilibrium point of the system (2.14), and the map $\mathbf{f} : \mathcal{X} \to \mathbb{R}^n$ is continuously differentiable in a neighborhood $\mathcal{B}$ of $\mathbf{x}^*$. The linearization*

$$\Delta\dot{\mathbf{x}} = \mathbf{A}\Delta\mathbf{x}, \qquad \mathbf{A} = \left.\frac{\partial \mathbf{f}}{\partial \mathbf{x}}\right|_{\mathbf{x}^*}, \tag{2.17}$$

where $\Delta\mathbf{x} = \mathbf{x} - \mathbf{x}^*$, locally approximates the behavior of (2.14). If $\Lambda(\mathbf{A})$, the set of eigenvalues of the matrix $\mathbf{A}$, strictly lies in the open left-half complex plane, then the equilibrium point $\mathbf{x}^*$ is asymptotically stable*. If at least one eigenvalue of $\mathbf{A}$ is strictly in the right-half complex plane, the equilibrium point $\mathbf{x}^*$ is* unstable*. In any other case, one cannot conclude stability or instability from the linearization (2.17).*

While the theorem provides information whether the equilibrium is stable or not, it does not reveal any data about the value of δ.

Definition 2.10 (Domain of attraction)**.** Suppose $\mathbf{x}^*$ is an asymptotically stable equilibrium point of the system (2.14). The domain of attraction (DA) of $\mathbf{x}^*$ is the set

$$\mathcal{A}(\mathbf{x}^*) = \left\{ \mathbf{x}_0 \in \mathcal{X} \mid \lim_{t\to\infty} \boldsymbol{\gamma}_{\mathbf{x}_0}(t) = \mathbf{x}^* \right\}. \tag{2.18}$$

The exact calculation of the DA, or stability region, of a particular asymptotically stable equilibrium $\mathbf{x}^*$ is generally a hard task and remains unsolved up to now. Nevertheless, the following theorem and corollary help to provide an estimation.

Theorem 2.3 (Lyapunov's direct method)**.** *Suppose there is a continuously differentiable function* $V : \mathcal{X} \to \mathbb{R}$ *satisfying*

$$V(\mathbf{x}) > V(\mathbf{x}^*), \qquad \forall\, \mathbf{x} \neq \mathbf{x}^* \tag{2.19}$$

in an open set $\mathcal{B}$ *containing* $\mathbf{x}^*$*. The equilibrium* $\mathbf{x}^*$ *is stable if*

$$\dot{V}(\mathbf{x}) = \frac{\partial V}{\partial \mathbf{x}} \mathbf{f}(\mathbf{x}) \leq 0, \qquad \forall\, \mathbf{x} \in \mathcal{B}. \tag{2.20}$$

The equilibrium $\mathbf{x}^*$ *is asymptotically stable if*

$$\dot{V}(\mathbf{x}) = \frac{\partial V}{\partial \mathbf{x}} \mathbf{f}(\mathbf{x}) < 0, \qquad \forall\, \mathbf{x} \in \mathcal{B} \setminus \{\mathbf{x}^*\}. \tag{2.21}$$

Corollary 2.1. *Let* V *be a function that satisfies (2.19) and (2.21). If*

$$\mathcal{S}_c = \{\mathbf{x} \in \mathcal{X} \mid V(\mathbf{x}) \leq c\} \tag{2.22}$$

is bounded and contained in $\mathcal{B}$*, then* $\mathcal{S}_c$ *is an estimate of the DA of* $\mathbf{x}^*$*, since all solutions of (2.14) starting in* $\mathcal{S}_c$ *remain in* $\mathcal{S}_c$*, and approach* $\mathbf{x}^*$ *as* $t \to \infty$*.*

A function $V(\mathbf{x})$ that satisfies the conditions of stability is called a *Lyapunov function*[8]. A big hurdle in using the above theorem lies in the difficulty of finding an appropriate Lyapunov function. A systematic procedure does not exist in general. If the system is mechanical, however, then its total energy is a good candidate. For that choice, $\dot{V}$ is only *negative semidefinite*, such that asymptotic stability cannot be shown from Theorem 2.3. The following invariance principle by LaSalle helps to conclude asymptotic stability nonetheless.

Theorem 2.4 (LaSalle's invariance principle)**.** *Let* $\mathcal{B} \subset \mathcal{X}$ *be a compact set that is positively invariant with respect to (2.14). Let* $V : \mathcal{X} \to \mathbb{R}$ *be a continuously differentiable function such that* $\dot{V} \leq 0$ *in* $\mathcal{B}$*. Let further* $\mathcal{S} = \{\mathbf{x} \in \mathcal{B} \mid \dot{V}(\mathbf{x}) = 0\}$*, and* $\mathcal{E}$ *be the largest invariant set in* $\mathcal{S}$*. Then every solution* $\boldsymbol{\gamma}_{\mathcal{B}}(t)$ *starting in* $\mathcal{B}$ *approaches* $\mathcal{E}$ *as* $t \to \infty$*.*

Corollary 2.2. *If* $\mathcal{E} = \mathbf{x}^*$*, then the equilibrium* $\mathbf{x}^*$ *is asymptotically stable.*

[8] The original definition assumes, without loss of generality, that $\mathbf{x}^* = \mathbf{0}$, and $V(\mathbf{0}) = 0$. The function $V(\mathbf{x})$ can be made positive definite by shifting $\mathbf{x}^*$ and $V(\mathbf{x}^*)$ to the origin.

The invariance principle expands Lyapunov's theory in three important ways. It relaxes the positive definiteness requirements of Lyapunov's original theory and gives an estimate of the domain of attraction that is not necessarily a level set of a Lyapunov function. The Lyapunov function, however, can be very useful for determining the invariant sets $\mathcal{B}$ and $\mathcal{S}$. The third, and most important extension for our purposes, is useful when dealing with nonholonomic constraints: The invariance principle can also be applied to asymptotically stable sets that are not just given by a single point.

2.2.2 Mechanical systems

Our interest is in showing asymptotic stability of the desired equilibrium point of a mechanical system. Let us apply the preceding results to a Lagrangian mechanical system

$$\mathbf{M}\ddot{\mathbf{q}} + \mathbf{C}\dot{\mathbf{q}} + \nabla_{\mathbf{q}} V = \mathbf{J}\dot{\mathbf{q}} - \mathbf{R}\dot{\mathbf{q}} \tag{2.23}$$

evolving on the smooth manifold $\mathcal{Q}$, where $\mathbf{J}(\mathbf{q}, \dot{\mathbf{q}}) = -\mathbf{J}^{\mathrm{T}}(\mathbf{q}, \dot{\mathbf{q}})$ is a skew-symmetric matrix linear in $\dot{\mathbf{q}}$ that corresponds to generalized gyroscopic forces, and $\mathbf{R}(\mathbf{q}) \geq \mathbf{0}$ is a symmetric matrix related to the dissipative forces in the system. To guarantee asymptotic stability, the positive semidefinite damping matrix needs to ensure *pervasive* damping.

Definition 2.11 (Pervasive damping [208])**.** The damping in a mechanical system is pervasive if every motion elicits energy dissipation.

As a consequence, if a system is pervasively damped, it cannot move indefinitely and will eventually come to rest. The following corollary is an immediate result from the preceding results.

Corollary 2.3. *The equilibrium $\mathbf{q}^*$ of the system (2.23) is locally stable if the potential energy V has a strict minimum at $\mathbf{q}^*$. The equilibrium is locally asymptotically stable if it is stable and the damping is pervasive.*

Proof. Since the inertia matrix $\mathbf{M}$ is positive definite, and $\mathbf{q}^* = \arg\min V$, the total mechanical energy

$$E = \frac{1}{2}\dot{\mathbf{q}}^{\mathrm{T}}\mathbf{M}\dot{\mathbf{q}} + V \tag{2.24}$$

qualifies as Lyapunov function in an open set $\mathcal{B} \subset \mathsf{T}\mathcal{Q}$ containing $(\mathbf{q}^*, \mathbf{0})$. The rate of

change of E along the trajectories of (2.23) is

$$\begin{aligned}\dot{E} &= \dot{\mathbf{q}}^{\mathrm{T}}\mathbf{M}\ddot{\mathbf{q}} + \frac{1}{2}\dot{\mathbf{q}}^{\mathrm{T}}\dot{\mathbf{M}}\dot{\mathbf{q}} + \nabla_{\mathbf{q}}^{\mathrm{T}}V\dot{\mathbf{q}} \\ &= \dot{\mathbf{q}}^{\mathrm{T}}(\mathbf{J}-\mathbf{R}-\mathbf{C})\dot{\mathbf{q}} - \dot{\mathbf{q}}^{\mathrm{T}}\nabla_{\mathbf{q}}V + \frac{1}{2}\dot{\mathbf{q}}^{\mathrm{T}}\dot{\mathbf{M}}\dot{\mathbf{q}} + \nabla_{\mathbf{q}}^{\mathrm{T}}V\dot{\mathbf{q}} \\ &= -\dot{\mathbf{q}}^{\mathrm{T}}\mathbf{R}\dot{\mathbf{q}},\end{aligned}$$

where $\dot{\mathbf{M}} = \mathbf{C} + \mathbf{C}^{\mathrm{T}}$ from Proposition 2.1 has been used. Stability of the equilibrium follows from Theorem 2.3, since $\mathbf{R} \geq \mathbf{0}$. If the damping is pervasive, the largest invariant set under the system dynamics (2.23) contained in

$$\left\{(\mathbf{q}, \dot{\mathbf{q}}) \in \mathsf{T}\mathcal{Q} \mid \dot{E} = 0\right\} \tag{2.25}$$

is given by $\nabla_{\mathbf{q}}V = \mathbf{0}$, and equals the equilibrium $\mathbf{q}^*$, since V has a strict minimum at $\mathbf{q}^*$. Asymptotic stability follows from LaSalle's invariance principle. An estimate of the domain of attraction is given by the largest bounded level set of E contained in $\mathcal{B}$. ■

2.2.3 Time-varying systems

Consider time-varying systems whose dynamics evolve on $\mathcal{X} \subset \mathbb{R}^n$

$$\dot{\mathbf{x}} = \mathbf{f}(t, \mathbf{x}), \qquad \mathbf{x}_0 = \mathbf{x}(t_0), \tag{2.26}$$

where the vector field $\mathbf{f} : [t_0, \infty[\times \mathcal{X} \to \mathbb{R}^n$ is locally Lipschitz in $\mathbf{x}$ and piecewise continuous in t. Let $\boldsymbol{\gamma}_{\mathbf{x}_0}^{t_0}(t) = \boldsymbol{\gamma}(t, \mathbf{x}_0, t_0)$ be the solution of (2.26) that starts at initial state $\mathbf{x}_0$ at time t_0, and let it be defined for all $t \geq t_0$. A point $\mathbf{x}^*$ is an equilibrium point of (2.26) at $t = t_0$ if, for all $t \geq t_0$, it holds that $\mathbf{f}(t, \mathbf{x}^*) = \mathbf{0}$. Since the conditions for stability of time-varying systems may also depend on the initial time t_0, we need to refine Definition 2.9:

Definition 2.12 (Lyapunov stability for non-autonomous systems)**.** The equilibrium point $\mathbf{x}^*$ of (2.26) is

- stable if, for each $\epsilon > 0$, there exists a $\delta = \delta(\epsilon, t_0) > 0$ such that

$$\|\mathbf{x}_0 - \mathbf{x}^*\| < \delta \implies \|\boldsymbol{\gamma}_{\mathbf{x}_0}^{t_0}(t) - \mathbf{x}^*\| < \epsilon, \qquad \forall\, t \geq t_0 \geq 0. \tag{2.27}$$

- uniformly stable if, for each $\epsilon > 0$, there exists a $\delta = \delta(\epsilon) > 0$, independent of t_0, such that (2.27) is satisfied.

- asymptotically stable if it is stable, and there is a positive constant $c = c(t_0)$ such that

$$\|\mathbf{x}_0 - \mathbf{x}^*\| < c \implies \lim_{t\to\infty} \boldsymbol{\gamma}_{\mathbf{x}_0}^{t_0}(t) = \mathbf{x}^*. \tag{2.28}$$

- uniformly asymptotically stable if it is uniformly stable, and there is a positive constant $c > 0$, independent of t_0, such that, for each $\eta > 0$, there is $T = T(\eta) > 0$ such that

$$\|\mathbf{x}_0 - \mathbf{x}^*\| < c \implies \|\boldsymbol{\gamma}_{\mathbf{x}_0}^{t_0}(t) - \mathbf{x}^*\| < \eta, \qquad \forall\, t \geq t_0 + T(\eta). \tag{2.29}$$

Definition 2.13 (Domain of attraction for nonautonomous systems)**.** Suppose that $\mathbf{x}^*$ is a uniformly asymptotically stable equilibrium point of the system (2.26). Its DA is the set

$$\mathcal{A}^{t_0}(\mathbf{x}^*) = \left\{ \mathbf{x}_0 \in \mathcal{X} \mid \lim_{t\to\infty} \boldsymbol{\gamma}_{\mathbf{x}_0}^{t_0}(t) = \mathbf{x}^* \right\}. \tag{2.30}$$

Note that in this definition, the DA depends on a particular initial time t_0. Lyapunov theory can as well be extended to this time-variant case. We can, accordingly, give an estimate of the DA of an equilibrium of (2.26) by means of a Lyapunov function.

Theorem 2.5. *Let $\mathbf{x}^*$ be an equilibrium point of (2.26). Let $\mathcal{B} \subset \mathcal{X}$ be a neighborhood of $\mathbf{x}^*$, and let $V\colon [t_0, \infty[\times \mathcal{X} \to \mathbb{R}$, $V(t, \mathbf{x}^*) = 0$ be a continuously differentiable function such that, for all $t \geq t_0$, and all $\mathbf{x} \in \mathcal{B}$, the inequalities*

$$W_1(\mathbf{x}) \leq V(t, \mathbf{x}) \leq W_2(\mathbf{x}) \tag{2.31}$$

$$\dot{V}(t, \mathbf{x}) = \frac{\partial V}{\partial t} + \frac{\partial V}{\partial \mathbf{x}} \mathbf{f}(t, \mathbf{x}) \leq -W_3(\mathbf{x}) \tag{2.32}$$

hold for continuous functions $W_i\colon \mathcal{X} \to \mathbb{R}$, $i = 1, 2, 3$ satisfying

$$W_i(\mathbf{x}^*) = 0, \quad W_i(\mathbf{x}) > W_i(\mathbf{x}^*), \qquad \forall\, \mathbf{x} \in \mathcal{B}. \tag{2.33}$$

Then $\mathbf{x}^*$ is uniformly asymptotically stable.

Corollary 2.4. *If $c > 0$ is such that the sets*

$$\mathcal{S}_c^{W_1} = \{\mathbf{x} \in \mathcal{X} \mid W_1(\mathbf{x}) \leq c\} \tag{2.34}$$

$$\mathcal{S}_c^{W_2} = \{\mathbf{x} \in \mathcal{X} \mid W_2(\mathbf{x}) \leq c\} \tag{2.35}$$

are bounded and contained in $\mathcal{B}$, then $\mathcal{S}_c^{W_2}$ is an estimate of the DA of $\mathbf{x}^*$, since all solutions of (2.26) starting in $\mathcal{S}_c^{W_2}$ remain in $\mathcal{S}_c^{W_1}$ and approach $\mathbf{x}^*$ as $t \to \infty$.

Note that we ask for a *positive definite* function $W_3(\mathbf{x})$ in the above theorem. Although there is no unifying formulation for the asymptotic stability of general non-autonomous systems when $\dot{V}(t,\mathbf{x})$ is only negative semidefinite, some extensions of the invariance principle to time-varying systems can be consulted in [102] and the references therein. The reader is also referred to [18], where the author considers time-varying systems of the form (2.26) and Lyapunov functions $V(\mathbf{x})$ independent from time for the formulation of the invariance principle. The celebrated Lemma of Barbalat in its "*Lyapunov-like*" version can also help to conclude asymptotic stability from $\dot{V}(t,\mathbf{x})\leq 0$ (see Section 4.5 in [189] for a short discussion and examples).

2.2.4 Input-to-state stability

The notion of input-to-state stability (ISS) was introduced by Sontag in [190], and is essentially the natural extension of the Lyapunov stability to systems with input

$$\dot{\mathbf{x}} = \mathbf{f}(t,\mathbf{x},\mathbf{u}), \qquad \mathbf{x}_0 = \mathbf{x}(t_0), \quad t_0 = 0 \tag{2.36}$$

where $\mathbf{u}\in\mathcal{U}\subset\mathbb{R}^m$. The vector field $\mathbf{f}:\mathbb{R}_0^+\mathcal{X}\times\mathcal{U}\rightarrow\mathbb{R}^n$ is piecewise continuous in t, and locally Lipschitz in $\mathbf{x}$ and $\mathbf{u}$. Suppose that the unforced system has an equilibrium point at $\mathbf{x}^*$

$$\mathbf{f}(t,\mathbf{x}^*,\mathbf{0}) = \mathbf{0}. \tag{2.37}$$

The stability of the unforced system can be nicely tackled by Lyapunov's stability theory. For some *bounded* input disturbance $\mathbf{u}\neq\mathbf{0}$, the ISS property provides a framework in which to formulate the notions of stability for the system (2.36). Basically, the question is whether the trajectories of (2.36) remain bounded under the effect of $\mathbf{u}$ (*bounded-inputs bounded-states*). Since its origins in the late eighties, the ISS property has constituted a central concept for the analysis of nonlinear systems. Let us first introduce the following comparison functions (cf. [81])

- A function $\alpha:\mathbb{R}_0^+\rightarrow\mathbb{R}_0^+$ belongs to class $\mathcal{K}$ ($\alpha\in\mathcal{K}$) if it is continuous, strictly increasing, and satisfies $\alpha(0)=0$. A function $\bar{\alpha}\in\mathcal{K}$ is in $\mathcal{K}_\infty$ if $\bar{\alpha}(t)\rightarrow\infty$ as $t\rightarrow\infty$.

- A function $\alpha:\mathbb{R}_0^+\rightarrow\mathbb{R}_0^+$ belongs to class $\mathcal{L}$ ($\alpha\in\mathcal{L}$) if it is continuous, strictly decreasing, and satisfies $\lim_{t\rightarrow\infty}\beta(t)=0$.

- A function $\alpha:\mathbb{R}_0^+\times\mathbb{R}_0^+\rightarrow\mathbb{R}_0^+$ belongs to class $\mathcal{KL}$ ($\alpha\in\mathcal{KL}$) if it is of class $\mathcal{K}$ on the first argument and of class $\mathcal{L}$ on the second argument.

Definition 2.14 (Input-to-state stability [102, 191])**.** Let $\mathcal{B}$ be an open set of $\mathcal{X}$ containing $\mathbf{x}^*$. The system (2.36) is said to be *locally* ISS if there exist functions $\gamma \in \mathcal{K}$ and $\beta \in \mathcal{KL}$, and constants $k_1, k_2 > 0$ such that

$$\|\mathbf{x}(t)\| \leq \beta(\|\mathbf{x}_0\|, t) + \gamma(\|\mathbf{u}\|_{\mathcal{L}_\infty}) \tag{2.38}$$

holds for all $\mathbf{x}_0 \in \mathcal{B}$ and $\mathbf{u} \in \mathcal{U}$ satisfying $\|\mathbf{x}_0\| < k_1$, and $\|\mathbf{u}\|_{\mathcal{L}_\infty} < k_2$ [9]. It is said to be globally ISS (or simply ISS) if $\mathcal{B} = \mathcal{X}$, $\gamma \in \mathcal{K}_\infty$, and (2.38) is satisfied for any bounded input ($k_2 = \infty$).

A further characterization of ISS can be given in terms of a Lyapunov-like function.

Definition 2.15 (ISS-Lyapunov function)**.** Let $\mathcal{U}_\mathcal{B} = \{\mathbf{u} \in \mathcal{U} \mid \|\mathbf{u}\| \leq \gamma^{-1} \circ \alpha(\|\mathbf{x}\|)\}$. A continuously differentiable function $V : \mathbb{R}_0^+ \times \mathcal{X} \to \mathbb{R}$ is called a local ISS-Lyapunov function if it is positive definite in $\mathcal{B}$ and its time derivative satisfies

$$\dot{V}(\mathbf{x}, \mathbf{u}) = \frac{\partial V}{\partial t} + \frac{\partial V}{\partial \mathbf{x}} \mathbf{f}(t, \mathbf{x}, \mathbf{u}) \leq -\alpha(\|\mathbf{x}\|) + \gamma(\|\mathbf{u}\|), \qquad \forall\, \mathbf{x} \in \mathcal{B},\ \mathbf{u} \in \mathcal{U}_\mathcal{B}, \tag{2.39}$$

for some functions $\alpha, \gamma \in \mathcal{K}$. The function V is called ISS-Lyapunov function if it is radially unbounded, $\mathcal{B} = \mathcal{X}$, and $\alpha \in \mathcal{K}_\infty$.

Theorem 2.6 ([192])**.** *A system is ISS if and only if it admits a smooth ISS-Lyapunov function $V(t, \mathbf{x})$.*

Globally speaking, ISS is a very strong condition and does not always hold for mechanical systems that are globally asymptotically stable (GAS) in the absence of inputs. See, e. g., the closed-loop system arising from a passivity-based tracking design for a mechanical system, where the "input" corresponds to a time-varying desired state, or to measurement noise [9]. This can be intuitively explained by some nonlinear resonance produced by bounded inputs. Nevertheless, GAS (closed-loop) mechanical systems do present some boundedness in the state trajectories with respect to certain inputs (measurement noise or time-varying desired state). To capture this property, the weaker form of *integral* input-to-state stability has been proposed, which relates the amplitude of the state to the *energy* of the input [9]. However, since our results hold only locally, we will restrict the analysis to the local version of ISS, which has been proven to be equivalent to the (local) asymptotic stability of the uncontrolled system (2.36) for $\mathbf{u} = \mathbf{0}$. Local input-to-state stability is, therefore, only of interest for robustness analysis if both the domain of attraction and the magnitude of the tolerated inputs can

[9] $\|\mathbf{u}\|_{\mathcal{L}_\infty}$ represents the sup norm of the input $\mathbf{u}$, i. e., $\|\mathbf{u}(t)\|_{\mathcal{L}_\infty} = \sup_{t \geq 0}(\|\mathbf{u}(t)\|)$.

be estimated. For further details on the ISS property and its variations, the reader is referred to [45, 191].

2.3 Passivity-based control and energy shaping

The term passivity-based control (PBC) was first introduced in the context of motion control of mechanical systems in [157]. Energy shaping is a PBC method used for the stabilization of mechanical systems, which has its roots in the work of Takegaki and Arimoto [11] long before it was related to passivity. The goal of energy shaping is to virtually modify the energy of the system, composed of kinetic and potential energy, in order to stabilize a desired equilibrium point.

In this thesis we focus our attention on two widespread energy shaping control methods for mechanical systems: the parametric form of *interconnection and damping assignment*, and the method of *Controlled Lagrangians*. Both methods have been proven to be equivalent formulations of the stabilization problem in [22, 47].

2.3.1 Dissipativity, passivity, and stability

This section revisits the notions of *dissipativity* and *passivity*, and how they are used in control theory for stabilization. Readers interested in a broader overview on the topic are referred to the books [153, 181, 187], and the papers [44, 151, 154]. Passivity is a structural property that stems from the fact that energy is dissipated in physical systems. It essentially states that the energy of the system cannot increase more than the amount of energy that flows into it. Mechanical systems naturally satisfy the energy conservation[10]

$$\text{Stored energy} = \text{Supplied energy} - \text{Dissipation},$$

and are, therefore, passive as we shall see later in the next section. The concept of passivity was long used in the context of network systems but it was not until the early 70's that Willems generalized it, and put it in a control theoretic framework [207]. Let us consider input affine systems of the form

$$\dot{\mathbf{x}} = \mathbf{f}(\mathbf{x}) + \mathbf{G}(\mathbf{x})\mathbf{u}, \tag{2.40a}$$

$$\mathbf{y} = \mathbf{h}(\mathbf{x}), \tag{2.40b}$$

[10] Dissipation is defined as a positive quantity.

where $\mathbf{x} \in \mathcal{X} \subseteq \mathbb{R}^n$ is the state, $\mathbf{u} \in \mathcal{U} \subseteq \mathbb{R}^m$ is the input, and $\mathbf{y} \in \mathcal{Y} \subseteq \mathbb{R}^m$ represents the output.

Definition 2.16 (Dissipative system)**.** The System (2.40) is called dissipative if it satisfies for all initial conditions $\mathbf{x}_0$, and all inputs $\mathbf{u}(t)$, $t \geq 0$ the inequality

$$S(\mathbf{x}(t)) - S(\mathbf{x}_0) \leq \int_0^t w(\mathbf{y}(\tau), \mathbf{u}(\tau))\, \mathrm{d}\tau \tag{2.41}$$

for a positive semidefinite storage function $S(\mathbf{x})$, and supply rate $w(\mathbf{y}(t), \mathbf{u}(t))$.

Definition 2.17 (Passive system)**.** The System (2.40) is passive if it is dissipative with supply rate $w = \mathbf{y}^{\mathrm{T}}\mathbf{u}$.

We assume $S(\mathbf{x})$ to be continuously differentiable, such that the passivity inequality

$$\dot{S}(\mathbf{x}) \leq \mathbf{y}^{\mathrm{T}}\mathbf{u} \tag{2.42}$$

holds. If $\mathbf{u} = \mathbf{0}$, then $\dot{S}(\mathbf{x}) \leq 0$ from (2.42), and $S(\mathbf{x})$ qualifies as a Lyapunov function if it is positive definite (cf. [88]). Passivity is, thus, a very attractive property of dynamical systems, which gave rise to the PBC methods, whose aim is to render the closed-loop system passive. Despite the term *passivity-based control* being first introduced by Ortega and Spong in 1989 [157], the idea of PBC for mechanical systems dates back to Takegaki and Arimoto, who in 1981 proposed the now well-known potential energy shaping and damping injection technique to solve set point regulation problems for fully actuated systems [11]. As of today, the PBC approach for mechanical systems aims at keeping the structure of the closed-loop system mechanical, and, thus, passive[11], but shaping its energy such that it exhibits a local minimum at the desired equilibrium point. A key advantage of passivity-based methods relies on passivity as a structural property, and as such, no exact knowledge of the system parameters is required.

2.3.2 Port-Hamiltonian systems

Port-Hamiltonian (pH) systems describe a class of intrinsically passive dynamical systems. Viewed as the generalization of the Hamiltonian representation of mechanical systems presented in Section 2.1.3, pH systems naturally arise from a *port-based* modeling of lumped-parameter physical systems and constitute an important class throughout this thesis. This section introduces pH systems and presents some of their key properties. For more detailed information, we recommend the textbook [181], and the survey

[11] Note that a realistic mechanical energy is always bounded from below.

paper [184], which gives a very nice introduction to the topic from a rather geometric point of view. For the use of pH systems as a unifying framework for the port-based modeling and control of complex physical systems, we refer to the more recent book [59], and to the papers [182, 183]. We consider port-Hamiltonian systems whose dynamics evolve on $\mathcal{X} \subset \mathbb{R}^n$, and which are of the form

$$\dot{\mathbf{x}} = (\mathbf{J}(\mathbf{x}) - \mathbf{R}(\mathbf{x}))\, \nabla_{\mathbf{x}} H(\mathbf{x}) + \mathbf{G}(\mathbf{x})\mathbf{u} \tag{2.43a}$$

$$\mathbf{y} = \mathbf{G}^{\mathrm{T}}(\mathbf{x}) \nabla_{\mathbf{x}} H(\mathbf{x}), \tag{2.43b}$$

where the continuously differentiable Hamiltonian function $H : \mathcal{X} \to \mathbb{R}$ is bounded from below, and represents the stored energy. Further, $\mathbf{J} : \mathcal{X} \to \mathbb{R}^{n \times n}$ is a skew-symmetric matrix representing the lossless energy exchange in the system, and $\mathbf{R} : \mathcal{X} \to \mathbb{R}^{n \times n}$ is a symmetric matrix, which characterizes the energy dissipation, and is positive semidefinite for physical systems. The input $\mathbf{u} \in \mathcal{U} \subseteq \mathbb{R}^m$ and the output $\mathbf{y} \in \mathcal{Y} \subseteq \mathbb{R}^m$ are *conjugate variables*, i. e., their product gives a power quantity.

The system (2.43) is passive with storage function $H(\mathbf{x})$, as the passivity inequality

$$\dot{H} = -\nabla_{\mathbf{x}}^{\mathrm{T}} H \mathbf{R} \nabla_{\mathbf{x}} H + \underbrace{\nabla_{\mathbf{x}}^{\mathrm{T}} H \mathbf{G}}_{\mathbf{y}^{\mathrm{T}}} \mathbf{u} \leq \mathbf{y}^{\mathrm{T}} \mathbf{u} \tag{2.44}$$

holds, since $\mathbf{J}$ is skew-symmetric, and $\mathbf{R}$ is positive semidefinite. If $\mathbf{u} = \mathbf{0}$, and

$$\mathbf{x}^* = \arg\min H, \tag{2.45}$$

then H is a Lyapunov function, and stability of the equilibrium point $\mathbf{x}^*$ follows from Theorem 2.3. Adding damping of the form $\mathbf{u} = -\boldsymbol{\phi}(\mathbf{y})$ for a function $\boldsymbol{\phi}(\mathbf{y})$ satisfying $\boldsymbol{\phi}(\mathbf{y})\mathbf{y} > 0$ for all $\mathbf{y} \neq \mathbf{0}$, guarantees asymptotic stability if the output $\mathbf{y}$ is zero-state detectable.

2.3.3 Interconnection and damping assignment

The passivity-based control method *interconnection and damping assignment* (IDA) exploits the aforementioned properties of pH systems for the stabilization of dynamical systems. The approach was first presented in [156] for pH systems and was generalized for input affine systems in [151]. The application to underactuated mechanical systems in Hamiltonian representation was introduced by Ortega et al. in [158]. The following is a short exposition of the method; for details and additional material, the reader is referred to the survey paper [151] and the references within. Consider the input affine

system

$$\dot{\mathbf{x}} = \mathbf{f}(\mathbf{x}) + \mathbf{G}(\mathbf{x})\mathbf{u}, \tag{2.46}$$

with drift vector field $\mathbf{f}$, and input matrix $\mathbf{G}$. The idea of IDA is to find a static state feedback $\mathbf{u} = \mathbf{u}(\mathbf{x})$, such that the closed-loop system is port-Hamiltonian

$$\mathbf{f}(\mathbf{x}) + \mathbf{G}(\mathbf{x})\mathbf{u} \overset{!}{=} (\mathbf{J}_\mathrm{d}(\mathbf{x}) - \mathbf{R}_\mathrm{d}(\mathbf{x}))\,\nabla_\mathbf{x} H_\mathrm{d}(\mathbf{x}). \tag{2.47}$$

To ensure (asymptotic) stability of the desired equilibrium $\mathbf{x}^*$ according to Theorem 2.3, we additionally impose the following definiteness constraints

1. The damping matrix $\mathbf{R}_\mathrm{d}$ is positive (semi-) definite
2. The desired Hamiltonian function H_d has a strict minimum at $\mathbf{x}^*$

We will often make use of following fundamental result (Lemma 2 in [154]):

Lemma 2.1. *Let* $\mathbf{G}$ *be a matrix-valued map* $\mathbf{G}\colon \mathcal{X} \to \mathbb{R}^{n\times m}$ *of constant rank* $\operatorname{rank}(\mathbf{G}) = m < n$. *Define* $\mathbf{G}_\perp \in \mathbb{R}^{(n-m)\times n}$ *as the full rank left annihilator of* $\mathbf{G}$, *i. e.,* $\mathbf{G}_\perp \mathbf{G} = \mathbf{0}$. *For any* $\mathbf{f} \in \mathbb{R}^n$, $\mathbf{u} \in \mathcal{U} \subseteq \mathbb{R}^m$

$$\mathbf{f} + \mathbf{G}\mathbf{u} = \mathbf{0} \quad \Leftrightarrow \quad \begin{cases} \mathbf{0} = \mathbf{G}_\perp \mathbf{f} \\ \mathbf{u} = -(\mathbf{G}^\mathrm{T}\mathbf{G})^{-1}\mathbf{G}^\mathrm{T}\mathbf{f} \end{cases} \tag{2.48}$$

Proof. The matrix

$$\begin{bmatrix} \mathbf{G}_\perp \\ \mathbf{G}^\mathrm{T} \end{bmatrix}$$

is full rank. Therefore

$$\mathbf{f} + \mathbf{G}\mathbf{u} = \mathbf{0} \quad \Leftrightarrow \quad \begin{bmatrix} \mathbf{G}_\perp \\ \mathbf{G}^\mathrm{T} \end{bmatrix} (\mathbf{f} + \mathbf{G}\mathbf{u}) = \mathbf{0}.$$

The proof is concluded using the annihilating property of $\mathbf{G}_\perp$, and noting that the matrix $\mathbf{G}^\mathrm{T}\mathbf{G}$ is invertible. ∎

According to Lemma 2.1, (2.47) is equivalent to

$$\mathbf{u} = (\mathbf{G}^\mathrm{T}\mathbf{G})^{-1}\mathbf{G}^\mathrm{T}\Big((\mathbf{J}_\mathrm{d} - \mathbf{R}_\mathrm{d})\,\nabla_\mathbf{x} H_\mathrm{d} - \mathbf{f}\Big), \tag{2.49a}$$

$$\mathbf{0} = \mathbf{G}_\perp\Big((\mathbf{J}_\mathrm{d} - \mathbf{R}_\mathrm{d})\,\nabla_\mathbf{x} H_\mathrm{d} - \mathbf{f}\Big). \tag{2.49b}$$

Therefore, the matching problem is solved if and only if the projected matching equation (2.49b) is satisfied, and the control law is chosen according to (2.49a). For underactuated systems, some restrictions on the design matrices $\mathbf{J}_\mathrm{d}$ and $\mathbf{R}_\mathrm{d}$, and/or on the closed-loop energy function H_d arise from the projected matching equation, since $\mathbf{G}_\perp \neq \mathbf{0}$. Finding a solution for (2.49b) can be very challenging, constituting therefore the major obstacle for the control design via IDA.

There are, roughly speaking, three ways to proceed for the solution of the matching problem (2.47). In the most common approach, known as the *non-parametrized* IDA, the idea is to fix the *desired* interconnection and dissipation matrices $\mathbf{J}_\mathrm{d}(\mathbf{x}) = -\mathbf{J}_\mathrm{d}^\mathrm{T}(\mathbf{x})$ and $\mathbf{R}_\mathrm{d}(\mathbf{x}) = \mathbf{R}_\mathrm{d}^\mathrm{T}(\mathbf{x}) \geq \mathbf{0}$—hence the name. The admissible energy functions $H_\mathrm{d}(\mathbf{x})$ are then described by the set of *partial differential equations* (PDEs) given by (2.49b). The energy function $H_\mathrm{d}(\mathbf{x})$ is chosen such that it has a strict minimum at the desired equilibrium $\mathbf{x}^*$.

In the *algebraic* IDA approach, one fixes the desired energy function[12]. The projected matching equations (2.49b) become algebraic equations in $\mathbf{J}_\mathrm{d}(\mathbf{x})$ and $\mathbf{R}_\mathrm{d}(\mathbf{x})$. The difficulty of the latter lies in choosing $H_\mathrm{d}(\mathbf{x})$ such that $\mathbf{R}_\mathrm{d}(\mathbf{x}) \geq \mathbf{0}$ is a possible solution of the matching problem.

The third approach is called *parametrized* IDA and is widely used for the stabilization of mechanical systems [158]. In this particular case, the structure of the closed-loop Hamiltonian function is physically motivated and chosen to be—in the context of mechanical systems—the sum of kinetic and potential energy. This choice results in a different (and simpler) set of PDEs (2.49b), but it also imposes some constraints on $\mathbf{J}_\mathrm{d}(\mathbf{x})$ and $\mathbf{R}_\mathrm{d}(\mathbf{x})$, as we shall see in the following. We consider (damped) mechanical systems with input in Hamiltonian representation

$$\begin{bmatrix} \dot{\mathbf{q}} \\ \dot{\mathbf{p}} \end{bmatrix} = \begin{bmatrix} \mathbf{0} & \mathbf{I} \\ -\mathbf{I} & -\mathbf{R} \end{bmatrix} \begin{bmatrix} \nabla_\mathbf{q} H \\ \nabla_\mathbf{p} H \end{bmatrix} + \begin{bmatrix} \mathbf{0} \\ \mathbf{G} \end{bmatrix} \mathbf{u}. \tag{2.50}$$

The dissipation matrix $\mathbf{R} = \mathbf{R}^\mathrm{T} \geq \mathbf{0}$ is assumed to satisfy $\mathbf{G}_\perp \mathbf{R} = \mathbf{0}$, which means that there is no physical dissipation in unactuated coordinates. We also assume—for obvious reasons—that the equilibrium to be stabilized is admissible.

Definition 2.18 (Admissible equilibrium)**.** An equilibrium $(\mathbf{q}^*, \mathbf{0})$ (or simply $\mathbf{q}^*$) of a mechanical system is called admissible if $\mathbf{G}_\perp \nabla_\mathbf{q} V \,|_{\mathbf{q}^*} = \mathbf{0}$.

[12] The name IDA here is somehow misleading.

Since the structure of the desired closed-loop energy is chosen to be of mechanical form

$$H_\mathrm{d} = \frac{1}{2}\,\mathbf{p}^\mathrm{T}\mathbf{M}_\mathrm{d}^{-1}\mathbf{p} + V_\mathrm{d} \tag{2.51}$$

for this particular case, the matching equation (2.47) becomes

$$\begin{bmatrix} \mathbf{0} & \mathbf{I} \\ -\mathbf{I} & -\mathbf{R} \end{bmatrix} \begin{bmatrix} \nabla_\mathbf{q} H \\ \nabla_\mathbf{p} H \end{bmatrix} + \begin{bmatrix} \mathbf{0} \\ \mathbf{G} \end{bmatrix} \mathbf{u} \overset{!}{=} \begin{bmatrix} \mathbf{0} & \mathbf{J}_1 \\ -\mathbf{J}_1^\mathrm{T} & \mathbf{J}_2 - \mathbf{R}_2 \end{bmatrix} \begin{bmatrix} \nabla_\mathbf{q} H_\mathrm{d} \\ \nabla_\mathbf{p} H_\mathrm{d} \end{bmatrix}. \tag{2.52}$$

It is necessary that $\mathbf{J}_1 = \mathbf{M}^{-1}\mathbf{M}_\mathrm{d}$, for the relation $\dot{\mathbf{q}} = \mathbf{M}^{-1}\mathbf{p}$ still needs to be satisfied in the closed-loop system. Based on the result of Lemma 2.1, (2.52) is satisfied by the control law

$$\mathbf{u} = (\mathbf{G}^\mathrm{T}\mathbf{G})^{-1}\mathbf{G}^\mathrm{T}\left(\nabla_\mathbf{q} H + \mathbf{R}\mathbf{M}^{-1}\mathbf{p} - \mathbf{M}_\mathrm{d}\mathbf{M}^{-1}\nabla_\mathbf{q} H_\mathrm{d} + (\mathbf{J}_2 - \mathbf{R}_2)\,\mathbf{M}_\mathrm{d}^{-1}\mathbf{p}\right) \tag{2.53}$$

if and only if

$$\mathbf{G}_\perp\left(\nabla_\mathbf{q} H - \mathbf{M}_\mathrm{d}\mathbf{M}^{-1}\nabla_\mathbf{q} H_\mathrm{d} + (\mathbf{J}_2 - \mathbf{R}_2)\,\mathbf{M}_\mathrm{d}^{-1}\mathbf{p}\right) = \mathbf{0} \tag{2.54}$$

holds. Assuming that $\mathbf{R}_2 = \mathbf{R}_2(\mathbf{q})$, and $\mathbf{J}_2 = \mathbf{J}_{20}(\mathbf{q}) + \mathbf{J}_{21}(\mathbf{q},\mathbf{p})$, with $\mathbf{J}_{21}$ linear in $\mathbf{p}$, the projected matching equation (2.54) can be naturally split according to the dependency on $\mathbf{p}$: The terms quadratic and independent from $\mathbf{p}$ correspond to the kinetic and potential energies, respectively. The terms linear in $\mathbf{p}$ correspond to the dissipation. Thus, (2.54) can be written as

$$\mathbf{G}_\perp\left(\nabla_\mathbf{q}(\mathbf{p}^\mathrm{T}\mathbf{M}^{-1}\mathbf{p}) - \mathbf{M}_\mathrm{d}\mathbf{M}^{-1}\nabla_\mathbf{q}(\mathbf{p}^\mathrm{T}\mathbf{M}_\mathrm{d}^{-1}\mathbf{p}) + 2\mathbf{J}_{21}\mathbf{M}_\mathrm{d}^{-1}\mathbf{p}\right) = \mathbf{0}, \tag{2.55a}$$

$$\mathbf{G}_\perp\left(\nabla_\mathbf{q} V - \mathbf{M}_\mathrm{d}\mathbf{M}^{-1}\nabla_\mathbf{q} V_\mathrm{d}\right) = \mathbf{0}, \tag{2.55b}$$

$$\mathbf{G}_\perp(\mathbf{J}_{20} - \mathbf{R}_2)\,\mathbf{M}_\mathrm{d}^{-1}\mathbf{p} = \mathbf{0}. \tag{2.55c}$$

The first equation is a nonlinear PDE that has to be solved for the unknown elements of the inertia matrix $\mathbf{M}_\mathrm{d}(\mathbf{q})$. For a given desired inertia matrix, the second equation becomes a linear PDE for the unknown function $V_\mathrm{d}(\mathbf{q})$, and the third equation is a simple algebraic equation, which can be solved by the choice

$$\mathbf{J}_{20} - \mathbf{R}_2 = \mathbf{G}\,(\mathbf{K}_\mathbf{J} - \mathbf{K}_\mathbf{R})\,\mathbf{G}^\mathrm{T}, \tag{2.56}$$

with free parameters $\mathbf{K}_\mathbf{R} = \mathbf{K}_\mathbf{R}^\mathrm{T} > \mathbf{0}$, and $\mathbf{K}_\mathbf{J} = -\mathbf{K}_\mathbf{J}^\mathrm{T}$. The following corollary results directly from Theorem 2.3:

Corollary 2.5 (Stability of the closed-loop system)**.** *If*

$$\mathbf{q}^* = \arg\min V_\mathrm{d},\ \mathbf{M}_\mathrm{d} > \mathbf{0} \text{ and } \mathbf{R}_2 \geq \mathbf{0} \tag{2.57}$$

in a neighborhood of $\mathbf{q}^*$*, then the equilibrium* $\mathbf{q}^*$ *is (locally) stable with Lyapunov function* H_d*. Local asymptotic stability follows if the damping is pervasive.*

Proof. Stability follows from Theorem 2.3 noting that H_d is positive definite, and $\dot{H}_\mathrm{d} \leq 0$. If the damping is pervasive, asymptotic stability can be shown by invoking LaSalle's invariance principle. ■

Remark 2.3.1. There is a significant difference between the zero-state detectability property and pervasive damping. The output $\mathbf{y}$ is zero-state detectable if $\mathbf{y} = \mathbf{0}$ implies, without loss of generality, that the state $\mathbf{x} \to \mathbf{0}$ as time goes to infinity. In the context of mechanical systems, zero-state detectability of $\mathbf{y}$ implies that if $\mathbf{y} = \mathbf{0}$, the system converges to the desired configuration $\mathbf{q}^*$. Pervasive damping, on the other hand, guarantees that the system will come to rest, since $\dot{\mathbf{q}} \to \mathbf{0}$ as time goes to infinity. However, it does not guarantee that the system will converge towards the desired equilibrium $\mathbf{q}^*$. For that reason, the damping matrix $\mathbf{R}_2 = \mathbf{G}\mathbf{K}_\mathbf{R}\mathbf{G}^\mathrm{T}$ ($\mathbf{K}_\mathbf{R} > \mathbf{0}$) induces pervasive damping if the output $\mathbf{y} = \mathbf{G}^\mathrm{T}\mathbf{M}_\mathrm{d}^{-1}\mathbf{p}$ is zero-state detectable, but the converse does not hold.

2.3.4 Method of Controlled Lagrangians

The method of *Controlled Lagrangians* (CL) as the Lagrangian counterpart to parametric IDA for mechanical systems aims at stabilizing an equilibrium point by shaping the system's total energy and, in its more general form, also includes generalized gyroscopic forces as additional degree of freedom. Damping is subsequently *injected* to achieve asymptotic stability of the desired equilibrium $\mathbf{q}^*$. In the following, we give the general idea of CL for the stabilization of an admissible equilibrium $\mathbf{q}^*$. Consider the mechanical system

$$\mathbf{M}\ddot{\mathbf{q}} + \mathbf{C}\dot{\mathbf{q}} + \nabla_\mathbf{q} V = \mathbf{G}\mathbf{u}. \tag{2.58}$$

The goal of the Controlled Lagrangians procedure is to transform (2.58) by static state feedback $\mathbf{u} = \mathbf{u}(\mathbf{q}, \dot{\mathbf{q}})$ into a target Lagrangian closed-loop system. Let

$$L_\mathrm{c} = \frac{1}{2}\,\dot{\mathbf{q}}^\mathrm{T}\mathbf{M}_\mathrm{c}\dot{\mathbf{q}} - V_\mathrm{c} \tag{2.59}$$

be the desired closed-loop Lagrangian with mass matrix $\mathbf{M}_\mathrm{c}(\mathbf{q}) = \mathbf{M}_\mathrm{c}^\mathrm{T}(\mathbf{q})$ and potential energy $V_\mathrm{c}(\mathbf{q})$, and let us consider the Euler-Lagrange equation for the target system with dissipation and generalized gyroscopic forces

$$\frac{\mathrm{d}}{\mathrm{d}t}\left(\frac{\partial L_\mathrm{c}}{\partial \dot{\mathbf{q}}}\right)^\mathrm{T} - \left(\frac{\partial L_\mathrm{c}}{\partial \mathbf{q}}\right)^\mathrm{T} = (\mathbf{J}_\mathrm{c} - \mathbf{R}_\mathrm{c})\,\dot{\mathbf{q}}, \tag{2.60}$$

where the matrix $\mathbf{J}_\mathrm{c} = \mathbf{J}_{\mathrm{c}0}(\mathbf{q}) + \mathbf{J}_{\mathrm{c}1}(\mathbf{q}, \dot{\mathbf{q}})$ ($\mathbf{J}_{\mathrm{c}1}$ linear in $\dot{\mathbf{q}}$) is skew-symmetric, and the closed-loop damping matrix $\mathbf{R}_\mathrm{c} = \mathbf{R}_\mathrm{c}(\mathbf{q})$ is symmetric and positive (semi-)definite. The target dynamics (2.60) can then be given in matrix form as

$$\mathbf{M}_\mathrm{c}\ddot{\mathbf{q}} + \mathbf{C}_\mathrm{c}\dot{\mathbf{q}} + \nabla_\mathbf{q} V_\mathrm{c} = (\mathbf{J}_\mathrm{c} - \mathbf{R}_\mathrm{c})\,\dot{\mathbf{q}}, \tag{2.61}$$

or equivalently

$$\ddot{\mathbf{q}} = -\mathbf{M}_\mathrm{c}^{-1}\mathbf{C}_\mathrm{c}\dot{\mathbf{q}} - \mathbf{M}_\mathrm{c}^{-1}\nabla_\mathbf{q} V_\mathrm{c} + \mathbf{M}_\mathrm{c}^{-1}(\mathbf{J}_\mathrm{c} - \mathbf{R}_\mathrm{c})\,\dot{\mathbf{q}}. \tag{2.62}$$

The following corollary follows directly from Corollary 2.3:

Corollary 2.6. *The desired closed-loop system (2.61) is asymptotically stable if*

$$\mathbf{q}^* = \arg\min V_\mathrm{c},\ \ \mathbf{M}_\mathrm{c} > \mathbf{0},\ \ \mathbf{R}_\mathrm{c} \geq \mathbf{0}, \tag{2.63}$$

and the damping is pervasive.

Conditions, under which both—the system (2.58) and the target Lagrangian system (2.61)—match, can be derived by inserting the target dynamics (2.62) into the system's equations of motion (2.58). The objective is to find an appropriate input $\mathbf{u}$, which solves the corresponding *matching equation*

$$-\mathbf{M}\mathbf{M}_\mathrm{c}^{-1}\mathbf{C}_\mathrm{c}\dot{\mathbf{q}} - \mathbf{M}\mathbf{M}_\mathrm{c}^{-1}\nabla_\mathbf{q} V_\mathrm{c} + \mathbf{M}\mathbf{M}_\mathrm{c}^{-1}(\mathbf{J}_\mathrm{c} - \mathbf{R}_\mathrm{c})\,\dot{\mathbf{q}} + \mathbf{C}\dot{\mathbf{q}} + \nabla_\mathbf{q} V = \mathbf{G}\mathbf{u}. \tag{2.64}$$

Splitting the equations by means of the dependency on the velocities $\dot{\mathbf{q}}$, leads to the matching equations for the potential (independent from $\dot{\mathbf{q}}$) and the kinetic (quadratic in $\dot{\mathbf{q}}$) energy, and for the dissipation, which consists of the terms linear in $\dot{\mathbf{q}}$. The resulting set of equations

$$\mathbf{G}\mathbf{u}_\mathrm{ke} = \mathbf{C}\dot{\mathbf{q}} - \mathbf{M}\mathbf{M}_\mathrm{c}^{-1}(\mathbf{C}_\mathrm{c} - \mathbf{J}_{\mathrm{c}1})\,\dot{\mathbf{q}}, \tag{2.65a}$$

$$\mathbf{G}\mathbf{u}_\mathrm{pe} = \nabla_\mathbf{q} V - \mathbf{M}\mathbf{M}_\mathrm{c}^{-1}\nabla_\mathbf{q} V_\mathrm{c}, \tag{2.65b}$$

$$\mathbf{G}\mathbf{u}_\mathrm{di} = \mathbf{M}\mathbf{M}_\mathrm{c}^{-1}(\mathbf{R}_\mathrm{c} - \mathbf{J}_{\mathrm{c}0})\,\dot{\mathbf{q}}, \tag{2.65c}$$

determines the components of the control law

$$\mathbf{u} = \mathbf{u}_{\text{ke}} + \mathbf{u}_{\text{pe}} + \mathbf{u}_{\text{di}} \tag{2.66}$$

related to the shaping of kinetic and potential energy, as well as damping injection. The solution of all three matching equations (2.65) is sufficient to satisfy (2.64).

Remark 2.3.2. As we will see in Chapter 6, the matching equations (2.65) in Controlled Lagrangians can be split into a non-actuated part, which is equivalent to the matching problem (2.55) in IDA, and a fully actuated part. From the latter we can directly compute the control law that renders the mechanical system (2.58) the desired closed-loop system (2.60), provided that the projected matching equations—the non-actuated part of (2.65)—are satisfied.

II

Physical Dissipation in Unactuated Coordinates

3 Augmented Interconnection and Damping Assignment

Physical dissipation in mechanical systems is mostly neglected in PBC for the sake of simplicity and mathematical elegance, especially in unactuated coordinates, where it is assumed to be small. Yet, it plays a crucial role in the applicability of energy shaping to mechanical systems. Intuitively, physical damping enhances stability, since it dissipates energy. However, if dissipation occurs in unactuated coordinates of the uncontrolled mechanical system, shaping the kinetic energy through feedback, e. g., via CL or IDA, might cause the dissipation terms to have a destabilizing effect on the closed-loop system. The so-called *dissipation condition*—firstly introduced in [74]—determines *a posteriori*, i. e., after the controller has been designed for the undamped system, if the required definiteness properties for the closed-loop system are also fulfilled in the presence of dissipation or not.

This chapter addresses the systematic design of passivity-based controllers for mechanical systems in the presence of dissipation in unactuated coordinates. In order to render a mechanical system passive by shaping its total energy, the dissipation condition has to be met. To bypass this obstacle, a more general, non-mechanical structure for the closed-loop energy is allowed. By doing so, we do not only counteract the dissipation related problems, we also increase the design freedom of the approach, but, at the same time, break the system's mechanical structure.

The chapter is organized as follows: After the formulation of the problem in Section 3.1, the *augmented* IDA approach for mechanical systems is motivated by means of a linear system in Section 3.2.1. The idea is then transfered to nonlinear systems in Section 3.2.2, for which the new matching equations are given. A solution to this new matching problem is then proposed in Section 3.3. In Section 3.4, we give the Lagrangian formulation of the closed-loop dynamics, and conclude the chapter with some final remarks.

3.1 Problem formulation

Let us first briefly recapitulate the IDA-PBC approach for underactuated mechanical systems as presented in Section 2.3.3. We consider Hamiltonian systems of the form

$$\begin{bmatrix} \dot{\mathbf{q}} \\ \dot{\mathbf{p}} \end{bmatrix} = \begin{bmatrix} \mathbf{0} & \mathbf{I} \\ -\mathbf{I} & -\mathbf{R} \end{bmatrix} \begin{bmatrix} \nabla_{\mathbf{q}} H \\ \nabla_{\mathbf{p}} H \end{bmatrix} + \begin{bmatrix} \mathbf{0} \\ \mathbf{G} \end{bmatrix} \mathbf{u}, \tag{3.1}$$

where $(\mathbf{q}, \mathbf{p}) \in \mathsf{T}^*\mathcal{Q}$ are the generalized local coordinates and momenta, respectively, $\mathbf{u} \in \mathcal{U} \subseteq \mathbb{R}^m$ is the input, and $\mathbf{G} \in \mathbb{R}^{n \times m}$ is the input matrix with $\operatorname{rank}(\mathbf{G}) = m < n$. The Hamiltonian

$$H = \frac{1}{2} \mathbf{p}^{\mathrm{T}} \mathbf{M}^{-1} \mathbf{p} + V \tag{3.2}$$

corresponds to the total energy with inertia matrix $\mathbf{M}(\mathbf{q}) > \mathbf{0}$ and potential energy $V(\mathbf{q})$. The goal is to stabilize the equilibrium $\mathbf{q}^*$ via total energy shaping. The state feedback

$$\mathbf{u} = (\mathbf{G}^{\mathrm{T}}\mathbf{G})^{-1}\mathbf{G}^{\mathrm{T}} \left(\nabla_{\mathbf{q}} H + \mathbf{R}\mathbf{M}^{-1}\mathbf{p} - \mathbf{M}_{\mathrm{d}}\mathbf{M}^{-1} \nabla_{\mathbf{q}} H_{\mathrm{d}} + (\mathbf{J}_2 - \mathbf{R}_2)\, \mathbf{M}_{\mathrm{d}}^{-1}\mathbf{p} \right) \tag{3.3}$$

transforms (3.1) into a pH system

$$\begin{bmatrix} \dot{\mathbf{q}} \\ \dot{\mathbf{p}} \end{bmatrix} = \begin{bmatrix} \mathbf{0} & \mathbf{M}^{-1}\mathbf{M}_{\mathrm{d}} \\ -\mathbf{M}_{\mathrm{d}}\mathbf{M}^{-1} & \mathbf{J}_2 - \mathbf{R}_2 \end{bmatrix} \begin{bmatrix} \nabla_{\mathbf{q}} H_{\mathrm{d}} \\ \nabla_{\mathbf{p}} H_{\mathrm{d}} \end{bmatrix} \tag{3.4}$$

with new (shaped) energy

$$H_{\mathrm{d}} = \frac{1}{2} \mathbf{p}^{\mathrm{T}} \mathbf{M}_{\mathrm{d}}^{-1} \mathbf{p} + V_{\mathrm{d}} \tag{3.5}$$

if the projected matching equations (2.55) are satisfied. According to Corollary 2.5, if further

$$\mathbf{q}^* = \arg\min V_{\mathrm{d}}, \;\; \mathbf{M}_{\mathrm{d}} > \mathbf{0}, \;\; \text{and} \;\; \mathbf{R}_2 \geq \mathbf{0}, \tag{3.6}$$

then $\mathbf{q}^*$ is stable, provided that $\mathbf{G}_\perp \mathbf{R} = \mathbf{0}$.

Unlike the common approach, in this chapter we consider physical dissipation in unactuated coordinates, such that $\mathbf{G}_\perp \mathbf{R} \neq \mathbf{0}$. For that reason, the matching equation related to the dissipation (2.55c) takes the new form

$$\mathbf{G}_\perp \left(\mathbf{R}\mathbf{M}^{-1}\mathbf{p} + (\mathbf{J}_{20} - \mathbf{R}_2)\mathbf{M}_{\mathrm{d}}^{-1}\mathbf{p} \right) = \mathbf{0}. \tag{3.7}$$

In [74], Gómez-Estern and van der Schaft derive the *dissipation condition*[1] (DC)

$$\mathbf{G}_\perp \left(\mathbf{R}\mathbf{M}^{-1}\mathbf{M}_\mathrm{d} + \mathbf{M}_\mathrm{d}\mathbf{M}^{-1}\mathbf{R} \right) \mathbf{G}_\perp^\mathrm{T} \geq \mathbf{0} \tag{3.8}$$

from (3.7), and show that it is a necessary and sufficient condition for the existence of a passive closed-loop system with given positive definite storage function H_d. Note that the DC depends on $\mathbf{M}_\mathrm{d}$. It, therefore, provides the information *after* the matching equation for the kinetic energy (2.55a) has been solved. If it turns out, for instance, that the DC is not satisfied, one cannot know for certain whether it will be satisfied for a different $\mathbf{M}_\mathrm{d}$ or not. Yet, it is well-known that in the presence of physical damping in unactuated degrees of freedom for many mechanical systems—such as the acrobot system, the Furuta and the inverted pendulum on a cart among others—it is not possible to find a solution for the matching equations (2.55a) and (2.55b) that simultaneously satisfies the definiteness requirements (3.6) and the DC (3.8) (see, e. g., the papers [43, 74] for the DC in IDA, or [209] for the CL point of view). Two questions naturally arise from this fact:

- Is it possible, nonetheless, to show stability of an equilibrium $\mathbf{q}^*$ that has been stabilized in the absence of damping, when damping is considered?
- How can the IDA approach be modified, such that it can cope with dissipation in unactuated coordinates from the very beginning, regardless of the dissipation condition?

The answer to the first question is given by Woolsey, Reddy, and others in [167, 168, 209]. Assuming small dissipation values, the authors prove stability of the desired equilibrium for appropriately chosen control parameters via spectral analysis of the linearized closed-loop system. However, even though it is possible to show asymptotic stability, the analysis is cumbersome, and one loses the estimate of the domain of attraction, which constitutes one of the advantages of the energy shaping methodology that we do not want to lose. The purpose of this chapter is to give an answer to the second question.

3.2 Non-mechanical PBC for mechanical systems

The central question that is addressed in this section is whether or not it is possible to transform a damped mechanical system into a closed-loop pH system by static state

[1] The DC is not to be confused with the *dissipation obstacle* also known from PBC approaches [155].

feedback if the DC is not satisfied. Indeed, the answer is yes. It can be achieved by augmenting the desired Hamiltonian function by a cross term between coordinates and momenta, *breaking* the mechanical structure of the closed-loop system[2].

3.2.1 Linear time-invariant systems

To motivate the approach, let us consider linear time-invariant (LTI) systems of the form

$$\dot{\mathbf{x}} = \mathbf{A}\mathbf{x} + \mathbf{B}\mathbf{u}, \qquad \mathbf{x} \in \mathbb{R}^n,\ \mathbf{u} \in \mathbb{R}^m. \tag{3.9}$$

A substantial analysis of IDA-PBC for general LTI systems can be found in [162] and [152]. The CL case is treated in [219]. For simplicity—and without loss of generality—the desired equilibrium to be stabilized is taken to be the origin. Applying IDA to LTI systems consists in finding a linear state feedback $\mathbf{u} = -\mathbf{D}\mathbf{x}$ such that

$$\mathbf{A}\mathbf{x} + \mathbf{B}\mathbf{u} \overset{!}{=} (\mathbf{J}_\mathrm{d} - \mathbf{R}_\mathrm{d})\,\mathbf{P}_\mathrm{d}\mathbf{x}. \tag{3.10}$$

The matrix $\mathbf{P}_\mathrm{d}$ is positive definite and defines the Hamiltonian of the closed-loop system, i. e., the Hamiltonian is given by

$$H_\mathrm{d} = \frac{1}{2}\mathbf{x}^\mathrm{T}\mathbf{P}_\mathrm{d}\mathbf{x}. \tag{3.11}$$

It has been shown in [152] that, for general LTI systems, IDA-PBC is equivalent to stabilizability: if the pair $(\mathbf{A}, \mathbf{B})$ is stabilizable, then there exists a matrix $\mathbf{D} \in \mathbb{R}^{m\times n}$, such that $\mathbf{A}_\mathrm{d} = \mathbf{A} - \mathbf{B}\mathbf{D}$ is Hurwitz. Further, given a positive definite matrix $\mathbf{R}_\mathrm{d}$, a unique solution $\mathbf{P}_\mathrm{d}^{-1} > \mathbf{0}$ to the Lyapunov equation

$$\mathbf{A}_\mathrm{d}\mathbf{P}_\mathrm{d}^{-1} + \mathbf{P}_\mathrm{d}^{-1}\mathbf{A}_\mathrm{d}^\mathrm{T} = -2\mathbf{R}_\mathrm{d} \tag{3.12}$$

exists. The projected matching equations—i. e., conditions that have to be satisfied independent from control—stem directly from (3.10): The applicability of IDA to a general LTI system (3.9) is equivalent to the solvability of the LMIs (Proposition 7 in [162] and Proposition 3.1 in [152])

$$\mathbf{P}_\mathrm{d} > \mathbf{0} \tag{3.13a}$$

$$\operatorname{sym}(\mathbf{B}_\perp\mathbf{A}\mathbf{P}_\mathrm{d}^{-1}\mathbf{B}_\perp^\mathrm{T}) \leq \mathbf{0}, \tag{3.13b}$$

[2] A PBC can be denoted non-mechanical if the energy term (Hamiltonian function) of the closed-loop system is not composed of the sum of kinetic and potential energy.

where $\mathbf{B}_\perp$ is a full rank left annihilator of $\mathbf{B}$, i. e., $\mathbf{B}_\perp\mathbf{B} = \mathbf{0}$.

When dealing with mechanical systems, the structure of the desired Hamiltonian function is restricted to be of mechanical form. This has some important repercussions as shown in the following. We consider linear mechanical systems in the Hamiltonian representation

$$\dot{\mathbf{x}} = \begin{bmatrix} \dot{\mathbf{q}} \\ \dot{\mathbf{p}} \end{bmatrix} = \begin{bmatrix} \mathbf{0} & \mathbf{I} \\ -\mathbf{I} & -\mathbf{R} \end{bmatrix} \begin{bmatrix} \nabla_{\mathbf{q}} H \\ \nabla_{\mathbf{p}} H \end{bmatrix} + \begin{bmatrix} \mathbf{0} \\ \mathbf{G} \end{bmatrix} \mathbf{u} = \mathbf{A}\mathbf{x} + \mathbf{B}\mathbf{u}, \tag{3.14}$$

with quadratic energy

$$H = \frac{1}{2}\,\mathbf{p}^{\mathrm{T}}\mathbf{M}^{-1}\mathbf{p} + \frac{1}{2}\,\mathbf{q}^{\mathrm{T}}\mathbf{Q}\mathbf{q}. \tag{3.15}$$

The aim of IDA is now to transform (3.14) by linear state feedback into a new LTI mechanical system

$$\dot{\mathbf{x}} = \begin{bmatrix} \dot{\mathbf{q}} \\ \dot{\mathbf{p}} \end{bmatrix} = \begin{bmatrix} \mathbf{0} & \mathbf{M}^{-1}\mathbf{M}_{\mathrm{d}} \\ -\mathbf{M}_{\mathrm{d}}\mathbf{M}^{-1} & \mathbf{J}_2 - \mathbf{R}_2 \end{bmatrix} \begin{bmatrix} \nabla_{\mathbf{q}} H_{\mathrm{d}} \\ \nabla_{\mathbf{p}} H_{\mathrm{d}} \end{bmatrix} = \mathbf{A}_{\mathrm{d}}\mathbf{x} \tag{3.16}$$

with shaped Hamiltonian composed of the sum of desired kinetic and potential energy

$$H_{\mathrm{d}} = \frac{1}{2}\,\mathbf{p}^{\mathrm{T}}\mathbf{M}_{\mathrm{d}}^{-1}\mathbf{p} + \frac{1}{2}\,\mathbf{q}^{\mathrm{T}}\mathbf{Q}_{\mathrm{d}}\mathbf{q}. \tag{3.17}$$

Notice that, in doing so, the matrix $\mathbf{P}_{\mathrm{d}}$ is restricted to be of a predefined block-diagonal form

$$\mathbf{P}_{\mathrm{d}} = \nabla^2_{(\mathbf{q},\mathbf{p})} H_{\mathrm{d}} = \begin{bmatrix} \mathbf{Q}_{\mathrm{d}} & \mathbf{0} \\ \mathbf{0} & \mathbf{M}_{\mathrm{d}}^{-1} \end{bmatrix}. \tag{3.18}$$

By imposing (3.18), the conditions (3.13) exhibit a familiar structure: On the one hand, the LMI (3.13a) demands positive definiteness of both matrices $\mathbf{M}_{\mathrm{d}}$ and $\mathbf{Q}_{\mathrm{d}}$, and thereby, positive definiteness of the kinetic and potential energy. On the other hand, the LMI (3.13b) characterizes the linear version of the potential energy matching equation (2.55b), and of the dissipation condition (3.8), which are given as

$$\mathbf{G}_\perp(\mathbf{M}_{\mathrm{d}}\mathbf{M}^{-1} - \mathbf{Q}\mathbf{Q}_{\mathrm{d}}^{-1}) = \mathbf{0}, \tag{3.19a}$$

$$-\mathbf{G}_\perp(\mathbf{R}\mathbf{M}^{-1}\mathbf{M}_{\mathrm{d}} + \mathbf{M}_{\mathrm{d}}\mathbf{M}^{-1}\mathbf{R})\mathbf{G}_\perp^{\mathrm{T}} \leq \mathbf{0}. \tag{3.19b}$$

According to Proposition 7 in [162], the linear state feedback

$$\mathbf{u} = (\mathbf{G}^{\mathrm{T}}\mathbf{G})^{-1}\mathbf{G}^{\mathrm{T}}\left[\left(\mathbf{Q} - \mathbf{M}_{\mathrm{d}}\mathbf{M}^{-1}\mathbf{Q}_{\mathrm{d}}\right)\mathbf{q} + \left(\mathbf{R}\mathbf{M}^{-1} + (\mathbf{J}_2 - \mathbf{R}_2)\,\mathbf{M}_{\mathrm{d}}^{-1}\right)\mathbf{p}\right] \tag{3.20}$$

renders (3.14) the closed loop-system (3.16) if a solution $\mathbf{P}_{\mathrm{d}}$ to the set of LMIs (3.13) restricted to (3.18) exists (cf. [219] and [112]), or, equivalently, a solution to the matching equations (3.19)[3] can be found. Yet, for many mechanical systems it is not possible to find positive definite matrices $\mathbf{M}_{\mathrm{d}}$ and $\mathbf{Q}_{\mathrm{d}}$ that solve (3.19a) and (3.19b) simultaneously [73, 111, 112].

In [152], Ortega and co-workers show that stabilizability is not sufficient for the applicability of parametrized IDA to linear (undamped) mechanical systems, since some conditions on the uncontrolled modes have to be additionally imposed. In addition, if physical damping is considered, then the dissipation condition needs to be satisfied to render the closed-loop system passive. However, as previously mentioned, stabilizability is indeed sufficient for the existence of an IDA controller if we relax the condition on the mechanical structure for the closed-loop system: By allowing off-diagonal entries in the matrix $\mathbf{P}_{\mathrm{d}}$—representing a cross term between coordinates and momenta in the energy function (3.17)—a positive definite solution $\mathbf{P}_{\mathrm{d}}$ to the set of LMIs (3.13) can always be found, assuming stabilizability of (3.9). It is, thus, possible to asymptotically stabilize linear mechanical systems via IDA-PBC regardless of the DC.

Remark 3.2.1. In [219], the stabilization of (conservative) linear mechanical systems using only position feedback in the CL framework is discussed. Therein, the closed-loop Hamiltonian is initially assumed to have a non-block-diagonal Hessian, which corresponds to the structure of the augmented closed-loop Hamiltonian in the next section.

3.2.2 Augmented Hamiltonian function and new matching equations

Starting from the premise that a stabilizing state feedback for systems with a stabilizable linearization always exists, it is intended to reformulate the target pH system such that a nonlinear IDA controller can be derived, although the DC is violated. The non-block-diagonal structure of the solution of the set of LMIs (3.13) gives rise to assume an augmented formulation of the closed-loop energy function

$$H_{\mathrm{d}} = \frac{1}{2}\,\mathbf{p}^{\mathrm{T}}\mathbf{M}_{\mathrm{d}}^{-1}(\mathbf{q})\mathbf{p} + V_{\mathrm{d}}(\mathbf{q}) + \mathbf{p}^{\mathrm{T}}\mathbf{n}_{\mathrm{d}}(\mathbf{q}) \tag{3.21}$$

[3] Note that the matching equation for the kinetic energy is obviated in the linear case.

for the generalized target pH system

$$\mathbf{F}_\mathrm{d}\,\nabla H_\mathrm{d} = \begin{bmatrix} \mathbf{W}(\mathbf{q}) & \mathbf{X}(\mathbf{q}) \\ \mathbf{Y}(\mathbf{q}) & \mathbf{Z}(\mathbf{q},\mathbf{p}) \end{bmatrix} \begin{bmatrix} \nabla_\mathbf{q} H_\mathrm{d} \\ \nabla_\mathbf{p} H_\mathrm{d} \end{bmatrix}, \tag{3.22}$$

where $\mathbf{Z} = \mathbf{Z}_0(\mathbf{q}) + \mathbf{Z}_1(\mathbf{q},\mathbf{p})$, and $\mathbf{Z}_1(\mathbf{q},\mathbf{p})$ is skew-symmetric and linear in $\mathbf{p}$. Because of the non-mechanical form of H_d, the closed-loop interconnection and damping matrices $\mathbf{F}_\mathrm{d} = \mathbf{J}_\mathrm{d}(\mathbf{q},\mathbf{p}) - \mathbf{R}_\mathrm{d}(\mathbf{q})$ are required to be of a more general form than in the classic approach. As $\dot{\mathbf{q}} = \mathbf{M}^{-1}\mathbf{p}$ still holds in the closed-loop system (3.22), the matrices $\mathbf{W}$ and $\mathbf{X}$ are required to satisfy $\mathbf{M}^{-1}\mathbf{p} = \mathbf{W}\nabla_\mathbf{q} H_\mathrm{d} + \mathbf{X}\nabla_\mathbf{p} H_\mathrm{d}$. Splitting the equation in different dependencies on $\mathbf{p}$—quadratic, linear, and independent—yields the sufficient conditions

$$\mathbf{W}\nabla_\mathbf{q}\left(\mathbf{p}^\mathrm{T}\mathbf{M}_\mathrm{d}^{-1}\mathbf{p}\right) = \mathbf{0}, \tag{3.23a}$$

$$\mathbf{W}\left(\frac{\partial \mathbf{n}_\mathrm{d}}{\partial \mathbf{q}}\right)^\mathrm{T} + \mathbf{X}\mathbf{M}_\mathrm{d}^{-1} - \mathbf{M}^{-1} = \mathbf{0}, \tag{3.23b}$$

$$\mathbf{W}\nabla_\mathbf{q} V_\mathrm{d} + \mathbf{X}\mathbf{n}_\mathrm{d} = \mathbf{0}. \tag{3.23c}$$

Furthermore, the unactuated part of the second rows of (3.1) and (3.22) must match. A sufficient condition is represented by the *new* projected matching equations (again, splitting the terms)

$$\mathbf{G}_\perp\left(\mathbf{Y}\nabla_\mathbf{q}\left(\mathbf{p}^\mathrm{T}\mathbf{M}_\mathrm{d}^{-1}\mathbf{p}\right) + 2\mathbf{Z}_1\mathbf{M}_\mathrm{d}^{-1}\mathbf{p} + \nabla_\mathbf{q}\left(\mathbf{p}^\mathrm{T}\mathbf{M}^{-1}\mathbf{p}\right)\right) = 0, \tag{3.24a}$$

$$\mathbf{G}_\perp\left(\mathbf{R}\mathbf{M}^{-1}\mathbf{p} + \mathbf{Z}_0\mathbf{M}_\mathrm{d}^{-1}\mathbf{p} + \mathbf{Z}_1\mathbf{n}_\mathrm{d} + \mathbf{Y}\left(\frac{\partial \mathbf{n}_\mathrm{d}}{\partial \mathbf{q}}\right)^\mathrm{T}\mathbf{p}\right) = 0, \tag{3.24b}$$

$$\mathbf{G}_\perp\left(\nabla_\mathbf{q} V + \mathbf{Y}\nabla_\mathbf{q} V_\mathrm{d} + \mathbf{Z}_0\mathbf{n}_\mathrm{d}\right) = 0. \tag{3.24c}$$

The computation of an analytical solution to the matching problem given by (3.23) and (3.24) subject to

$$H_\mathrm{d} > 0, \qquad \mathbf{R}_\mathrm{d} \geq \mathbf{0}, \tag{3.25}$$

is, in general, far from trivial. The next section presents a way to systematically compute a solution for a class of mechanical systems.

3.3 Solving the matching problem in augmented IDA

One of the main difficulties of the IDA-PBC approach lies in finding a solution to the projected matching equations. Not all degrees of freedom being equipped with actuators results in certain restrictions on the achievable closed-loop dynamics of underactuated systems. These restrictions are given in the form of algebraic equations and PDEs: the matching equations. Whilst in its parametric mechanical form the restrictions are given by two PDEs and one LMI—the matching equations for the potential and kinetic energy, and the dissipation condition—the matching problem in augmented IDA is much more challenging. Even though the structure of the desired Hamiltonian (3.21) is not left completely free, the closed-loop system still possesses a vast amount of degrees of freedom that need to be tuned appropriately to guarantee the definiteness conditions (3.25). As mentioned earlier in Section 2.3.3, there are, basically, two ways of solving (3.23) and (3.24): On the one hand, one can fix the desired interconnection and damping matrices—in terms of $\mathbf{W}$, $\mathbf{X}$, $\mathbf{Y}$, and $\mathbf{Z}$—and then try to solve the PDEs. The solution to the corresponding homogeneous PDEs needs to be fixed such that $H_\mathrm{d} > 0$. This results in the non-algebraic approach, which is discussed in Section 3.3.1. On the other hand, one can fix the Hamiltonian H_d. The conditions for matching (3.23) and (3.24) become algebraic equations for the desired interconnection and damping matrices, and need to be satisfied for $\mathbf{R}_\mathrm{d} \geq \mathbf{0}$. This concept is treated in Section 3.3.2.

In the following, we generalize the theory developed in the papers [52, 112] for the simplification and solution of the new matching equations (3.23) and (3.24). In the process, we impose some conditions on the closed-loop system, and restrict the analysis to a special class of mechanical systems. Initially, our concern is to find a general solution to the matching equations. Its parametrization, such that it also satisfies the definiteness requirements (3.25), will be addressed in Chapter 4.

Assumption 3.1. The underactuation degree is one, i. e., $\operatorname{rank}(\mathbf{G}_\perp) = n - m = 1$.

Assumption 3.2. The closed-loop inertia matrix $\mathbf{M}_\mathrm{d}$ is chosen to be constant, i. e., $\nabla_\mathbf{q}\left(\mathbf{p}^\mathrm{T}\mathbf{M}_\mathrm{d}^{-1}\mathbf{p}\right) = \mathbf{0}$. For convenience of notation, it will be denoted as $\mathbf{M}_{\mathrm{d}*}$.

Assumption 3.1 is often made for the application of IDA to underactuated mechanical systems, see, e. g., the representative papers [5, 151, 158]. The reason for that is twofold: On the one hand, the PDEs are significantly simplified. In fact, it is possible to construct an analytical solution to the classic matching problem for this class of systems if damping is not considered [5]. On the other hand, the matching conditions are given in terms of scalar PDEs, and are, therefore, always integrable according to the

Frobenius Theorem 2.1. That is, the existence of a solution is guaranteed, in contrast to the case $m<n-1$, where a system of PDEs with non-constant coefficients has to be examined for solvability first, and then has to be solved. In the following, the matrix $\mathbf{W}$ is assumed to be full rank, such that Assumption 3.2 is necessary for the solution of (3.23a).

3.3.1 Non-algebraic approach

One way of solving (3.24) is fixing a parametrization for the matrices $\mathbf{Y}$ and $\mathbf{Z}_0$, and solving $n+1$ PDEs for V_d, and the elements of $\mathbf{n}_\mathrm{d}$. The idea was first presented in [112] for the benchmark system *acrobot*, for which the mass matrix is independent of unactuated coordinates, i. e., $\mathbf{G}_\perp \nabla_\mathbf{q}\left(\mathbf{p}^\mathrm{T}\mathbf{M}^{-1}\mathbf{p}\right)=0$. Then, equation (3.24a) is trivially satisfied for $\mathbf{Z}_1=\mathbf{0}$. It remains to find solutions $V_\mathrm{d}(\mathbf{q})$ and $\mathbf{n}_\mathrm{d}(\mathbf{q})$ to the PDEs (3.24b) and (3.24c). In [112], a parametrized solution to these PDEs has been constructed. The subsequent parametrization of the closed-loop system and the stability analysis have been carried out via *local linear dynamics assignment* (LLDA) (see Section 4.1).

This method provides a solution for the problem of designing a passivity-based controller via IDA even though the DC is violated. However, a series of practical difficulties arises in the application of non-algebraic augmented IDA: The solution of additional PDEs for the vector-valued function $\mathbf{n}_\mathrm{d}(\mathbf{q})$ is required, the estimate of the region of attraction is shown to be poor, and the controller becomes confusingly complicated. The *algebraic approach* aims at solving some of these issues.

3.3.2 Algebraic approach

In the algebraic approach of IDA, the closed-loop Hamiltonian H_d is fixed. By doing so, the matching problem is reduced to a set of algebraic equations for the interconnection and damping matrices. The condition $\dot{\mathbf{q}} = \mathbf{M}^{-1}\mathbf{p}$ for the closed-loop system (3.22) is represented by the set of equations (3.23). Assumption 3.2 guarantees the solution of (3.23a). Without loss of generality, and in order to provide an expression for the matrices $\mathbf{W}(\mathbf{q})$ and $\mathbf{X}(\mathbf{q})$ in closed form, the vector-valued function $\mathbf{n}_\mathrm{d}(\mathbf{q})$ is given as

$$\mathbf{n}_\mathrm{d}(\mathbf{q}) = -\mathbf{K}_\mathrm{d}(\mathbf{q})\nabla_\mathbf{q} V_\mathrm{d}(\mathbf{q}), \tag{3.26}$$

where $\mathbf{K}_\mathrm{d} \in \mathbb{R}^{n\times n}$ is a smooth matrix-valued function. For a given closed-loop Hamiltonian (3.21), equations (3.23b) and (3.23c) are, consequently, satisfied by

$$\mathbf{W} = \mathbf{X}\mathbf{K}_\mathrm{d}, \qquad \mathbf{X} = \mathbf{M}^{-1}\left(\mathbf{K}_\mathrm{d}\left(\frac{\partial \mathbf{n}_\mathrm{d}}{\partial \mathbf{q}}\right)^\mathrm{T} + \mathbf{M}_{\mathrm{d}*}^{-1}\right)^{-1}, \tag{3.27}$$

assuming regularity of $\left(\mathbf{K}_\mathrm{d}\left(\frac{\partial \mathbf{n}_\mathrm{d}}{\partial \mathbf{q}}\right)^\mathrm{T} + \mathbf{M}_{\mathrm{d}*}^{-1}\right)$. For a systematic solution of the projected matching equations (3.24), it is convenient to first express (3.24a) and (3.24b) in an alternative, equivalent form.

Proposition 3.1. *Let Assumption 3.1 and Assumption 3.2 hold. Equation (3.24a) is equivalent to*

$$\mathbf{\Gamma}\mathbf{M}_{\mathrm{d}*}^{-1} + \mathbf{M}_{\mathrm{d}*}^{-1}\mathbf{\Gamma}^\mathrm{T} + \sum_{j=1}^{n} G_{\perp j}(\partial_{q_j}\mathbf{M}^{-1}) = \mathbf{0}, \tag{3.28}$$

where

$$\mathbf{\Gamma} = \sum_{i=1}^{N} \mathbf{f}_i(\mathbf{q})\mathbf{G}_\perp \boldsymbol{\mathcal{J}}_i, \qquad N = \frac{n^2-n}{2}, \tag{3.29}$$

the N free vector-valued functions $\mathbf{f}_i(\mathbf{q})$ are free parameters, and the N matrices $\boldsymbol{\mathcal{J}}_i$ constitute a basis for the set of n-dimensional skew-symmetric matrices. The scalar $G_{\perp j}$ denotes the j-th coefficient of $\mathbf{G}_\perp$, and $\partial_{q_j}\mathbf{M}^{-1}$ represents the element-wise derivative of the matrix $\mathbf{M}^{-1}$ with respect to the configuration variable q_j.

Proof. See Appendix A.1. ∎

We are now ready to formulate the main result of this chapter.

Theorem 3.1. *Let the desired Hamiltonian function H_d be defined as in (3.21) with fixed $V_\mathrm{d}(\mathbf{q})$, $\mathbf{M}_{\mathrm{d}*}$, and $\mathbf{n}_\mathrm{d}(\mathbf{q}) = -\mathbf{K}_\mathrm{d}(\mathbf{q})\nabla_\mathbf{q} V_\mathrm{d}(\mathbf{q})$. Suppose that one can find m functions $\mathbf{f}_i(\mathbf{q})$, such that the matrix $\mathbf{\Gamma}$ is a solution for (3.28), and define*

$$\mathbf{S}_\mathrm{d} = \frac{\mathbf{V}\mathbf{G}_\perp^\mathrm{T}\mathbf{n}_\mathrm{d}^\mathrm{T}\mathbf{\Gamma}^\mathrm{T}}{\mathbf{G}_\perp\mathbf{V}\mathbf{G}_\perp^\mathrm{T}}\mathbf{M}, \tag{3.30}$$

for an arbitrary matrix $\mathbf{V}(\mathbf{q}) \in \mathbb{R}^{n\times n}$ satisfying $\mathbf{G}_\perp\mathbf{V}\mathbf{G}_\perp^\mathrm{T} \neq 0$. Further, let $\mathbf{L}_\mathrm{d}(\mathbf{q})$ be a solution of

$$\mathbf{G}_\perp\left(\nabla_\mathbf{q} V - \mathbf{L}_\mathrm{d}\mathbf{K}_\mathrm{d}\nabla_\mathbf{q} V_\mathrm{d}\right) = 0, \tag{3.31}$$

and set

$$\mathbf{Y} = -\left(\mathbf{L}_{\mathrm{d}}\mathbf{M}_{\mathrm{d}*}^{-1}\mathbf{M} + \mathbf{R} + \mathbf{S}_{\mathrm{d}}\right)\mathbf{W}, \tag{3.32}$$

$$\mathbf{Z}_0 = -\left(\mathbf{Y}\left(\frac{\partial \mathbf{n}_{\mathrm{d}}}{\partial \mathbf{q}}\right)^{\mathrm{T}} + \mathbf{R}\mathbf{M}^{-1} + \mathbf{S}_{\mathrm{d}}\mathbf{M}^{-1}\right)\mathbf{M}_{\mathrm{d}*} + \mathbf{G}\boldsymbol{\eta}^{\mathrm{T}}, \tag{3.33}$$

where $\boldsymbol{\eta}(\mathbf{q}) \in \mathbb{R}^n$ *is an arbitrary vector-valued function, and* $\mathbf{W}$ *is defined according to (3.27). Then, the state feedback*

$$\mathbf{u} = (\mathbf{G}^{\mathrm{T}}\mathbf{G})^{-1}\mathbf{G}^{\mathrm{T}}\left(\nabla_{\mathbf{q}}H + \mathbf{R}\mathbf{M}^{-1}\mathbf{p} + \mathbf{Y}\nabla_{\mathbf{q}}H_{\mathrm{d}} + \mathbf{Z}_0\nabla_{\mathbf{p}}H_{\mathrm{d}}\right) \tag{3.34}$$

transforms (3.1) into the closed-loop system (3.22).

Proof. According to (2.49), the solution of (3.24) is sufficient to render (3.1) the desired closed-loop system (3.22) using the state feedback (3.34). From Assumption 3.2 and Proposition 3.1, we can conclude that if a matrix $\boldsymbol{\Gamma}$ satisfying (3.28) exists, then it also satisfies (3.24a). Additionally, Assumption 3.2 and Proposition 3.1 imply that the matching equation (3.24b) can be rewritten as

$$\mathbf{G}_{\perp}\left(\mathbf{R}\mathbf{M}^{-1} + \mathbf{Z}_0\mathbf{M}_{\mathrm{d}*}^{-1} + \mathbf{Y}\left(\frac{\partial \mathbf{n}_{\mathrm{d}}}{\partial \mathbf{q}}\right)^{\mathrm{T}}\right) + \mathbf{n}_{\mathrm{d}}^{\mathrm{T}}\boldsymbol{\Gamma}^{\mathrm{T}} = \mathbf{0}. \tag{3.35}$$

One can show by direct calculation that the matrix $\mathbf{Z}_0$ defined by (3.33) is a solution to (3.35), and thus, to (3.24b). Finally, from (3.23b) and (3.23c), it can be concluded that

$$\mathbf{W}\left(\nabla_{\mathbf{q}}V_{\mathrm{d}} - \left(\frac{\partial \mathbf{n}_{\mathrm{d}}}{\partial \mathbf{q}}\right)^{\mathrm{T}}\mathbf{M}_{\mathrm{d}*}\mathbf{n}_{\mathrm{d}}\right) = -\mathbf{M}^{-1}\mathbf{M}_{\mathrm{d}*}\mathbf{n}_{\mathrm{d}}, \tag{3.36}$$

such that replacing (3.33) in (3.24c) yields

$$\begin{aligned}
0 &= \mathbf{G}_{\perp}\left(\nabla_{\mathbf{q}}V + \mathbf{Y}\nabla_{\mathbf{q}}V_{\mathrm{d}} - \left(\mathbf{Y}\left(\frac{\partial \mathbf{n}_{\mathrm{d}}}{\partial \mathbf{q}}\right)^{\mathrm{T}} + \mathbf{R}\mathbf{M}^{-1} + \mathbf{S}_{\mathrm{d}}\mathbf{M}^{-1}\right)\mathbf{M}_{\mathrm{d}*}\mathbf{n}_{\mathrm{d}}\right) \\
&= \mathbf{G}_{\perp}\left(\nabla_{\mathbf{q}}V + \mathbf{Y}\underbrace{\left(\nabla_{\mathbf{q}}V_{\mathrm{d}} - \left(\frac{\partial \mathbf{n}_{\mathrm{d}}}{\partial \mathbf{q}}\right)^{\mathrm{T}}\mathbf{M}_{\mathrm{d}*}\mathbf{n}_{\mathrm{d}}\right)}_{\overset{(3.36)}{=} -\mathbf{W}^{-1}\mathbf{M}^{-1}\mathbf{M}_{\mathrm{d}*}\mathbf{n}_{\mathrm{d}}} - \left(\mathbf{R} + \mathbf{S}_{\mathrm{d}}\right)\mathbf{M}^{-1}\mathbf{M}_{\mathrm{d}*}\mathbf{n}_{\mathrm{d}}\right) \\
&= \mathbf{G}_{\perp}\left(\nabla_{\mathbf{q}}V - \left(\mathbf{Y}\mathbf{W}^{-1} + \mathbf{R} + \mathbf{S}_{\mathrm{d}}\right)\mathbf{M}^{-1}\mathbf{M}_{\mathrm{d}*}\mathbf{n}_{\mathrm{d}}\right).
\end{aligned} \tag{3.37}$$

Defining

$$\mathbf{L}_{\mathrm{d}} = -\left(\mathbf{Y}\mathbf{W}^{-1} + \mathbf{R} + \mathbf{S}_{\mathrm{d}}\right)\mathbf{M}^{-1}\mathbf{M}_{\mathrm{d}*}, \tag{3.38}$$

and rewriting equation (3.37) with (3.38) and $\mathbf{n}_{\mathrm{d}} = -\mathbf{K}_{\mathrm{d}}\nabla_{\mathbf{q}}V_{\mathrm{d}}$ finishes the proof. ■

3.4 Concluding remarks

The procedure presented in this chapter breaks the mechanical structure of the closed-loop system. Nonetheless, also in this augmented formulation, there is still a relation between the Hamiltonian and the Lagrangian framework as we can see in the following. Introducing the Lagrangian

$$L_{\mathrm{d}}(\mathbf{q}, \mathbf{y}) = \mathbf{p}^{\mathrm{T}}\mathbf{y} - H_{\mathrm{d}}(\mathbf{q}, \mathbf{p}), \tag{3.39}$$

where the new pseudo-velocities $\mathbf{y}$ satisfy

$$\mathbf{y} = \nabla_{\mathbf{p}}H_{\mathrm{d}}, \tag{3.40}$$

the closed-loop dynamics (3.22) can be written in the form

$$\frac{\mathrm{d}}{\mathrm{d}t}\left(\frac{\partial L_{\mathrm{d}}}{\partial \mathbf{y}}\right)^{\mathrm{T}} + \mathbf{Y}\left(\frac{\partial L_{\mathrm{d}}}{\partial \mathbf{q}}\right)^{\mathrm{T}} = \mathbf{Z}\,\mathbf{y}. \tag{3.41}$$

For the classical IDA approach (2.52) with $\mathbf{n}_{\mathrm{d}} = \mathbf{0}$, (3.41) describes the closed-loop system with $\mathbf{y} = \mathbf{M}_{\mathrm{d}}^{-1}\mathbf{M}\dot{\mathbf{q}}$, $\mathbf{Z} = \mathbf{J}_2 - \mathbf{R}_2$, and $\mathbf{Y} = -\mathbf{M}_{\mathrm{d}}\mathbf{M}^{-1}$ (cf. [22]). Notice also that (3.41) represents the Euler-Lagrange equations of motion for standard mechanical systems with velocity-proportional damping if $\mathbf{y} = \dot{\mathbf{q}}$, $\mathbf{Z} = -\mathbf{R}$, and $\mathbf{Y} = -\mathbf{I}$. Based thereupon, we can as well give the augmented formulation of the dynamics in Lagrangian form for the controller design and stability analysis as in [127]. However, for simplicity, and since IDA is not restricted to mechanical systems in its original formulation, we will restrict the analysis to the Hamiltonian representation (cf. Chapters 4 and 5).

In this chapter, we introduced a novel IDA controller design approach for underactuated mechanical systems based on a more general closed-loop Hamiltonian function—yet not completely free—that is not affected by physical damping, since dissipation is considered for the controller design from the very beginning. Additionally, the methodology is attractive from a practical point of view, for it does not require the solution of PDEs. The next chapter presents the controller parametrization via LLDA, and provides a framework consisting of five simple steps for the systematic controller design.

4 Controller Design Implementation

In Chapter 3, we assumed an augmented formulation for the desired Hamiltonian H_d in order to bypass the dissipation condition. This leads to a more general representation of the closed-loop pH system and a considerable amount of free parameters. Since the approach breaks the physical structure of the system, it is no longer possible to achieve a *physically motivated* choice of the design parameters by means of the potential energy and inertia matrix of the closed-loop system. This chapter shows that transparency with respect to achievable dynamics can be provided by *local linear dynamics assignment* (LLDA), nonetheless.

The remainder of the chapter is organized as follows: After the introduction of LLDA in Section 4.1, we show stability of the closed-loop system and provide an estimation of the domain of attraction of the equilibrium in Section 4.2. Section 4.3 gives a step-by-step guideline to systematically design augmented IDA controllers for the class of mechanical systems in consideration. Section 4.4 concludes the chapter with some final remarks.

4.1 Local linear dynamics assignment

In general, the control design via IDA requires the tuning of free parameters such that, besides from stability, the closed-loop system exhibits desired properties in terms of performance and/or robustness. By fixing $H_\mathrm{d} > 0$, the matching conditions are given by a set of algebraic equations. As mentioned earlier in Section 2.3.3, the main obstacle of the algebraic IDA-PBC approach lies, in fact, in choosing a positive definite desired Hamiltonian H_d such that $\mathbf{R}_\mathrm{d} \geq \mathbf{0}$ is a possible solution to the matching problem. Even if we manage to guarantee stability, it is uncertain how individual parameters affect the robustness, the estimate of the domain of attraction, or the transient dynamics.

The method of LLDA was first introduced in [113] to provide transparency in the parametrization of IDA controllers. Essentially, the idea is to parametrize the closed-loop dynamics according to a desired local behavior predefined by the designer. By

doing so, not only the choice of the free parameters is reduced to the election of appropriate eigenvalues for the linearized closed-loop dynamics—arising, e. g., from a linear quadratic regulator (LQR) [38, 103]—but also $\mathbf{R}_\mathrm{d} > \mathbf{0}$ is guaranteed in a neighborhood of the desired equilibrium $\mathbf{q}^*$, such that stability is provided. The adaptation of LLDA to time-varying systems, particularly to the design of an error controller for trajectory tracking, has been presented in [114]. The method has been later adapted to mechanical systems with underactuation degree one in [109], and it has been finally synthesized in [110].

The original approach was designed for the parametric and non-algebraic IDA. As we make use of the algebraic procedure from the previous chapter to solve the matching equations, we proceed slightly differently than in the original formulation. The principle, however, remains the same: The design parameters of the controller are chosen such that desired local dynamics are achieved by means of the eigenvalues of the linearized closed-loop system

$$\Delta\dot{\mathbf{x}} = \mathbf{A}_\mathrm{d}\Delta\mathbf{x}. \tag{4.1}$$

Remark 4.1.1. When applying LLDA to mechanical systems in the classical IDA formulation, the number of assignable eigenvalues is, in general, larger than the number of free parameters [109], such that LLDA can be applied only to some extent. On the contrary, the augmented formulation *always* provides enough design degrees of freedom to place all eigenvalues of the linearized closed-loop as desired if the linearized system is controllable.

Since LLDA relies on the assignment of desired closed-loop eigenvalues, the following assumption is required for its applicability

Assumption 4.1. The mechanical system is given by (3.1), and its linearization at the desired (admissible) equilibrium $\mathbf{q}^*$ is controllable.

Let

$$\Delta\dot{\mathbf{x}} = \mathbf{A}\Delta\mathbf{x} + \mathbf{B}\Delta\mathbf{u}, \qquad \Delta\mathbf{x} = \mathrm{col}(\mathbf{q}-\mathbf{q}^*, \mathbf{p}) \in \mathbb{R}^{2n}, \tag{4.2}$$

be the linearized mechanical system at $\mathbf{q} = \mathbf{q}^*$, $\mathbf{p}^* = \mathbf{0}$. Assumption 4.1 guarantees the existence of a linear state feedback $\Delta\mathbf{u} = -\mathbf{D}\Delta\mathbf{x}$, such that the matrix $\mathbf{A}_\mathrm{d} = \mathbf{A}–\mathbf{BD}$ has eigenvalues as requested. Then, a unique, positive definite matrix $\mathbf{P}_\mathrm{d}$ exists that solves the Lyapunov equation

$$\mathbf{A}_\mathrm{d}\mathbf{P}_\mathrm{d}^{-1} + \mathbf{P}_\mathrm{d}^{-1}\mathbf{A}_\mathrm{d}^\mathrm{T} = -2\mathbf{R}_{\mathrm{d}*} \tag{4.3}$$

for any $\mathbf{R}_{\mathrm{d}*} > \mathbf{0}$ (cf. [38]).

4.2 Stability and estimation of the domain of attraction

The parametrization of the closed-loop system via LLDA guarantees asymptotic stability of the equilibrium and, at least locally, desired transient dynamics. The following theorem synthesizes the result:

Theorem 4.1. *Let the conditions of Theorem 3.1 be satisfied. Let the stabilizing linear feedback* $\Delta\mathbf{u} = -\mathbf{D}\Delta\mathbf{x}$ *for the damped underactuated mechanical system (3.1) result in a closed-loop system locally approximated by the state matrix* $\mathbf{A}_\mathrm{d}$*. Fix* $\mathbf{R}_{\mathrm{d}*} > \mathbf{0}$ *and compute the solution*

$$\mathbf{P}_\mathrm{d} = \begin{bmatrix} \mathbf{P}_{\mathrm{d},11} & \mathbf{P}_{\mathrm{d},12} \\ \mathbf{P}_{\mathrm{d},12}^\mathrm{T} & \mathbf{P}_{\mathrm{d},22} \end{bmatrix} > \mathbf{0} \tag{4.4}$$

of (4.3). Set

$$\mathbf{Q}_\mathrm{d} = \mathbf{P}_{\mathrm{d},11}, \quad \mathbf{M}_{\mathrm{d}*} = \mathbf{P}_{\mathrm{d},22}^{-1}, \quad \mathbf{K}_{\mathrm{d}*} = -\mathbf{P}_{\mathrm{d},12}^\mathrm{T}\mathbf{P}_{\mathrm{d},11}^{-1}, \quad \begin{bmatrix} \mathbf{W}_* & \mathbf{X}_* \\ \mathbf{Y}_* & \mathbf{Z}_* \end{bmatrix} = \mathbf{A}_\mathrm{d}\mathbf{P}_\mathrm{d}^{-1}. \tag{4.5}$$

Fix V_d*, such that*

$$\nabla_\mathbf{q} V_\mathrm{d}|_{\mathbf{q}^*} = \mathbf{0}, \qquad \nabla_\mathbf{q}^2 V_\mathrm{d}\Big|_{\mathbf{q}^*} = \mathbf{Q}_\mathrm{d}, \tag{4.6}$$

and suppose one can find a solution $\mathbf{L}_\mathrm{d}$ *of (3.31) that satisfies* $\mathbf{L}_\mathrm{d}(\mathbf{q}^*) = \mathbf{Y}_*\mathbf{W}_*^{-1}$*. Then, the static state feedback (3.34) asymptotically stabilizes the equilibrium* $\mathbf{q}^*$*. According to Theorem 2.3, from the largest bounded level set of* H_d*, where* $\mathbf{R}_\mathrm{d} > \mathbf{0}$ *holds, an estimate of the domain of attraction can be derived. The closed-loop system is locally approximated by (4.1).*

Proof. The state feedback (3.34) transforms (3.1) into a pH system (3.22) according to Theorem 3.1. From the parameter choice in (4.5), and from the structure of the closed-loop energy (3.21),

$$\nabla_{(\mathbf{q},\mathbf{p})}^2 H_\mathrm{d}\Big|_{(\mathbf{q}^*,\mathbf{0})} = \mathbf{P}_\mathrm{d} > \mathbf{0} \tag{4.7}$$

can be deduced, i. e., positive definiteness of H_d in an open neighborhood of $(\mathbf{q}^*, \mathbf{0})$ is guaranteed. The dissipation matrix at the equilibrium is

$$\mathbf{R}_\mathrm{d}(\mathbf{q}^*) = -\frac{1}{2}\left(\mathbf{A}_\mathrm{d}\mathbf{P}_\mathrm{d}^{-1} + \mathbf{P}_\mathrm{d}^{-1}\mathbf{A}_\mathrm{d}^\mathrm{T}\right) = \mathbf{R}_{\mathrm{d}*} > \mathbf{0}. \tag{4.8}$$

Since the elements of $\mathbf{R}_\mathrm{d}$ are continuous functions in $\mathbf{q}$, strong dissipativity in an open neighborhood of $(\mathbf{q}^*, \mathbf{0})$ is guaranteed. An estimate of the region of attraction follows

from usual Lyapunov arguments. The linearization of the closed-loop pH system around $(\mathbf{q}^*, \mathbf{0})$ directly yields (4.1). ■

The difficulty in augmented IDA mainly lies in the vast amount of free parameters and functions to be tuned. Even after the parametrization via LLDA, fixing the function V_d, the matrix $\mathbf{R}_{\mathrm{d}*}$, and the matrix-valued function $\mathbf{K}_\mathrm{d}$ still possesses great optimization potential. Apart from their local approximation at the equilibrium, V_d and $\mathbf{K}_\mathrm{d}$ can be freely chosen; the matrix $\mathbf{R}_{\mathrm{d}*}$ is only required to be positive definite. In [104], the authors introduced a procedure to optimally determine remaining degrees of freedom after the application of LLDA for IDA controllers. The algorithm maximizes the domain of attraction of the desired equilibrium together with its estimation.

4.3 Constructive augmented IDA for a class of mechanical systems

In this section, we present a scheme to compute the augmented IDA controller for the class of systems that satisfy the condition of Theorem 3.1. The approach is systematic and, therefore, easy to implement. The following five steps summarize the controller design procedure:

Step 1: Finding a stabilizing linear state feedback. In this initial step, we design a linear state feedback $\mathbf{u} = -\mathbf{D}\Delta\mathbf{x}$ to both stabilize the equilibrium $(\mathbf{q}^*, \mathbf{0})$ and achieve desired dynamical behavior in terms of robustness and performance. Since the linearized system is assumed to be controllable, it is always possible to find a feedback matrix $\mathbf{D}$ such that all eigenvalues of the linearized closed-loop system

$$\Delta\dot{\mathbf{x}} = \mathbf{A}_\mathrm{d}\Delta\mathbf{x}, \qquad \Delta\mathbf{x} = (\mathbf{q} - \mathbf{q}^*, \mathbf{p}) \in \mathbb{R}^{2n}, \tag{4.9}$$

can be placed as requested. The designer can either directly choose the eigenvalues or, alternatively, optimally determine $\mathbf{D}$ via LQR design.

Step 2: Solving the Lyapunov equation. In this step, we are interested in the solution $\mathbf{P}_\mathrm{d}^{-1}$ of the Lyapunov equation

$$\mathbf{A}_\mathrm{d}\mathbf{P}_\mathrm{d}^{-1} + \mathbf{P}_\mathrm{d}^{-1}\mathbf{A}_\mathrm{d}^\mathrm{T} = -2\mathbf{R}_{\mathrm{d}*}. \tag{4.10}$$

The matrix $\mathbf{R}_{\mathrm{d}*} = \mathbf{R}_{\mathrm{d}*}^\mathrm{T} > \mathbf{0}$ is a free parameter that does not affect the local behavior, as it is completely specified by the choice of eigenvalues in Step 1. However, the choice of $\mathbf{R}_{\mathrm{d}*}$ has some implications regarding the estimate of the region of attraction. The

elements of $\mathbf{R}_{\mathrm{d}*}$ can, for instance, be optimized employing the procedure presented in [104] to maximize the estimate of the DA. The matrix $\mathbf{P}_{\mathrm{d}}$, which stems from the solution of (4.10), is the Hessian of the closed-loop Hamiltonian at $(\mathbf{q}^*, \mathbf{0})$

$$\nabla^2_{(\mathbf{q},\mathbf{p})} H_{\mathrm{d}} \Big|_{(\mathbf{q}^*,\mathbf{0})} = \begin{bmatrix} \mathbf{Q}_{\mathrm{d}} & -\mathbf{Q}_{\mathrm{d}}\mathbf{K}_{\mathrm{d}*}^{\mathrm{T}} \\ -\mathbf{K}_{\mathrm{d}*}\mathbf{Q}_{\mathrm{d}} & \mathbf{M}_{\mathrm{d}*}^{-1} \end{bmatrix} = \mathbf{P}_{\mathrm{d}}. \tag{4.11}$$

From the closed-loop state matrix in (4.9) and the local approximation of the Hamiltonian (4.11), the desired interconnection and damping matrices at the equilibrium can be directly computed as

$$\begin{bmatrix} \mathbf{W}_* & \mathbf{X}_* \\ \mathbf{Y}_* & \mathbf{Z}_* \end{bmatrix} = \mathbf{J}_{\mathrm{d}}(\mathbf{q}^*, \mathbf{0}) - \mathbf{R}_{\mathrm{d}}(\mathbf{q}^*) = \mathbf{A}_{\mathrm{d}}\mathbf{P}_{\mathrm{d}}^{-1}. \tag{4.12}$$

Step 3: Fixing of the Hamiltonian. As we are considering the algebraic problem, the closed-loop Hamiltonian needs to be fixed in advance. In order to guarantee the desired local behavior from Step 1, the matrix-valued function $\mathbf{K}_{\mathrm{d}}(\mathbf{q})$, and the potential energy $V_{\mathrm{d}}(\mathbf{q})$ have to satisfy

$$\nabla^2_{\mathbf{q}} V_{\mathrm{d}}(\mathbf{q})\Big|_{\mathbf{q}^*} = \mathbf{Q}_{\mathrm{d}}, \qquad \nabla_{\mathbf{q}} V_{\mathrm{d}}(\mathbf{q})|_{\mathbf{q}^*} = \mathbf{0}, \qquad \mathbf{K}_{\mathrm{d}}(\mathbf{q}^*) = \mathbf{K}_{\mathrm{d}*}. \tag{4.13}$$

How to specifically choose both functions cannot be generalized. However, the simplest choice

$$V_{\mathrm{d}} = \frac{1}{2}\mathbf{q}^{\mathrm{T}}\mathbf{Q}_{\mathrm{d}}\mathbf{q}, \qquad \mathbf{K}_{\mathrm{d}}(\mathbf{q}) = \mathbf{K}_{\mathrm{d}*}$$

fulfills the conditions (4.13).

Step 4: Solving the matching equation. According to Theorem 3.1, for the computation of the stabilizing controller, it is sufficient to find a solution $\mathbf{L}_{\mathrm{d}}$ to the *scalar* matching equation

$$\mathbf{G}_{\perp}\left(\nabla_{\mathbf{q}} V - \mathbf{L}_{\mathrm{d}}\mathbf{K}_{\mathrm{d}}\nabla_{\mathbf{q}} V_{\mathrm{d}}\right) = 0.$$

To guarantee the local behavior specified in Step 1, the matrix $\mathbf{L}_{\mathrm{d}}(\mathbf{q})$ is required to satisfy $\mathbf{L}_{\mathrm{d}}(\mathbf{q}^*) = \mathbf{Y}_*\mathbf{W}_*^{-1}$ as specified in Theorem 4.1. It is not difficult to find such a matrix $\mathbf{L}_{\mathrm{d}}$. However, this step should be done with care: Some elements of $\mathbf{L}_{\mathrm{d}}(\mathbf{q})$ might need to be smartly fixed in advance to ensure a suitable solution (cf. Chapter 5).

Step 5: Computation of remaining matrices and control law. In this final

step, the matrix-valued functions $\mathbf{Y}$ and $\mathbf{Z}_0$ are calculated from

$$\mathbf{Y} = -\left(\mathbf{L}_\mathrm{d}\mathbf{M}_{\mathrm{d}*}^{-1}\mathbf{M} + \mathbf{R} + \mathbf{S}_\mathrm{d}\right)\mathbf{M}^{-1}\left(\mathbf{K}_\mathrm{d}\left(\frac{\partial \mathbf{n}_\mathrm{d}}{\partial \mathbf{q}}\right)^\mathrm{T} + \mathbf{M}_{\mathrm{d}*}^{-1}\right)^{-1}\mathbf{K}_\mathrm{d},$$

and

$$\mathbf{Z}_0 = -\left(\mathbf{Y}\left(\frac{\partial \mathbf{n}_\mathrm{d}}{\partial \mathbf{q}}\right)^\mathrm{T} + \mathbf{R}\mathbf{M}^{-1} + \mathbf{S}_\mathrm{d}\mathbf{M}^{-1}\right)\mathbf{M}_{\mathrm{d}*} + \mathbf{G}\boldsymbol{\eta}^\mathrm{T},$$

according to Theorem 3.1. The vector-valued function $\boldsymbol{\eta} = \boldsymbol{\eta}(\mathbf{q})$ has to be chosen such that $\mathbf{Z}_0(\mathbf{q}^*) = \mathbf{Z}_*$. Otherwise, it is free to shape and can be used, for instance, to inject nonlinear damping. See, e. g., Section 5.3. Finally, the control law is computed from (3.34).

4.4 Concluding remarks

This chapter presented the parametrization via LLDA for the augmented IDA approach of the previous chapter. We presented a scheme of five simple steps for the computation and parametrization of a stabilizing controller. Based on the design of a desired Hamiltonian for the closed-loop system that is not of mechanical form, we were able to overcome three of the main obstacles arising in IDA-PBC: First, even if the dissipation condition is not satisfied, we are able to systematically design energy-based stabilizing controllers. Second, the closed-loop system can be entirely parametrized via LLDA. Third, the solution of PDEs is obviated, as we consider the algebraic matching problem by fixing the closed-loop Hamiltonian. The resulting nonlinear controller guarantees desired local behavior and provides an estimate of the domain of attraction based on standard Lyapunov arguments. There is, however, a significant amount of free degrees of freedom that can be exploited for the controller design: Apart from the desired eigenvalues of the closed-loop system, the right hand side $\mathbf{R}_{\mathrm{d}*}$ of the Lyapunov equation (4.10) is a free design parameter. Additionally, besides from conditions (4.13), the matrix-valued function $\mathbf{K}_\mathrm{d}(\mathbf{q})$, and the potential energy $V_\mathrm{d}(\mathbf{q})$ are free functions, just as the matrix $\mathbf{L}_\mathrm{d}(\mathbf{q})$ and the vector-valued function $\boldsymbol{\eta}(\mathbf{q})$, which are only fixed at the equilibrium $\mathbf{q}^*$. Due to the large number of design quantities it is indispensable to integrate the controller design sketched above into an optimization loop. One possibility is to maximize the domain of attraction as presented in [104].

The next chapter shows the applicability of the method with a series of simulations and experiments using well-known benchmark systems.

5 Applications

In this chapter, we demonstrate the applicability and performance of the augmented IDA approach developed in Chapter 3 and Chapter 4. We consider three different well-known benchmark systems: the acrobot, the inertia wheel pendulum (IWP), and the inverted pendulum on a cart (IP). These underactuated mechanical systems are widely employed for nonlinear control problems and robotics, for they are *"complex enough to yield a rich source of nonlinear control problems, yet simple enough to permit a complete mathematical analysis"* [195]. The motivation for the acrobot and the pendulum systems is more than only academical, though. Take, for instance, the liftoff of a space shuttle. While the main thruster pushes the rocket upwards, smaller thrusters actively stabilize the pitch angle of the system for it to remain stable. The problem is not very different from the inverted pendulum on a cart. The same stabilization problem is again found in Segway-like systems used for human transportation [128, 186], and even in ship dynamics: Although capsize in large ships is rare, roll instabilities can occur with a catastrophic outcome. Thus, the response of the ship dynamics to sea waves, and, in particular, the roll motion, needs to be passively or actively stabilized [120]. The inertia wheel pendulum is found in [72] as a model for a monorail tramway, whose roll motion is stabilized by an inertia wheel. In biomechanics, the pendulum and the acrobot are used for the modeling of bipedal walking as can be found in [75]. During the leg-swinging period, the leg in contact with the ground can be seen as an acrobot-like system; the hanging leg as a free swinging pendulum.

The dynamics of all three benchmark systems can be described by the well-known second order differential equation

$$\mathbf{M}\ddot{\mathbf{q}} + \mathbf{C}\dot{\mathbf{q}} + \nabla_{\mathbf{q}} V = \mathbf{G}\mathbf{u} - \mathbf{R}\dot{\mathbf{q}}. \tag{5.1}$$

All three systems are controllable (at the equilibrium point of interest), have two degrees of freedom and just one input, and all three fail to satisfy the dissipation condition[1] for a matrix $\mathbf{R} \neq \mathbf{0}$, satisfying $\mathbf{G}_\perp \mathbf{R} \neq \mathbf{0}$, which is assumed in the following. In other words,

[1] Although the DC depends on the chosen closed-loop inertia matrix $\mathbf{M}_\mathrm{d}$, it can be shown that the DC can never be satisfied.

since energy gets dissipated in the unactuated coordinate, the conventional passivity-based stability analysis in IDA fails.

There is a large number of studies about the analysis and control of underactuated mechanical systems. In particular, the three benchmark systems considered in this chapter are found in countless publications. Their simple construction and the inherent nonlinear and unstable dynamics make them appropriate test-beds for the design of a variety of classical and novel control techniques. For it is impossible to give a complete overview of the past work, we simply refer to the following relevant contributions [141, 150, 194, 196, 198], and the references therein. For the sake of clarity and consistency, in the following we compare the augmented IDA approach with a classical IDA controller found in the literature, and with a linear quadratic optimal state feedback (LQR). The augmented IDA controller and the LQR are equally parametrized in terms of the eigenvalues of the linearized closed-loop system; the free parameters of the classical IDA controller are chosen according to the reference the controller is taken from.

Remark 5.0.1. The configuration space of the benchmark systems can be seen either locally as $\mathcal{Q} = \mathbb{R}^2$ or, taking into account the periodicity of the angular variables, as $\mathcal{Q} = \mathbb{S}^2$ (for the acrobot and the IWP), or $\mathcal{Q} = \mathbb{R} \times \mathbb{S}^1$ (for the IP). However, we adopt the local form for the controller design to allow for feedback laws that are not necessarily periodic in their variables. Although it constitutes a parametrization that does not globally represent the dynamics accurately, this simplification is often valid for the practical implementation, as the dynamics of each system are usually restricted to a region of physical interest.

5.1 The acrobot

The term *acrobot* was coined at Berkeley by Murray and Hauser in the nineties as an abbreviation for *acrobatic robot* [84, 140]. Basically, the acrobot is a two-link planar robot arm with an actuator at the elbow and no actuator at the shoulder. Figure 5.1 shows the schematic construction of the acrobot, which resembles a gymnast performing on a single bar. The dynamical model can be found, e. g., in [131, 150, 195], and is uniquely characterized by the system's mass matrix

$$\mathbf{M}(\mathbf{q}) = \begin{bmatrix} c_1 + c_2 + 2c_3 \cos q_2 & c_2 + c_3 \cos q_2 \\ c_2 + c_3 \cos q_2 & c_2 \end{bmatrix}, \tag{5.2}$$

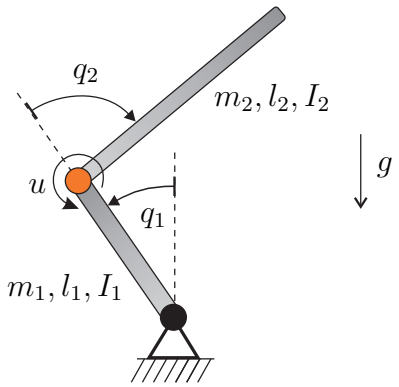

Figure 5.1: The acrobot. The elbow is actuated (orange joint); the shoulder unactuated (black joint).

its potential energy

$$V(\mathbf{q}) = c_4 g \cos q_1 + c_5 g \cos(q_1 + q_2), \tag{5.3}$$

and the input matrix

$$\mathbf{G} = \begin{bmatrix} 1 \\ 0 \end{bmatrix}. \tag{5.4}$$

The configuration space is parametrized by q_1 and q_2, where q_1 denotes the angle of the first link with respect to the vertical position, and q_2 denotes the relative angle of rotation of the second link with respect to q_1. The acrobot is subject to the gravitational acceleration g. We assume massless joints and homogeneous links such that the constant parameters c_i are given as

$$c_1 = \frac{1}{4} m_1 l_1^2 + m_2 l_1^2 + I_1, \quad c_2 = \frac{1}{4} m_2 l_2^2 + I_2,$$
$$c_3 = \frac{1}{2} m_2 l_1 l_2, \quad c_4 = \frac{1}{4} m_1 l_1 + m_2 l_1, \quad c_5 = \frac{1}{2} m_2 l_2,$$

where m_i, l_i, and I_i represent the mass, the length, and the moment of inertia of the i-th link, respectively. Additionally, we consider only dissipation in the unactuated coordinate[2] given by the viscous damping matrix

$$\mathbf{R} = \begin{bmatrix} r_1 & 0 \\ 0 & 0 \end{bmatrix}. \tag{5.5}$$

Especially, the swing-up problem of the acrobot attracted the attention of researchers in the past decades [195, 210, 211]. Energy-based swing-up control laws have been

[2]The dissipation in the actuated coordinate is assumed to be fully compensated.

designed, which have been again inspired by the gymnast: by swinging the legs, the gymnast is able to bring himself up into a vertical position above the bar. In the upward (unstable) equilibrium, a second controller is required for the stabilization of the acrobot. The stabilizing controller is usually a linear or a stabilizing energy-based state feedback [109, 131]. Our goal is to design an augmented IDA controller capable of stabilizing the upward (unstable) equilibrium of the acrobot with dissipation in the unactuated joint. Note that the admissible equilibria are characterized by

$$\mathbf{G}_\perp \nabla_{\mathbf{q}} V(\mathbf{q}) = c_4 g \sin q_1 + c_5 g \sin(q_1 + q_2) = 0. \tag{5.6}$$

We will, however, restrict the analysis to the upward equilibrium given by $\mathbf{q}^* = \mathbf{0}$. The parameters of the acrobot are borrowed from [131] and are given in Table 5.1.

Table 5.1: Model parameters for the acrobot.

Parameter	Value	Unit
c_1	2.333	$\mathrm{kg\,m^2}$
c_2	5.333	$\mathrm{kg\,m^2}$
c_3	2.0	$\mathrm{kg\,m^2}$
c_4	3.0	$\mathrm{kg\,m}$
c_5	2.0	$\mathrm{kg\,m}$
r_1	0.2	$\mathrm{kg\,m^2/s}$
g	9.81	$\mathrm{m/s^2}$

Controller design

In this section, we apply the procedure developed in Chapter 4 to design a stabilizing controller. To that end, and according to Theorem 3.1, we first need to check if a solution $\mathbf{\Gamma}$ to (3.28) exists. Clearly, the inertia matrix $\mathbf{M} = \mathbf{M}(q_2)$ does not depend on unactuated coordinates. As a consequence, $\mathbf{G}_\perp \nabla_{\mathbf{q}} \left(\mathbf{p}^{\mathrm{T}} \mathbf{M}^{-1} \mathbf{p} \right) = \mathbf{0}$, and the matching equation for the kinetic energy (3.28) is trivially satisfied setting $\mathbf{\Gamma} = \mathbf{0}$. For consistency, for the remaining of the controller design procedure, we follow the steps of Section 4.3. The first three steps are straightforward: we choose the linear controller $u = -\mathbf{D}\mathbf{x}$ to be a LQR that minimizes the cost function

$$J = \frac{1}{2} \int_0^\infty \mathbf{q}^{\mathrm{T}} \mathbf{Q}_{\mathbf{q}} \mathbf{q} + \mathbf{p}^{\mathrm{T}} \mathbf{Q}_{\mathbf{p}} \mathbf{p} + r u^2 \, \mathrm{d}t, \tag{5.7}$$

with weighting factors

$$\mathbf{Q}_\mathbf{q} = \begin{bmatrix} 1 & 0 \\ 0 & 1 \end{bmatrix}, \qquad \mathbf{Q}_\mathbf{p} = \begin{bmatrix} 100 & 0 \\ 0 & 100 \end{bmatrix}, \qquad r = 1. \tag{5.8}$$

This choice results in the feedback gain $\mathbf{D} = [-449.1, -179.7, -33.8, 19.3]$, and leads to closed-loop eigenvalues $\Lambda(\mathbf{A}_\mathrm{d}) = \{-11.07, -4.01+j1.84, -4.01-j1.84, -0.32\}$. To compute the solution to the Lyapunov equation (4.10), the positive definite matrix on the right hand side is set as $\mathbf{R}_{\mathrm{d}*} = \mathrm{diag}(0.5, 2.25, 1200, 50)$[3]. Finally, and for simplicity, the closed-loop potential energy is chosen to be quadratic

$$V_\mathrm{d}(\mathbf{q}) = \frac{1}{2}\,\mathbf{q}^\mathrm{T}\mathbf{Q}_\mathrm{d}\mathbf{q}, \tag{5.9}$$

and $\mathbf{K}_\mathrm{d}(\mathbf{q}) = \mathbf{K}_{\mathrm{d}*}$ is fixed. In the fourth step, we are concerned with the solution $\mathbf{L}_\mathrm{d}$ to the matching equation (3.31). For the acrobot example, (3.31) can be explicitly given as

$$c_4 g \sin q_1 + c_5 g \sin(q_1+q_2) - \begin{bmatrix} L_{\mathrm{d},21} & L_{\mathrm{d},22} \end{bmatrix} \begin{bmatrix} a_1 q_1 + a_2 q_2 \\ a_3 q_1 + a_4 q_2 \end{bmatrix} = 0, \tag{5.10}$$

for some constants a_i. In order to avoid singularities in the solution, we use the relation

$$\sin(q_1+q_2) = \sin q_1 \cos q_2 + \cos q_1 \sin q_2$$

to split (5.10) into two equations

$$(c_4 + c_5 \cos q_2)\, g \sin q_1 - (L_{\mathrm{d},21} a_1 + L_{\mathrm{d},22} a_3)\, q_1 = 0 \tag{5.11a}$$

$$c_5 g \cos q_1 \sin q_2 - (L_{\mathrm{d},21} a_2 + L_{\mathrm{d},22} a_4)\, q_2 = 0 \tag{5.11b}$$

that are solved for $L_{\mathrm{d},21}$ and $L_{\mathrm{d},22}$ independently. The two remaining coefficients of the matrix $\mathbf{L}_\mathrm{d}$, namely $L_{\mathrm{d},11}$ and $L_{\mathrm{d},12}$, are chosen to be constant and such that $\mathbf{L}_\mathrm{d}(\mathbf{0}) = \mathbf{Y}_* \mathbf{W}_*^{-1}$ holds. The fifth and last step is kept simple: We set the vector-valued function $\boldsymbol{\eta}(\mathbf{q})$ to be constant, and determine its coefficients to satisfy $\mathbf{Z}_0(\mathbf{0}) = \mathbf{Z}_*$.

[3] For simplicity, the matrix $\mathbf{R}_{\mathrm{d}*}$ is assumed to be of diagonal form. We have used a heuristic approach to optimize the value of the diagonal coefficients: the space $\mathbb{R}^4$ is discretized in an interval $[\underline{r}_{\mathrm{d}*,j}, \bar{r}_{\mathrm{d}*,j}]$ $(j = 1, \ldots 4)$ using equidistant discrete points. Thereafter, we determine the estimate of the DA of the equilibrium for each of the possible combinations, and finally fix $\mathbf{R}_{\mathrm{d}*}$ with the coefficients that maximize the estimate of the DA.

Comparison with benchmark controllers

In order to illustrate the effectiveness of the method proposed in this thesis, we compare our controller with a LQR, and a classical IDA controller, which was desinged by Mahindrakar and coworkers for the undamped system [131]. Figure 5.2 shows the estimated (left) and simulated (right) stability margins of the closed-loop system for the three different controllers. In the left figure, the white area represents the set where the dissipation matrix $\mathbf{R}_\mathrm{d}$ is positive definite. Although the real stability margins show that both the LQR and the augmented IDA controller lead to a similar DA, the blue ellipse limits an area 34 times larger than the estimate of the DA given by the linear controller. As the DC is not satisfied, no estimation for the DA for IDA can be given. It should be noted that the DA is defined in the phase-space, which consists of the configuration variables as well as the generalized momenta. For that reason, the DA is a four-dimensional set. Figure 5.2 shows only a two-dimensional subset thereof. However, since $\mathbf{R}_\mathrm{d}$ only depends on $\mathbf{q}$, and the energy function is quadratic, the ellipses in the two-dimensional plane accurately represent the level sets that estimates the boundary of the DA for $\mathbf{p}_0 = \mathbf{0}$.

By adding damping in the unactuated coordinate, the IDA-PBC controller developed in [131] yields a closed-loop with indefinite dissipation matrix $\mathbf{R}_\mathrm{d}$. For that reason, no stability of the equilibrium can be proven by standard Lyapunov arguments. However, as the real (simulated) stability margins in Figure 5.2 (right) show, the IDA controller does, in fact, stabilize the equilibrium $\mathbf{q}^* = \mathbf{0}$.

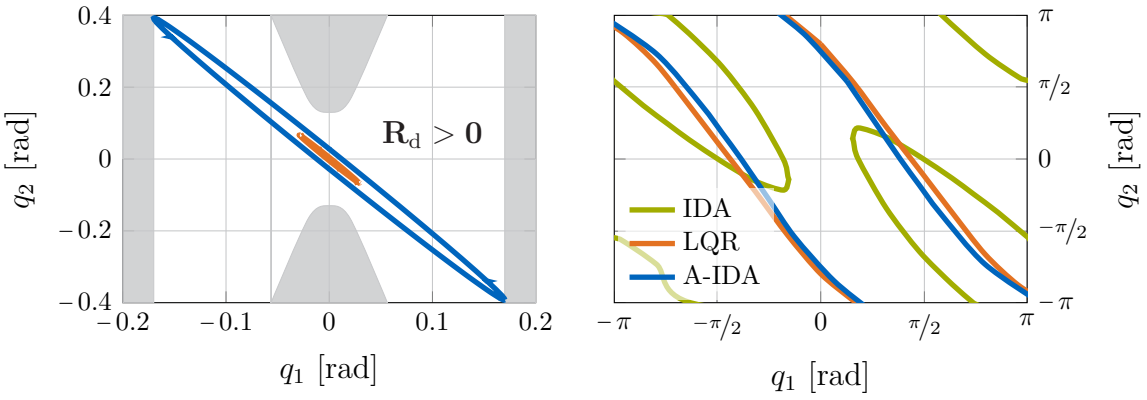

Figure 5.2: Comparison of the estimated (left) and real (right) stability boundaries of the acrobot with respect to the equilibrium $\mathbf{q}^* = \mathbf{0}$ for the different controllers. In the left figure, the white area represents the set, where the closed-loop dissipation matrix $\mathbf{R}_\mathrm{d}$ is positive definite. As the DC is not satisfied, no estimation for the DA for IDA can be given.

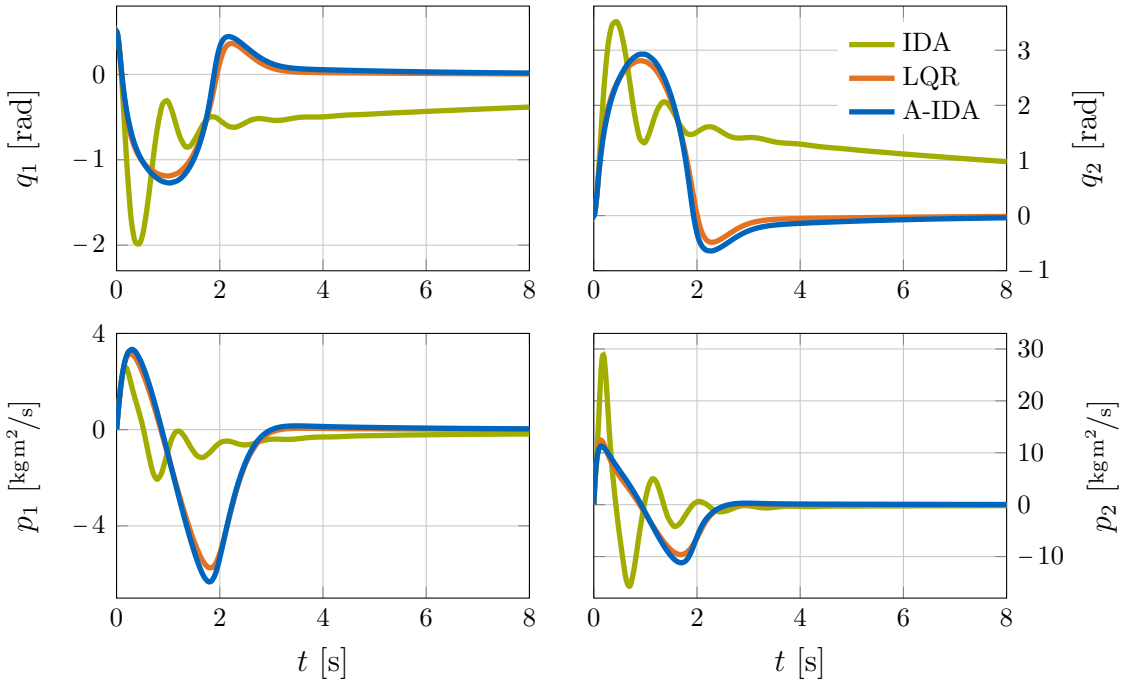

Figure 5.3: The acrobot's transient dynamics for an initial error $\mathbf{q}_0 = (0.5, 0)$, $\mathbf{p}_0 = \mathbf{0}$. While both the LQR and the augmented IDA controller show similar behaviors, the classical IDA approach exhibits oscillations and slow convergence towards the desired equilibrium.

Figure 5.3 shows the time evolution of the states for initial values $\mathbf{q}_0 = (0.5, 0)$ and $\mathbf{p}_0 = \mathbf{0}$. While all three controllers stabilize the system, the classical IDA controller shows oscillating behavior and a slower transient response. Different parameter choices only result in slightly different transient dynamics. With regard to the method proposed in this thesis, it clearly shows similar transient dynamics compared to the linear controller. This result was also expected, as the LQR was used for the parametrization of the augmented IDA via LLDA.

5.2 The inertia wheel pendulum

Spong et al. [197] introduced the *reaction wheel pendulum*—also known as inertia wheel pendulum (IWP)—in 2001. In their work, the authors present two different nonlinear control laws based on a feedback linearization to swing-up and stabilize the system. Since then, the IWP has served as a benchmark for the implementation of a vast number of control laws [36], including passivity-based approaches for stabilization and tracking [80, 158, 199]. As shown in Figure 5.4, the system consists of a simple pendulum with an inertia wheel at the end. Both the pendulum's and the wheel's axis

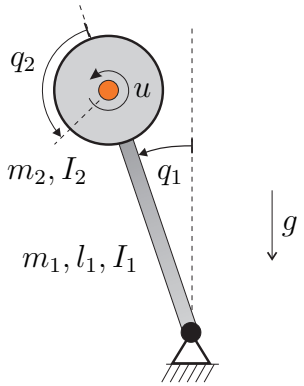

Figure 5.4: The inertia wheel pendulum.

of rotation are parallel, such that the acceleration of the wheel by the motor torque generates a reaction torque on the pendulum's axis. The configuration $\mathbf{q}$ consists of the pitch angle q_1, and the relative angle of rotation q_2 of the reaction wheel with respect to the pendulum. The model parameters of the IWP are given as

$$\mathbf{M} = \begin{bmatrix} c_1 & 0 \\ 0 & c_2 \end{bmatrix}, \quad V(\mathbf{q}) = c_3 \cos q_1, \quad \mathbf{G} = \begin{bmatrix} -1 \\ 1 \end{bmatrix}, \tag{5.12}$$

where

$$c_1 = \frac{1}{4} m_1 l_1^2 + m_2 l_1^2 + I_1 + I_2, \quad c_2 = I_2, \quad c_3 = g l_1 (\frac{1}{2} m_1 + m_2).$$

Here again, the parameters m_i and I_i represent the mass and the moment of inertia of the i-th link, respectively. The length of the pendulum is given by l_1 and g denotes the gravitational acceleration. In the same manner as the acrobot example, we consider physical dissipation in the unactuated coordinate given by the viscous damping matrix

$$\mathbf{R} = \begin{bmatrix} r_1 & 0 \\ 0 & 0 \end{bmatrix}. \tag{5.13}$$

The parameters of the IWP are borrowed from [158] and are given in Table 5.2.

Controller design

Since the inertia matrix of the IWP is constant, the matching equation for the kinetic energy (3.28) is satisfied for $\mathbf{\Gamma} = \mathbf{0}$. In the first step of the design procedure, we let the

Table 5.2: Model parameters for the inertia wheel pendulum.

Parameter	Value	Unit
c_1	0.1	$\mathrm{kg\,m^2}$
c_2	0.2	$\mathrm{kg\,m^2}$
c_3	10	$\mathrm{kg\,m^2}$
r_1	0.2	$\mathrm{kg\,m^2/s}$
g	9.81	$\mathrm{m/s^2}$

linear controller be a LQR that minimizes the cost function

$$J = \frac{1}{2} \int_0^\infty \mathbf{q}^\mathrm{T} \mathbf{Q}_\mathbf{q} \mathbf{q} + \mathbf{p}^\mathrm{T} \mathbf{Q}_\mathbf{p} \mathbf{p} + r u^2 \,\mathrm{d}t, \tag{5.14}$$

with the same weighting factors from the acrobot example

$$\mathbf{Q}_\mathbf{q} = \begin{bmatrix} 1 & 0 \\ 0 & 1 \end{bmatrix}, \qquad \mathbf{Q}_\mathbf{p} = \begin{bmatrix} 100 & 0 \\ 0 & 100 \end{bmatrix}, \qquad r = 1. \tag{5.15}$$

For the IWP, this choice results in $\mathbf{D} = [-45.1, -1.0, -42.0, -11.6]$, and leads to eigenvalues $\Lambda(\mathbf{A}_\mathrm{d}) = \{-17.83, -7.03 + j2.56, -7.03 - j2.56, -0.5\}$. Using the same heuristic approach from the previous example to determine the desired dissipation matrix at the equilibrium $\mathbf{q}^* = \mathbf{0}$, we set $\mathbf{R}_{\mathrm{d}*} = \mathrm{diag}(0.3, 16, 1.2, 0.4)$. To maintain the controller design as simple as possible, we choose $\mathbf{K}_\mathrm{d}(\mathbf{q}) = \mathbf{K}_{\mathrm{d}*}$, and set

$$V_\mathrm{d}(\mathbf{q}) = \frac{1}{2} \mathbf{q}^\mathrm{T} \mathbf{Q}_\mathrm{d} \mathbf{q} \tag{5.16}$$

for the closed-loop potential energy. The next step consists of determining the solution $\mathbf{L}_\mathrm{d}$ to the matching equation (3.31). For the IWP, (3.31) can be given as

$$c_3 \sin q_1 + \begin{bmatrix} L_{\mathrm{d},11} + L_{\mathrm{d},21} & L_{\mathrm{d},12} + L_{\mathrm{d},22} \end{bmatrix} \begin{bmatrix} a_1 q_1 + a_2 q_2 \\ a_3 q_1 + a_4 q_2 \end{bmatrix} = 0, \tag{5.17}$$

for some constants a_i. As in the previous example, we assign $L_{\mathrm{d},11}$ and $L_{\mathrm{d},12}$ constant values and solve the equations

$$c_3 \sin q_1 - \left(\left(L_{\mathrm{d},11} + L_{\mathrm{d},21} \right) a_1 + \left(L_{\mathrm{d},12} + L_{\mathrm{d},22} \right) a_3 \right) q_1 = 0 \tag{5.18}$$

$$\left(L_{\mathrm{d},11} + L_{\mathrm{d},21} \right) a_2 + \left(L_{\mathrm{d},12} + L_{\mathrm{d},22} \right) a_4 = 0 \tag{5.19}$$

for $L_{\mathrm{d},21}$ and $L_{\mathrm{d},22}$. In the last step, we set the vector-valued function $\boldsymbol{\eta}(\mathbf{q})$ to be constant.

Comparison with benchmark controllers

In one of the first works on IDA for mechanical systems, Ortega et al. [158] develop a controller capable of asymptotically stabilizing the IWP at the equilibrium $\mathbf{q}^* = \mathbf{0}$ without velocity feedback. The required velocities are generated by filtering the position measurements. For the sake of fairness in the comparison, we consider the IDA controller from [158] including velocity feedback. As we consider damping in the unactuated coordinates, this controller fails to provide an estimate for the DA of the equilibrium; the estimated stability margins of the closed-loop system for the proposed approach and for the LQR are shown in Figure 5.5. Although both the linear controller and the controller proposed in this work provide a large estimate of the DA, the area estimated by the blue ellipse (A-IDA) is 28% larger than the area enclosed by the orange ellipse (LQR).

In order to illustrate the differences in the transient dynamics, we have run the simulations choosing a rather large initial error in the pendulum's angle as shown in Figure 5.6. A simple observation shows that all three controllers—including the IDA controller from

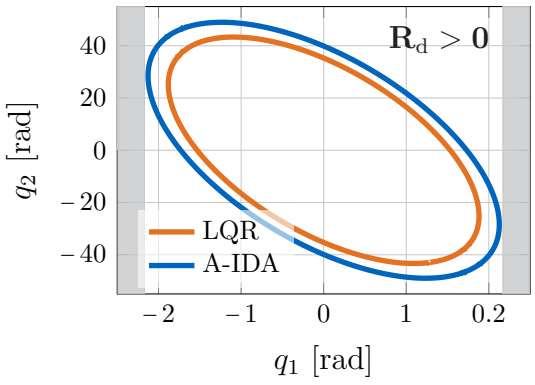

Figure 5.5: Estimated stability boundaries of the IWP with respect to the equilibrium $\mathbf{q}^* = \mathbf{0}$ for the LQR (orange) and the augmented IDA controller (blue).

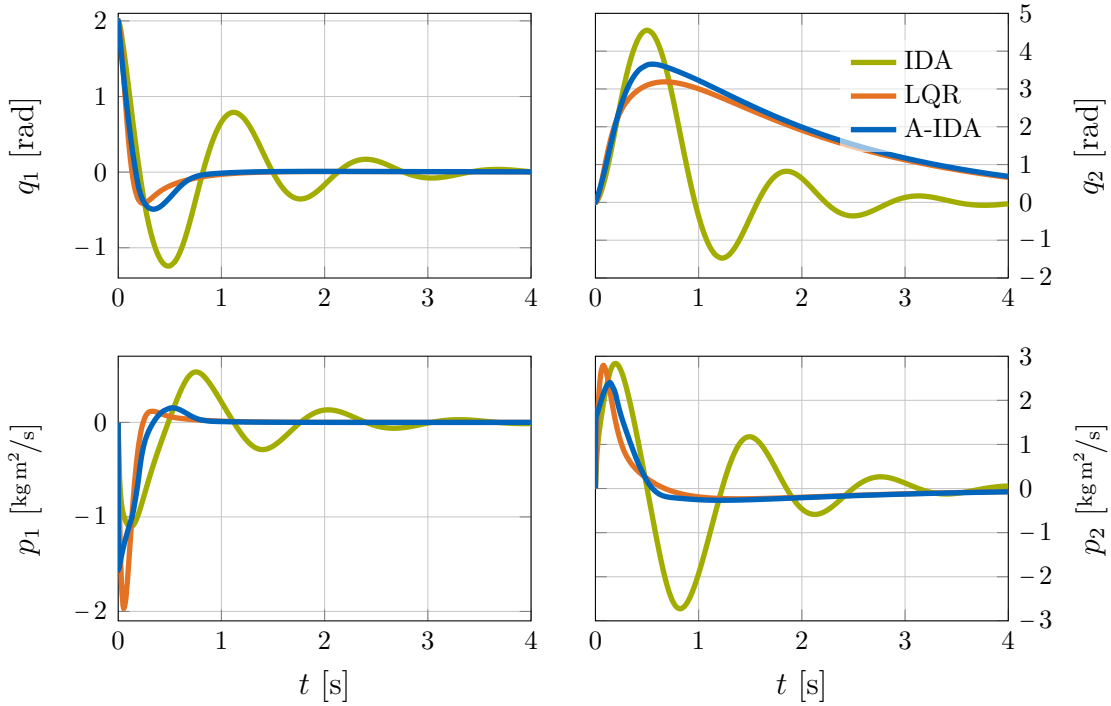

Figure 5.6: Transient dynamics of the IWP for an initial error $\mathbf{q}_0 = (2, 0)$, $\mathbf{p}_0 = \mathbf{0}$. The proposed approach shows fast convergence towards the equilibrium without undesired oscillations.

[158]—stabilize the desired equilibrium. In fact, simulations show that all three controllers stabilize the desired equilibrium for arbitrary initial conditions up to a set of Lebesgue measure 0, which corresponds to the stable equilibrium point. However, in contrast to the classical IDA approach, the augmented IDA shows fast convergence and oscillation-free transient dynamics. Additionally, the proposed controller is transparent to parametrize via LLDA, as we can assign, locally, arbitrary desired linear dynamics. The conventional IDA design does not provide enough degrees of freedom to eliminate the undesired oscillations of the closed-loop transient dynamics.

5.3 The inverted pendulum on a cart

One of the most common examples of underactuated mechanical systems in control theory is the inverted pendulum on a cart (IP), or cart-pole, shown in Figure 5.7. A lot of effort has been put in the design of nonlinear controllers for stabilization and tracking of the IP: the approaches are diverse and range from the classical linear state feedback and control laws based on a partial feedback linearization (PFL) [2, 194], to energy shaping methods [32, 43, 83, 205, 214], immersion and invariance [3], backstepping [149], sliding

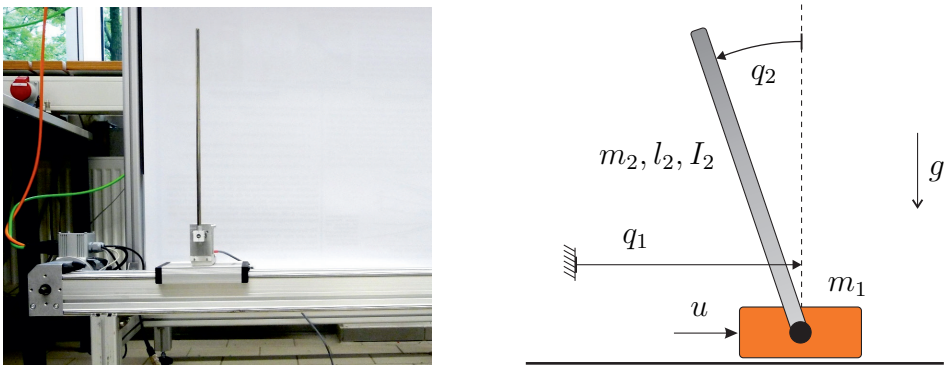

Figure 5.7: The inverted pendulum on a cart: lab setup (left) and schematic diagram (right).

mode [203], neural networks [8], model predictive control [130], and others. The IP consists of a base, or cart, that is actuated and can move horizontally, and a pendulum fixed to the cart. As the pendulum is not actuated and swings freely about the rotation axis perpendicular to the cart's motion, moving the cart back and forth is necessary to stabilize the pendulum at its unstable upward equilibrium. The configuration $\mathbf{q}$ consists of the linear displacement of the cart, represented by q_1, and the rotation angle of the pendulum with respect to its upward position q_2. The dynamics of the IP can be found in any of the aforementioned articles. A closer examination of the dynamics shows that the mass matrix depends on the unactuated coordinate q_2, which significantly complicates the controller design. For that reason, we apply a PFL [194] to simplify the dynamics. The model parameters of the IP after the PFL are given as

$$\mathbf{M} = \begin{bmatrix} 1 & 0 \\ 0 & 1 \end{bmatrix}, \quad V(\mathbf{q}) = cg\cos q_2, \quad \mathbf{G}(\mathbf{q}) = \begin{bmatrix} 1 \\ c\cos q_2 \end{bmatrix}, \tag{5.20}$$

with the constant parameter

$$c = \frac{\frac{1}{2}m_2 l_2}{\frac{1}{4}m_2 l_2^2 + I_2}.$$

The pendulum's mass, its length, and its moment of inertia with respect to the center of mass are denoted by m_2, l_2, and I_2. Again, the system is subject to the gravitational acceleration g. Note that, as the PFL aims at transforming the dynamics such that the acceleration of the cart is directly commanded by the input, the mass m_1 of the cart does not appear explicitly in the model. Yet, its exact value is necessary to compute the input required for the PFL. The damping in the unactuated coordinate is given by

the matrix

$$\mathbf{R} = \begin{bmatrix} 0 & 0 \\ 0 & r_1 \end{bmatrix}. \tag{5.21}$$

Note that the damping parameter r_1 does not directly represent the physical viscous damping coefficient, since $\mathbf{R}$ has been altered by the PFL. The numerical values of the parameters are given in Table 5.3, and correspond to the test bed at the Institute of Automatic Control at the Technische Universität München (cf. Figure 5.7). The specific units for the parameters arise from the PFL.

Table 5.3: Model parameters for the inverted pendulum on a cart.

Parameter	Value	Unit
c	3.9	$1/\mathrm{m}$
g	9.81	m/s^2
r_1	$4.7 \cdot 10^{-2}$	$1/\mathrm{s}$

Controller design

The controller design for the IP based on the augmented IDA approach was previously presented in [52]. For completeness, we summarize the main design steps according to Section 4.3. Note that, since the inertia matrix is the identity matrix, the trivial choice $\mathbf{\Gamma} = \mathbf{0}$ solves (3.28). For the linear controller $u = \mathbf{D}\mathbf{x}$ required in the first step of the design procedure, we choose the feedback gain $\mathbf{D} = [-168.45,\ 631.02,\ -219.31,\ 101.66]$. The feedback gain $\mathbf{D}$ has been identified by designing a LQR for the full model of the test bed. The linearized closed-loop system has eigenvalues $\Lambda(\mathbf{A}_\mathrm{d}) = \{-163.61,\ -6.18 + j5.9 \cdot 10^{-2},\ -6.18 - j5.9 \cdot 10^{-2},\ -1.03\}$. In the second step of the procedure, we choose the matrix $\mathbf{R}_{\mathrm{d}*} = \mathrm{diag}(1,\ 1,\ \frac{1}{3},\ \frac{1}{3})$ for the right hand side of the Lyapunov equation (4.10). To simplify the third step, we choose a quadratic form for the potential energy

$$V_\mathrm{d}(\mathbf{q}) = \frac{1}{2}\,\mathbf{q}^\mathrm{T}\mathbf{Q}_\mathrm{d}\mathbf{q}, \tag{5.22}$$

and a constant $\mathbf{K}_\mathrm{d}(\mathbf{q}) = \mathbf{K}_{\mathrm{d}*}$. In the fourth step, we are concerned with the solution $\mathbf{L}_\mathrm{d}$ of the matching equation

$$gc\sin q_2 - \begin{bmatrix} L_{\mathrm{d},11}\,a\cos q_2 - L_{\mathrm{d},21} & L_{\mathrm{d},12}\,a\cos q_2 - L_{\mathrm{d},22} \end{bmatrix} \begin{bmatrix} a_1 q_1 + a_2 q_2 \\ a_3 q_1 + a_4 q_2 \end{bmatrix} = 0. \tag{5.23}$$

To determine the matrix $\mathbf{L}_\mathrm{d}$, we first assign to $L_{\mathrm{d},21}$ and $L_{\mathrm{d},22}$ constant values, and then solve the equations

$$(L_{\mathrm{d},11} a \cos q_2 - L_{\mathrm{d},21})\, a_1 + (L_{\mathrm{d},12} a \cos q_2 - L_{\mathrm{d},22})\, a_3 = 0 \tag{5.24}$$

$$gc \sin q_2 - ((L_{\mathrm{d},11} a \cos q_2 - L_{\mathrm{d},21})\, a_2 + (L_{\mathrm{d},12} a \cos q_2 - L_{\mathrm{d},22})\, a_4)\, q_2 = 0 \tag{5.25}$$

for the remaining coefficients $L_{\mathrm{d},11}$ and $L_{\mathrm{d},12}$. In the fifth and last step, we set the vector-valued function as

$$\boldsymbol{\eta}(\mathbf{q}) = \boldsymbol{\eta}^* + \mathbf{G} k_{IP}, \qquad k_{IP} = 1200 \left(\frac{1}{\cos \varphi} - 1 \right), \tag{5.26}$$

where $\boldsymbol{\eta}^*$ is a constant vector. This nonlinear damping term has an influence on the estimate of the DA and on the transient dynamics of the closed-loop system.

Comparison with benchmark controllers

In this section, we demonstrate the applicability and practicability of our approach with a series of simulations and experimental results. The proposed controller is compared to a linear and an IDA-PBC controller as found in the literature [5]. In [5], Acosta et al. develop an IDA controller using a constructive approach that directly yields the solution to the matching equations if some conditions are satisfied. The controller is characterized by a large DA in the absence of dissipation. However, the transient dynamics are not fully satisfactory.

Let us begin by characterizing the DA. Figure 5.8 shows the estimated and simulated

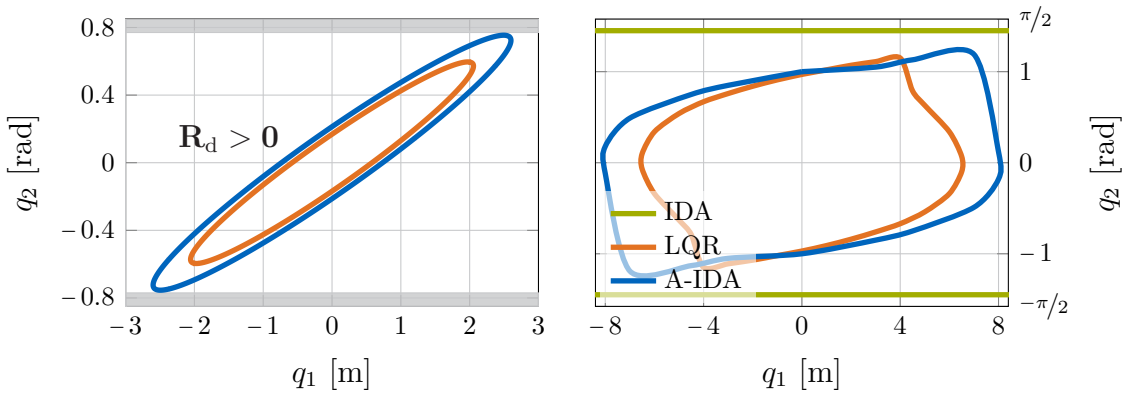

Figure 5.8: Comparison of the estimated (left) and real (right) stability boundaries of the inverted pendulum on a cart with respect to the equilibrium $\mathbf{q}^* = \mathbf{0}$ for the different controllers. As the DC is not satisfied, no estimation for the DA for IDA can be given.

stability margins of the equilibrium $\mathbf{q}^* = \mathbf{0}$ for the different controllers. For the LQR and the augmented approach, the region bounded by the largest level set of the potential function V_d (cf. (5.22)) represents an estimate of the DA of the equilibrium point: Since the energy function H_d is of quadratic form (given by the solution $\mathbf{P}_\mathrm{d}$ to the Lyapunov equation (4.10)), and the dissipation solely depends on the pendulum's angle q_2, the four-dimensional sublevel set of H_d that completely contained in the region where $\mathbf{R}_\mathrm{d} > \mathbf{0}$ is an estimate for the DA. The area enclosed by the largest level set of the potential function V_d (blue ellipse), where $\mathbf{R}_\mathrm{d} > \mathbf{0}$ (A-IDA) is 60% larger than the area enclosed by the orange ellipse, which represents an estimate of the DA given by the linear controller. As we consider dissipation in unactuated coordinates, and the system fails to satisfy the DC, no analytic estimate for the DA can be given for the IDA-PBC controller. The simulated stability margins show, however, that all controllers stabilize the desired equilibrium, with the classic IDA approach exhibiting the largest DA, and the LQR the smallest.

Figure 5.9 shows the response of the system controlled with the LQR, with the IDA-PBC controller as found in [5] for the undamped system, and with the augmented IDA proposed in this thesis. A closer look at the simulations reveals the nonlinear nature of the augmented approach, especially provided by the injection of the nonlinear damping

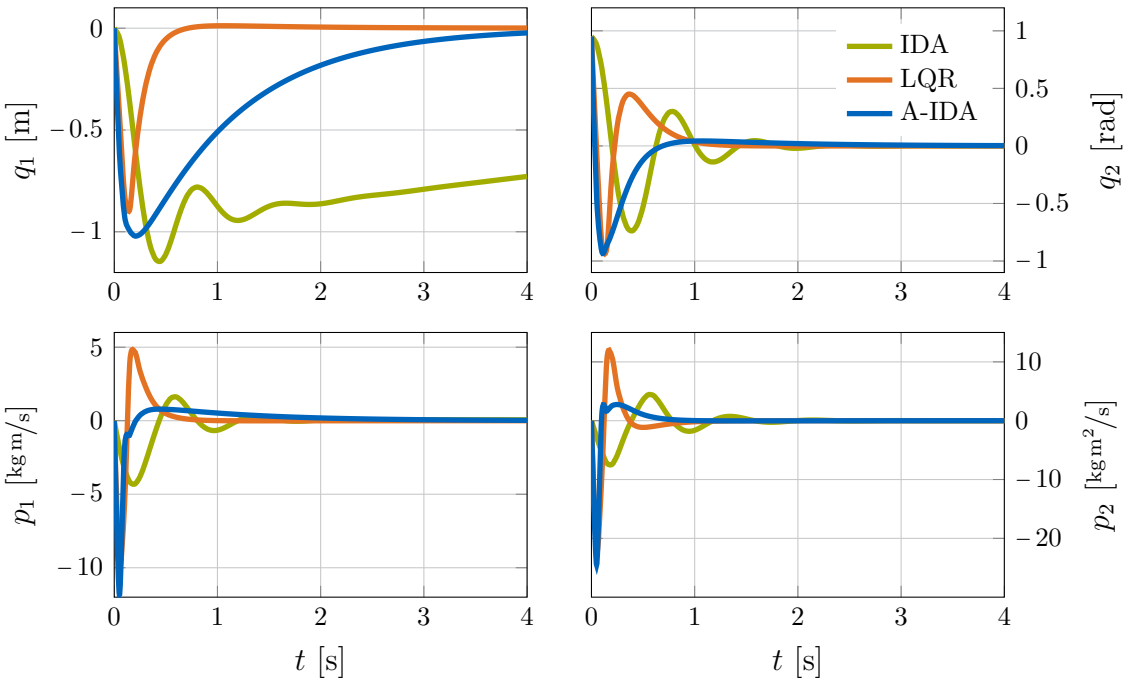

Figure 5.9: Transient dynamics of the inverted pendulum on a cart for an initial error $\mathbf{q}_0 = (0,\ 0.95)$, $\mathbf{p}_0 = \mathbf{0}$.

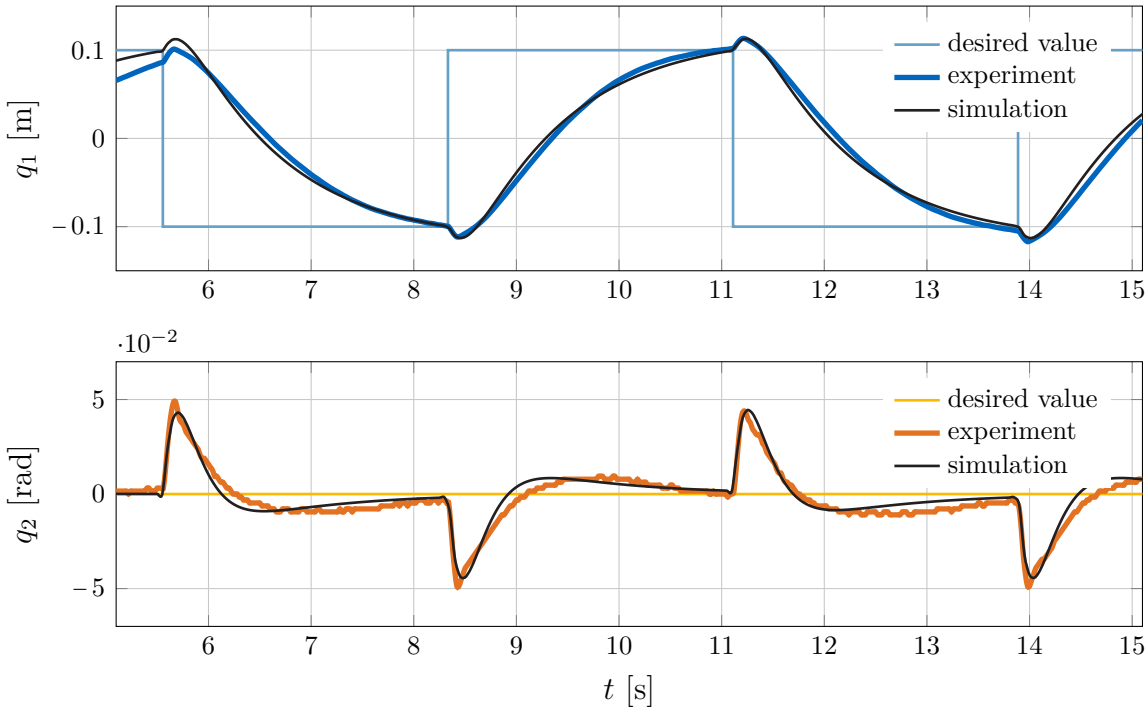

Figure 5.10: Experimental results versus simulation for the inverted pendulum on a cart stabilized using the augmented IDA methodology.

term (5.26): For small angles q_2, both the linear controller and the augmented IDA show identical responses; for larger pitch angles—as shown in the simulation—the augmented approach exhibits a smoother convergence to the origin and less overshoot in the q_2 dynamics. The system controlled with the IDA-PBC controller presents oscillations in the pitch angle and slow convergence of the cart position. The few tuning parameters do not allow to completely eliminate the undesired oscillations.

Figure 5.10 shows the behavior of the augmented IDA-PBC controlled test rig. The same controller parametrization from the simulation has also been used for the experiments, which has been chosen rather slow to clearly visualize the results. The desired position of the cart continuously changes from -0.1m to 0.1m and back. As the results show, the cart smoothly reaches the desired position as expected, keeping the pendulum close to its desired equilibrium and showing a similar transient to that of the simulations.

5.4 Concluding remarks

In this chapter, we have demonstrated through three benchmark examples how the methods proposed in the last chapters can be applied to systematically design and

parametrize passivity-based controllers via IDA while considering dissipation in unactuated coordinates from the very beginning. On the one hand, the parametrization via LLDA guarantees transparency in the controller tuning and required performance; on the other hand, the systematic design not only copes with the dissipation in unactuated coordinates but it also provides a Lyapunov function for the stability analysis and the estimation of the DA, without requiring the solution of PDEs.

III

Nonholonomic Mechanical Systems

6 Total Energy Shaping for Nonholonomic Systems

This chapter presents the position and velocity control for a class of nonholonomic systems. Since no configuration $\mathbf{q}^* \in \mathcal{Q}$ can be asymptotically stabilized using a continuous control law, we restrict the analysis, if not stated otherwise, to a reduced space $\mathcal{Q}_{\mathrm{R}}$, in which the system evolves unconstrained. Additionally, we assume that the DC is satisfied, such that no augmentation of the closed-loop energy function is necessary to render the closed-loop system passive with respect to the closed-loop energy. Therefore, we consider in the following the conventional total energy shaping approach. The chapter is organized as follows. The problem setting is formulated in Section 6.1, nonholonomic mechanical systems and their properties are presented in Section 6.2. Section 6.3 discusses the position control via energy shaping, and in Section 6.4, the results from position control are used for velocity control. In Section 6.5, we show robustness of both the position and the velocity controller by means of input-to-state stability. Section 6.6 deals with actuator dynamics, and how they can be included in the energy shaping framework via backstepping design. Finally, the chapter concludes with some final comments and remarks in Section 6.7.

6.1 Problem formulation

Nonholonomic systems have been studied for more than a century, but they have become the focus of attention of many researchers around the globe only recently [106], partially due to the fast development and commercialization of mobile robots and autonomous vehicles. This chapter deals, specifically, with the position and speed stabilization via energy shaping for a class of nonholonomic systems. In particular, we are interested in the following:

i) Systematically designing smooth stabilizing control laws, while exploiting the intrinsic properties of the system.

ii) Studying the robustness of the controllers by means of input-to-state stability.

iii) Developing a procedure to include actuator dynamics in the controller design.

One of the central issues for control theorists in the field of nonholonomic mechanical systems concerns the asymptotic stabilization of a certain configuration $\mathbf{q}^* \in \mathcal{Q}$. It has been known since the work of Brockett (cf. [39]) that time-varying or discontinuous control laws are necessary to asymptotically stabilize a desired $\mathbf{q}^*$. For over two decades, many researchers around the globe have been working on these control laws for the asymptotic stabilization of nonholonomic systems (cf. Chapter 6 of [24] and the references therein). One approach, introduced by Astolfi in 1994 [13], relies on a non-smooth coordinate transformation in the states. In the new (non-smooth) coordinates, a smooth control can be designed to asymptotically stabilize a desired configuration $\mathbf{q}^*$. This idea was later generalized in [14]. A second approach rests upon the fact that many nonholonomic systems—such as chained systems—are controllable in the sense that it is possible to steer them in any direction applying Lie bracket motion (cf. Chow's Theorem [142], Example 2.1.2). Based thereon, switching and time-varying control laws in form of sinusoidal functions emerged [142, 213]. A further idea is to employ non-smooth potential functions for the asymptotic stabilization of constrained systems. The approach was presented in [66] for fully actuated nonholonomic systems. However, assuming a non-smooth closed-loop potential energy not only leads to a weak performance of the closed-loop system, but also significantly complicates the solution of the matching problem for underactuated systems. Although discontinuous and time-varying control laws are available for the asymptotic stabilization of a desired $\mathbf{q}^*$, their design procedure is cumbersome and they often exhibit a bad performance and slow convergence [106, 174, 177]. Additionally, infinite switching leads to undesired *chattering* effects [213]. Thus, for the sake of practicability, we consider time-invariant smooth control laws.

Furthermore, we wish to consider the structural benefits of mechanical systems for the controller design. Some preliminary results on exploiting the system's intrinsic structure employing geometric control techniques for nonholonomic systems are provided in [35]. In [33], the authors introduce an energy-momentum-based technique (cf. [218]) that takes advantage of quasi-velocities for the controller design. The approach is based on *"controlled conservation laws"*, and takes into account the geometric structure of the mechanical system. However, it is hard to implement, since *"the functions that define these conservation laws are typically difficult or impossible to find explicitly"*. Due to the difficulties of geometric control for the practical implementation, we consider total energy shaping—a technique that benefits from the structural features of mechanical systems and allows for a systematic controller design. The stabilization of nonholonomic

systems via energy shaping was introduced by Maschke and van der Schaft in 1994 (cf. [134]). In their work, the authors assign virtual potential forces and damping through feedback, and show that the closed-loop system is stable and asymptotically converges to an invariant set. This situation can be easily visualized with the following example:

Example 6.1.1 (Vertical coin rolling on a horizontal plane). Let us now consider the vertical coin rolling on a horizontal plane from Example 2.1.2. The system's normalized dynamics are given as

$$\dot{\boldsymbol{\nu}} = \mathbf{u}, \qquad \mathbf{u} \in \mathbb{R}^2, \tag{6.1}$$

for admissible velocities $\boldsymbol{\nu} = (v, \dot{\theta})$, where v is the forward velocity of the coin. As we are not interested in the absolute rotation of the coin φ, we restrict the analysis to the coordinates $\boldsymbol{\eta} = (x, y, \theta)$, $\boldsymbol{\eta} \in \mathcal{Q}_\mathrm{C}$, where $\mathcal{Q}_\mathrm{C}$ is a subset of the configuration space $\mathcal{Q}$ that is still subject to nonholonomic constraints characterized by the matrix

$$\mathbf{S} = \begin{bmatrix} \cos\theta & 0 \\ \sin\theta & 0 \\ 0 & 1 \end{bmatrix}. \tag{6.2}$$

To stabilize the origin $\boldsymbol{\eta}^* = \mathbf{0}$, we assign the virtual potential $V_\mathbf{u}(\boldsymbol{\eta}) = \frac{1}{2}\,x^2 + \frac{1}{2}\,y^2 + \frac{1}{2}\,\theta^2$ through feedback. In addition to the virtual potential forces $\nabla_{\boldsymbol{\eta}} V_\mathbf{u}$, it is necessary to inject damping forces $\mathbf{F}_\mathrm{damp} = -\mathbf{R}\boldsymbol{\nu}$ with $\mathbf{R} > \mathbf{0}$ for asymptotic stability. The stabilizing control law takes the form $\mathbf{u} = -\mathbf{S}^\mathrm{T}\nabla_\mathbf{q} V_\mathbf{u} - \mathbf{R}\boldsymbol{\nu}$, and asymptotically stabilizes[1] the set

$$\mathcal{X}^* = \left\{ \boldsymbol{\eta} \in \mathcal{Q}_\mathrm{C} \mid \mathbf{S}^\mathrm{T}\nabla_{\boldsymbol{\eta}} V_\mathbf{u} = \mathbf{0} \right\}. \tag{6.3}$$

The set $\mathcal{X}^*$ is characterized by $x = \theta = 0$ with arbitrary y. Since the potential forces arising from $V_\mathbf{u}$ are projected onto the admissible coordinates via $\mathbf{S}^\mathrm{T}$, potential forces acting perpendicular to the admissible motion direction of the coin get annihilated. □

One can see from the example above that the simplest—and most intuitive—potential energy does not lead to the asymptotic stabilization of $(x^*, y^*, \theta^*) = (0, 0, 0)$, as the matrix $\mathbf{S}^\mathrm{T}$ cancels the forces acting perpendicular to the admissible motion direction.

Since energy shaping for constrained systems stabilizes a set (and not a point) as discussed in [21] in the Hamiltonian framework, or in [82] and [220] in the Lagrangian counterpart, we restrict the control synthesis to a reduced space $\mathcal{Q}_\mathrm{R}$, in which the nonholonomic system evolves unconstrained. Based thereon, we systematically design

[1] Asymptotic stability of the set can be shown invoking LaSalle's invariance principle (cf. Theorem 2.4).

smooth control strategies for the position stabilization.

The second concern of this chapter is speed stabilization of nonholonomic systems by shaping their total energy. To the best of our knowledge, classical total energy shaping approaches, like IDA, have only been developed for velocity control of electrical machines (cf. [165]) and not for mechanical systems. However, one often wants to stabilize a specific motion velocity of a mobile robot or vehicle [144, 161, 176]. We show in this chapter that energy-based control approaches allow to transfer the results from position stabilization to velocity control of mechanical systems and, later on, to tracking (cf. Chapter 7).

In addition to the design of stabilizing control laws, we consider two aspects of practical relevance in this chapter. On the one hand, we study the robustness properties of the stabilizing controllers by means of input-to-state stability. On the other hand, we present a procedure to include actuator dynamics for the controller design via backstepping.

We consider the *vertical rolling coin* as an illustrative example to highlight the properties of the dynamics evolving on different spaces (reduced, constrained), and to clarify the symbols and definitions required for the unified position and speed stabilization approach.

The position and velocity control approaches of this chapter have been partially presented in [50, 53].

6.2 Mechanical systems with nonholonomic constraints

In this section, we recapitulate the modeling of nonholonomic systems and characterize the class of systems that is of relevance for the remainder of the thesis.

6.2.1 Equations of motion

There are several ways of deriving the dynamical model of mechanical systems subject to nonholonomic constraints in both Lagrangian and Hamiltonian representation [24, 27, 159, 185]. Andrew D. Lewis, one of the experts on the field, states that *"Sometimes it seems to me as if there are as many techniques for deriving the equations of motion in the presence of nonholonomic constraints as there are people who have thought about doing this. These methods are, at least the correct ones, all distinguished by one simple fact: they are all the same!"* [119]. Since all *correct* methods are equivalent, there are no intrinsic advantages in employing one method over the other. However, some researchers

are more comfortable using geometric methods like the constrained Hamel equations[2] [34], or employing a so-called Ehresmann connection[3] that allows the description of the equations of motion in terms of the constrained Lagrangian L_r (cf. [51]), while some researchers tend to employ more classical approaches.

In this section, we restrict the analysis to the well-known Lagrange-d'Alembert equations (2.12) in the Lagrangian representation, and to the corresponding Hamiltonian form as presented in [185]. It is known that the correct equations of motions of a nonholonomic mechanical system cannot be simply derived from the Euler-Lagrange equations restricting the Lagrangian to the admissible coordinates [24]. However, as a direct result from both the Lagrangian and the Hamiltonian frameworks, the coordinate form of the Hamel equations emerges (see, e.,g., [34]), which is given by means of the constrained Lagrangian L_r.

Let us begin with the widely used Lagrange-d'Alembert equations

$$\frac{\mathrm{d}}{\mathrm{d}t}\left(\frac{\partial L}{\partial \dot{\mathbf{q}}}\right)^{\mathrm{T}} - \left(\frac{\partial L}{\partial \mathbf{q}}\right)^{\mathrm{T}} = \mathbf{F}_{\mathrm{ext}} + \mathbf{A}\boldsymbol{\lambda}, \tag{6.4}$$

which describe the dynamics of systems subject to k nonholonomic (Pfaffian) constraints of the form

$$\mathbf{A}^{\mathrm{T}}\dot{\mathbf{q}} = \mathbf{0}. \tag{6.5}$$

The matrix form of (6.4) is given as

$$\tilde{\mathbf{M}}\ddot{\mathbf{q}} + \tilde{\mathbf{C}}\dot{\mathbf{q}} + \nabla_{\mathbf{q}} V = \mathbf{F}_{\mathrm{ext}} + \mathbf{A}\boldsymbol{\lambda}. \tag{6.6}$$

The constraints have been adjoined to the system using Lagrange multipliers $\boldsymbol{\lambda} \in \mathbb{R}^k$ that represent the constraint forces, which oblige the system to satisfy the constraints (6.5). The work done by these forces vanishes as can be seen by looking at the corresponding power

$$P_{\mathrm{constr}} = \dot{\mathbf{q}}^{\mathrm{T}}\mathbf{A}\boldsymbol{\lambda} = \boldsymbol{\lambda}^{\mathrm{T}}\mathbf{A}^{\mathrm{T}}\dot{\mathbf{q}} = 0. \tag{6.7}$$

Due to the nonholonomic constraints (6.5), the admissible velocities at $\mathbf{q} \in \mathcal{Q}$ must be of the form

$$\dot{\mathbf{q}} = \mathbf{S}\boldsymbol{\nu}, \tag{6.8}$$

with a smooth full rank matrix $\mathbf{S}(\mathbf{q})$ satisfying $\mathbf{A}^{\mathrm{T}}\mathbf{S} = \mathbf{0}$, for all $\mathbf{q} \in \mathcal{Q}$, and local coor-

[2] The Hamel equations are characterized by replacing the canonical velocities $\dot{\mathbf{q}}$ by generalized velocities—so-called quasi-velocities—that are expressed in a non-coordinate frame.

[3] An Ehresmann connection is nothing but a way to split the tangent space (velocity phase space) into two parts and relate these two tangent subspaces to each other according to the constraints.

dinates of the constrained tangent space $\boldsymbol{\nu} \in \mathbb{R}^{n-k}$. The admissible velocities at $\mathbf{q}$ lie in the subspace of $\mathsf{T}_{\mathbf{q}}\mathcal{Q}$ spanned by the columns of $\mathbf{S}$, which is the $(n-k)$-dimensional space $\mathcal{D}_q$, that is, the subspace of $\mathsf{T}_{\mathbf{q}}\mathcal{Q}$ given by the constraint distribution $\mathcal{D}$. Now, replace $\dot{\mathbf{q}} = \mathbf{S}\boldsymbol{\nu}$ and $\ddot{\mathbf{q}} = \mathbf{S}\dot{\boldsymbol{\nu}} + \dot{\mathbf{S}}\boldsymbol{\nu}$ in (6.6), and eliminate the constraints by pre-multiplying the result by $\mathbf{S}^{\mathrm{T}}$ to get

$$\mathbf{S}^{\mathrm{T}}\tilde{\mathbf{M}}\mathbf{S}\dot{\boldsymbol{\nu}} + \mathbf{S}^{\mathrm{T}}\left(\tilde{\mathbf{M}}\dot{\mathbf{S}} + \tilde{\mathbf{C}}\mathbf{S}\right)\boldsymbol{\nu} + \mathbf{S}^{\mathrm{T}}\nabla_{\mathbf{q}}V = \mathbf{S}^{\mathrm{T}}\tilde{\boldsymbol{\tau}}. \tag{6.9}$$

The dynamical system represented by (6.9) can also be written in the known mechanical form

$$\mathbf{M}\dot{\boldsymbol{\nu}} + \mathbf{C}\boldsymbol{\nu} + \mathbf{S}^{\mathrm{T}}\nabla_{\mathbf{q}}V = \boldsymbol{\tau} + \mathbf{J}\boldsymbol{\nu}, \tag{6.10}$$

where $\mathbf{M} = \mathbf{S}^{\mathrm{T}}\tilde{\mathbf{M}}\mathbf{S}$, and $\boldsymbol{\tau} = \mathbf{S}^{\mathrm{T}}\tilde{\boldsymbol{\tau}}$. Since the matrix $\mathbf{C}$ is solely defined by the *Christoffel symbols* of $\mathbf{M}$, the matching of the systems (6.9) and (6.10) requires, in general, additional gyroscopic forces $\mathbf{J}\boldsymbol{\nu}$, where $\mathbf{J}(\mathbf{q}, \boldsymbol{\nu}) = -\mathbf{J}^{\mathrm{T}}(\mathbf{q}, \boldsymbol{\nu})$.

There is also the possibility of describing the equations of motion of nonholonomic systems in the Hamiltonian framework as shown in [21, 66, 185]. The reduced equations are obtained after applying a coordinate transformation to the full state model with a subsequent truncation.

Let us consider the Lagrange-d'Alembert equations (6.4) in the Hamiltonian representation

$$\begin{bmatrix} \dot{\mathbf{q}} \\ \dot{\mathbf{p}} \end{bmatrix} = \begin{bmatrix} \mathbf{0} & \mathbf{I} \\ -\mathbf{I} & \mathbf{0} \end{bmatrix} \begin{bmatrix} \nabla_{\mathbf{q}}H \\ \nabla_{\mathbf{p}}H \end{bmatrix} + \begin{bmatrix} \mathbf{0} \\ \tilde{\boldsymbol{\tau}} \end{bmatrix} + \begin{bmatrix} \mathbf{0} \\ \mathbf{A} \end{bmatrix} \boldsymbol{\lambda}, \tag{6.11}$$

with total energy $H = \dot{\mathbf{q}}^{\mathrm{T}}\mathbf{p} - L$, and where[4] $(\mathbf{q}, \mathbf{p}) \in \mathsf{T}^*\mathcal{Q}$, and $\mathbf{p} = \nabla_{\dot{\mathbf{q}}}L$. The constraint forces $\mathbf{A}\boldsymbol{\lambda}$ are uniquely determined by (6.5): Their magnitude is such that the dynamics of the system evolve in the constrained phase space given by

$$\mathcal{X}_{\mathrm{R}} = \left\{(\mathbf{q}, \mathbf{p}) \in \mathsf{T}^*\mathcal{Q} \mid \mathbf{A}^{\mathrm{T}}\nabla_{\mathbf{p}}H = \mathbf{0}\right\}. \tag{6.12}$$

According to [185], the equations of motion (6.11) subject to (6.12) can also be locally described using a coordinate transformation in the momenta $\mathbf{z} = \mathbf{T}\mathbf{p}$, where

$$\mathbf{T} = \begin{bmatrix} \mathbf{S}^{\mathrm{T}} \\ \mathbf{A}^{\mathrm{T}} \end{bmatrix}, \qquad \text{with} \qquad \mathbf{A}^{\mathrm{T}}\mathbf{S} = \mathbf{0}. \tag{6.13}$$

[4] The cotangent bundle $\mathsf{T}^*\mathcal{Q}$ is dual to the tangent bundle $\mathsf{T}\mathcal{Q}$.

The system in the transformed coordinates $(\mathbf{q}, \mathbf{z})$ becomes

$$\begin{bmatrix} \dot{\mathbf{q}} \\ \dot{\mathbf{z}} \end{bmatrix} = \begin{bmatrix} \mathbf{0} & \mathbf{T}^{\mathrm{T}} \\ -\mathbf{T} & \tilde{\mathbf{J}} \end{bmatrix} \begin{bmatrix} \nabla_{\mathbf{q}} H_{\mathrm{T}} \\ \nabla_{\mathbf{z}} H_{\mathrm{T}} \end{bmatrix} + \begin{bmatrix} \mathbf{0} \\ \mathbf{T}\tilde{\boldsymbol{\tau}} \end{bmatrix} + \begin{bmatrix} \mathbf{0} \\ \mathbf{T}\mathbf{A} \end{bmatrix} \boldsymbol{\lambda} \tag{6.14}$$

where $H_{\mathrm{T}}(\mathbf{q}, \mathbf{z}) = H(\mathbf{q}, \mathbf{T}^{-1}\mathbf{z})$ is the total energy expressed in new coordinates. Note that the gyroscopic forcing term in the structure matrix

$$\tilde{\mathbf{J}} = \mathbf{T}\left(\nabla_{\mathbf{q}}\left(\mathbf{T}^{-1}\mathbf{z}\right) - \nabla_{\mathbf{q}}^{\mathrm{T}}\left(\mathbf{T}^{-1}\mathbf{z}\right)\right)\mathbf{T}^{\mathrm{T}} \tag{6.15}$$

arises from the transformation (6.13). The nonholonomic constraints (6.5) can be expressed by

$$\mathbf{A}^{\mathrm{T}}\mathbf{T}^{\mathrm{T}}\nabla_{\mathbf{z}} H_{\mathrm{T}} = \mathbf{0}. \tag{6.16}$$

To eliminate the constraint forces, just truncate the last k rows of (6.14) and the last k columns of the structure matrix. This is justified, since $\mathbf{q}$ and the first n–k elements of $\mathbf{z}$ serve as local coordinates for the constrained space $\mathcal{X}_{\mathrm{R}}$ (see [185]). Additionally, the last k elements of $\nabla_{\mathbf{z}} H_{\mathrm{T}}$ must vanish according to (6.16).

For the equivalence of both the Lagrangian and the Hamiltonian approach to become clear, we define the quasi-velocities $\tilde{\boldsymbol{\nu}} = \nabla_{\mathbf{z}} H_{\mathrm{T}}$ and apply to (6.14) the inverse Legendre transform $L_{\mathrm{r}} = \mathbf{z}^{\mathrm{T}}\tilde{\boldsymbol{\nu}} - H_{\mathrm{T}}$ to express the equations of motion in Lagrangian form

$$\frac{\mathrm{d}}{\mathrm{d}t}\left(\frac{\partial L_{\mathrm{r}}}{\partial \tilde{\boldsymbol{\nu}}}\right)^{\mathrm{T}} - \mathbf{T}\left(\frac{\partial L_{\mathrm{r}}}{\partial \mathbf{q}}\right)^{\mathrm{T}} = \mathbf{T}\tilde{\boldsymbol{\tau}} + \tilde{\mathbf{J}}\big|_{\mathbf{z}=\mathbf{z}(\tilde{\nu})}\,\tilde{\boldsymbol{\nu}} + \mathbf{T}\mathbf{A}\boldsymbol{\lambda}, \tag{6.17}$$

where

$$L_{\mathrm{r}} = \frac{1}{2}\,\tilde{\boldsymbol{\nu}}^{\mathrm{T}}\mathbf{T}\tilde{\mathbf{M}}\mathbf{T}^{\mathrm{T}}\tilde{\boldsymbol{\nu}} - V. \tag{6.18}$$

Equation (6.16) implies that the last k velocities in $\tilde{\boldsymbol{\nu}}$ must vanish, i. e., $\tilde{\boldsymbol{\nu}} = \mathrm{col}(\boldsymbol{\nu}, \mathbf{0})$. This property simplifies the constrained Lagrangian, which can now be written as

$$L_{\mathrm{r}} = \frac{1}{2}\,\boldsymbol{\nu}^{\mathrm{T}}\mathbf{S}^{\mathrm{T}}\tilde{\mathbf{M}}\mathbf{S}\boldsymbol{\nu} - V = \frac{1}{2}\,\boldsymbol{\nu}^{\mathrm{T}}\mathbf{M}\boldsymbol{\nu} - V. \tag{6.19}$$

The equations of motion (6.17) in terms of the admissible coordinates $(\mathbf{q}, \boldsymbol{\nu}) \in \mathcal{Q} \times \mathbb{R}^{n-k}$ become

$$\frac{\mathrm{d}}{\mathrm{d}t}\left(\frac{\partial L_{\mathrm{r}}}{\partial \boldsymbol{\nu}}\right)^{\mathrm{T}} - \mathbf{S}^{\mathrm{T}}\left(\frac{\partial L_{\mathrm{r}}}{\partial \mathbf{q}}\right)^{\mathrm{T}} = \mathbf{S}^{\mathrm{T}}\tilde{\boldsymbol{\tau}} + \mathbf{J}_{\mathrm{S}}\big|_{\mathbf{z}=\mathbf{z}(\nu)}\,\boldsymbol{\nu}, \tag{6.20}$$

where $\mathbf{J}_{\mathrm{S}}$ consists of the first n–k rows and columns of $\tilde{\mathbf{J}}$ and is equal to the matrix $\mathbf{J}$ in (6.10), setting $\mathbf{z} = \mathbf{T}\tilde{\mathbf{M}}\mathbf{S}\boldsymbol{\nu}$. We consider only input affine systems, such that $\mathbf{S}^{\mathrm{T}}\tilde{\boldsymbol{\tau}} = \mathbf{G}\mathbf{u}$

for some input matrix $\mathbf{G} \in \mathbb{R}^{(n-k)\times m}$. The following result follows directly from the Hamiltonian representation (cf. [139]):

Proposition 6.1. *Let Σ be a (simple) mechanical system with (generalized) input forces $\tilde{\boldsymbol{\tau}}$, Lagrangian $L : \mathsf{T}\mathcal{Q} \to \mathbb{R}$, defined as kinetic minus potential energy, and subject to k nonholonomic (Pfaffian) constraints $\mathbf{A}^{\mathrm{T}}\dot{\mathbf{q}} = \mathbf{0}$. Let $L_{\mathrm{r}} : \mathcal{D} \to \mathbb{R}$ be the constrained Lagrangian defined as $L_{\mathrm{r}}(\mathbf{q}, \boldsymbol{\nu}) = L(\mathbf{q}, \mathbf{S}\boldsymbol{\nu})$, where $\mathbf{S} \in \mathbb{R}^{n\times(n-k)}$ is a full rank matrix satisfying $\mathbf{A}^{\mathrm{T}}\mathbf{S} = \mathbf{0}$, and $\boldsymbol{\nu} \in \mathbb{R}^{n-k}$ are local coordinates for the admissible velocity space at $\mathbf{q}$. Then, the equations of motion for Σ in $(\mathbf{q}, \boldsymbol{\nu}) \in \mathcal{Q} \times \mathbb{R}^{n-k}$ are given as*

$$\frac{\mathrm{d}}{\mathrm{d}t}\left(\frac{\partial L_{\mathrm{r}}}{\partial \boldsymbol{\nu}}\right)^{\mathrm{T}} - \mathbf{S}^{\mathrm{T}}\left(\frac{\partial L_{\mathrm{r}}}{\partial \mathbf{q}}\right)^{\mathrm{T}} = \mathbf{G}\mathbf{u} + \mathbf{J}\boldsymbol{\nu}, \tag{6.21a}$$

$$\dot{\mathbf{q}} = \mathbf{S}\boldsymbol{\nu}, \tag{6.21b}$$

where the skew-symmetric matrix $\mathbf{J}$ is defined as

$$\mathbf{J} = \left\{\mathbf{S}^{\mathrm{T}}\left(\nabla_{\mathbf{q}}\left(\mathbf{T}^{-1}\mathbf{z}\right) - \nabla_{\mathbf{q}}^{\mathrm{T}}\left(\mathbf{T}^{-1}\mathbf{z}\right)\right)\mathbf{S}\right\}\Big|_{\mathbf{z}=\mathbf{T}\tilde{\mathbf{M}}\mathbf{S}\boldsymbol{\nu}}. \tag{6.22}$$

Proof. The equations (6.21) follow directly from (6.14) restricting the dynamics to the admissible space (6.12). ∎

The equations of motion (6.21a) are the coordinate form of the constrained Hamel equations (see, e. g., [34]) for the admissible quasi-velocities $\boldsymbol{\nu} = \mathbf{S}\dot{\mathbf{q}}$; the reconstruction equation is simply given by (6.21b). If required, the magnitude of the constraint forces $\boldsymbol{\lambda}$ can be computed evaluating the last k rows of (6.17).

Nonholonomic systems are underactuated as per the most common definition, since the number of configuration variables $\mathbf{q}$ is strictly larger than the number of independent inputs $\mathbf{u}$. However, we consider in this thesis underactuation in the admissible space $\mathcal{D}$.

Definition 6.1 (Underactuated nonholonomic system)**.** We call a nonholonomic system underactuated if the dimension of the input is strictly lower than the rank of the constrained distribution $\mathcal{D}$ that defines the constraints.

According to this definition, the vertical coin rolling on a plane is a fully actuated system. In this thesis we consider systems with underactuation degree one ($m = n - k - 1$). The dynamics of this class of systems are represented by (6.21), with a non-invertible input matrix $\mathbf{G}$. Shaping the total energy, therefore, is restricted to the solution to the projected matching equations (cf. Section 6.3.1).

6.2.2 Reduced space

In order to exploit the structural advantages of energy shaping and smooth control laws for underactuated nonholonomic systems, we restrict the analysis to the reduced space[5] $\mathcal{Q}_{\mathrm{R}}$.

Proposition 6.2 (Reduced space)**.** *Suppose there are coordinates $\boldsymbol{\xi} \in \mathcal{Q}_R$, and a basis $\boldsymbol{\nu}$ for the velocity space $\mathcal{D}$ such that $\dot{\boldsymbol{\xi}} = \boldsymbol{\nu}$. If the matrices $\mathbf{M}$ and $\mathbf{S}$, and the potential forces $\nabla_{\mathbf{q}} V$ in (6.10) depend only on $\boldsymbol{\xi}$, then the equations of motion can be written in the equivalent unconstrained form*

$$\mathbf{M}\dot{\boldsymbol{\nu}} + \mathbf{C}\boldsymbol{\nu} - \mathbf{F}_{\mathrm{pot}} = \mathbf{G}\mathbf{u} + \mathbf{J}\boldsymbol{\nu} \tag{6.23}$$

in the reduced space $\mathcal{Q}_R$, where $\mathbf{S}^{\mathrm{T}} \nabla_{\mathbf{q}} V = -\mathbf{F}_{\mathrm{pot}}$. If $\mathbf{F}_{\mathrm{pot}}(\boldsymbol{\xi})$ can be derived from a potential $V_{\mathrm{R}}(\boldsymbol{\xi})$, then (6.23) can be given as

$$\mathbf{M}\dot{\boldsymbol{\nu}} + \mathbf{C}\boldsymbol{\nu} + \nabla_{\boldsymbol{\xi}} V_{\mathrm{R}} = \mathbf{G}\mathbf{u} + \mathbf{J}\boldsymbol{\nu}. \tag{6.24}$$

Proof. If the matrix $\mathbf{M}$ only depends on $\boldsymbol{\xi}$, so does $\mathbf{C}$, since $\mathbf{C}$ depends on the coefficients of $\mathbf{M}$ alone. In the same manner, if the elements of $\mathbf{S}$ are only functions of $\boldsymbol{\xi}$, so is $\mathbf{J} = \mathbf{J}(\boldsymbol{\xi}, \boldsymbol{\nu})$. Thus, the coordinates $(\boldsymbol{\xi}, \boldsymbol{\nu})$ fully describe the dynamics (6.23). If, additionally, the potential forces $\mathbf{F}_{\mathrm{pot}}$ can be derived from a scalar function $V_{\mathrm{R}}(\boldsymbol{\xi})$, then $\nabla_{\boldsymbol{\xi}} V_{\mathrm{R}} = -\mathbf{F}_{\mathrm{pot}}$, and the equations of motion in reduced space can be given in the mechanical form (6.24). ■

The matrix $\mathbf{S}^{\mathrm{T}}$ projects the potential forces onto the admissible space $\mathcal{D}$. If all external and potential forces lie already in the admissible space, then the projection is unnecessary.

Example 6.2.1 (Rolling coin on different surfaces). Consider the vertical coin from Example 2.1.2 with coordinates $\mathbf{q} = (x, y, \theta, \phi)$ rolling on 1) a pan's surface, 2) a plane inclined in x-direction, and 3) a horizontal plane. The mass matrix $\mathbf{M}$ is constant, and

[5] With some abuse of terminology, we call the space $\mathcal{Q}_{\mathrm{R}}$ *reduced space*. It should be clarified that the space $\mathcal{Q}_{\mathrm{R}}$ does not constitute a reduction of the configuration space $\mathcal{Q}$. Rather, we employ a different set of variables for the purpose of control that do not fully characterize the dynamics of the system

the matrix $\mathbf{S}$ is given as

$$\mathbf{S} = \begin{bmatrix} \cos\theta & 0 \\ \sin\theta & 0 \\ 1 & 0 \\ 0 & 1 \end{bmatrix}.$$

In the first case, the potential is given by $V_1 = x^2 + y^2$, such that the potential forces $\nabla_{\mathbf{q}} V_1 = \nabla_{\mathbf{q}} V_1(\mathbf{q}) = \mathrm{col}(2x, 2y)$. As $\mathbf{S}^{\mathrm{T}} \nabla_{\mathbf{q}} V_1$ depends on x and y, the equations of motion do not accept a formulation in reduced coordinates $\boldsymbol{\xi} = (\phi, \theta)$. In the second case, the potential can be given as $V_2 = kx$, for a constant k. Thus, $\mathbf{S}^{\mathrm{T}} \nabla_{\mathbf{q}} V_2 = -\mathbf{F}_{\mathrm{pot}}(\boldsymbol{\xi}) = \mathrm{col}(rk\cos\theta, 0)$, and the dynamics can be completely given in the reduced space $\mathcal{Q}_{\mathrm{R}}$ with coordinates $\boldsymbol{\xi} = (\phi, \theta)$. However, note that the resulting *potential* forces $\mathbf{F}_{\mathrm{pot}}(\boldsymbol{\xi})$ cannot be given in terms of the gradient of a scalar function $V_{\mathrm{R}_2}(\boldsymbol{\xi})$. In the third case, $V_3 = V_{\mathrm{R}_3} = 0$, and the equations of motion accept the formulation (6.24) for coordinates $\boldsymbol{\xi} \in \mathcal{Q}_{\mathrm{R}}$. □

In $\mathcal{Q}_{\mathrm{R}}$, the system evolves *unconstrained*, allowing the asymptotic stabilization of an admissible equilibrium $\boldsymbol{\xi}^*$ using smooth control laws. For the remainder of the thesis, the nonholonomic systems are assumed to accept either formulation (6.23) or (6.24). In the following, we show how to develop an energy-based controller to asymptotically stabilize an admissible equilibrium $\boldsymbol{\xi}^* \in \mathcal{Q}_{\mathrm{R}}$ in reduced space, and, additionally, we illustrate how the result can be utilized to asymptotically stabilize an invariant set in the configuration space or a subset $\mathcal{Q}_{\mathrm{C}} \subseteq \mathcal{Q}$ thereof.

6.3 Position control

This section discusses the systematic design of an energy-based controller that is capable of asymptotically stabilizing an admissible equilibrium $\boldsymbol{\xi}^* \in \mathcal{Q}_{\mathrm{R}}$. We formulate the conditions for the desired closed-loop equilibrium $\boldsymbol{\xi}^*$ to be (asymptotically) stable based on the matching of the system (6.23) with a Lagrangian target system. For the reduced space $\mathcal{Q}_{\mathrm{R}}$, the matching problem in IDA and CL resemble the well-known matching problem for holonomic systems as presented in Section 2.3.3 and Section 2.3.4. Therefore, known methods for the solution of the matching equations can be used for this class of nonholonomic systems. Since the Lagrangian and the Hamiltonian representations are equivalent—and also the procedures IDA-PBC and Controlled Lagrangians for simple mechanical systems [23, 47]—the following controller design can be done in both frameworks analogously. However, we put the focus on the Lagrangian case, for

velocities are more intuitive than momenta.

As introduced in Section 2.3.4, the goal of the Controlled Lagrangians procedure is to transform (6.23) by static state feedback $\mathbf{u} = \mathbf{u}(\boldsymbol{\xi}, \boldsymbol{\nu})$ into a Lagrangian closed-loop system

$$\mathbf{M}_\mathrm{c}\dot{\boldsymbol{\nu}} + \mathbf{C}_\mathrm{c}\boldsymbol{\nu} + \nabla_{\boldsymbol{\xi}} V_\mathrm{c} = (\mathbf{J}_\mathrm{c} - \mathbf{R}_\mathrm{c})\,\boldsymbol{\nu}, \tag{6.25}$$

where the matrix $\mathbf{J}_\mathrm{c} = \mathbf{J}_{\mathrm{c}0}(\boldsymbol{\xi}) + \mathbf{J}_{\mathrm{c}1}(\boldsymbol{\xi}, \boldsymbol{\nu})$ ($\mathbf{J}_{\mathrm{c}1}$ linear in $\boldsymbol{\nu}$) is skew-symmetric, and the closed-loop damping matrix $\mathbf{R}_\mathrm{c}(\boldsymbol{\xi})$ is symmetric. According to Corollary 2.6, the equilibrium $\boldsymbol{\xi}^*$ of (6.25) is asymptotically stable if

$$\boldsymbol{\xi}^* = \arg\min V_\mathrm{c}, \quad \mathbf{M}_\mathrm{c} > \mathbf{0}, \quad \mathbf{R}_\mathrm{c} \geq \mathbf{0}, \tag{6.26}$$

and the damping is pervasive. For the stabilization of (6.23) it suffices to solve the matching equations for the kinetic and potential energy, and for the dissipation

$$\mathbf{G}\mathbf{u}_\mathrm{ke} = (\mathbf{C} - \mathbf{J})\,\boldsymbol{\nu} - \mathbf{M}\mathbf{M}_\mathrm{c}^{-1}(\mathbf{C}_\mathrm{c} - \mathbf{J}_{\mathrm{c}1})\,\boldsymbol{\nu}, \tag{6.27a}$$

$$\mathbf{G}\mathbf{u}_\mathrm{pe} = -\mathbf{F}_\mathrm{pot} - \mathbf{M}\mathbf{M}_\mathrm{c}^{-1}\nabla_{\boldsymbol{\xi}} V_\mathrm{c}, \tag{6.27b}$$

$$\mathbf{G}\mathbf{u}_\mathrm{di} = \mathbf{M}\mathbf{M}_\mathrm{c}^{-1}(\mathbf{J}_{\mathrm{c}0} - \mathbf{R}_\mathrm{c})\,\boldsymbol{\nu}, \tag{6.27c}$$

for closed-loop parameters that satisfy the definiteness requirements (6.26). In the following, we assume that $\mathbf{J}_{\mathrm{c}0} = \mathbf{0}$, such that $\mathbf{J}_\mathrm{c} = \mathbf{J}_{\mathrm{c}1}$.

Remark 6.3.1. The parametrization of the closed-loop system can be realized in a transparent matter either physically motivated by tuning the closed-loop mechanical parameters, or via LLDA. In Chapter 8, we show how the LLDA technique can be applied to the WIP to achieve prescribed local dynamics in terms of the closed-loop eigenvalues.

6.3.1 Solving the matching equations

Shaping the kinetic energy. Unlike fully actuated systems, underactuated mechanical systems often require the shaping of both kinetic and potential energy for stabilization. It is, thus, necessary to solve (6.27) for a positive definite closed-loop matrix $\mathbf{M}_\mathrm{c} \neq \mathbf{M}$. Since $\mathbf{J}_\mathrm{c}$ and $\mathbf{C}_\mathrm{c}$ are linear in the velocities, and assuming that the kinetic shaping input is of the form

$$\mathbf{u}_\mathrm{ke} = \mathbf{F}^\mathrm{T}\boldsymbol{\nu}, \tag{6.28}$$

with $\mathbf{F}(\boldsymbol{\xi}, \boldsymbol{\nu}) \in \mathbb{R}^{n-k\times m}$ also linear in the velocities, more modest sufficient conditions

for matching are obtained (cf. [209]). By doing so, (6.27a) becomes

$$\left(\mathbf{C}-\mathbf{J}-\mathbf{M}\mathbf{M}_{\mathrm{c}}^{-1}(\mathbf{C}_{\mathrm{c}}-\mathbf{J}_{\mathrm{c}})-\mathbf{G}\mathbf{F}^{\mathrm{T}}\right)\boldsymbol{\nu}=\mathbf{0}, \tag{6.29}$$

and as it has to be satisfied for all $\boldsymbol{\nu}$, we get

$$\mathbf{J}_{\mathrm{c}}=\mathbf{C}_{\mathrm{c}}+\mathbf{M}_{\mathrm{c}}\mathbf{M}^{-1}(\mathbf{J}-\mathbf{C}+\mathbf{G}\mathbf{F}^{\mathrm{T}}). \tag{6.30}$$

For the mechanical target system $\dot{\mathbf{M}}_{\mathrm{c}}=\mathbf{C}_{\mathrm{c}}+\mathbf{C}_{\mathrm{c}}^{\mathrm{T}}$ holds. Expressing the skew-symmetry of $\mathbf{J}_{\mathrm{c}}$ in (6.30) by $\mathbf{J}_{\mathrm{c}}+\mathbf{J}_{\mathrm{c}}=\mathbf{0}$, we obtain

$$\mathbf{M}_{\mathrm{c}}\mathbf{M}^{-1}(\mathbf{J}-\mathbf{C}+\mathbf{G}\mathbf{F}^{\mathrm{T}})+(\mathbf{J}-\mathbf{C}+\mathbf{G}\mathbf{F}^{\mathrm{T}})^{\mathrm{T}}\mathbf{M}^{-1}\mathbf{M}_{\mathrm{c}}=-\dot{\mathbf{M}}_{\mathrm{c}}. \tag{6.31}$$

To extract the conditions that have to be satisfied independently from control, we pre-multiply (6.31) by $\mathbf{G}_{\perp}\mathbf{M}\bar{\mathbf{M}}_{\mathrm{c}}$ and post-multiply it by $\bar{\mathbf{M}}_{\mathrm{c}}\mathbf{M}\mathbf{G}_{\perp}^{\mathrm{T}}$, which leads to the projected matching equation

$$\mathbf{G}_{\perp}\left((\mathbf{J}-\mathbf{C})\bar{\mathbf{M}}_{\mathrm{c}}\mathbf{M}+\mathbf{M}\bar{\mathbf{M}}_{\mathrm{c}}(\mathbf{J}-\mathbf{C})^{\mathrm{T}}\right)\mathbf{G}_{\perp}^{\mathrm{T}}=\mathbf{G}_{\perp}\mathbf{M}\dot{\bar{\mathbf{M}}}_{\mathrm{c}}\mathbf{M}\mathbf{G}_{\perp}^{\mathrm{T}}, \tag{6.32}$$

where $\bar{\mathbf{M}}_{\mathrm{c}}=\mathbf{M}_{\mathrm{c}}^{-1}$. In order to transform the PDE (6.32)—which is usually hard to solve—into an ODE, we make the following assumptions:

Assumption 6.1. The inertia matrices $\mathbf{M}$ and $\mathbf{M}_{\mathrm{c}}$ are constant or depend only on one configuration variable ξ_j. That is, $\mathbf{M}(\boldsymbol{\xi})=\mathbf{M}(\xi_j)$, $\mathbf{M}_{\mathrm{c}}(\boldsymbol{\xi})=\mathbf{M}_{\mathrm{c}}(\xi_j)$. Consequently, $\dot{\bar{\mathbf{M}}}_{\mathrm{c}}=\bar{\mathbf{M}}_{\mathrm{c}}'\dot{\xi}_j$, where $\bar{\mathbf{M}}_{\mathrm{c}}'$ represents the element-wise derivative of the matrix $\bar{\mathbf{M}}_{\mathrm{c}}$ with respect to ξ_j.

Assumption 6.2. The matrices $\mathbf{J}$ and $\mathbf{C}$ are such that the row vector $\mathbf{G}_{\perp}(\mathbf{J}-\mathbf{C})$ can be given as $\dot{\xi}_j\mathbf{f}_C^{\mathrm{T}}(\xi_j)$, for a vector-valued function $\mathbf{f}_C\colon\mathcal{Q}_{\mathrm{R}}\to\mathbb{R}^{n-k}$.

Note that with Assumptions 6.1 and 6.2, (6.32) is an ODE for the elements of the inverse closed-loop inertia matrix $\bar{\mathbf{M}}_{\mathrm{c}}$, since it can be written as

$$2\mathbf{f}_C^{\mathrm{T}}\bar{\mathbf{M}}_{\mathrm{c}}\mathbf{f}_M=\mathbf{f}_M^{\mathrm{T}}\bar{\mathbf{M}}_{\mathrm{c}}'\mathbf{f}_M, \tag{6.33}$$

where $\mathbf{f}_M=\mathbf{M}\mathbf{G}_{\perp}^{\mathrm{T}}$. Thus, shaping the kinetic energy only requires a solution $\bar{\mathbf{M}}_{\mathrm{c}}>\mathbf{0}$ of (6.33)[6]. Assuming that a solution has been found, the kinetic energy shaping control

[6]Note that equation (6.33) has infinite solutions, as it represents a scalar ODE for all elements of $\bar{\mathbf{M}}_{\mathrm{c}}$.

(6.28) is given as

$$\mathbf{u}_{\text{ke}} = (\mathbf{G}^{\text{T}}\mathbf{G})^{-1}\mathbf{G}^{\text{T}}\left(\mathbf{C} - \mathbf{J} - \mathbf{M}\mathbf{M}_{\text{c}}^{-1}(\mathbf{C}_{\text{c}} - \mathbf{J}_{\text{c}})\right)\boldsymbol{\nu}. \tag{6.34}$$

The matrix $\mathbf{C}_{\text{c}}$ can be easily computed from the Christoffel symbols of $\mathbf{M}_{\text{c}}$; the matrix $\mathbf{J}_{\text{c}}$ by pre-multiplying (6.30) by $\mathbf{G}_{\perp}\mathbf{M}\mathbf{M}_{\text{c}}^{-1}$, and fixing the coefficients to satisfy the skew-symmetry.

Shaping the potential energy. With the help of the shaped mass matrix $\mathbf{M}_{\text{c}}$, we can proceed to shape the potential energy by solving (6.27b). The equivalent projected matching equation is

$$\mathbf{G}_{\perp}\left(\mathbf{F}_{\text{pot}} + \mathbf{M}\mathbf{M}_{\text{c}}^{-1}\nabla_{\boldsymbol{\xi}}V_{\text{c}}\right) = 0, \tag{6.35}$$

which represents a set of linear first order PDEs that can be easily solved using a computer algebra system. The closed-loop potential energy V_{c} is composed of a heterogeneous solution $\Phi_{\text{het}}(\boldsymbol{\xi})$, and a free function $\Pi(\Phi_{\text{hom}}(\boldsymbol{\xi}))$ of the homogeneous solution $\Phi_{\text{hom}}(\boldsymbol{\xi})$. If $\Phi_{\text{het}}(\boldsymbol{\xi})$ has a minimum at $\boldsymbol{\xi}^*$—which can be ensured by appropriately shaping the kinetic energy—then one can always choose the function Π such that V_{c} has an isolated minimum at $\boldsymbol{\xi}^*$. The potential energy shaping control is then given by

$$\mathbf{u}_{\text{pe}} = -(\mathbf{G}^{\text{T}}\mathbf{G})^{-1}\mathbf{G}^{\text{T}}\left(\mathbf{F}_{\text{pot}} + \mathbf{M}\mathbf{M}_{\text{c}}^{-1}\nabla_{\boldsymbol{\xi}}V_{\text{c}}\right). \tag{6.36}$$

Damping injection. To achieve asymptotic stability of $\boldsymbol{\xi}^*$, it is necessary to add (pervasive) damping according to Corollary 2.5, for which we need the solution of (6.27c) for a dissipation matrix $\mathbf{R}_{\text{c}} \geq \mathbf{0}$, such that any possible system motion elicits energy dissipation. First, let us define $\mathbf{R}_{\text{c}} = \mathbf{M}_{\text{c}}\mathbf{M}^{-1}\breve{\mathbf{R}}\mathbf{M}^{-1}\mathbf{M}_{\text{c}}$, such that (6.27c) is written as

$$\mathbf{G}\mathbf{u}_{\text{di}} = -\breve{\mathbf{R}}\mathbf{M}^{-1}\mathbf{M}_{\text{c}}\boldsymbol{\nu}. \tag{6.37}$$

Choosing the damping matrix as $\breve{\mathbf{R}} = \mathbf{G}\mathbf{K}_{\text{di}}\mathbf{G}^{\text{T}}$, for $\mathbf{K}_{\text{di}} = \text{diag}(k_{\text{d},1}, \ldots, k_{\text{d},m}) > \mathbf{0}$, the damping injection part of the control law is

$$\mathbf{u}_{\text{di}} = -\mathbf{K}_{\text{di}}\mathbf{G}^{\text{T}}\mathbf{M}^{-1}\mathbf{M}_{\text{c}}\boldsymbol{\nu}. \tag{6.38}$$

The following proposition gives a necessary and sufficient condition for pervasive damping:

Proposition 6.3. *Let $\mathbf{M}_{\text{c}} > \mathbf{0}$, and the function V_{c} be positive semidefinite. The damping injection term (6.38) ensures pervasive damping for a positive definite matrix $\mathbf{K}_{\text{di}}$*

if and only if, for $\boldsymbol{\nu} = \beta \mathbf{M}_\mathrm{c}^{-1} \mathbf{M} \mathbf{G}_\perp^\mathrm{T}$*, the equation*

$$\dot{\beta} \mathbf{M} \mathbf{G}_\perp^\mathrm{T} + \beta \left(\mathbf{C} - \mathbf{J} \right) \mathbf{G}_\perp^\mathrm{T} + \nabla_{\boldsymbol{\xi}} V_\mathrm{c} = \mathbf{0} \tag{6.39}$$

is only satisfied for $\beta = 0$*.*

Proof. See Appendix A.2. ∎

Remark 6.3.2. The DC (3.8) is assumed to be satisfied in the following. Small damping terms in unactuated coordinates that have not been included in the model enter as dissipation with respect to the closed-loop energy. Thus, damping in the unactuated coordinates does not represent a threat to the stability of the system.

6.3.2 Asymptotic stabilization in $\mathcal{Q}_\mathrm{R}$

The following result summarizes the asymptotic stabilization in reduced space $\mathcal{Q}_\mathrm{R}$:

Theorem 6.1. *Consider the mechanical system (6.23). Assume there is a matrix* $\mathbf{M}_\mathrm{c}(\boldsymbol{\xi}) > \mathbf{0}$ *and a scalar function* $V_\mathrm{c}(\boldsymbol{\xi})$ *that verify (6.33) and (6.35), where the function* V_c *is such that* $\boldsymbol{\xi}^* = \arg\min V_\mathrm{c}$*. Then, the control law*

$$\mathbf{u} = \mathbf{u}_\mathrm{ke} + \mathbf{u}_\mathrm{pe} + \mathbf{u}_\mathrm{di} \tag{6.40}$$

according to (6.34), (6.36), and (6.38), asymptotically stabilizes the equilibrium $\boldsymbol{\xi}^*$ *for* $\mathbf{K}_\mathrm{di} > \mathbf{0}$ *if the closed-loop damping is pervasive.*

Proof. Assumption 6.1 and Assumption 6.2 imply that the ODE (6.33) is equivalent to the the non-actuated part of (6.27a)—that is, the projection of (6.27a) onto the kernel of $\mathbf{G}$ by pre-multiplying (6.27a) with the left annihilator $\mathbf{G}_\perp$. Thus, according to Lemma 2.1, the matching equations (6.27) are satisfied if and only if a solution to (6.27c), (6.35), and (6.33) can be found and, additionally, the input (6.40) is chosen according to (6.34), (6.36), and (6.38).

Note that the damping matching equation (6.27c) is trivially solved by choosing the closed-loop matrix as $\breve{\mathbf{R}} = \mathbf{G} \mathbf{K}_\mathrm{di} \mathbf{G}^\mathrm{T}$. Furthermore, as the projected matching equations (6.33) and (6.35) are assumed to be satisfied for the matrix $\mathbf{M}_\mathrm{c}(\boldsymbol{\xi})$ and the scalar function $V_\mathrm{c}(\boldsymbol{\xi})$, the control law (6.40) renders (6.23) the closed-loop Lagrangian system (6.25). Stability and asymptotic stability of the desired equilibrium $\boldsymbol{\xi}^*$ follow from Corollary 2.3, since the closed-loop damping is pervasive. ∎

6.3.3 Asymptotic stabilization in $\mathcal{Q}_\mathrm{C}$

Suppose now that we want to solve the matching problem for the configuration space, or a subset $\mathcal{Q}_\mathrm{C} \subseteq \mathcal{Q}$ thereof, which comprises coordinates that are not included in the reduced space $\mathcal{Q}_\mathrm{R}$. Although it is not possible to asymptotically stabilize a point using a continuous controller—since the dynamics evolving on $\mathcal{Q}_\mathrm{C}$ are subject to nonholonomic constraints—it can be helpful to consider the constrained space[7] $\mathcal{Q}_\mathrm{C}$, for instance, to develop controllers that stabilize a specific position of a mobile robot in the horizontal plane (cf. Section 8.4.1). As it is usually easier to postulate and solve the matching problem in unconstrained reduced coordinates $\boldsymbol{\xi} \in \mathcal{Q}_\mathrm{R}$ than to employ constrained coordinates $\boldsymbol{\eta} \in \mathcal{Q}_\mathrm{C}$ (cf. Chapter 8), we are interested in making use of the solution to the matching equations in $\mathcal{Q}_\mathrm{R}$ to find a solution to the matching problem in $\mathcal{Q}_\mathrm{C}$. To that end, we make the following assumption:

Assumption 6.3. The space $\mathcal{Q}_\mathrm{C}$ is a submersion. That is, the set of coordinates $\boldsymbol{\eta} \in \mathcal{Q}_\mathrm{C}$ can be given as $\boldsymbol{\eta} = \boldsymbol{\phi}(\mathbf{q})$, where $\boldsymbol{\phi}$ is smooth and onto, and its differential is of constant rank. Further, $\boldsymbol{\eta} \in \mathcal{Q}_\mathrm{C}$ includes, at least, the configuration variable $\eta_j = \xi_j$ from Assumption 6.1, and all coordinates $\eta_i = q_i$ the potential energy V depends on.

Assumption 6.3 implies that the dynamical system (6.10) can be given in new coordinates $\boldsymbol{\eta} \in \mathcal{Q}_\mathrm{C}$ as

$$\mathbf{M}(\eta_j)\dot{\boldsymbol{\nu}} + \mathbf{C}(\eta_j, \boldsymbol{\nu})\boldsymbol{\nu} + \mathbf{S}_\eta^\mathrm{T}(\boldsymbol{\eta})\nabla_\eta V(\boldsymbol{\eta}) = \mathbf{G}\mathbf{u} + \mathbf{J}(\boldsymbol{\eta}, \boldsymbol{\nu})\boldsymbol{\nu} \tag{6.41a}$$

$$\dot{\boldsymbol{\eta}} = \mathbf{S}_\eta(\boldsymbol{\eta})\boldsymbol{\nu}, \tag{6.41b}$$

where

$$\mathbf{S}_\eta = \frac{\partial \boldsymbol{\eta}}{\partial \mathbf{q}}\mathbf{S}. \tag{6.42}$$

Example 6.3.1 (Rolling coin.). Let us consider the vertical coin from Example 2.1.2 rolling on a horizontal plane. The configuration space $\mathcal{Q}$ is parametrized by the coordinates $\mathbf{q} = (x, y, \theta, \phi)$, where (x, y) denotes the position of the contact point, and θ and ϕ describe the coin's orientation and its absolute rotation angle, respectively. As, in general, we are not interested whether the figure on the coin is right side up, we may study the dynamics of the system on the three-dimensional manifold $\mathcal{Q}_\mathrm{C} \subseteq \mathcal{Q}$, parametrized by $\boldsymbol{\eta} = \boldsymbol{\phi}(\mathbf{q}) = (x, y, \theta)$. □

As no diffeomorphism (continuously differentiable coordinate transformation) exists that directly relates $\boldsymbol{\xi}$ and $\boldsymbol{\eta}$, the solution of the matching equations (6.27) in $\mathcal{Q}_\mathrm{R}$ does

[7] With some abuse of terminology, we call the space $\mathcal{Q}_\mathrm{C} \subset \mathcal{Q}$ *constrained space*, although, strictly speaking, the velocity space is constrained and not the space $\mathcal{Q}_\mathrm{C}$ as such.

not imply the solution to the matching problem in $\mathcal{Q}_\mathrm{C}$. However, from Assumption 6.3 and the fact that the constraint distribution $\mathcal{D}$ represents the space of admissible velocities $\boldsymbol{\nu}$, which remains unchanged after the transformation, the kinetic energy and damping matching equations are equal as in Section 6.3.1 and admit the same solution. The potential energy PDE, however, changes to

$$\mathbf{G}_\perp \left(\mathbf{S}_{\boldsymbol{\eta}}^\mathrm{T} \nabla_{\boldsymbol{\eta}} V - \mathbf{M}\mathbf{M}_\mathrm{c}^{-1} \mathbf{S}_{\boldsymbol{\eta}}^\mathrm{T} \nabla_{\boldsymbol{\eta}} \tilde{V}_\mathrm{c} \right) = 0, \tag{6.43}$$

for the potentials $V(\boldsymbol{\eta})$ and $\tilde{V}_\mathrm{c}(\boldsymbol{\eta})$ given in coordinates $\boldsymbol{\eta}$. The following result holds for the solution of the new potential energy matching equation (6.43):

Theorem 6.2. *Assume that $V_\mathrm{c}(\boldsymbol{\xi})$ is a solution to the potential energy PDE (6.35), and suppose that one can find a vector-valued function $\boldsymbol{\vartheta}(\boldsymbol{\eta})$, such that*

$$\mathbf{G}_\perp \mathbf{M}\mathbf{M}_\mathrm{c}^{-1} \mathbf{S}_{\boldsymbol{\eta}}^\mathrm{T} \left(\frac{\partial \boldsymbol{\vartheta}}{\partial \boldsymbol{\eta}} \right)^\mathrm{T} = \mathbf{G}_\perp \mathbf{M}\mathbf{M}_\mathrm{c}^{-1} \tag{6.44}$$

holds. Then, the potential function

$$\tilde{V}_\mathrm{c}(\boldsymbol{\eta}) = V_\mathrm{c}(\boldsymbol{\xi} = \boldsymbol{\vartheta}(\boldsymbol{\eta})) \tag{6.45}$$

is a solution to (6.43).

Proof. For the gradient of $\tilde{V}_\mathrm{c}$ we can write

$$\frac{\partial \tilde{V}_\mathrm{c}}{\partial \boldsymbol{\eta}} = \frac{\partial V_\mathrm{c}}{\partial \boldsymbol{\xi}} \frac{\partial \boldsymbol{\xi}}{\partial \boldsymbol{\eta}} \;\Rightarrow\; \nabla_{\boldsymbol{\eta}} \tilde{V}_\mathrm{c} = \left(\frac{\partial \boldsymbol{\vartheta}}{\partial \boldsymbol{\eta}} \right)^\mathrm{T} \nabla_{\boldsymbol{\xi}} V_\mathrm{c}.$$

As $\mathbf{S}_{\boldsymbol{\eta}}^\mathrm{T} \nabla_{\boldsymbol{\eta}} V = -\mathbf{F}_\mathrm{pot}$, replacing $\nabla_{\boldsymbol{\eta}} \tilde{V}_\mathrm{c}$ into (6.43) yields

$$\mathbf{G}_\perp \left(\mathbf{F}_\mathrm{pot} + \mathbf{M}\mathbf{M}_\mathrm{c}^{-1} \mathbf{S}_{\boldsymbol{\eta}}^\mathrm{T} \left(\frac{\partial \boldsymbol{\vartheta}}{\partial \boldsymbol{\eta}} \right)^\mathrm{T} \nabla_{\boldsymbol{\xi}} V_\mathrm{c} \right) = 0. \tag{6.46}$$

As (6.44) is assumed to hold, (6.46) equals (6.35), and is satisfied by $V_\mathrm{c}(\boldsymbol{\xi} = \boldsymbol{\vartheta}(\boldsymbol{\eta}))$, as $V_\mathrm{c}(\boldsymbol{\xi})$ solves (6.35) according to the theorem. ∎

The result allows to consider stabilization in a constrained space $\mathcal{Q}_\mathrm{C}$, once we have found the solution to the matching equations in reduced (unconstrained) space $\mathcal{Q}_\mathrm{R}$. If the developed controller in reduced space stabilizes the admissible equilibrium $\boldsymbol{\xi}^* \in \mathcal{Q}_\mathrm{R}$,

then, setting $\boldsymbol{\xi} = \boldsymbol{\vartheta}(\boldsymbol{\eta})$, asymptotically stabilizes the invariant set given by

$$\mathcal{X}^* = \left\{ \boldsymbol{\eta} \in \mathcal{Q}_{\mathrm{C}} \mid \mathbf{S}_{\boldsymbol{\eta}}^{\mathrm{T}} \nabla_{\boldsymbol{\eta}} \tilde{V}_{\mathrm{c}} = \mathbf{0} \right\}, \tag{6.47}$$

provided that (6.44) is satisfied.

6.4 Velocity control

This chapter deals with the energy shaping procedure for speed control. In some applications, it is desired not just to stabilize a static equilibrium, for which the velocities vanish, but to stabilize a so-called dynamical equilibrium.

Definition 6.2 (Dynamical equilibrium)**.** A mechanical system is at a dynamical equilibrium (DE) if the sum of forces and momenta acting on the system is zero, yet it moves with constant velocity. Hence, an admissible DE only accepts nonzero velocities in cyclic coordinates of the uncontrolled system.

Let us introduce the following notation for the characterization of a DE: Let us split the coordinates $\boldsymbol{\xi} \in \mathcal{Q}_{\mathrm{R}}$ into $\boldsymbol{\xi}^{\mathrm{d}}$ and $\boldsymbol{\xi}^{\mathrm{s}}$, and the corresponding velocities $\boldsymbol{\nu} \in \mathsf{T}_{\boldsymbol{\xi}} \mathcal{Q}_{\mathrm{R}}$, and $\hat{\boldsymbol{\nu}} \in \mathsf{T}_{\boldsymbol{\xi}} \mathcal{Q}_{\mathrm{R}}$ into $\boldsymbol{\nu}^{\mathrm{d}}$ and $\boldsymbol{\nu}^{\mathrm{s}}$ (resp. $\hat{\boldsymbol{\nu}}^{\mathrm{d}}$ and $\hat{\boldsymbol{\nu}}^{\mathrm{s}}$). The vector $\boldsymbol{\xi}^{\mathrm{d}}$ contains only the cyclic variables with nonzero reference velocities $\hat{\boldsymbol{\nu}}^{\mathrm{d}}$, while $\boldsymbol{\xi}^{\mathrm{s}}$ contains the remaining configuration variables, which are to be stabilized at a constant value $\hat{\boldsymbol{\xi}}^{\mathrm{s}}$. Since the relationship $\dot{\boldsymbol{\xi}} = \boldsymbol{\nu}$ holds, one has $\boldsymbol{\nu}^{\mathrm{d}} = \dot{\boldsymbol{\xi}}^{\mathrm{d}}$ and $\boldsymbol{\nu}^{\mathrm{s}} = \dot{\boldsymbol{\xi}}^{\mathrm{s}}$ as well.

Example 6.4.1 (Rolling coin). Consider the rolling coin on a horizontal plane with (cyclic) coordinates $\boldsymbol{\xi} = (\theta, \phi)$. If the goal was to stabilize a specific forward velocity that is characterized by $\dot{\phi}$, while maintaining a constant orientation θ^*, then $\xi^{\mathrm{d}} = \phi$, and $\xi^{\mathrm{s}} = \theta$. □

By defining the reference value $\hat{\boldsymbol{\xi}}^{\mathrm{d}} = \boldsymbol{\xi}^{\mathrm{d}}$, such that $\boldsymbol{\xi}_{\mathrm{e}}^{\mathrm{d}} = \mathbf{0}$ for all times $t > 0$, the potential energy $V_{\mathrm{c}}^{\mathrm{e}}$ does not depend on $\boldsymbol{\xi}^{\mathrm{d}}$. Thus, for the stabilization of a constant (nonzero) reference velocity $\hat{\boldsymbol{\nu}}^{\mathrm{d}}$, we completely ignore the configuration variables $\boldsymbol{\xi}^{\mathrm{d}}$. That is,

$$\nabla_{\boldsymbol{\xi}} V_{\mathrm{c}}^{\mathrm{e}} = \begin{bmatrix} \nabla_{\boldsymbol{\xi}^{\mathrm{d}}} V_{\mathrm{c}}^{\mathrm{e}} \\ \nabla_{\boldsymbol{\xi}^{\mathrm{s}}} V_{\mathrm{c}}^{\mathrm{e}} \end{bmatrix} = \begin{bmatrix} \mathbf{0} \\ \nabla_{\boldsymbol{\xi}^{\mathrm{s}}} V_{\mathrm{c}} \end{bmatrix}. \tag{6.48}$$

Additionally, the following relations hold for an admissible DE:

$$\hat{\boldsymbol{\xi}} = \begin{bmatrix} \hat{\boldsymbol{\xi}}^{\mathrm{d}} \\ \hat{\boldsymbol{\xi}}^{\mathrm{s}} \end{bmatrix} = \begin{bmatrix} \boldsymbol{\xi}^{\mathrm{d}} \\ \hat{\boldsymbol{\xi}}^{\mathrm{s}*} \end{bmatrix}, \qquad \hat{\boldsymbol{\nu}} = \begin{bmatrix} \hat{\boldsymbol{\nu}}^{\mathrm{d}} \\ \hat{\boldsymbol{\nu}}^{\mathrm{s}} \end{bmatrix} = \begin{bmatrix} \hat{\boldsymbol{\nu}}^{\mathrm{d}*} \\ \mathbf{0} \end{bmatrix}, \tag{6.49}$$

for constant $\hat{\boldsymbol{\xi}}^{\mathrm{s}*}$ and $\hat{\boldsymbol{\nu}}^{\mathrm{d}*}$.

Remark 6.4.1. It makes sense to define the dynamical equilibrium in this fashion, as demanding a constant velocity $\hat{\nu}_i$ and at the same time, a constant position $\hat{\xi}_i$ are contradictory requests.

For the stabilization of a DE via energy shaping, we need to find a static state feedback $\mathbf{u}=\mathbf{u}(\boldsymbol{\xi},\boldsymbol{\nu},t)$ that renders (6.23) the closed-loop system[8]

$$\mathbf{M}_{\mathrm{c}}\dot{\boldsymbol{\nu}}+\mathbf{C}_{\mathrm{c}}\boldsymbol{\nu}_{\mathrm{e}}+\nabla_{\boldsymbol{\xi}}V_{\mathrm{c}}^{\mathrm{e}}=(\mathbf{J}_{\mathrm{c}}-\mathbf{R}_{\mathrm{c}})\boldsymbol{\nu}_{\mathrm{e}}, \tag{6.50}$$

where $V_{\mathrm{c}}^{\mathrm{e}}=V_{\mathrm{c}}(\boldsymbol{\xi}_{\mathrm{e}})$[9], and $\boldsymbol{\xi}_{\mathrm{e}}=\boldsymbol{\xi}-\hat{\boldsymbol{\xi}}$ and $\boldsymbol{\nu}_{\mathrm{e}}=\boldsymbol{\nu}-\hat{\boldsymbol{\nu}}$ are the configuration and the velocity errors from the reference values $\hat{\boldsymbol{\xi}}$ and $\hat{\boldsymbol{\nu}}$, respectively.

Theorem 6.3. *Let $(\hat{\boldsymbol{\xi}},\hat{\boldsymbol{\nu}})$ be an admissible DE with constant $\hat{\boldsymbol{\nu}}^{\mathrm{d}}$ and $\hat{\boldsymbol{\nu}}^{\mathrm{s}}=\mathbf{0}$. Define $\hat{\boldsymbol{\xi}}^{\mathrm{d}}=\boldsymbol{\xi}^{\mathrm{d}}$, such that the potential energy $V_{\mathrm{c}}^{\mathrm{e}}$ is only a function of the coordinates $\boldsymbol{\xi}^{\mathrm{s}}$. The admissible DE $(\hat{\boldsymbol{\xi}},\hat{\boldsymbol{\nu}})$ of (6.50) is stable if $\mathbf{M}_{\mathrm{c}}>\mathbf{0}$, $V_{\mathrm{c}}^{\mathrm{e}}$ is such that $\mathbf{0}=\arg\min V_{\mathrm{c}}^{\mathrm{e}}$, and $\mathbf{R}_{\mathrm{c}}\geq\mathbf{0}$. The DE is asymptotically stable if $\mathbf{R}_{\mathrm{c}}\geq\mathbf{0}$ ensures pervasive damping*[10].

Proof. Consider the time-invariant Lyapunov function

$$E_{\nu}=\frac{1}{2}\boldsymbol{\nu}_{\mathrm{e}}^{\mathrm{T}}\mathbf{M}_{\mathrm{c}}\boldsymbol{\nu}_{\mathrm{e}}+V_{\mathrm{c}}^{\mathrm{e}}. \tag{6.51}$$

Its derivative along the trajectories of (6.50) is given by

$$\dot{E}_{\nu}=-\boldsymbol{\nu}_{\mathrm{e}}^{\mathrm{T}}\mathbf{R}_{\mathrm{c}}\boldsymbol{\nu}_{\mathrm{e}}+\nabla_{\boldsymbol{\xi}}^{\mathrm{T}}V_{\mathrm{c}}^{\mathrm{e}}\left(\hat{\boldsymbol{\nu}}-\dot{\hat{\boldsymbol{\xi}}}\right). \tag{6.52}$$

The second term in (6.52) is always zero, since

$$\nabla_{\boldsymbol{\xi}}^{\mathrm{T}}V_{\mathrm{c}}^{\mathrm{e}}\left(\hat{\boldsymbol{\nu}}-\dot{\hat{\boldsymbol{\xi}}}\right)=\underbrace{\nabla_{\boldsymbol{\xi}^{\mathrm{d}}}^{\mathrm{T}}V_{\mathrm{c}}^{\mathrm{e}}}_{=\mathbf{0}}\left(\hat{\boldsymbol{\nu}}^{\mathrm{d}}-\dot{\hat{\boldsymbol{\xi}}}^{\mathrm{d}}\right)+\nabla_{\boldsymbol{\xi}^{\mathrm{s}}}^{\mathrm{T}}V_{\mathrm{c}}^{\mathrm{e}}\underbrace{\left(\hat{\boldsymbol{\nu}}^{\mathrm{s}}-\dot{\hat{\boldsymbol{\xi}}}^{\mathrm{s}}\right)}_{=\mathbf{0}}=0. \tag{6.53}$$

Stability of the DE $(\hat{\boldsymbol{\xi}},\hat{\boldsymbol{\nu}})$ follows, as $\dot{E}_{\nu}\leq 0$. Asymptotic stability can be shown invoking La Salle's invariance principle if $\mathbf{R}_{\mathrm{c}}\geq\mathbf{0}$ ensures pervasive damping. ■

In order to find a control law $\mathbf{u}=\mathbf{u}(\boldsymbol{\xi},\boldsymbol{\nu})$ that renders (6.23) the closed-loop system (6.50), consider the matching equations for the kinetic and potential energy, and for

[8] These equations have been motivated by the Controlled Lagrangians procedure for the stabilization of an admissible equilibrium. Note that they cannot be derived from a Lagrangian function.

[9] The function $V_{\mathrm{c}}^{\mathrm{e}}$ is a so-called tracking error function (cf. Section 7.2).

[10] Note that for $\hat{\boldsymbol{\nu}}^{\mathrm{d}}=\mathbf{0}$ and constant $\hat{\boldsymbol{\xi}}^{\mathrm{d}}$, the closed-loop system (6.50) equals (6.25).

the dissipation

$$\mathbf{G}\mathbf{u}_{\mathrm{ke}} = (\mathbf{C} - \mathbf{J})\,\boldsymbol{\nu} - \mathbf{M}\mathbf{M}_{\mathrm{c}}^{-1}\,(\mathbf{C}_{\mathrm{c}} - \mathbf{J}_{\mathrm{c}})\,\boldsymbol{\nu}_{\mathrm{e}}, \tag{6.54a}$$

$$\mathbf{G}\mathbf{u}_{\mathrm{pe}} = -\mathbf{M}\mathbf{M}_{\mathrm{c}}^{-1}\nabla_{\boldsymbol{\xi}} V_{\mathrm{c}}^{\mathrm{e}} - \mathbf{F}_{\mathrm{pot}}, \tag{6.54b}$$

$$\mathbf{G}\mathbf{u}_{\mathrm{di}} = -\mathbf{M}\mathbf{M}_{\mathrm{c}}^{-1}\mathbf{R}_{\mathrm{c}}\boldsymbol{\nu}_{\mathrm{e}}, \tag{6.54c}$$

respectively. The equations for the kinetic and potential energy (6.54a) (setting $\boldsymbol{\nu} = \boldsymbol{\nu}_{\mathrm{e}} + \hat{\boldsymbol{\nu}}$) and (6.54b), and for the dissipation (6.54c), are very similar to (6.27a), (6.27b), and (6.27c), and have a structurally identical solution of their projected part if

$$\mathbf{G}_{\perp}\,(\mathbf{C} - \mathbf{J})\,\hat{\boldsymbol{\nu}} = 0. \tag{6.55}$$

From Lemma 2.1, the speed control law can be given as

$$\mathbf{u} = (\mathbf{G}^{\mathrm{T}}\mathbf{G})^{-1}\mathbf{G}^{\mathrm{T}}\left((\mathbf{C} - \mathbf{J})\,\hat{\boldsymbol{\nu}} - \mathbf{F}_{\mathrm{pot}} - \mathbf{M}\mathbf{M}_{\mathrm{c}}^{-1}\nabla_{\boldsymbol{\xi}} V_{\mathrm{c}}^{\mathrm{e}}\right) + \mathbf{F}^{\mathrm{T}}\boldsymbol{\nu}_{\mathrm{e}} - \mathbf{K}_{\mathrm{di}}\mathbf{G}^{\mathrm{T}}\mathbf{M}^{-1}\mathbf{M}_{\mathrm{c}}\boldsymbol{\nu}_{\mathrm{e}}, \tag{6.56}$$

and can be computed without much effort, since the matching equations involved have been previously solved: Note that in order to get (6.56) from (6.28), (6.36), and (6.38), it is merely necessary to add an extra term and replace some $\boldsymbol{\nu}$ by $\boldsymbol{\nu}_{\mathrm{e}}$.

Theorem 6.4. *Assume there is a scalar function $V_{\mathrm{c}}^{\mathrm{e}}$ with a strict minimum at $\mathbf{0}$, and matrices $\mathbf{M}_{\mathrm{c}} > \mathbf{0}$ and $\mathbf{R}_{\mathrm{c}} \geq \mathbf{0}$, which verify the equations (6.27) and ensure pervasive damping. Further, define the vector $\boldsymbol{\nu}_{\mathrm{e}} = \boldsymbol{\nu} - \hat{\boldsymbol{\nu}}$, where $(\hat{\boldsymbol{\xi}}, \hat{\boldsymbol{\nu}})$ is an admissible dynamical equilibrium with constant $\hat{\boldsymbol{\nu}}^{\mathrm{d}}$, $\hat{\boldsymbol{\xi}}^{\mathrm{s}}$, and with $\hat{\boldsymbol{\nu}}^{\mathrm{s}} = \mathbf{0}$, and $\hat{\boldsymbol{\xi}}^{\mathrm{d}} = \boldsymbol{\xi}^{\mathrm{d}}$. Additionally, assume that (6.55) holds true. Then, the control law (6.56) asymptotically stabilizes the admissible equilibrium $(\hat{\boldsymbol{\xi}}, \hat{\boldsymbol{\nu}})$.*

Proof. In the same manner as in Theorem 6.1, the input (6.56) transforms (6.23) into (6.50), since $\mathbf{G}_{\perp}(\mathbf{C} - \mathbf{J})\hat{\boldsymbol{\nu}} = 0$. Stability and asymptotic stability follow from Theorem 6.3. ■

6.5 Input-to-state stability

In Section 6.3, we designed a controller that is capable of stabilizing a desired admissible equilibrium $\boldsymbol{\xi}^*$. How the stability of the system is affected by varying this equilibrium is the topic of this section. Let, without loss of generality, $\mathbf{0} = \arg\min V_{\mathrm{c}}$, and let $V_{\mathrm{c}}^{\mathrm{e}} = V_{\mathrm{c}}(\boldsymbol{\xi} - \boldsymbol{\xi}^*)$, such that $\boldsymbol{\xi}^* = \arg\min V_{\mathrm{c}}^{\mathrm{e}}$. We analyze the input-to-state stability of

the closed-loop system[11]

$$\mathbf{M}_{\mathrm{c}}\dot{\boldsymbol{\nu}} + \mathbf{C}_{\mathrm{c}}\boldsymbol{\nu} + \nabla_{\boldsymbol{\xi}} V_{\mathrm{c}}^{\mathrm{e}} = (\mathbf{J}_{\mathrm{c}} - \mathbf{R}_{\mathrm{c}})\,\boldsymbol{\nu} \tag{6.57}$$

with respect to the "disturbance" $\mathbf{d}_{\boldsymbol{\xi}} = \boldsymbol{\xi}^*$. ISS is locally equivalent to asymptotic stability. In this section, we give explicit bounds for the input disturbance $\mathbf{d}_{\boldsymbol{\xi}}$ such that boundedness of all closed-loop signals is guaranteed. For that purpose, we make the following assumptions:

Assumption 6.4. A constant positive definite matrix $\mathbf{K} = \mathbf{K}^{\mathrm{T}}$ exists, such that the matrix

$$\mathbf{R}_{\varepsilon}^{\boldsymbol{\xi}} = \mathbf{R}_{\mathrm{c}} - \frac{\varepsilon}{2}\left(\mathbf{M}_{\mathrm{c}}\mathbf{K}\nabla_{\boldsymbol{\xi}}^2 V_{\mathrm{c}} + \nabla_{\boldsymbol{\xi}}^2 V_{\mathrm{c}}\,\mathbf{K}\mathbf{M}_{\mathrm{c}}\right) \tag{6.58}$$

is positive definite in a neighborhood of $\boldsymbol{\xi} = \mathbf{0}$ for small values of ε. Note that it always holds true for $\mathbf{R}_{\mathrm{c}} > \mathbf{0}$.

Assumption 6.5. The potential function V_{c} satisfies

$$\nabla_{\boldsymbol{\xi}} V_{\mathrm{c}}(\boldsymbol{\xi} - \mathbf{d}_{\boldsymbol{\xi}}) - \nabla_{\boldsymbol{\xi}} V_{\mathrm{c}}(\boldsymbol{\xi}) = \boldsymbol{\Pi}_{\boldsymbol{\xi}}\mathbf{d}_{\boldsymbol{\xi}}, \tag{6.59}$$

for a matrix-valued function $\boldsymbol{\Pi}_{\boldsymbol{\xi}} \colon \mathcal{Q}_{\mathrm{R}} \to \mathbb{R}^{(n-k)\times(n-k)}$.

Assumption 6.5 indicates that the closed-loop system (6.57) can be given as

$$\mathbf{M}_{\mathrm{c}}\dot{\boldsymbol{\nu}} + \mathbf{C}_{\mathrm{c}}\boldsymbol{\nu} + \nabla_{\boldsymbol{\xi}} V_{\mathrm{c}} = (\mathbf{J}_{\mathrm{c}} - \mathbf{R}_{\mathrm{c}})\,\boldsymbol{\nu} - \boldsymbol{\Pi}_{\boldsymbol{\xi}}\mathbf{d}_{\boldsymbol{\xi}}, \tag{6.60}$$

with input matrix $\boldsymbol{\Pi}_{\boldsymbol{\xi}}$, and input disturbance $\mathbf{d}_{\boldsymbol{\xi}}$. Recall that a system is ISS if the states remain bounded in the presence of a disturbance in the sense that a positive definite function exists—an ISS Lyapunov function—whose time derivative is negative semidefinite for bounded input disturbances $\mathbf{d}_{\boldsymbol{\xi}}$.

Theorem 6.5. *Let $\varepsilon > 0$ be a sufficiently small scalar. The system (6.60) is (locally) input-to-state stable with respect to input disturbances satisfying*

$$\|\mathbf{d}_{\boldsymbol{\xi}}\| \leq \frac{\gamma\lambda_{\min}}{\sigma_{\max}}\,\|\boldsymbol{\chi}\|, \tag{6.61}$$

where $\boldsymbol{\chi} = \mathrm{col}(\nabla_{\boldsymbol{\xi}} V_{\mathrm{c}},\, \boldsymbol{\nu})$, the scalar $\gamma =]0,\, 1[$ is free, $\sigma_{\max}$ represents the largest singular

[11] Note that (6.57) is equivalent to (6.25) for a constant $\boldsymbol{\xi}^*$ if $\mathbf{0} = \arg\min V_{\mathrm{c}}$, and $V_{\mathrm{c}}^{\mathrm{e}} = V_{\mathrm{c}}(\boldsymbol{\xi} - \boldsymbol{\xi}^*)$.

value of the matrix

$$\boldsymbol{\Sigma} = \begin{bmatrix} \varepsilon \mathbf{K} \boldsymbol{\Pi}_{\boldsymbol{\xi}} \\ \boldsymbol{\Pi}_{\boldsymbol{\xi}} \end{bmatrix}, \tag{6.62}$$

and $\lambda_{\min}$ *is the smallest eigenvalue of the positive definite matrix*

$$\mathbf{R}_{\boldsymbol{\chi}} = \begin{bmatrix} \varepsilon \mathbf{K} & -\frac{\varepsilon}{2} \mathbf{K} \left(\mathbf{J}_{\mathrm{c}} + \mathbf{C}_{\mathrm{c}}^{\mathrm{T}} - \mathbf{R}_{\mathrm{c}} \right) \\ \frac{\varepsilon}{2} \left(\mathbf{J}_{\mathrm{c}} + \mathbf{R}_{\mathrm{c}} + \mathbf{C}_{\mathrm{c}} \right) \mathbf{K} & \mathbf{R}_{\varepsilon}^{\boldsymbol{\xi}} \end{bmatrix}. \tag{6.63}$$

Proof. Consider the (local) ISS Lyapunov function

$$E_{\mathrm{ISS}}^{\boldsymbol{\xi}} = \frac{1}{2} \boldsymbol{\nu}^{\mathrm{T}} \mathbf{M}_{\mathrm{c}} \boldsymbol{\nu} + V_{\mathrm{c}} + \varepsilon \nabla_{\boldsymbol{\xi}}^{\mathrm{T}} V_{\mathrm{c}} \mathbf{K} \mathbf{M}_{\mathrm{c}} \boldsymbol{\nu}, \tag{6.64}$$

which clearly is positive definite for small values of ε. The time derivative along the trajectories of (6.60) is

$$\begin{aligned} \dot{E}_{\mathrm{ISS}}^{\boldsymbol{\xi}} &= \boldsymbol{\nu}^{\mathrm{T}} \left(\left(\mathbf{J}_{\mathrm{c}} - \mathbf{R}_{\mathrm{c}} - \mathbf{C}_{\mathrm{c}} \right) \boldsymbol{\nu} - \nabla_{\boldsymbol{\xi}} V_{\mathrm{c}} - \boldsymbol{\Pi}_{\boldsymbol{\xi}} \mathbf{d}_{\boldsymbol{\xi}} \right) + \frac{1}{2} \boldsymbol{\nu}^{\mathrm{T}} \dot{\mathbf{M}}_{\mathrm{c}} \boldsymbol{\nu} + \boldsymbol{\nu}^{\mathrm{T}} \nabla_{\boldsymbol{\xi}} V_{\mathrm{c}} + \varepsilon \nabla_{\boldsymbol{\xi}}^{\mathrm{T}} V_{\mathrm{c}} \mathbf{K} \dot{\mathbf{M}}_{\mathrm{c}} \boldsymbol{\nu} \\ &\quad + \varepsilon \nabla_{\boldsymbol{\xi}}^{\mathrm{T}} V_{\mathrm{c}} \mathbf{K} \left(\left(\mathbf{J}_{\mathrm{c}} - \mathbf{R}_{\mathrm{c}} - \mathbf{C}_{\mathrm{c}} \right) \boldsymbol{\nu} - \nabla_{\boldsymbol{\xi}} V_{\mathrm{c}} - \boldsymbol{\Pi}_{\boldsymbol{\xi}} \mathbf{d}_{\boldsymbol{\xi}} \right) + \varepsilon \boldsymbol{\nu}^{\mathrm{T}} \mathbf{M}_{\mathrm{c}} \mathbf{K} \nabla_{\boldsymbol{\xi}}^{2} V_{\mathrm{c}} \, \boldsymbol{\nu} \\ &= - \boldsymbol{\nu}^{\mathrm{T}} \underbrace{\left(\mathbf{R}_{\mathrm{c}} - \frac{\varepsilon}{2} \left(\mathbf{M}_{\mathrm{c}} \mathbf{K} \nabla_{\boldsymbol{\xi}}^{2} V_{\mathrm{c}} + \nabla_{\boldsymbol{\xi}}^{2} V_{\mathrm{c}} \, \mathbf{K} \mathbf{M}_{\mathrm{c}} \right) \right)}_{\mathbf{R}_{\varepsilon}^{\boldsymbol{\xi}}} \boldsymbol{\nu} - \boldsymbol{\nu}^{\mathrm{T}} \boldsymbol{\Pi}_{\boldsymbol{\xi}} \mathbf{d}_{\boldsymbol{\xi}} - \varepsilon \nabla_{\boldsymbol{\xi}}^{\mathrm{T}} V_{\mathrm{c}} \mathbf{K} \nabla_{\boldsymbol{\xi}} V_{\mathrm{c}} \\ &\quad + \varepsilon \nabla_{\boldsymbol{\xi}}^{\mathrm{T}} V_{\mathrm{c}} \mathbf{K} \left(\mathbf{J}_{\mathrm{c}} - \mathbf{R}_{\mathrm{c}} + \mathbf{C}_{\mathrm{c}}^{\mathrm{T}} \right) \boldsymbol{\nu} - \varepsilon \nabla_{\boldsymbol{\xi}}^{\mathrm{T}} V_{\mathrm{c}} \mathbf{K} \boldsymbol{\Pi}_{\boldsymbol{\xi}} \mathbf{d}_{\boldsymbol{\xi}}. \end{aligned} \tag{6.65}$$

Defining $\boldsymbol{\chi} = \mathrm{col}(\nabla_{\boldsymbol{\xi}} V_{\mathrm{c}}, \, \boldsymbol{\nu})$, expression (6.65) can be given as

$$\dot{E}_{\mathrm{ISS}}^{\boldsymbol{\xi}} = - \boldsymbol{\chi}^{\mathrm{T}} \mathbf{R}_{\boldsymbol{\chi}} \boldsymbol{\chi} + \boldsymbol{\chi}^{\mathrm{T}} \boldsymbol{\Sigma} \mathbf{d}_{\boldsymbol{\xi}}, \tag{6.66}$$

where

$$\mathbf{R}_{\boldsymbol{\chi}} = \begin{bmatrix} \varepsilon \mathbf{K} & -\frac{\varepsilon}{2} \mathbf{K} \left(\mathbf{J}_{\mathrm{c}} + \mathbf{C}_{\mathrm{c}}^{\mathrm{T}} - \mathbf{R}_{\mathrm{c}} \right) \\ \frac{\varepsilon}{2} \left(\mathbf{J}_{\mathrm{c}} + \mathbf{R}_{\mathrm{c}} + \mathbf{C}_{\mathrm{c}} \right) \mathbf{K} & \mathbf{R}_{\varepsilon}^{\boldsymbol{\xi}} \end{bmatrix}, \qquad \boldsymbol{\Sigma} = \begin{bmatrix} \varepsilon \mathbf{K} \boldsymbol{\Pi}_{\boldsymbol{\xi}} \\ \boldsymbol{\Pi}_{\boldsymbol{\xi}} \end{bmatrix}. \tag{6.67}$$

For any number $0 < \gamma < 1$, we have for the derivative of the ISS Lyapunov function

$$\dot{E}_{\mathrm{ISS}}^{\boldsymbol{\xi}} = - (1 - \gamma) \boldsymbol{\chi}^{\mathrm{T}} \mathbf{R}_{\boldsymbol{\chi}} \boldsymbol{\chi} - \boldsymbol{\chi}^{\mathrm{T}} \left(\gamma \mathbf{R}_{\boldsymbol{\chi}} \boldsymbol{\chi} - \boldsymbol{\Sigma} \mathbf{d}_{\boldsymbol{\xi}} \right) \leq 0,$$

provided

$$\boldsymbol{\chi}^{\mathrm{T}}\left(\gamma \mathbf{R}_{\boldsymbol{\chi}} \boldsymbol{\chi}-\boldsymbol{\Sigma} \mathbf{d}_{\boldsymbol{\xi}}\right) \geq 0. \tag{6.68}$$

Using the relations $\boldsymbol{\chi}=\|\boldsymbol{\chi}\| \bar{\boldsymbol{\chi}}$ and $\mathbf{d}_{\boldsymbol{\xi}}=\|\mathbf{d}_{\boldsymbol{\xi}}\| \bar{\mathbf{d}}_{\boldsymbol{\xi}}$, where $\|\bar{\boldsymbol{\chi}}\|=\|\bar{\mathbf{d}}_{\boldsymbol{\xi}}\|=1$, the latter inequality can be given as

$$\|\boldsymbol{\chi}\| \gamma \bar{\boldsymbol{\chi}}^{\mathrm{T}} \mathbf{R}_{\boldsymbol{\chi}} \bar{\boldsymbol{\chi}} \geq\left\|\mathbf{d}_{\boldsymbol{\xi}}\right\| \bar{\boldsymbol{\chi}}^{\mathrm{T}} \boldsymbol{\Sigma} \bar{\mathbf{d}}_{\boldsymbol{\xi}}. \tag{6.69}$$

As $\bar{\boldsymbol{\chi}}^{\mathrm{T}} \mathbf{R}_{\boldsymbol{\chi}} \bar{\boldsymbol{\chi}} \geq \lambda_{\min}$, where $\lambda_{\min}$ is the smallest eigenvalue of $\mathbf{R}_{\boldsymbol{\chi}}$, and $\bar{\boldsymbol{\chi}}^{\mathrm{T}} \boldsymbol{\Sigma} \bar{\mathbf{d}}_{\boldsymbol{\xi}} \leq \sigma_{\max}$, where $\sigma_{\max}=\|\boldsymbol{\Sigma}\|_2$ represents the spectral norm—or largest singular value—of the matrix $\boldsymbol{\Sigma}$, the inequality (6.69) is always satisfied for

$$\left\|\mathbf{d}_{\boldsymbol{\xi}}\right\| \leq \frac{\gamma \lambda_{\min }}{\sigma_{\max }}\|\boldsymbol{\chi}\|. \tag{6.70}$$

Note that the right hand side of (6.70) is a class $\mathcal{K}$ function of $\boldsymbol{\chi}$, and, therefore, also a class $\mathcal{K}$ function of the state variables $(\boldsymbol{\xi}, \boldsymbol{\nu}) \in \mathsf{T}\mathcal{Q}_{\mathrm{R}}$, as $\nabla_{\boldsymbol{\xi}} V_{\mathrm{c}}(\|\boldsymbol{\xi}\|) \in \mathcal{K}$, and the composition of class $\mathcal{K}$ functions is again a class $\mathcal{K}$ function. Thus, the system (6.60) is ISS according to Theorem 2.6. ■

Let us now analyze the robustness of the velocity controller of Section 6.4 with respect to the "disturbance" $\mathbf{d}_{\boldsymbol{\nu}}=\hat{\boldsymbol{\nu}}$. To that end, we make the following assumption:

Assumption 6.6. A constant positive definite matrix $\mathbf{K}=\mathbf{K}^{\mathrm{T}}$ exists, such that the matrix

$$\mathbf{R}_{\varepsilon}^{\nu}=\mathbf{R}_{\mathrm{c}}-\frac{\varepsilon}{2}\left(\mathbf{M}_{\mathrm{c}} \mathbf{K} \nabla_{\boldsymbol{\xi}}^2 V_{\mathrm{c}}^{\mathrm{e}}+\nabla_{\boldsymbol{\xi}}^2 V_{\mathrm{c}}^{\mathrm{e}} \mathbf{K} \mathbf{M}_{\mathrm{c}}\right) \tag{6.71}$$

is positive definite in a neighborhood of the DE $(\hat{\boldsymbol{\xi}}, \hat{\boldsymbol{\nu}})$ for small values of ε.

Further, let us define the matrix $\boldsymbol{\Pi}_{\boldsymbol{\nu}}=\mathbf{J}_{\mathrm{c}}-\mathbf{C}_{\mathrm{c}}-\mathbf{R}_{\mathrm{c}}$, such that the closed-loop system (6.50) is given as

$$\mathbf{M}_{\mathrm{c}} \dot{\boldsymbol{\nu}}+\mathbf{C}_{\mathrm{c}} \boldsymbol{\nu}+\nabla_{\boldsymbol{\xi}} V_{\mathrm{c}}^{\mathrm{e}}=\left(\mathbf{J}_{\mathrm{c}}-\mathbf{R}_{\mathrm{c}}\right) \boldsymbol{\nu}-\boldsymbol{\Pi}_{\boldsymbol{\nu}} \mathbf{d}_{\boldsymbol{\nu}}. \tag{6.72}$$

The following theorem illustrates the ISS property of the speed controller:

Theorem 6.6. *Let $(\hat{\boldsymbol{\xi}}, \hat{\boldsymbol{\nu}})$ be an admissible DE with constant $\hat{\boldsymbol{\nu}}^{\mathrm{d}}$ and $\hat{\boldsymbol{\nu}}^{\mathrm{s}}=\mathbf{0}$, and define $\hat{\boldsymbol{\xi}}^{\mathrm{d}}=\boldsymbol{\xi}^{\mathrm{d}}$, such that the potential energy $V_{\mathrm{c}}^{\mathrm{e}}$ is only a function of the coordinates $\boldsymbol{\xi}^{\mathrm{s}}$. Let, further, $\varepsilon>0$ be a sufficiently small scalar. The system (6.72) is (locally) input-to-state stable for input disturbances $\mathbf{d}_{\boldsymbol{\nu}}$ satisfying*

$$\left\|\mathbf{d}_{\boldsymbol{\nu}}\right\| \leq \frac{\gamma \lambda_{\min }}{\sigma_{\max }}\|\boldsymbol{\chi}\|, \tag{6.73}$$

where $\boldsymbol{\chi}=\mathrm{col}(\nabla_{\boldsymbol{\xi}} V_{\mathrm{c}},\, \boldsymbol{\nu})$, *the scalar* $\gamma=]0,\, 1[$ *is free,* $\sigma_{\max}$ *represents the largest singular value of the matrix*

$$\boldsymbol{\Sigma} = \begin{bmatrix} \varepsilon \mathbf{K} \boldsymbol{\Pi}_{\boldsymbol{\nu}} \\ \boldsymbol{\Pi}_{\boldsymbol{\nu}} \end{bmatrix}, \tag{6.74}$$

and $\lambda_{\min}$ *is the smallest eigenvalue of the positive definite matrix*

$$\mathbf{R}_{\boldsymbol{\chi}} = \begin{bmatrix} \varepsilon \mathbf{K} & -\frac{\varepsilon}{2} \mathbf{K} \left(\mathbf{J}_{\mathrm{c}} + \mathbf{C}_{\mathrm{c}}^{\mathrm{T}} - \mathbf{R}_{\mathrm{c}} \right) \\ \frac{\varepsilon}{2} \left(\mathbf{J}_{\mathrm{c}} + \mathbf{R}_{\mathrm{c}} + \mathbf{C}_{\mathrm{c}} \right) \mathbf{K} & \mathbf{R}_{\varepsilon}^{\boldsymbol{\nu}} \end{bmatrix}. \tag{6.75}$$

Proof. Consider the (local) ISS Lyapunov function

$$E_{\mathrm{ISS}}^{\boldsymbol{\nu}} = \frac{1}{2} \boldsymbol{\nu}^{\mathrm{T}} \mathbf{M}_{\mathrm{c}} \boldsymbol{\nu} + V_{\mathrm{c}}^{\mathrm{e}} + \varepsilon \nabla_{\boldsymbol{\xi}}^{\mathrm{T}} V_{\mathrm{c}}^{\mathrm{e}} \mathbf{K} \mathbf{M}_{\mathrm{c}} \boldsymbol{\nu}, \tag{6.76}$$

which is positive definite for small values of ε. Its rate of change along the trajectories of (6.72) is given as

$$\begin{aligned} \dot{E}_{\mathrm{ISS}}^{\boldsymbol{\nu}} = {} & \boldsymbol{\nu}^{\mathrm{T}} \left(\left(\mathbf{J}_{\mathrm{c}} - \mathbf{R}_{\mathrm{c}} - \mathbf{C}_{\mathrm{c}} \right) \boldsymbol{\nu} - \nabla_{\boldsymbol{\xi}} V_{\mathrm{c}}^{\mathrm{e}} - \boldsymbol{\Pi}_{\boldsymbol{\nu}} \mathbf{d}_{\boldsymbol{\nu}} \right) + \frac{1}{2} \boldsymbol{\nu}^{\mathrm{T}} \dot{\mathbf{M}}_{\mathrm{c}} \boldsymbol{\nu} + \nabla_{\boldsymbol{\xi}}^{\mathrm{T}} V_{\mathrm{c}}^{\mathrm{e}} \left(\dot{\boldsymbol{\xi}} - \dot{\hat{\boldsymbol{\xi}}} \right) \\ & + \varepsilon \nabla_{\boldsymbol{\xi}}^{\mathrm{T}} V_{\mathrm{c}}^{\mathrm{e}} \mathbf{K} \dot{\mathbf{M}}_{\mathrm{c}} \boldsymbol{\nu} + \varepsilon \nabla_{\boldsymbol{\xi}}^{\mathrm{T}} V_{\mathrm{c}}^{\mathrm{e}} \mathbf{K} \left(\left(\mathbf{J}_{\mathrm{c}} - \mathbf{R}_{\mathrm{c}} - \mathbf{C}_{\mathrm{c}} \right) \boldsymbol{\nu} - \nabla_{\boldsymbol{\xi}} V_{\mathrm{c}}^{\mathrm{e}} - \boldsymbol{\Pi}_{\boldsymbol{\nu}} \mathbf{d}_{\boldsymbol{\nu}} \right) \\ & + \varepsilon \boldsymbol{\nu}^{\mathrm{T}} \mathbf{M}_{\mathrm{c}} \mathbf{K} \nabla_{\boldsymbol{\xi}}^{2} V_{\mathrm{c}}^{\mathrm{e}} \left(\dot{\boldsymbol{\xi}} - \dot{\hat{\boldsymbol{\xi}}} \right). \end{aligned}$$

From the characterization of the DE (6.48) and (6.49), we conclude

$$\nabla_{\boldsymbol{\xi}}^{\mathrm{T}} V_{\mathrm{c}}^{\mathrm{e}} \dot{\hat{\boldsymbol{\xi}}} = 0, \qquad \nabla_{\boldsymbol{\xi}}^{2} V_{\mathrm{c}}^{\mathrm{e}} \dot{\hat{\boldsymbol{\xi}}} = \mathbf{0}. \tag{6.77}$$

The latter relationships imply

$$\begin{aligned} \dot{E}_{\mathrm{ISS}}^{\boldsymbol{\nu}} = {} & -\boldsymbol{\nu}^{\mathrm{T}} \underbrace{\left(\mathbf{R}_{\mathrm{c}} - \frac{\varepsilon}{2} \left(\mathbf{M}_{\mathrm{c}} \mathbf{K} \nabla_{\boldsymbol{\xi}}^{2} V_{\mathrm{c}}^{\mathrm{e}} + \nabla_{\boldsymbol{\xi}}^{2} V_{\mathrm{c}}^{\mathrm{e}} \mathbf{K} \mathbf{M}_{\mathrm{c}} \right) \right)}_{\mathbf{R}_{\varepsilon}^{\boldsymbol{\nu}}} \boldsymbol{\nu} - \varepsilon \nabla_{\boldsymbol{\xi}}^{\mathrm{T}} V_{\mathrm{c}}^{\mathrm{e}} \mathbf{K} \nabla_{\boldsymbol{\xi}} V_{\mathrm{c}}^{\mathrm{e}} \\ & + \varepsilon \nabla_{\boldsymbol{\xi}}^{\mathrm{T}} V_{\mathrm{c}}^{\mathrm{e}} \mathbf{K} \left(\mathbf{J}_{\mathrm{c}} - \mathbf{R}_{\mathrm{c}} + \mathbf{C}_{\mathrm{c}}^{\mathrm{T}} \right) \boldsymbol{\nu} - \boldsymbol{\nu}^{\mathrm{T}} \boldsymbol{\Pi}_{\boldsymbol{\nu}} \mathbf{d}_{\boldsymbol{\nu}} - \varepsilon \nabla_{\boldsymbol{\xi}}^{\mathrm{T}} V_{\mathrm{c}}^{\mathrm{e}} \mathbf{K} \boldsymbol{\Pi}_{\boldsymbol{\nu}} \mathbf{d}_{\boldsymbol{\nu}}. \end{aligned} \tag{6.78}$$

The rest of the proof is analogous to the proof of Theorem 6.5 for the input matrix $\boldsymbol{\Pi}_{\boldsymbol{\nu}}$, and the disturbance $\mathbf{d}_{\boldsymbol{\nu}}$, defining $\boldsymbol{\chi}=\mathrm{col}(\nabla_{\boldsymbol{\xi}} V_{\mathrm{c}}^{\mathrm{e}},\, \boldsymbol{\nu})$, and noting that

$$\mathbf{R}_{\boldsymbol{\chi}} = \begin{bmatrix} \varepsilon \mathbf{K} & -\frac{\varepsilon}{2} \mathbf{K} \left(\mathbf{J}_{\mathrm{c}} + \mathbf{C}_{\mathrm{c}}^{\mathrm{T}} - \mathbf{R}_{\mathrm{c}} \right) \\ \frac{\varepsilon}{2} \left(\mathbf{J}_{\mathrm{c}} + \mathbf{R}_{\mathrm{c}} + \mathbf{C}_{\mathrm{c}} \right) \mathbf{K} & \mathbf{R}_{\varepsilon}^{\boldsymbol{\nu}} \end{bmatrix} \tag{6.79}$$

is positive definite for ε sufficiently small. ■

Remark 6.5.1. The ISS property can be also invoked to study the robustness of controllers to model uncertainties by reformulating the modeling errors as input disturbances. By doing so, one can show that, to a certain extent, energy-based controllers are intrinsically robust to model uncertainties.

6.6 Motor dynamics

Many robotic platforms are actuated by DC motors, for instance, such that the input forces (and/or torques) $\boldsymbol{\tau}$ cannot be directly commanded. Rather, the armature voltage of the motors $\mathbf{u}_\mathrm{A}$ is the input, and the torques are governed by the motor dynamics

$$\dot{\boldsymbol{\tau}} = \tilde{\mathbf{f}}_\mathrm{A} + \tilde{\mathbf{G}}_\mathrm{A}\mathbf{u}_\mathrm{A}, \tag{6.80}$$

which can be given in terms of the system's input $\mathbf{u}$ as

$$\dot{\mathbf{u}} = \mathbf{f}_\mathrm{A} + \mathbf{G}_\mathrm{A}\mathbf{u}_\mathrm{A}, \tag{6.81}$$

where $\mathbf{f}_\mathrm{A} = \mathbf{f}_\mathrm{A}(\boldsymbol{\xi}, \boldsymbol{\nu}, \mathbf{u})$ is the drift vector field, and $\mathbf{G}_\mathrm{A}$ is the new (invertible) constant input matrix (cf. (B.4) in Appendix B.1). In the case that the motor dynamics (6.81) cannot be neglected, the backstepping method—introduced in [105]—can be used to include the actuator dynamics in the energy shaping procedure to design a control law that asymptotically stabilizes the mechanical system (6.23) with actuator dynamics (6.81). The following proposition summarizes the result for the position stabilization. The same procedure, however, can be applied to include actuator dynamics for speed stabilization.

Proposition 6.4. *Let* $\tilde{\mathbf{u}}$ *be the* desired *input defined as in (6.40), which asymptotically stabilizes the system (6.23) according to Theorem 6.1. Further, assume that the input* $\mathbf{u}$ *cannot be commanded directly, but rather it is subject to the dynamics (6.81). Then, the control law*

$$\mathbf{u}_\mathrm{A} = \mathbf{G}_\mathrm{A}^{-1}\left(\dot{\tilde{\mathbf{u}}} - \mathbf{G}^\mathrm{T}\mathbf{M}^{-1}\mathbf{M}_\mathrm{c}\boldsymbol{\nu} - \mathbf{f}_\mathrm{A} - \mathbf{K}_\mathrm{A}(\mathbf{u} - \tilde{\mathbf{u}})\right), \qquad \mathbf{K}_\mathrm{A} > \mathbf{0}, \tag{6.82}$$

asymptotically stabilizes the equilibrium $\boldsymbol{\xi}^*$.

Proof. As $\tilde{\mathbf{u}}$ cannot be commanded directly, let us consider the Lyapunov function

candidate

$$E_{\mathrm{bs}} = \frac{1}{2}\,\boldsymbol{\nu}^{\mathrm{T}}\mathbf{M}_{\mathrm{c}}\boldsymbol{\nu} + V_{\mathrm{c}} + \frac{1}{2}\,(\mathbf{u}-\tilde{\mathbf{u}})^{\mathrm{T}}(\mathbf{u}-\tilde{\mathbf{u}}) \tag{6.83}$$

for the system (6.23) including the motor dynamics (6.81). The function E_{bs} clearly is positive definite in a neighborhood of the equilibrium $\boldsymbol{\xi}^*$, as $\mathbf{M}_{\mathrm{c}}(\boldsymbol{\xi}) > \mathbf{0}$ and $\boldsymbol{\xi}^* = \arg\min V_{\mathrm{c}}$. The rate of change of E_{bs} along the trajectories of (6.23) and (6.81) is given as

$$\begin{aligned}\dot{E}_{\mathrm{bs}} &= \boldsymbol{\nu}^{\mathrm{T}}\mathbf{M}_{\mathrm{c}}\dot{\boldsymbol{\nu}} + \frac{1}{2}\,\boldsymbol{\nu}^{\mathrm{T}}\dot{\mathbf{M}}_{\mathrm{c}}\boldsymbol{\nu} + \nabla_{\boldsymbol{\xi}}^{\mathrm{T}}V_{\mathrm{c}}\boldsymbol{\nu} + (\dot{\mathbf{u}}-\dot{\tilde{\mathbf{u}}})^{\mathrm{T}}(\mathbf{u}-\tilde{\mathbf{u}}) \\ &\overset{(6.23)}{=} \boldsymbol{\nu}^{\mathrm{T}}\mathbf{M}_{\mathrm{c}}\mathbf{M}^{-1}(\mathbf{G}\mathbf{u} + \mathbf{J}\boldsymbol{\nu} + \mathbf{F}_{\mathrm{pot}} - \mathbf{C}\boldsymbol{\nu}) + \frac{1}{2}\,\boldsymbol{\nu}^{\mathrm{T}}\dot{\mathbf{M}}_{\mathrm{c}}\boldsymbol{\nu} + \nabla_{\boldsymbol{\xi}}^{\mathrm{T}}V_{\mathrm{c}}\boldsymbol{\nu} + (\dot{\mathbf{u}}-\dot{\tilde{\mathbf{u}}})^{\mathrm{T}}(\mathbf{u}-\tilde{\mathbf{u}})\end{aligned}$$

As known from the backstepping design, we add a zero in form of $\mathbf{G}\tilde{\mathbf{u}} - \mathbf{G}\tilde{\mathbf{u}}$. Since $\tilde{\mathbf{u}}$ is defined as in (6.40) and asymptotically stabilizes (6.23), we get

$$\begin{aligned}\dot{E}_{\mathrm{bs}} &= \boldsymbol{\nu}^{\mathrm{T}}\mathbf{M}_{\mathrm{c}}\mathbf{M}^{-1}\left(\mathbf{G}(\mathbf{u}-\tilde{\mathbf{u}}) + \mathbf{G}\tilde{\mathbf{u}} + \mathbf{J}\boldsymbol{\nu} + \mathbf{F}_{\mathrm{pot}} - \mathbf{C}\boldsymbol{\nu}\right) + \frac{1}{2}\,\boldsymbol{\nu}^{\mathrm{T}}\dot{\mathbf{M}}_{\mathrm{c}}\boldsymbol{\nu} \\ &\quad + \nabla_{\boldsymbol{\xi}}^{\mathrm{T}}V_{\mathrm{c}}\boldsymbol{\nu} + (\dot{\mathbf{u}}-\dot{\tilde{\mathbf{u}}})^{\mathrm{T}}(\mathbf{u}-\tilde{\mathbf{u}}) \\ &\overset{(6.40)}{=} -\boldsymbol{\nu}^{\mathrm{T}}\mathbf{R}_{\mathrm{c}}\boldsymbol{\nu} + \left(\dot{\mathbf{u}} - \dot{\tilde{\mathbf{u}}} + \mathbf{G}^{\mathrm{T}}\mathbf{M}^{-1}\mathbf{M}_{\mathrm{c}}\boldsymbol{\nu}\right)^{\mathrm{T}}(\mathbf{u}-\tilde{\mathbf{u}}) \\ &\overset{(6.81)}{=} -\boldsymbol{\nu}^{\mathrm{T}}\mathbf{R}_{\mathrm{c}}\boldsymbol{\nu} + \left(\mathbf{f}_{\mathrm{A}} + \mathbf{G}_{\mathrm{A}}\mathbf{u}_{\mathrm{A}} - \dot{\tilde{\mathbf{u}}} + \mathbf{G}^{\mathrm{T}}\mathbf{M}^{-1}\mathbf{M}_{\mathrm{c}}\boldsymbol{\nu}\right)^{\mathrm{T}}(\mathbf{u}-\tilde{\mathbf{u}})\end{aligned} \tag{6.84}$$

If one chooses the control law (6.82), then (6.84) becomes

$$\dot{E}_{\mathrm{bs}} = -\boldsymbol{\nu}^{\mathrm{T}}\mathbf{R}_{\mathrm{c}}\boldsymbol{\nu} - (\mathbf{u}-\tilde{\mathbf{u}})^{\mathrm{T}}\,\mathbf{K}_{\mathrm{A}}\,(\mathbf{u}-\tilde{\mathbf{u}}) \leq 0. \tag{6.85}$$

The latter inequality proves asymptotic stability of the equilibrium $\boldsymbol{\xi}^*$ according to Corollary 2.3, as $\mathbf{R}_{\mathrm{c}}$ ensures pervasive damping. ■

6.7 Concluding remarks

In this chapter, we considered the stabilization problem for underactuated nonholonomic mechanical systems via total energy shaping. We presented a systematic solution to the matching problem in reduced space $\mathcal{Q}_{\mathrm{R}}$, and showed how a coordinate transformation allows us to consider the stabilizing problem also in a constrained space $\mathcal{Q}_{\mathrm{C}}$ for a class of nonholonomic systems. Further, we illustrated how the results from the position controller are applied to design a speed control law that asymptotically

stabilizes an admissible dynamical equilibrium if some conditions are satisfied.

In a following step, we showed robustness of the closed-loop system for both the position and the velocity controller by means of ISS. This property allows us to continuously vary the desired equilibrium (or dynamical equilibrium) within specific bounds without threatening the stability of the system.

Finally, we showed how actuator dynamics can be easily embedded into the design procedure via backstepping. By doing so, we are able to compute position and velocity stabilizing control laws for mechanical systems with motor dynamics that cannot be neglected.

Based on the stabilization and ISS results presented in this chapter, the next chapter deals with trajectory tracking and path following strategies for nonholonomic systems.

7 Trajectory Tracking and Path Following

Motion control for mechanical systems can be practically divided into three categories: stabilization, trajectory tracking and path following. In the last chapter, we considered the stabilization problem; this chapter is concerned with trajectory tracking and path following for nonholonomic underactuated mechanical systems via total energy shaping. The control problem is specified in Section 7.1. Section 7.2 discusses the trajectory tracking problem. As admissible reference trajectories are often hard and even impossible to compute, we also consider stability with respect to reference trajectories that are not compatible with the system's dynamics. Section 7.3 covers the path following approach. Specifically, we present a vector field control strategy, and study the stability of the closed-loop system. The chapter concludes with a final remark in Section 7.4.

7.1 Problem formulation

Mobile robots and vehicles are designed to move from one place to another. We are mostly familiar with manned vehicles that are directly steered by humans. However, drones, unmanned vehicles and mobile robots are being developed at a fast pace. In the absence of a pilot, automatic control accounts for the navigation. In the course of the years, different strategies have been developed for wheeled systems to automatically displace from one point to another, or to execute a desired maneuver. In this chapter, we are concerned with reference tracking and path following for underactuated nonholonomic systems. Often, and in order to simplify the problem setting, some authors employ kinematic models of nonholonomic systems for tracking [97] and path following [137] (see also [57]). However, in this thesis we study underactuated systems, whose behavior can only be accurately described including the inertial and/or potential couplings. For that reason, it is necessary to consider the dynamical model.

The first approach we deal with is trajectory tracking, or reference tracking, which aims at steering the mobile robot to asymptotically converge towards a reference trajectory. A trajectory is a curve on the configuration (or reduced) manifold that is

parametrized by time. That is, in trajectory tracking, the system is commanded to be in a specific position with a specific velocity at a particular time. For simplicity, we consider trajectory tracking in the reduced space $\mathcal{Q}_{\mathrm{R}}$.

Definition 7.1 (Admissible reference trajectory.)**.** A reference trajectory $\hat{\boldsymbol{\xi}}(t)$ is said to be admissible if it is compatible with the system's dynamics (6.23). In other words, if $\boldsymbol{\xi}(0) = \hat{\boldsymbol{\xi}}(0)$, and $\boldsymbol{\nu}(0) = \hat{\boldsymbol{\nu}}(0)$, then, in the absence of disturbances, an input $\mathbf{u}_{\mathrm{ff}}(t)$ exists, such that $\boldsymbol{\xi}(t) \equiv \hat{\boldsymbol{\xi}}(t)$, $\forall t > 0$.

Using the result from Lemma 2.1, we can express the set of admissible trajectories for the mechanical system (6.23) by the differential equation

$$\mathbf{G}_{\perp}\left(\mathbf{M}(\hat{\boldsymbol{\xi}})\dot{\hat{\boldsymbol{\nu}}} + \mathbf{C}(\hat{\boldsymbol{\xi}}, \hat{\boldsymbol{\nu}})\hat{\boldsymbol{\nu}} - \mathbf{F}_{\mathrm{pot}}(\hat{\boldsymbol{\xi}}) - \mathbf{J}(\hat{\boldsymbol{\xi}}, \hat{\boldsymbol{\nu}})\hat{\boldsymbol{\nu}}\right) = \mathbf{0}, \tag{7.1}$$

where $\hat{\boldsymbol{\nu}}(t) = \dot{\hat{\boldsymbol{\xi}}}(t)$. If a solution $\hat{\boldsymbol{\xi}}(t)$ to (7.1) can be found, then (6.23) with input

$$\mathbf{u}_{\mathrm{ff}} = \mathbf{G}^{\mathrm{T}}\mathbf{G}^{-1}\mathbf{G}^{\mathrm{T}}\left(\mathbf{M}(\hat{\boldsymbol{\xi}})\dot{\hat{\boldsymbol{\nu}}} + \mathbf{C}(\hat{\boldsymbol{\xi}}, \hat{\boldsymbol{\nu}})\hat{\boldsymbol{\nu}} - \mathbf{F}_{\mathrm{pot}}(\hat{\boldsymbol{\xi}}) - \mathbf{J}(\hat{\boldsymbol{\xi}}, \hat{\boldsymbol{\nu}})\hat{\boldsymbol{\nu}}\right) \tag{7.2}$$

exactly follows the reference $\hat{\boldsymbol{\xi}}(t)$ if the initial conditions coincide. In addition to the feedforward term $\mathbf{u}_{\mathrm{ff}}$, a state feedback term $\mathbf{u}_{\mathrm{fb}}$ is necessary to account for modeling errors, initial offsets, and external disturbances.

The trajectory tracking problem can be stated as follows. Let $\boldsymbol{\xi}_{\mathrm{e}} = \boldsymbol{\xi}(t) - \hat{\boldsymbol{\xi}}(t)$ be the tracking error, and let $\mathcal{B}$ be a neighborhood of $(\boldsymbol{\xi}_{\mathrm{e}}, \dot{\boldsymbol{\xi}}_{\mathrm{e}}) = (\mathbf{0}, \mathbf{0})$. Design a controller $\mathbf{u} = \mathbf{u}_{\mathrm{ff}} + \mathbf{u}_{\mathrm{fb}}$ for the system (6.23) such that all closed-loop signals are bounded, and the tracking error $\boldsymbol{\xi}_{\mathrm{e}}$, with $(\boldsymbol{\xi}_{\mathrm{e}}(0), \dot{\boldsymbol{\xi}}_{\mathrm{e}}(0)) \in \mathcal{B}$, converges to the origin in the absence of disturbances. That is, find a control law $\mathbf{u}$, such that

$$(\boldsymbol{\xi}_{\mathrm{e}}(0), \dot{\boldsymbol{\xi}}_{\mathrm{e}}(0)) \in \mathcal{B} \implies \lim_{t\to\infty} \boldsymbol{\xi}(t) = \hat{\boldsymbol{\xi}}(t). \tag{7.3}$$

Note the local property of the result, as (7.3) holds for initial errors lying in a neighborhood of the origin. For unconstrained fully actuated mechanical systems, the tracking control problem is well understood and can be consulted in standard textbooks on control (cf. [118, 147, 189]) and robotics (cf. [42, 141]). Still, finding admissible trajectories for underactuated systems is difficult and might be even unfeasible, as $\hat{\boldsymbol{\xi}}(t)$ is subject to (7.1). One possibility to find an admissible trajectory between two given states is to employ stable nonlinear inversion approaches for output tracking [54, 76].

As we are not always able to compute admissible trajectories, there arises the question whether the closed-loop system is stable with respect to reference trajectories $\hat{\boldsymbol{\xi}}(t)$ that

are not compatible with the system's dynamics (6.23). That is, trajectories for which no feedforward input term $\mathbf{u}_{\text{ff}}$ exists, such that $\boldsymbol{\xi}(t) \equiv \hat{\boldsymbol{\xi}}(t)$ for all times $t > 0$, if their initial conditions match. The tracking problem for non-admissible trajectories can be stated as follows. Design a controller $\mathbf{u} = \mathbf{u}_{\text{ff}} + \mathbf{u}_{\text{fb}}$ for the system (6.23) such that, for all $(\boldsymbol{\xi}_{\text{e}}(0), \dot{\boldsymbol{\xi}}_{\text{e}}(0)) \in \mathcal{B}$, all closed-loop signals as well as the tracking error $\boldsymbol{\xi}_{\text{e}}$ remain bounded. Furthermore, $\boldsymbol{\xi}_{\text{e}}$ converges towards the origin if $\hat{\boldsymbol{\xi}}(t)$ is admissible.

The second approach we study in this chapter is path following, for which the primary goal is to steer the system towards a desired geometric path, and then to regulate a given, usually constant, velocity along the path. For simplicity, we consider geometric paths in the two-dimensional Euclidean space, piecewise defined as

$$\mathcal{P} = \left\{ (x, y, \theta) \in \mathbb{R}^2 \times \mathbb{S}^1 \mid \boldsymbol{\Phi}(x, y, \theta) = \mathbf{0} \right\}, \tag{7.4}$$

where the function $\boldsymbol{\Phi}(x, y, \theta)$ is sufficiently smooth, and the path is admissible by the nonholonomic constraints. In contrast to the holonomic case, in which the path can be given as a function of x and y, the nonholonomic case demands a specific orientation θ at every point of the path in accordance with the constraints. The approach can be, if necessary, easily expanded to the three-dimensional Euclidean space $\mathbb{R}^3$. Although, in general, no time dependency is assigned to the path, the dynamics along the path can be further specified by assigning a desired velocity profile. However, in this chapter we restrict the analysis to a constant velocity along the path. The control scheme consists, therefore, of a passivity-based velocity controller together with a heading regulation to approach and stay on the path. By doing so, large initial deviations to $\mathcal{P}$ do not affect the magnitude of the input. As a result, the control signals are less prone to reach saturation using path following strategies instead of reference tracking.

The goal of path following is to design feedback control laws for (6.23), such that all the closed-loop signals are bounded, the position of the system converges to and remains inside an arbitrarily small tube centered around the desired path $\mathcal{P}$, and the system travels along the path with desired constant speed v^*, i. e., the speed error $v_{\text{e}} = v - v^*$ converges to zero, as $t \to \infty$. Even though path following has received much less attention than reference tracking in the literature, it has been widely used for flying, underwater, and wheeled robots, especially since the introduction of the passive vector field control (PVFC) in the nineties [123, 126, 146].

7.2 Trajectory tracking

As mentioned before, in trajectory tracking, the goal is to steer the system such that it converges toward a reference trajectory. We want, therefore, to control the system to be in a defined position, and to move with a defined velocity, at a particular time. To do so, the idea is to define the error from the actual trajectory with respect to the reference, and then to control the system such that the error vanishes as time goes to infinity.

Since the reference velocity $\hat{\boldsymbol{\nu}}$ and the actual velocity $\boldsymbol{\nu}$ live in different tangent spaces $\mathsf{T}_{\hat{\boldsymbol{\xi}}}\mathcal{Q}_{\mathrm{R}}$ and $\mathsf{T}_{\boldsymbol{\xi}}\mathcal{Q}_{\mathrm{R}}$, to measure the distance between actual and reference velocity, we require the notion of a *transport map* to take vectors from one tangent space to another. Let us for a moment denote the pair $(\boldsymbol{\xi}, \boldsymbol{\nu}) \in \mathsf{T}\mathcal{Q}_{\mathrm{R}}$ as $\boldsymbol{\nu}_{\boldsymbol{\xi}}$, i. e., the velocity $\boldsymbol{\nu}$ at $\boldsymbol{\xi}$.

Definition 7.2 (Transport map [42])**.** A transport map $\mathfrak{I}\colon \mathcal{Q}_{\mathrm{R}} \times \mathsf{T}\mathcal{Q}_{\mathrm{R}} \to \mathsf{T}\mathcal{Q}_{\mathrm{R}} \times \mathcal{Q}_{\mathrm{R}}$ is a smooth map that satisfies

i) $\mathfrak{I}(\boldsymbol{\xi}, \boldsymbol{\nu}_{\boldsymbol{\xi}}) = \boldsymbol{\nu}_{\boldsymbol{\xi}}, \qquad \forall\, \boldsymbol{\xi} \in \mathcal{Q}_{\mathrm{R}}$ and $\boldsymbol{\nu}_{\boldsymbol{\xi}} \in \mathsf{T}\mathcal{Q}_{\mathrm{R}}$.

This object plays an important role in control design, as it is necessary to define the notion of a *velocity error*

$$\boldsymbol{\nu}_{\boldsymbol{\xi}} - \mathfrak{I}(\boldsymbol{\xi}, \hat{\boldsymbol{\nu}}_{\hat{\boldsymbol{\xi}}}) = \boldsymbol{\nu}_{\boldsymbol{\xi}} - \hat{\boldsymbol{\nu}}_{\boldsymbol{\xi}} = \boldsymbol{\nu}_{\mathrm{e}}. \tag{7.5}$$

We will normally drop the index and write $\boldsymbol{\nu}_{\mathrm{e}} = \boldsymbol{\nu} - \hat{\boldsymbol{\nu}}$ with some abuse of notation. Figure 7.1 illustrates the transport map.

In addition to the velocity error, for reference tracking we also require the error in the configuration. To measure the distance between reference and actual position, we make use of the *tracking error function*.

Definition 7.3 (Tracking error function [42])**.** A symmetric map $\Psi\colon \mathcal{Q}_{\mathrm{R}} \times \mathcal{Q}_{\mathrm{R}} \to \mathbb{R}$ is a tracking error function if, for all $\hat{\boldsymbol{\xi}} \in \mathcal{Q}_{\mathrm{R}}$, it satisfies

i) $\Psi(\hat{\boldsymbol{\xi}}, \hat{\boldsymbol{\xi}}) \leq \Psi(\hat{\boldsymbol{\xi}}, \boldsymbol{\xi}), \qquad \forall\, \boldsymbol{\xi} \neq \hat{\boldsymbol{\xi}}$,

ii) $\nabla_{\boldsymbol{\xi}} \Psi(\hat{\boldsymbol{\xi}}, \boldsymbol{\xi})\,|_{\boldsymbol{\xi}=\hat{\boldsymbol{\xi}}} = \mathbf{0}$, and

iii) $\nabla^2_{\boldsymbol{\xi}} \Psi(\hat{\boldsymbol{\xi}}, \boldsymbol{\xi})\,|_{\boldsymbol{\xi}=\hat{\boldsymbol{\xi}}}$ is positive definite.

A tracking function can be easily found via energy shaping: Suppose that V_{c} is a solution to (6.35), i. e., the shaped potential energy, with a strict minimum at $\mathbf{0}$. For

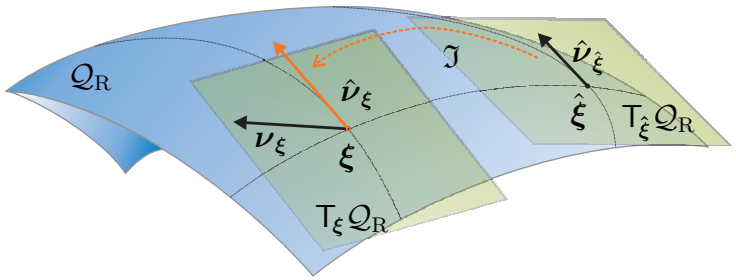

Figure 7.1: The notion of the transport map $\mathfrak{I}$ to measure the velocity error between velocity vectors living in different tangent spaces.

arbitrary reference values $\hat{\boldsymbol{\xi}} \in \mathcal{Q}_\mathrm{R}$, the function $V_\mathrm{c}^\mathrm{e} = V_\mathrm{c}(\boldsymbol{\xi}_\mathrm{e})$ is locally a tracking error function, where $\boldsymbol{\xi}_\mathrm{e} = \boldsymbol{\xi} - \hat{\boldsymbol{\xi}}$ denotes the configuration error.

Definition 7.4 (Compatibility of the tracking error function and the transport map)**.** A pair $(\Psi, \mathfrak{I})$ is said to be compatible if for all $(\boldsymbol{\xi}, \hat{\boldsymbol{\xi}}) \in \mathcal{Q}_\mathrm{R} \times \mathcal{Q}_\mathrm{R}$, the following relationship holds

$$\nabla_{\hat{\boldsymbol{\xi}}} \Psi(\boldsymbol{\xi}, \hat{\boldsymbol{\xi}}) = -\mathfrak{I}^*(\nabla_{\boldsymbol{\xi}} \Psi(\boldsymbol{\xi}, \hat{\boldsymbol{\xi}}), \hat{\boldsymbol{\xi}}),$$

where the map $\mathfrak{I}^*$ is the dual of the transport map $\mathfrak{I}$.

The map $\mathfrak{I}^* : \mathsf{T}^*\mathcal{Q}_\mathrm{R} \times \mathcal{Q}_\mathrm{R} \to \mathcal{Q}_\mathrm{R} \times \mathsf{T}^*\mathcal{Q}_\mathrm{R}$ is necessary to compare elements of the cotangent bundle—generalized forces—living in different cotangent spaces. It takes the elements from one cotangent space to another as shown in Figure 7.2.

The choice of the tracking error function Ψ has an effect on the performance of the closed-loop system; the choice of a suitable (and compatible) transport map $\mathfrak{I}$ has an effect on the complexity of the controller. As the choice of the tracking error function $V_\mathrm{c}^\mathrm{e} = V_\mathrm{c}(\boldsymbol{\xi}_\mathrm{e})$ is natural in the energy shaping framework, and $\nabla_{\hat{\boldsymbol{\xi}}} V_\mathrm{c}^\mathrm{e} = -\nabla_{\boldsymbol{\xi}} V_\mathrm{c}^\mathrm{e}$ holds, the identity map is a compatible transport map.

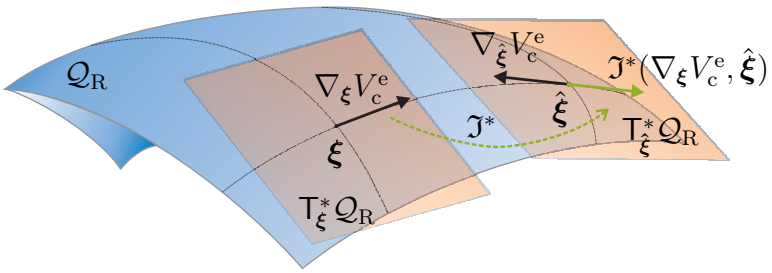

Figure 7.2: The dual of the transport map $\mathfrak{I}^*$ is necessary to compare elements of the cotangent bundle—generalized forces—that live in different cotangent spaces.

7.2.1 Tracking admissible trajectories in reduced space

Reference tracking in reduced space is straightforward for admissible reference trajectories $\hat{\boldsymbol{\xi}}(t)$, as it resembles the holonomic case. We will, however, present the problem setting in the energy-based framework for completeness. We want to design a controller such that the closed-loop signals remain bounded, and the position and velocity errors $\boldsymbol{\xi}_\mathrm{e} = \boldsymbol{\xi} - \hat{\boldsymbol{\xi}}$, and $\boldsymbol{\nu}_\mathrm{e} = \boldsymbol{\nu} - \hat{\boldsymbol{\nu}}$, respectively, converge to zero as $t \to \infty$. To put it in energy shaping words, the idea is to find a control law that renders (6.23) the closed-loop system

$$\mathbf{M}_\mathrm{c}\dot{\boldsymbol{\nu}}_\mathrm{e} + \mathbf{C}_\mathrm{c}\boldsymbol{\nu}_\mathrm{e} + \nabla_{\boldsymbol{\xi}} V_\mathrm{c}^\mathrm{e} = (\mathbf{J}_\mathrm{c} - \mathbf{R}_\mathrm{c})\,\boldsymbol{\nu}_\mathrm{e}, \tag{7.6}$$

where $\hat{\boldsymbol{\xi}}(t)$ is an admissible trajectory for (6.23), and $\hat{\boldsymbol{\nu}}(t) = \dot{\hat{\boldsymbol{\xi}}}(t)$. The following theorem proves asymptotic stability of the error $\boldsymbol{\xi}_\mathrm{e}$ for admissible trajectories $\hat{\boldsymbol{\xi}}(t)$.

Theorem 7.1. *Let (7.6) describe the closed-loop dynamics, where $\mathbf{M}_\mathrm{c} > \mathbf{0}$, V_c^e is a tracking error function, and $\mathbf{J}_\mathrm{c}$ is skew-symmetric. Further, let the condition of Assumption 6.6 hold in a neighborhood of $\boldsymbol{\xi}_\mathrm{e} = \mathbf{0}$, and let the initial errors $\boldsymbol{\xi}_\mathrm{e}(0)$ and $\boldsymbol{\nu}_\mathrm{e}(0)$ be sufficiently close to the origin. Then, the position and velocity error signals $\boldsymbol{\xi}_\mathrm{e} = \boldsymbol{\xi} - \hat{\boldsymbol{\xi}}$ and $\boldsymbol{\nu}_\mathrm{e} = \boldsymbol{\nu} - \hat{\boldsymbol{\nu}}$, respectively, remain bounded and converge to zero as $t \to \infty$.*

Proof. Consider the time-varying Lyapunov function[1]

$$E_\varepsilon = \frac{1}{2}\boldsymbol{\nu}_\mathrm{e}^\mathrm{T}\mathbf{M}_\mathrm{c}\boldsymbol{\nu}_\mathrm{e} + V_\mathrm{c}^\mathrm{e} + \varepsilon\nabla_{\boldsymbol{\xi}}^\mathrm{T} V_\mathrm{c}^\mathrm{e}\mathbf{K}\mathbf{M}_\mathrm{c}\boldsymbol{\nu}_\mathrm{e}. \tag{7.7}$$

Its derivative along the trajectories of (7.6) is

$$\begin{aligned}\dot{E}_\varepsilon = &-\boldsymbol{\nu}_\mathrm{e}^\mathrm{T}\left(\mathbf{R}_\mathrm{c} - \varepsilon\mathbf{M}_\mathrm{c}\mathbf{K}\nabla_{\boldsymbol{\xi}}^2 V_\mathrm{c}^\mathrm{e}\right)\boldsymbol{\nu}_\mathrm{e} - \varepsilon\nabla_{\boldsymbol{\xi}}^\mathrm{T} V_\mathrm{c}^\mathrm{e}\mathbf{K}\nabla_{\boldsymbol{\xi}} V_\mathrm{c}^\mathrm{e} \\ &+ \varepsilon\nabla_{\boldsymbol{\xi}}^\mathrm{T} V_\mathrm{c}^\mathrm{e}\mathbf{K}\left(\mathbf{J}_\mathrm{c} - \mathbf{C}_\mathrm{c} - \mathbf{R}_\mathrm{c}\right)\boldsymbol{\nu}_\mathrm{e} + \varepsilon\nabla_{\boldsymbol{\xi}}^\mathrm{T} V_\mathrm{c}^\mathrm{e}\mathbf{K}\dot{\mathbf{M}}_\mathrm{c}\boldsymbol{\nu}_\mathrm{e}.\end{aligned} \tag{7.8}$$

Defining $\boldsymbol{\chi} = \mathrm{col}(\nabla_{\boldsymbol{\xi}} V_\mathrm{c}^\mathrm{e},\, \boldsymbol{\nu}_\mathrm{e})$, expression (7.8) can be given as

$$\dot{E}_\varepsilon = -\boldsymbol{\chi}^\mathrm{T}\mathbf{R}_{\boldsymbol{\chi}}\boldsymbol{\chi}, \tag{7.9}$$

where

$$\mathbf{R}_{\boldsymbol{\chi}} = \begin{bmatrix} \varepsilon\mathbf{K} & -\frac{\varepsilon}{2}\mathbf{K}\left(\mathbf{J}_\mathrm{c} + \mathbf{C}_\mathrm{c}^\mathrm{T} - \mathbf{R}_\mathrm{c}\right) \\ \frac{\varepsilon}{2}\left(\mathbf{J}_\mathrm{c} + \mathbf{R}_\mathrm{c} + \mathbf{C}_\mathrm{c}\right)\mathbf{K} & \mathbf{R}_\varepsilon^\nu \end{bmatrix}. \tag{7.10}$$

Since $\mathbf{R}_\varepsilon^\nu$ is assumed to be positive definite (Assumption 6.6), it can be locally ensured

[1] A similar Lyapunov function can be found in [141] for trajectory tracking of fully actuated systems. It is clearly positive definite for small values of ε.

that $\mathbf{R}_{\boldsymbol{\chi}} > \mathbf{0}$ for ε sufficiently small, and, thus, $\dot{E}_\varepsilon < 0$. Uniformly asymptotic convergence towards the reference trajectory $\hat{\boldsymbol{\xi}}(t)$ follows from Theorem 2.5, since both $\boldsymbol{\xi}_\mathrm{e}$ and $\boldsymbol{\nu}_\mathrm{e}$ converge to the origin. ■

Note, again, the local nature of the result. To achieve the desired behavior (7.6), we need to find an admissible trajectory $\hat{\boldsymbol{\xi}}(t)$ for (6.23), and an input $\mathbf{u}$ that satisfies the matching condition (comparing (6.23) with (7.6))

$$\mathbf{M}\mathbf{M}_\mathrm{c}^{-1}\left((\mathbf{J}_\mathrm{c} - \mathbf{R}_\mathrm{c} - \mathbf{C}_\mathrm{c})\,\boldsymbol{\nu}_\mathrm{e} - \nabla_{\boldsymbol{\xi}} V_\mathrm{c}^\mathrm{e}\right) + \mathbf{M}\dot{\hat{\boldsymbol{\nu}}} + (\mathbf{C} - \mathbf{J})\,\boldsymbol{\nu} - \mathbf{F}_\mathrm{pot} = \mathbf{G}\mathbf{u}. \tag{7.11}$$

The solution of

$$\mathbf{G}\mathbf{u}_\mathrm{ke} = -\mathbf{M}\mathbf{M}_\mathrm{c}^{-1}(\mathbf{C}_\mathrm{c} - \mathbf{J}_\mathrm{c})\boldsymbol{\nu} + (\mathbf{C} - \mathbf{J})\boldsymbol{\nu}, \tag{7.12a}$$

$$\mathbf{G}\mathbf{u}_\mathrm{pe} = -\mathbf{M}\mathbf{M}_\mathrm{c}{}^{-1}\nabla_{\boldsymbol{\xi}} V_\mathrm{c}^\mathrm{e}, \tag{7.12b}$$

$$\mathbf{G}\mathbf{u}_\mathrm{di} = -\mathbf{M}\mathbf{M}_\mathrm{c}^{-1}\mathbf{R}_\mathrm{c}\boldsymbol{\nu}_\mathrm{e}, \tag{7.12c}$$

$$\mathbf{G}\mathbf{u}_\mathrm{ff} = \mathbf{M}\mathbf{M}_\mathrm{c}^{-1}(\mathbf{C}_\mathrm{c} - \mathbf{J}_\mathrm{c})\hat{\boldsymbol{\nu}} + \mathbf{M}\dot{\hat{\boldsymbol{\nu}}} - \mathbf{F}_\mathrm{pot}, \tag{7.12d}$$

is sufficient to satisfy (7.11). In contrast to the potential energy PDE of the previous chapters, the projected part of (7.12b) is a homogeneous PDE, as the system's potential forces $\mathbf{F}_\mathrm{pot}$ have been assigned to the equation for the feedforward term (7.12d). Nonetheless, by means of Lemma 2.1, the matching equation for the kinetic and potential energy, and for the dissipation, equations (7.12a), (7.12b), (7.12c), respectively, accept the same solution from Section 6.3.1 (with the exception of the inhomogeneous solution to the potential energy PDE) if the input $\mathbf{u}$ is chosen accordingly.

Pre-multiplying (7.12a) by $\mathbf{G}_\perp$ yields

$$\mathbf{G}_\perp\mathbf{M}\mathbf{M}_\mathrm{c}^{-1}(\mathbf{C}_\mathrm{c} - \mathbf{J}_\mathrm{c}) = \mathbf{G}_\perp(\mathbf{C} - \mathbf{J}). \tag{7.13}$$

The latter equation implies that, in accordance to Lemma 2.1, equation (7.12d) is satisfied for any admissible trajectory $\hat{\boldsymbol{\xi}}(t)$ (cf. (7.1)) if $\mathbf{u}_\mathrm{ff}$ is chosen as (7.2).

7.2.2 Tracking non-admissible trajectories in reduced space

The observation above reveals that extending the energy-based stabilizing approach to the tracking problem in reduced coordinates is a simple task if we are able to compute admissible trajectories. A much more interesting question is whether the energy shaping approach can be applied to (approximately) track non-admissible trajectories. Let us

consider the mechanical system (6.23), and assume that the relationships

$$\mathbf{G}\mathbf{u}_{\mathrm{ke}} = -\mathbf{M}\mathbf{M}_{\mathrm{c}}^{-1}(\mathbf{C}_{\mathrm{c}} - \mathbf{J}_{\mathrm{c}})\boldsymbol{\nu} + (\mathbf{C} - \mathbf{J})\boldsymbol{\nu}, \tag{7.14a}$$

$$\mathbf{G}\mathbf{u}_{\mathrm{pe}} = -\mathbf{M}\mathbf{M}_{\mathrm{c}}{}^{-1}\nabla_{\boldsymbol{\xi}} V_{\mathrm{c}}^{\mathrm{e}} - \mathbf{F}_{\mathrm{pot}}, \tag{7.14b}$$

$$\mathbf{G}\mathbf{u}_{\mathrm{di}} = -\mathbf{M}\mathbf{M}_{\mathrm{c}}^{-1}\mathbf{R}_{\mathrm{c}}\boldsymbol{\nu}_{\mathrm{e}} \tag{7.14c}$$

hold. Then, the closed-loop system (6.23) with input $\mathbf{u} = \mathbf{u}_{\mathrm{ke}} + \mathbf{u}_{\mathrm{pe}} + \mathbf{u}_{\mathrm{di}} + \hat{\mathbf{u}}$ is given as

$$\underbrace{\mathbf{M}_{\mathrm{c}}\dot{\boldsymbol{\nu}}_{\mathrm{e}} + \mathbf{C}_{\mathrm{c}}\boldsymbol{\nu}_{\mathrm{e}} + \nabla_{\boldsymbol{\xi}} V_{\mathrm{c}}^{\mathrm{e}} - (\mathbf{J}_{\mathrm{c}} - \mathbf{R}_{\mathrm{c}})\,\boldsymbol{\nu}_{\mathrm{e}}}_{\text{LHS}} = \underbrace{\mathbf{M}_{\mathrm{c}}\mathbf{M}^{-1}\mathbf{G}\hat{\mathbf{u}} - (\mathbf{C}_{\mathrm{c}} - \mathbf{J}_{\mathrm{c}})\hat{\boldsymbol{\nu}} - \mathbf{M}_{\mathrm{c}}\dot{\hat{\boldsymbol{\nu}}}}_{\text{RHS}}. \tag{7.15}$$

The control objective is to design a state feedback controller such that the closed–loop system ensures some stability properties in spite of considering non-admissible trajectories. In particular, we are interested in the following:

i) Preserving asymptotic stability for admissible trajectories $\hat{\boldsymbol{\xi}}(t)$.

ii) Ensuring ISS with respect to a disturbance $\mathbf{d}_{\boldsymbol{\Delta}}$ that characterizes the divergence of the desired trajectory to an admissible reference.

To compute the disturbance $\mathbf{d}_{\boldsymbol{\Delta}}$, we use the following elementary result:

Lemma 7.1. *For an arbitrary matrix* $\mathbf{G}$*, the inverse of the regular matrix*

$$\begin{bmatrix} \mathbf{G}_{\perp} \\ \mathbf{G}^{\mathrm{T}} \end{bmatrix}$$

is given by

$$\begin{bmatrix} \mathbf{G}_{\perp}^{\mathrm{T}}(\mathbf{G}_{\perp}\mathbf{G}_{\perp}^{\mathrm{T}})^{-1} & \mathbf{G}(\mathbf{G}^{\mathrm{T}}\mathbf{G})^{-1} \end{bmatrix}. \tag{7.16}$$

Proof. A direct computation yields

$$\begin{bmatrix} \mathbf{G}_{\perp} \\ \mathbf{G}^{\mathrm{T}} \end{bmatrix} \begin{bmatrix} \mathbf{G}_{\perp}^{\mathrm{T}}(\mathbf{G}_{\perp}\mathbf{G}_{\perp}^{\mathrm{T}})^{-1} & \mathbf{G}(\mathbf{G}^{\mathrm{T}}\mathbf{G})^{-1} \end{bmatrix} = \begin{bmatrix} \mathbf{I} & \mathbf{0} \\ \mathbf{0} & \mathbf{I} \end{bmatrix}.$$

The proof is completed noting that the inverse is unique. ■

By means of Lemma 7.1, the closed-loop dynamics (7.15) can be rewritten as

$$\begin{aligned}
(\text{LHS}) &= \underbrace{\mathbf{M}_\text{c}\mathbf{M}^{-1}\begin{bmatrix}\mathbf{G}_\perp^\text{T}(\mathbf{G}_\perp\mathbf{G}_\perp^\text{T})^{-1} & \mathbf{G}(\mathbf{G}^\text{T}\mathbf{G})^{-1}\end{bmatrix}}_{\boldsymbol{\Sigma}}\begin{bmatrix}\mathbf{G}_\perp\\ \mathbf{G}^\text{T}\end{bmatrix}\mathbf{M}\mathbf{M}_\text{c}^{-1}\,(\text{RHS})\\
&= \boldsymbol{\Sigma}\begin{bmatrix}-\mathbf{G}_\perp\mathbf{M}\mathbf{M}_\text{c}^{-1}\left(\mathbf{C}_\text{c}-\mathbf{J}_\text{c}\right)\hat{\boldsymbol{\nu}}-\mathbf{G}_\perp\mathbf{M}\dot{\hat{\boldsymbol{\nu}}}\\ \mathbf{G}^\text{T}\mathbf{G}\hat{\mathbf{u}}-\mathbf{G}^\text{T}\mathbf{M}\mathbf{M}_\text{c}^{-1}\left(\mathbf{C}_\text{c}-\mathbf{J}_\text{c}\right)\hat{\boldsymbol{\nu}}-\mathbf{G}^\text{T}\mathbf{M}\dot{\hat{\boldsymbol{\nu}}}\end{bmatrix}\\
&= \boldsymbol{\Sigma}\begin{bmatrix}-\mathbf{G}_\perp\mathbf{M}\mathbf{M}_\text{c}^{-1}\left(\mathbf{C}_\text{c}-\mathbf{J}_\text{c}\right)\hat{\boldsymbol{\nu}}-\mathbf{G}_\perp\mathbf{M}\dot{\hat{\boldsymbol{\nu}}}\\ \mathbf{0}\end{bmatrix}\\
&\overset{(7.13)}{=} -\mathbf{M}_\text{c}\mathbf{M}^{-1}\mathbf{G}_\perp^\text{T}(\mathbf{G}_\perp\mathbf{G}_\perp^\text{T})^{-1}\mathbf{G}_\perp\left(\left(\mathbf{C}-\mathbf{J}\right)\hat{\boldsymbol{\nu}}+\mathbf{M}\dot{\hat{\boldsymbol{\nu}}}\right)\\
&= \boldsymbol{\Delta}_1\hat{\boldsymbol{\nu}}+\boldsymbol{\Delta}_2\dot{\hat{\boldsymbol{\nu}}},
\end{aligned}\tag{7.17}$$

provided that $\hat{\mathbf{u}}$ is chosen as

$$\hat{\mathbf{u}} = (\mathbf{G}^\text{T}\mathbf{G})^{-1}\mathbf{G}^\text{T}\left(\mathbf{M}\dot{\hat{\boldsymbol{\nu}}}+\mathbf{M}\mathbf{M}_\text{c}^{-1}\left(\mathbf{C}_\text{c}-\mathbf{J}_\text{c}\right)\hat{\boldsymbol{\nu}}\right).\tag{7.18}$$

The dynamics of the closed-loop system (6.23) with input $\mathbf{u}=\mathbf{u}_\text{ke}+\mathbf{u}_\text{pe}+\mathbf{u}_\text{di}+\hat{\mathbf{u}}$ according to (7.14) and (7.18), and for a non-admissible trajectory $\hat{\boldsymbol{\xi}}$ are given by

$$\mathbf{M}_\text{c}\dot{\boldsymbol{\nu}}_\text{e}+\mathbf{C}_\text{c}\boldsymbol{\nu}_\text{e}+\nabla_{\boldsymbol{\xi}}V_\text{c}^\text{e} = \left(\mathbf{J}_\text{c}-\mathbf{R}_\text{c}\right)\boldsymbol{\nu}_\text{e}+\boldsymbol{\Pi}_{\boldsymbol{\Delta}}\mathbf{d}_{\boldsymbol{\Delta}},\tag{7.19}$$

where $V_\text{c}^\text{e}=V_\text{c}(\boldsymbol{\xi}-\hat{\boldsymbol{\xi}})$, $\boldsymbol{\nu}_\text{e}=\boldsymbol{\nu}-\hat{\boldsymbol{\nu}}$, and $\mathbf{d}_{\boldsymbol{\Delta}}=\text{col}(\hat{\boldsymbol{\nu}},\dot{\hat{\boldsymbol{\nu}}})$ is a disturbance. In the following, we study the stability of (7.19) for a bounded disturbance $\mathbf{d}_{\boldsymbol{\Delta}}$ via ISS. The following theorem directly results from Theorem 6.5.

Theorem 7.2. *Let $\varepsilon>0$ be a sufficiently small scalar. The system (7.19) is (locally) input-to-state stable for input disturbances $\mathbf{d}_{\boldsymbol{\Delta}}$ satisfying*

$$\|\mathbf{d}_{\boldsymbol{\Delta}}\| \leq \frac{\gamma\lambda_\text{min}}{\sigma_\text{max}}\|\boldsymbol{\chi}\|,\tag{7.20}$$

where $\boldsymbol{\chi}=\text{col}(\nabla_{\boldsymbol{\xi}}V_\text{c}^\text{e},\,\boldsymbol{\nu}_\text{e})$, the scalar $\gamma=]0,\,1[$ is free, σ_max represents the largest singular value of the matrix

$$\boldsymbol{\Sigma} = \begin{bmatrix}\varepsilon\mathbf{K}\boldsymbol{\Delta}_1 & \varepsilon\mathbf{K}\boldsymbol{\Delta}_2\\ \boldsymbol{\Delta}_1 & \boldsymbol{\Delta}_2\end{bmatrix} = \begin{bmatrix}\varepsilon\mathbf{K}\boldsymbol{\Pi}_{\boldsymbol{\Delta}}\\ \boldsymbol{\Pi}_{\boldsymbol{\Delta}}\end{bmatrix},\tag{7.21}$$

and λ_min is the smallest eigenvalue of the positive definite matrix $\mathbf{R}_{\boldsymbol{\chi}}$ (cf. (7.10)).

Proof. Consider the time-varying ISS Lyapunov function

$$E_\varepsilon = \frac{1}{2}\boldsymbol{\nu}_\mathrm{e}^\mathrm{T}\mathbf{M}_\mathrm{c}\boldsymbol{\nu}_\mathrm{e} + V_\mathrm{c}^\mathrm{e} + \varepsilon\nabla_{\boldsymbol{\xi}}^\mathrm{T}V_\mathrm{c}^\mathrm{e}\mathbf{K}\mathbf{M}_\mathrm{c}\boldsymbol{\nu}_\mathrm{e}. \tag{7.22}$$

Its derivative along the trajectories of (7.19) is

$$\begin{aligned}\dot{E}_\varepsilon = &-\boldsymbol{\nu}_\mathrm{e}^\mathrm{T}\left(\mathbf{R}_\mathrm{c} - \varepsilon\mathbf{M}_\mathrm{c}\mathbf{K}\nabla_{\boldsymbol{\xi}}^2 V_\mathrm{c}^\mathrm{e}\right)\boldsymbol{\nu}_\mathrm{e} - \varepsilon\nabla_{\boldsymbol{\xi}}^\mathrm{T}V_\mathrm{c}^\mathrm{e}\mathbf{K}\nabla_{\boldsymbol{\xi}}V_\mathrm{c}^\mathrm{e} + \boldsymbol{\nu}_\mathrm{e}^\mathrm{T}\boldsymbol{\Pi}_{\boldsymbol{\Delta}}\mathbf{d}_{\boldsymbol{\Delta}} \\ &+ \varepsilon\nabla_{\boldsymbol{\xi}}^\mathrm{T}V_\mathrm{c}^\mathrm{e}\mathbf{K}\left(\mathbf{J}_\mathrm{c} - \mathbf{C}_\mathrm{c} - \mathbf{R}_\mathrm{c} + \dot{\mathbf{M}}_\mathrm{c}\right)\boldsymbol{\nu}_\mathrm{e} + \varepsilon\nabla_{\boldsymbol{\xi}}^\mathrm{T}V_\mathrm{c}^\mathrm{e}\mathbf{K}\boldsymbol{\Pi}_{\boldsymbol{\Delta}}\mathbf{d}_{\boldsymbol{\Delta}}.\end{aligned} \tag{7.23}$$

Defining $\boldsymbol{\chi} = \mathrm{col}(\nabla_{\boldsymbol{\xi}}V_\mathrm{c}^\mathrm{e},\, \boldsymbol{\nu}_\mathrm{e})$, expression (7.23) can be given as

$$\dot{E}_\varepsilon = -\boldsymbol{\chi}^\mathrm{T}\mathbf{R}_{\boldsymbol{\chi}}\boldsymbol{\chi} + \boldsymbol{\chi}^\mathrm{T}\boldsymbol{\Sigma}\mathbf{d}_{\boldsymbol{\Delta}}, \tag{7.24}$$

where

$$\mathbf{R}_{\boldsymbol{\chi}} = \begin{bmatrix} \varepsilon\mathbf{K} & -\frac{\varepsilon}{2}\mathbf{K}\left(\mathbf{J}_\mathrm{c} + \mathbf{C}_\mathrm{c}^\mathrm{T} - \mathbf{R}_\mathrm{c}\right) \\ \frac{\varepsilon}{2}\left(\mathbf{J}_\mathrm{c} + \mathbf{R}_\mathrm{c} + \mathbf{C}_\mathrm{c}\right)\mathbf{K} & \mathbf{R}_\varepsilon^\nu \end{bmatrix}, \qquad \boldsymbol{\Sigma} = \begin{bmatrix} \varepsilon\mathbf{K}\boldsymbol{\Delta}_1 & \varepsilon\mathbf{K}\boldsymbol{\Delta}_2 \\ \boldsymbol{\Delta}_1 & \boldsymbol{\Delta}_2 \end{bmatrix}. \tag{7.25}$$

Since $\mathbf{R}_\varepsilon^\nu$ is assumed to be positive definite (Assumption 6.6), it can be locally ensured that $\mathbf{R}_{\boldsymbol{\chi}} > \mathbf{0}$ for $\varepsilon > 0$ sufficiently small. The remaining of the proof is analogous to the proof of Theorem 6.5 for the disturbance $\mathbf{d}_{\boldsymbol{\Delta}}$. ■

7.2.3 Hybrid position and speed controller

In Section 6.4 (Theorem 6.4), we introduced a strategy for the stabilization of a dynamical equilibrium (DE) that corresponds to a classical speed controller. In this section, a second type—given in Corollary 7.1—also considers the configuration error $\boldsymbol{\xi}_\mathrm{e}^\mathrm{d}$. The idea is to stabilize a constant reference velocity $\hat{\boldsymbol{\nu}}^\mathrm{d}$, and, at the same time, a *time-varying consistent* position given as $\hat{\boldsymbol{\xi}}^\mathrm{d} = \hat{\boldsymbol{\nu}}^\mathrm{d}t + \boldsymbol{\xi}_0^\mathrm{d}$, where $\boldsymbol{\xi}_0^\mathrm{d}$ is a constant value for the initial (admissible) equilibrium.

Corollary 7.1. *Let $(\hat{\boldsymbol{\xi}}, \hat{\boldsymbol{\nu}})$ be an admissible DE. Let, further, the condition of Assumption 6.4 be satisfied. Define $\hat{\boldsymbol{\xi}}^\mathrm{d} = \hat{\boldsymbol{\nu}}^\mathrm{d}t + \boldsymbol{\xi}_0^\mathrm{d}$, where $\boldsymbol{\xi}_0^\mathrm{d}$ is an admissible equilibrium of (6.23). Let, further, $\hat{\boldsymbol{\nu}}^\mathrm{s} = \mathbf{0}$, and $\hat{\boldsymbol{\nu}}^\mathrm{d}$ be constant, and assume that $\mathbf{G}_\perp(\mathbf{C} - \mathbf{J})\hat{\boldsymbol{\nu}} = 0$. The admissible DE $(\hat{\boldsymbol{\xi}}, \hat{\boldsymbol{\nu}})$ of (7.19) is uniformly asymptotically stable if $\mathbf{M}_\mathrm{c} > \mathbf{0}$, and V_c^e is such that $\mathbf{0} = \arg\min V_\mathrm{c}^\mathrm{e}$.*

Proof. From Theorem 7.2, we know that the system (7.19) is ISS with respect to the disturbance $\mathbf{d}_{\boldsymbol{\Delta}}$. As $\dot{\hat{\boldsymbol{\nu}}} = \mathbf{0}$, and $\mathbf{G}_\perp(\mathbf{C} - \mathbf{J})\hat{\boldsymbol{\nu}} = 0$ is assumed to hold, we have

for the disturbance term $\mathbf{\Pi}_{\boldsymbol{\Delta}}\mathbf{d}_{\boldsymbol{\Delta}} = \mathbf{0}$. The ISS property implies that the time-varying dynamical equilibrium $(\hat{\boldsymbol{\xi}}, \hat{\boldsymbol{\nu}})$ is, thus, uniformly asymptotically stable. ■

7.3 Path following

Some maneuvers are better described in the path following setting rather than reference tracking. Consider, for instance, an industrial welding or paint robot, or a mobile robot that should cover a specific area for surveillance. Nonetheless, even in cases for which reference tracking is better suited for the description of the problem setting, its inherent disadvantages may justify path following strategies. In this section, we aim at designing a control law to stabilize a given, constant forward velocity v^*, and at finding an appropriate *passive velocity field control* (PVFC) strategy to determine the required steering commands for the system to approach and remain on a geometric path $\mathcal{P}$.

From a practical point of view, the velocity field control can be easily embedded in the energy shaping framework, even though, strictly speaking, no energy is being shaped. As systems controlled via PVFC interact in a passive way with its environment, the vector field can be used to extend the classic PBC stabilizing controllers [70] to path following. The notion of vector (velocity) fields is similar to that of potential fields in the sense that the control forces are commanded by these fields. Yet, the velocity fields simply specify the desired direction of motion and do not necessarily represent the gradient of a scalar function.

Let us begin by describing the idea of PVFC. Path following via vector field control relies on using a speed control law for the forward velocity of the system, designing a vector field that assigns to every point $\mathbf{q} \in \mathcal{Q}$ a vector, whose direction specifies the desired orientation $\hat{\theta}$, and controlling the orientation error $\theta_{\mathrm{e}} = \theta - \hat{\theta}$ via energy shaping. Note that path following is defined in the configuration space $\mathcal{Q}$. There are different ways of constructing an appropriate vector field. In this thesis, we use a strategy introduced by Nelson and co-workers in [146]. Yet, in contrast to the work of Nelson et al., we consider one single strategy as a unified procedure to construct vector fields for arbitrary paths. For simplicity, let us consider mobile robots and two dimensional paths $\mathcal{P}$ defined on the plane as in (7.4).

The point $\mathbf{p} \in \mathbb{R}^2$ characterizes the closest point of the path with respect to the actual position (x, y). For simplicity, we assume that $\mathbf{p}$ is unique. The vector field is characterized by

$$\hat{\theta} = \theta_{\mathbf{p}} - \epsilon \arctan(k\rho), \tag{7.26}$$

where $\theta_{\mathbf{p}}$ is the orientation at $\mathbf{p}$ (given by the tangent line at this point), $\rho > 0$ is the distance of the system to the nearest point $\mathbf{p}$ of the path, and $\epsilon = \{-1, 1\}$ depends whether the actual position lies on the right or left hand side of the path with respect to the desired travel direction. The parameter k characterizes the shape of the vector field: Large values of k correspond to faster convergence, but also to an abrupt transition between *approaching* and *moving along* the path; small values of k lead to a slower, but smoother convergence to the path, as the vector field flattens softer the closer the system gets to the path. The effect of the parameter k is shown in Figure 7.3. An advantageous feature of PVFC compared to reference tracking is the fact that the input signal is not likely to reach saturation even for initial conditions far away from the desired path $\mathcal{P}$, as the commanded velocity v^* is constant and does not depend on the magnitude of the error ρ to the path.

Example 7.3.1 (Rolling coin.). Consider the vertical coin from Example 2.1.2 rolling on a horizontal plane. Suppose that we want to steer the coin such that it tracks a circular path of radius $R=1$ with constant velocity $v^* = r\dot{\phi}^*$. The path is defined as[2]

$$\mathcal{P} = \left\{ \mathbf{q} \in \mathcal{Q} \,|\, x^2 + y^2 - 1 = 0,\ \theta = \begin{matrix} + \\ - \end{matrix} \frac{\pi}{2} + \arctan\left(\frac{y}{x}\right) \right\}. \tag{7.27}$$

The vector field that provides the commands for the desired orientation is defined as

$$\hat{\theta} = \theta_{\mathbf{p}} + \arctan(k\rho), \tag{7.28}$$

for all points outside the circle, or

$$\hat{\theta} = \theta_{\mathbf{p}} - \arctan(k\rho), \tag{7.29}$$

[2]Note that the oriantation angle θ is not free, as the system is subject to nonholonomic constraints. The case differentiation *plus* or *minus* is necessary, since the arctangent is only defined for the first and the fourth quadrants.

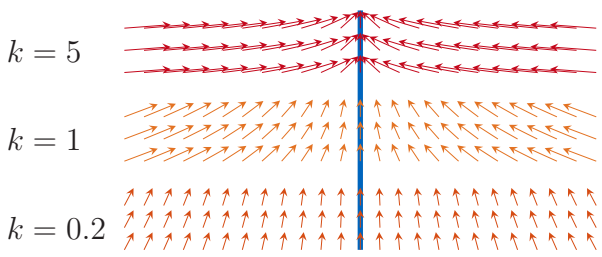

Figure 7.3: Effect of the parameter k for the velocity field control. The smaller the values of k, the slower, but also smoother the convergence to the path $\mathcal{P}$.

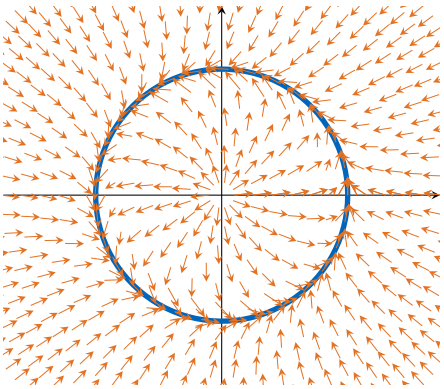

Figure 7.4: Vector field control for the vertical coin rolling on a horizontal plane for $k=5$. The direction of each vector characterizes the desired orientation for the coin at the respective position.

for all points inside thereof. Figure 7.4 illustrates the vector field for $k=5$. □

To study the boundedness of the closed-loop signals and the convergence of the mechanical system to the path, we first show that the vector field given by (7.26) in fact converges to the desired path $\mathcal{P}$.

Proposition 7.1. *Let $\mathcal{P}$ be an arbitrary path defined as in (7.4), and let $\mathbf{p}=(x_\mathbf{p}, y_\mathbf{p})$ be the nearest point thereon. Further, let $\theta_\mathbf{p}$ denote the orientation of the path at $\mathbf{p}$. The course commands (7.26) converge to the path for a constant forward velocity $v^*>0$.*

Proof. The distance ρ of a particle moving with constant velocity $v^*>0$ according to the vector field (7.26) from its actual position to the path evolves according to the ODE

$$\dot{\rho} = v^* \sin(\hat{\theta}-\theta_\mathbf{p}) = -v^* \frac{k\rho}{\sqrt{k^2\rho^2+1}}. \tag{7.30}$$

Consider the Lyapunov function

$$V_\mathbf{p} = \frac{1}{2}\rho^2, \tag{7.31}$$

whose rate of change along the dynamics of ρ is given as

$$\dot{V}_\mathbf{p} = \rho\dot{\rho} = -v^* \frac{k\rho^2}{\sqrt{k^2\rho^2+1}}, \tag{7.32}$$

which is clearly negative definite for $k>0$ and $v^*>0$. Thus, the distance ρ converges to zero as $t\to\infty$, which implies that also $\hat{\theta}\to\theta_\mathbf{p}$ as time goes to infinity. ■

Proposition 7.1 implies that if the system satisfies $\theta=\hat{\theta}$, and $v=v^*$ for all times $t>0$, then it also converges to the path as $t\to\infty$. The following result follows from the ISS property of the position and velocity controllers, and proves boundedness of the closed-

loop signals with respect to the path as well as convergence of the velocity towards v^*.

Theorem 7.3. *Let $\mathcal{P}$ be an arbitrary path defined as in (7.4), and let $\mathbf{p}$ be the nearest point thereon. Further, let $\theta_{\mathbf{p}}$ denote the orientation of the path at $\mathbf{p}$, and let (6.50) describe the dynamics of the closed-loop system with $\mathbf{M}_c > \mathbf{0}$, $\mathbf{0} = \arg\min V_c^e$, and $\mathbf{R}_c \geq \mathbf{0}$. Let v^* be the desired forward velocity along the path, and let $\hat{\theta} = \theta_{\mathbf{p}} - \epsilon \arctan(k\rho)$ be the desired orientation. Then, the velocity error $v_e = v - v^*$ converges towards the origin, and both the errors $\theta_e = \theta - \theta_{\mathbf{p}}$ and ρ are bounded, and can be made arbitrary small for sufficiently small desired forward velocities $v^* > 0$. Additionally, for constant $\theta_{\mathbf{p}}$, the errors $\theta_e = \theta - \theta_{\mathbf{p}}$ and ρ converge towards zero as $t \to \infty$.*

Proof. According to Theorem 6.3, the desired velocity v^* is asymptotically stabilized. Furthermore, the system is ISS with respect to the disturbance $\hat{\theta}$ (Theorem 6.5), which implies that the system's response to $\hat{\theta}$ is bounded, and converges towards $\hat{\theta}$ if the course commands $\hat{\theta}$ are constant. The rate of change of the course commands directly depends on the desired forward velocity v^*. Regardless of the shape of the path and the vector field, a sufficiently small v^* can always be found such that the rate of change of $\hat{\theta}$ remains within given bounds. Since the error $\theta - \hat{\theta}$ is bounded, and $\hat{\theta}$ converges towards $\theta_{\mathbf{p}}$, also the error $\theta_e = \theta - \theta_{\mathbf{p}}$ is bounded. As a result, the system remains as closed as desired to the path $\mathcal{P}$. ■

The theorem above implies that the system asymptotically converges towards a desired path in the form of a straight line, where the orientation commands $\hat{\theta}$ evolve into constant values, as $\theta_{\mathbf{p}}$ is constant, whereas the error is only guaranteed to be bounded for more complex and curved path geometries like circles.

Corollary 7.2. *Let the assumptions of Theorem 7.3 hold, and let us augment the velocity stabilizing controller by the yaw angular velocity $\dot{\hat{\theta}} = \dot{\theta}_{\mathbf{p}}$. Then, the error $\dot{\theta}_e = \dot{\theta} - \dot{\theta}_{\mathbf{p}}$ is bounded and converges towards the origin for constant $\dot{\theta}_{\mathbf{p}}$.*

Proof. The proof follows directly from the ISS property of both the position and the velocity controllers, and noting that the velocity controller asymptotically stabilizes a desired constant yaw rate $\dot{\hat{\theta}}$. ■

7.4 Concluding remarks

In this chapter, we have addressed trajectory tracking and path following for underactuated nonholonomic systems. Due to the intrinsic disadvantages of trajectory tracking, especially the need of an admissible trajectory, we studied stability with respect

to non-admissible trajectories. We introduced sufficient conditions in terms of ISS to prove boundedness of the tracking error. In particular, for a hybrid velocity and position control, we showed that, if a condition is satisfied, then the error converges to zero.

The second half of the chapter was dedicated to the path following problem. Employing a unified passive velocity field control approach found in the literature, we showed that the system will remain arbitrarily close to the path for sufficiently small desired velocities v^*.

Reduced coordinates $\boldsymbol{\xi} \in \mathcal{Q}_{\mathrm{R}}$, in general, do not provide any information about the position of the nonholonomic system in the Euclidean space $\mathbb{R}^3$. As the desired motion of mobile robots is often specified in the Euclidean space, considering path following strategies together with reference tracking can be useful to track more complex maneuvers.

In the next chapter, we evaluate the results of both Chapter 6 and Chapter 7 on a wheeled inverted pendulum (WIP) system, which is an underactuated nonholonomic system with unstable pitch dynamics. Preliminary ideas on the combination of path following and reference tracking is shown in Section 8.4.2 for the WIP.

8 The Wheeled Inverted Pendulum

The *wheeled inverted pendulum* (WIP)—and its most popular commercial version, the *Segway* (cf. [186])—has gained interest for human assistance and transportation in the past several years due to its high maneuverability and simple construction [128]. A WIP—shown from the side in Figure 8.1 (left)—consists of a vertical body with two coaxial driven wheels mounted on the body. The actuation of both wheels in the same direction generates a forward (or backward) motion; opposite wheel velocities lead to a turning motion around the vertical axis.

Although WIPs are statically unstable, two-wheeled robots have many advantages over three- or four-wheeled vehicles and mobile robots: They require less space, can turn on a spot—which makes them highly maneuverable—and being actively stabilized increases their robustness, as they constantly counteract all types of disturbances, some of which could, e. g., tip over a three-wheeled robot.

Mobile robotic systems based on the WIP, like the intelligent two wheeled road vehicle *B2* presented in [17], or the novel and more car-like *Segway PUMA* and *Chevrolet En-V*, are being developed to be used as personal urban transportation systems in the near future [163, 204]. Apart from this emerging transportation industry, WIPs are being developed at institutes all over the world for research purposes, e. g., *Yamabico Kurara* [78], *JOE* [77] and *InPeRo* [145], to name only three examples. These systems can be further used as service robots like *KOBOKER* [117], or moving information platforms like the Ballbot *mObi* [136][1].

The stabilization and tracking control for the WIP is not trivial: First, the system is nonholonomic, for the rolling-without-slipping constraints of the wheels prevent the WIP from moving sideways, and the forward velocity of the WIP and its yaw rate are directly given by the angular velocity of the wheels. Second, the WIP belongs to the class of underactuated mechanical systems, since two control inputs—corresponding to the independent driving torques of the wheels—are used to control three degrees of

[1] Ballbots are robots balancing on a sphere, and thus, capable of omnidirectional movement [89, 143].

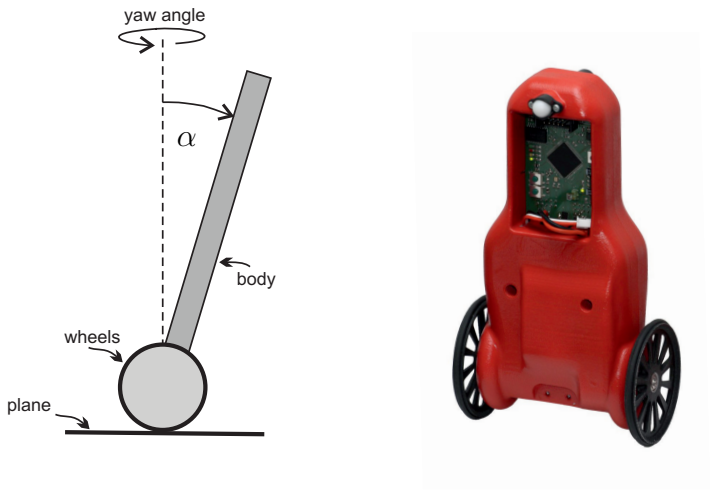

Figure 8.1: A wheeled inverted pendulum from the side (left). *KRT32*—the wheeled inverted pendulum developed at the Institute of Automatic control of the Technische Universität München (right).

freedom[2]. Third, the upward position of the body represents an unstable equilibrium that needs to be stabilized by feedback. And finally, since, to the best of our knowledge, no flat output has been found for wheeled inverted pendulum systems, being underactuated significantly complicates the computation of admissible trajectories.

This chapter generalizes and completes the results of the conference paper [50], and the article [53]. After the formulation of the problem in Section 8.1, we briefly present the dynamic model of the WIP in Section 8.2. Instead of considering the six-dimensional manifold $\mathcal{Q}$, which represents the configuration space of the WIP, we restrict our analysis to a lower dimensional space $\mathcal{Q}_{\mathrm{R}}$, on which the system evolves *unconstrained*. In Section 8.3, and based on the nonlinear model in $\mathcal{Q}_{\mathrm{R}}$, we present the solution to the matching equations, and parametrize the closed-loop system applying local linear dynamics assignment (LLDA). The applicability and performance of a number of energy shaping controllers is shown with a series of simulations and experiments in Section 8.4. The chapter includes, besides stabilization, strategies for path following, for non-admissible reference tracking, and for the stabilization of a point in the horizontal plane. Finally, the chapter concludes with some final remarks in Section 8.5.

[2]The constraint distribution $\mathcal{D}$ of the WIP has rank three.

8.1 Problem formulation

The WIP is very attractive from a control theoretic point of view, as it is statically unstable, shows nonlinear behavior, is restricted by nonholonomic constraints, and no flat output has yet been found. Several control laws have been applied for the stabilization and speed control of the WIP, mostly using linearized models [77, 78, 79, 128, 138]. While these models are simple and useful for many applications, they do not reflect the system's nonlinear behavior and are, thus, restricted to small pitch angles and yawing velocities. To satisfy the increasing demand on performance and robustness in control applications, more accurate models are necessary. Therefore, researchers have put a strong focus on the nonlinear model during the last decade. A complete controllability analysis of the WIP has been carried out in the works of Pathak et al. [161], Nasrallah et al. [145], and Salerno and Ángeles [175]. Based on the analysis of the nonlinear system, nonlinear control strategies have been developed for different purposes, including pitch stabilization [139, 215], stabilization of a specific position in the horizontal plane [138, 161], velocity control [93, 145, 161], disturbance rejection [166] as well as trajectory planning and adaptive control [212]. The employed control methods range from Lyapunov-based controller design [99, 100] to sliding-mode [93] and backstepping [48] approaches, neural networks [96, 170], and even Takagi-Sugeno modeling and controller design [121, 164]. For a very complete overview of the existing work on modeling and control of WIPs until 2012, the reader is referred to [46].

Most existing methods do not exploit the intrinsic mechanical structure of the system, as they rely on a partial feedback linearization (cf. [161]), or are designed for the linearized model (cf. [138]). Additionally, some methods feature a cumbersome and nonintuitive design procedure. Furthermore, the current literature is full with completely different control strategies to tackle diverse control tasks. As a consequence, the combination of existing methods for the solution of new tasks requires a lot of effort.

We would like, therefore, to use a single, unified framework for the position and speed control of the WIP that can be easily enhanced to tackle trajectory as well as path following problems, and which is flexible and modular enough to be adaptable to accomplish new tasks and satisfy further demands.

The total energy shaping approach provides such a framework, as it preserves the nonlinear mechanical structure of the system. By doing so, the closed-loop system retains the mechanical structure that, in turn, guarantees its stability and robustness. The approach is physically motivated, and the controller design is transparent and remarkably intuitive.

The goal of this chapter is to present the design of a stabilizing and speed controller for the WIP, based on the theory developed in Chapter 6. We show a feasible and elegant solution for the matching problem for position and speed control of the WIP. Based on this controller—which is easy to parametrize, either tuning the closed-loop dynamic parameters, or applying LLDA—the approach is adapted for the stabilization of a position in the horizontal plane, and for path following control and non-admissible trajectory tracking according to the theory developed in Chapter 7.

8.2 Dynamical model

In this section, we briefly present the dynamical model of the WIP. For a detailed development of the equations of motion, the reader is referred to Appendix B, and to the conference paper [51], where the dynamical model is derived from a geometric point of view. Figure 8.2 shows the coordinates used for the modeling of the WIP. Let the configuration space be $\mathcal{Q} = \mathbb{R}^2 \times \mathbb{S}^1 \times \mathbb{S}^1 \times \mathbb{S}^1 \times \mathbb{S}^1$ and define local coordinates $\mathbf{q} = (x,\, y,\, \theta,\, \alpha,\, \varphi_\mathrm{r},\, \varphi_\mathrm{l}) \in \mathcal{Q}$. The position of the WIP on the horizontal plane is given by $\mathbf{r} = (x,\, y)$. The yawing and pitching angles are each identified by θ and α. The coordinates $\varphi_\mathrm{r} = \phi_\mathrm{r} + \alpha$ and $\varphi_\mathrm{l} = \phi_\mathrm{l} + \alpha$ represent the absolute rotations of the right and left wheel, respectively, for relative rotation angles ϕ_l and ϕ_r. Let $2d$ be the distance between the wheels. For a given wheel radius r, the equations

$$\mathbf{A}^\mathrm{T}\dot{\mathbf{q}} = \begin{bmatrix} -\sin\theta & \cos\theta & 0 & 0 & 0 & 0 \\ \cos\theta & \sin\theta & d & 0 & -r & 0 \\ \cos\theta & \sin\theta & -d & 0 & 0 & -r \end{bmatrix} \dot{\mathbf{q}} = \mathbf{0} \tag{8.1}$$

represent the rolling-without-slipping constraints of the wheels. The natural choice of admissible velocities $\boldsymbol{\nu} = (v,\, \dot{\alpha},\, \dot{\theta})$, where v is the forward velocity of the WIP, results in the reconstruction equation

$$\dot{\mathbf{q}} = \mathbf{S}\boldsymbol{\nu} = \begin{bmatrix} \cos\theta & 0 & 0 \\ \sin\theta & 0 & 0 \\ 0 & 0 & 1 \\ 0 & 1 & 0 \\ \frac{1}{r} & 0 & \frac{d}{r} \\ \frac{1}{r} & 0 & -\frac{d}{r} \end{bmatrix} \begin{bmatrix} v \\ \dot{\alpha} \\ \dot{\theta} \end{bmatrix}. \tag{8.2}$$

Let us define reduced local coordinates $\boldsymbol{\xi} = (s, \alpha, \theta) \in \mathcal{Q}_{\mathrm{R}}$, such that[3] $\dot{\boldsymbol{\xi}} = \boldsymbol{\nu}$. Using this particular choice of coordinates $(\boldsymbol{\xi}, \boldsymbol{\nu})$, the equations of motion in reduced space $\mathcal{Q}_{\mathrm{R}}$ are given by[4]

$$\mathbf{M}\dot{\boldsymbol{\nu}} + \mathbf{C}\boldsymbol{\nu} + \nabla_{\boldsymbol{\xi}} V = \mathbf{G}\mathbf{u} + \mathbf{J}\boldsymbol{\nu} \tag{8.3}$$

with potential energy $V = c_2 g \sin\alpha$, and matrices

$$\mathbf{M} = \begin{bmatrix} c_1 & c_2\cos\alpha - c_3 & 0 \\ c_2\cos\alpha - c_3 & c_4 & 0 \\ 0 & 0 & \Theta(\alpha) \end{bmatrix}, \qquad \mathbf{J} = \begin{bmatrix} 0 & 0 & c_2\dot{\theta}\sin\alpha \\ 0 & 0 & 0 \\ -c_2\dot{\theta}\sin\alpha & 0 & 0 \end{bmatrix},$$

[3] The variable s defines the path length.

[4] The matrix $\mathbf{S}$ does not explicitly appear in the model (8.3), because the conditions of Proposition 6.2 are satisfied for the WIP.

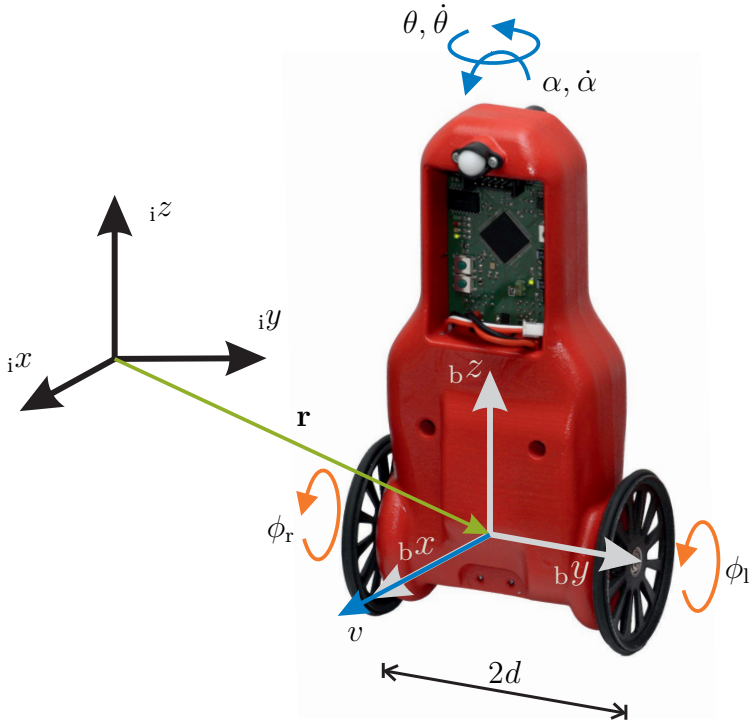

Figure 8.2: Coordinate systems and actuation of the WIP. The right (ϕ_{r}) and left (ϕ_{l}) wheels can be independently actuated. The actuation of both wheels in the same direction generates a forward (or backward) motion, characterized by the velocity v; wheel actuation in opposite directions lead to a turning motion around the vertical axis, given by the yaw angle θ. The pitch angle α is unactuated and has to be actively stabilized by a back and forth motion. The position in the horizontal plane $\mathbf{r} = (x, y)$ can be determined according to the reconstruction equation (8.2).

$$\mathbf{C} = \begin{bmatrix} 0 & -c_2\dot{\alpha}\sin\alpha & 0 \\ 0 & 0 & -c_5\dot{\theta}\sin\alpha\cos\alpha \\ 0 & c_5\dot{\theta}\sin\alpha\cos\alpha & c_5\dot{\alpha}\sin\alpha\cos\alpha \end{bmatrix}, \qquad \mathbf{G} = \begin{bmatrix} \frac{1}{r} & 0 \\ -1 & 0 \\ 0 & 1 \end{bmatrix}, \tag{8.4}$$

where $\Theta = c_5 \sin^2\alpha + c_6$, and c_i, $i = 1, ..., 6$, are constant parameters.

8.3 Total energy shaping controller

The control laws presented in the following are all based on the model (8.3). Figure 8.3 gives an overview of the control system. The feedforward term $\hat{\mathbf{u}}$ is computed according to (7.18). The feedback controller comprises the terms $\mathbf{u}_{\text{ke}}$, $\mathbf{u}_{\text{pe}}$, and $\mathbf{u}_{\text{di}}$, given as

$$\mathbf{u}_{\text{ke}} = (\mathbf{G}^{\text{T}}\mathbf{G})^{-1}\mathbf{G}^{\text{T}}\left((\mathbf{C} - \mathbf{J})\boldsymbol{\nu} - \mathbf{M}\mathbf{M}_{\text{c}}^{-1}(\mathbf{C}_{\text{c}} - \mathbf{J}_{\text{c}})\boldsymbol{\nu}_{\text{e}}\right), \tag{8.5a}$$

$$\mathbf{u}_{\text{pe}} = -(\mathbf{G}^{\text{T}}\mathbf{G})^{-1}\mathbf{G}^{\text{T}}\left(\mathbf{M}\mathbf{M}_{\text{c}}^{-1}\nabla_{\boldsymbol{\xi}}V_{\text{c}}^{\text{e}} + \mathbf{F}_{\text{pot}}\right), \tag{8.5b}$$

$$\mathbf{u}_{\text{di}} = -(\mathbf{G}^{\text{T}}\mathbf{G})^{-1}\mathbf{G}^{\text{T}}\mathbf{M}\mathbf{M}_{\text{c}}^{-1}\mathbf{R}_{\text{c}}\boldsymbol{\nu}_{\text{e}}. \tag{8.5c}$$

Essentially, the controller is equal for all different regulation tasks (stabilization, speed stabilization, reference tracking, and path following). The differences consist in the computation and the definition of the desired values $\hat{\boldsymbol{\xi}}$ and $\hat{\boldsymbol{\nu}}$ in the *task specification* block. A series of sensors—the system is equipped with two encoders that measure the rotation of the wheels relative to the body, an accelerometer and a gyroscope—directly provides the information about the velocities $\boldsymbol{\nu}$, and the relative rotation of the right and left wheel ϕ_{r} and ϕ_{l}. This information is, in turn, processed to compute $\boldsymbol{\xi}$. The detailed sensor fusion can be consulted in [98]. In addition to the actual state ($\boldsymbol{\xi}$, $\boldsymbol{\nu}$), the controller is provided with the desired values ($\hat{\boldsymbol{\xi}}$, $\hat{\boldsymbol{\nu}}$), as the control input $\mathbf{u}$ is computed based on the errors $\boldsymbol{\xi}_{\text{e}} = \boldsymbol{\xi} - \hat{\boldsymbol{\xi}}$ and $\boldsymbol{\nu}_{\text{e}} = \boldsymbol{\nu} - \hat{\boldsymbol{\nu}}$. In the following, limited by the physical nature of the problem setting, we restrict the analysis to $-\pi/2 < \alpha < \pi/2$.

8.3.1 Controller design

Let us begin by solving the matching problem (6.27), as it constitutes the basis for all control strategies. In accordance to the solution developed in Section 6.3.1, we show an elegant way to solve the matching problem for the WIP in reduced space $\mathcal{Q}_{\text{R}}$.

Shaping the kinetic energy. As shown in Section 6.3.1, shaping the kinetic energy only requires the solution $\bar{\mathbf{M}}_{\text{c}}$ of (6.33) for $\bar{\mathbf{M}}_{\text{c}} = \mathbf{M}_{\text{c}}^{-1}$. Due to the large number of

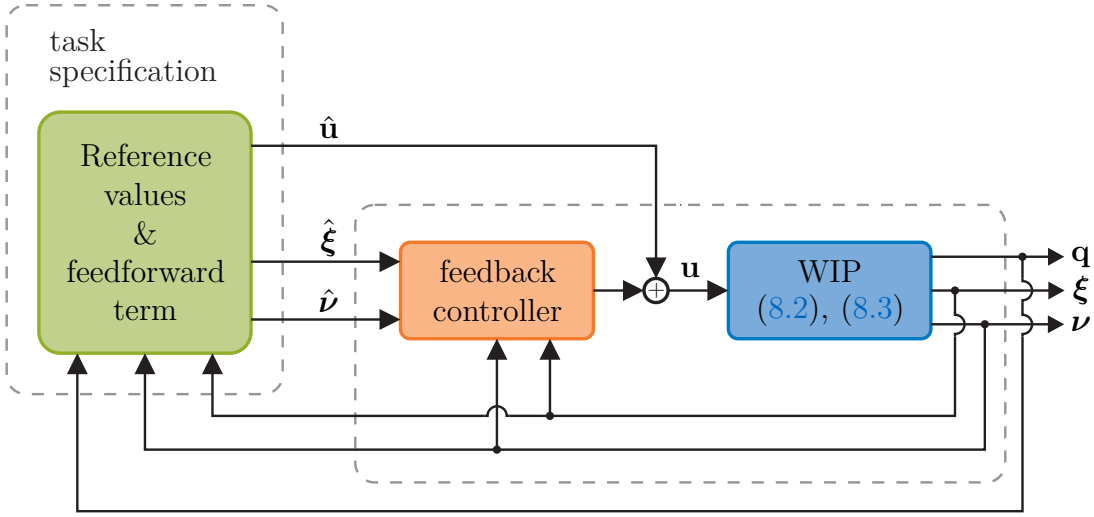

Figure 8.3: Feedforward and feedback scheme for the WIP. The controller is fed by the desired and actual values of the state.

design degrees of freedom, let us assume that $\mathbf{M}_\mathrm{c}$ only depends on the pitch angle α and has a block-diagonal structure. Further, fix the two coefficients k_1 and k_2 to be constant, such that

$$\mathbf{M}_\mathrm{c}^{-1} = \begin{bmatrix} k_1 & h(\alpha) & 0 \\ h(\alpha) & w(\alpha) & 0 \\ 0 & 0 & \frac{1}{k_2} \end{bmatrix}, \tag{8.6}$$

where $h(\alpha)$ and $w(\alpha)$ are free functions. By doing so, the projected matching equation (6.33) is substantially simplified: The left hand side (lhs) of (6.33) is given as

$$\text{lhs} = 2\,r c_2\,(h\psi_1 + w\psi_2)\,\dot{\alpha}\sin\alpha, \tag{8.7}$$

where

$$\psi_1(\alpha) = c_1 r + c_2\cos\alpha - c_3 \tag{8.8}$$

$$\psi_2(\alpha) = c_4 + r\,(c_2\cos\alpha - c_3) \tag{8.9}$$

are computed from

$$\mathbf{f}_M^\mathrm{T} = \mathbf{G}_\perp \mathbf{M} = \begin{bmatrix} \psi_1(\alpha) & \psi_2(\alpha) & 0 \end{bmatrix}. \tag{8.10}$$

The right hand side (rhs) of (6.33) becomes

$$\text{rhs} = \left(2h'\psi_1\psi_2 + w'\psi_2^2\right)\dot{\alpha}, \tag{8.11}$$

where $(\cdot)'$ denotes the derivative with respect to α. A possible solution is

$$w = \frac{k_3 \psi_1^2(\alpha)}{\psi_2^2(\alpha)}, \tag{8.12}$$

$$h = -\frac{\gamma k_3 \psi_1(\alpha) + g}{\gamma \psi_2(\alpha)}, \tag{8.13}$$

for constant positive parameters k_1, k_2, k_3, and γ, which need to be chosen such that $\mathbf{M}_\mathrm{c} > \mathbf{0}$ for $-\pi/2 < \alpha < \pi/2$. For the kinetic energy shaping control law (6.34), also $\mathbf{C}_\mathrm{c}$ and $\mathbf{J}_\mathrm{c}$ are necessary. The matrix $\mathbf{C}_\mathrm{c}$ can be easily calculated from the Christoffel symbols of $\mathbf{M}_\mathrm{c}$; the matrix $\mathbf{J}_\mathrm{c}$ takes the form

$$\mathbf{J}_\mathrm{c} = \begin{bmatrix} 0 & -f_2 v - f_3 \dot{\alpha} & 0 \\ f_2 v + f_3 \dot{\alpha} & 0 & -f_1 \dot{\theta} \\ 0 & f_1 \dot{\theta} & 0 \end{bmatrix} \tag{8.14}$$

for some functions[5] $f_i(\boldsymbol{\xi})$. Note that many other solutions to the matching equation (6.33) exist. However, as it turns out, this particular solution simplifies the parametrization via LLDA.

Shaping the potential energy. The solution to the PDE (6.35) for the shaping of the potential energy can be easily solved using a computer algebra system. The closed-loop potential energy takes the form

$$V_\mathrm{c}(\boldsymbol{\xi}) = \gamma \left(\ln(\psi_1(\alpha))(r^2 c_1 - c_3) - r c_2 \cos\alpha \right) + \Pi_1(\Phi(s,\alpha)) + \Pi_2(\theta), \tag{8.15}$$

where $\Pi_1(\Phi(s,\alpha))$ is a free function of the homogeneous solution[6]

$$\begin{aligned} \Phi(s,\alpha) = s - r\alpha + \frac{\gamma}{g}(k_1 - k_3)((c_4 - c_3 r)\alpha + c_2 r \sin\alpha) \\ + 2\,\frac{c_4 - c_1 r^2}{\sqrt{c_2^2 - (c_1 r - c_3)^2}} \arctan\left(\frac{(c_1 r - c_2 - c_3)(1 - \cos\alpha)}{\sqrt{c_2^2 - (c_1 r - c_3)^2}\,\sin\alpha} \right), \end{aligned} \tag{8.16}$$

and $\Pi_2(\theta)$ is a free function of θ. Both Π_1 and Π_2 need to be chosen such that $V_\mathrm{c}(\boldsymbol{\xi})$

[5] The explicit form of the functions $f_i(\boldsymbol{\xi})$ is omitted for brevity.

[6] We assume that $c_2^2 > (c_1 r - c_3)^2$ holds, which applies for the considered WIP. If this is not the case, a similar function $\Phi(s,\alpha)$ can be computed.

has an isolated minimum at the desired value $\boldsymbol{\xi}=\hat{\boldsymbol{\xi}}$. We choose

$$\Pi_1 = \frac{1}{2}\,\mu\,\Phi^2(s\text{–}\hat{s},\alpha), \qquad \mu > 0 \tag{8.17}$$

$$\Pi_2 = k_\mathrm{p}\left(1-\cos(\theta\text{–}\hat{\theta})\right), \qquad k_\mathrm{p} > 0, \tag{8.18}$$

to account for the periodic property of $\theta \in \mathbb{S}^1$.

Damping injection. The damping injection term is given as

$$\mathbf{u}_\mathrm{di} = -\mathbf{K}_\mathrm{di}\mathbf{G}^\mathrm{T}\mathbf{M}^{-1}\mathbf{M}_\mathrm{c}\boldsymbol{\nu}_\mathrm{e}, \tag{8.19}$$

where $\mathbf{K}_\mathrm{di}=\mathrm{diag}(k_{\mathrm{d},1},k_{\mathrm{d},2})>\mathbf{0}$.

Proposition 8.1. *The matrix* $\mathbf{R}_\mathrm{c}=\mathbf{M}_\mathrm{c}\mathbf{M}^{-1}\mathbf{G}\mathbf{K}_\mathrm{di}\mathbf{G}^\mathrm{T}\mathbf{M}^{-1}\mathbf{M}_\mathrm{c}$ *for the WIP ensures pervasive damping.*

Proof. See Appendix A.3. ■

8.3.2 Some remarks on the parameter choice

The desired eigenvalues for the linearized closed-loop system were computed in [10], and are given as follows:

Forward and pitch dynamics		Yaw dynamics	
λ_1	-3.94	λ_5	-2.38
λ_2	-35.96	λ_6	-62.34
λ_3	$-3+j0.77$		
λ_4	$-3-j0.77$		

For the potential function (8.18) and the damping injection (8.19), the closed-loop yaw dynamics are of the form

$$k_2\ddot{\theta} + k_\mathrm{p}\sin(\theta\text{–}\hat{\theta}) = f_1\dot{\theta}\dot{\alpha} - \frac{k_2^2}{c_6^2}\,k_{\mathrm{d},2}\dot{\theta}. \tag{8.20}$$

Note that the term quadratic in the velocities arises from (8.14). The free parameters k_2, k_p, and $k_{\mathrm{d},2}$ are chosen—similar to a PD controller—such that the linearized yawing dynamics have closed-loop eigenvalues $\{\lambda_5,\lambda_6\}$. Their value is given in Table 8.1.

For the parametrization of the remaining dynamics we apply the following procedure. First, let us replace the remaining five free parameters k_1, k_3, γ, μ, and $k_{\mathrm{d},1}$ in the following manner:

$$
\begin{aligned}
k_1 &= \frac{\psi_2^*(\pi_4 - \pi_2\pi_3) + \pi_2 c_2 g}{c_2 g \psi_1^* \psi_2^*}\,\pi_1 \\
k_3 &= \frac{\psi_1^*(\pi_4 - \pi_2\pi_3) - c_2 g}{c_2 g (\psi_1^*)^2}\,\pi_1 \\
\gamma &= \frac{g\psi_1^*}{\pi_1} \\
\mu &= \frac{\pi_3 c_2 g \psi_1^* \psi_2^*}{\pi_1\left((\psi_2^* - \pi_2\psi_1^*)(\pi_4 - \pi_2\pi_3) + \pi_2 c_2 g\right)} \\
k_{\mathrm{d},1} &= \frac{\pi_1\pi_5}{\pi_2 c_2 g \psi_1^* (\psi_2^*)^3}\left((c_3 - c_2)(\psi_2^* + \psi_1^* r) + \psi_1^*\psi_2^*\right)^2\left((\psi_2^* - \pi_2\psi_1^*)(\pi_4 - \pi_2\pi_3) + \pi_2 c_2 g\right),
\end{aligned}
$$

where $\psi_1^* = \psi_1(0)$ and $\psi_2^* = \psi_2(0)$, and π_i, $i = 1...5$ are new free parameters. By doing so, the linearized closed-loop system around the equilibrium point ($\boldsymbol{\xi}^* = \mathbf{0}$, $\boldsymbol{\nu}^* = \mathbf{0}$) is simplified to

$$
\begin{bmatrix} v \\ \dot{\alpha} \\ \dot{\theta} \\ \dot{v} \\ \ddot{\alpha} \\ \ddot{\theta} \end{bmatrix} = \begin{bmatrix} 0 & 0 & 0 & 1 & 0 & 0 \\ 0 & 0 & 0 & 0 & 1 & 0 \\ 0 & 0 & 0 & 0 & 0 & 1 \\ \pi_3 & \pi_4 & 0 & -\frac{\pi_5}{\pi_2} & -\pi_5 & 0 \\ -\frac{\psi_1^*}{\psi_2^*}\pi_3 & \frac{c_2 g - \psi_1^*\pi_4}{\psi_2^*} & 0 & \frac{\psi_1^*}{\pi_2\psi_2^*}\pi_5 & \frac{\psi_1^*}{\psi_2^*}\pi_5 & 0 \\ 0 & 0 & -\frac{k_{\mathrm{p}}}{k_2} & 0 & 0 & -\frac{k_2}{c_6^2}\,k_{\mathrm{d},2} \end{bmatrix} \begin{bmatrix} s \\ \alpha \\ \theta \\ v \\ \dot{\alpha} \\ \dot{\theta} \end{bmatrix}. \tag{8.21}
$$

The remaining eigenvalues $\{\lambda_1, \ldots, \lambda_4\}$ corresponding to the forward and pitch dynamics determine the values of the parameters π_i, $i = 2...5$. Note that the characteristic polynomial of the system's matrix (8.21) does not depend on π_1. The parameter π_1 is used to satisfy the definiteness requirements of the function V_{c}, and of the closed-loop matrices $\mathbf{M}_{\mathrm{c}}$ and $\mathbf{R}_{\mathrm{c}}$. Additionally, it can be used to optimize the domain of attraction and its estimate by employing the technique presented in [104]. For a particular choice of π_1, the values of the parameters k_1, k_3, γ, μ, and $k_{\mathrm{d},1}$ are given in Table 8.1.

Remark 8.3.1. The DC (3.8) is satisfied for the WIP. Small damping terms in unactuated coordinates that have not been included in the model enter as dissipation with respect to the closed-loop energy. Thus, damping in the unactuated coordinates does not represent a threat to the stability of the system.

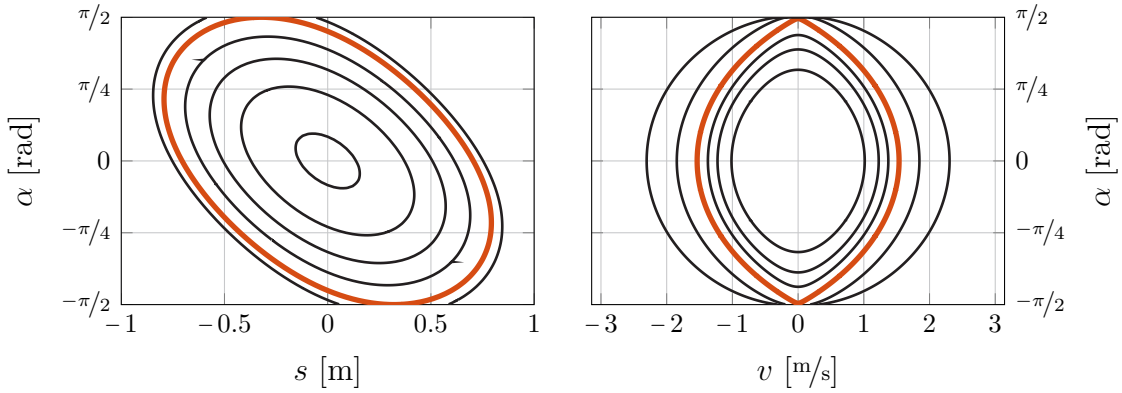

Figure 8.4: Level sets of the total closed-loop energy $E_c = \frac{1}{2}\boldsymbol{\nu}^T\mathbf{M}_c\boldsymbol{\nu} + V_c$. Left: Level sets of the potential energy V_c for $\theta = 0$. Right: Level sets of the closed-loop energy E_c for $\theta = \dot{\theta} = s = \dot{\alpha} = 0$.

Figure 8.4 shows the level sets of the potential energy V_c that correspond to the stability margins of the WIP without input saturation.

8.4 Simulations and experimental results

This section presents the implementation of the control framework developed in Chapter 6 and Chapter 7 on the WIP. The experimental setup consists of the WIP *KRT32*, the small scale WIP developed at the Institute of Automatic Control of the Technische Universität München. Figure 8.5 shows the internal structure of the WIP. The system is equipped with an accelerometer, a gyroscope, and encoders that enable the direct measurement of the relative rotation of the wheels with respect to the body. The ab-

Table 8.1: Closed-loop parameters for the wheel inverted pendulum.

Parameter	Value
k_1	14315.93852
k_2	1
k_3	5075.031964
μ	0.0009039394410
γ	0.2299298661
k_p	155.67438789
$k_{d,1}$	1192.763201
$k_{d,2}$	0.0008437349532

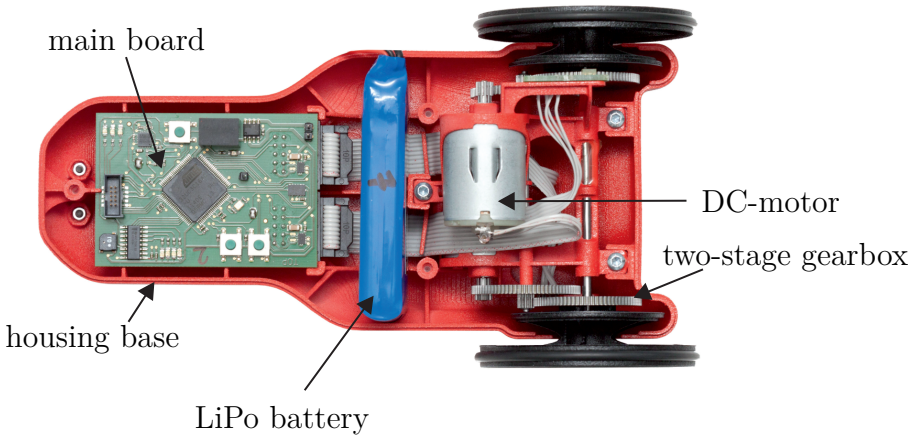

Figure 8.5: Configuration of the WIP.

solute position of the WIP on the plane is computed by means of the reconstruction equation (8.2). The actuation of the wheels is provided by two DC motors, each of them linked to one wheel by a two-stage gearbox. A Lithium Polymer battery serves as the power supply for the DC-motors. Data exchange is possible via a Bluetooth module. During the experiments, the armature voltage U_A to control the motors is bounded by the battery charge, which fluctuates approximately between 8.0V and 8.4V while fully charged. We, thus, assume $|U_\mathrm{A}| \leq 8.0\mathrm{V}$ for the simulations and experiments. Additionally, the current is limited by the *H-bridge* to 3.0A. All simulations and experiments are run within the input limits to avoid saturation. The controllers are implemented as continuous-time control laws in *Simulink*. For the experiments, the compiler automatically converts the controllers to discrete-time. The code can then be flashed via the Bluetooth module. For the simulations to reflect the micro-controller's sample time $T_\mathrm{s} = 5\mathrm{ms}$, the (continuous-time) controller is accordingly simulated in discrete-time with the same sample time T_s. It was shown in [169] that the motor dynamics are fast enough to be neglected. Therefore, we use the static model for the DC motors for the controller design.

8.4.1 Stabilization

In this section, we consider two different scenarios to demonstrate the performance of the stabilizing controller. The first scenario represents set point changes in the yaw angle θ and the path length s, and illustrates the transient behavior of the stabilizing controller in reduced space $\mathcal{Q}_\mathrm{R}$. The second scenario shows how the stabilization results can be applied to stabilize a specific point on the xy-plane.

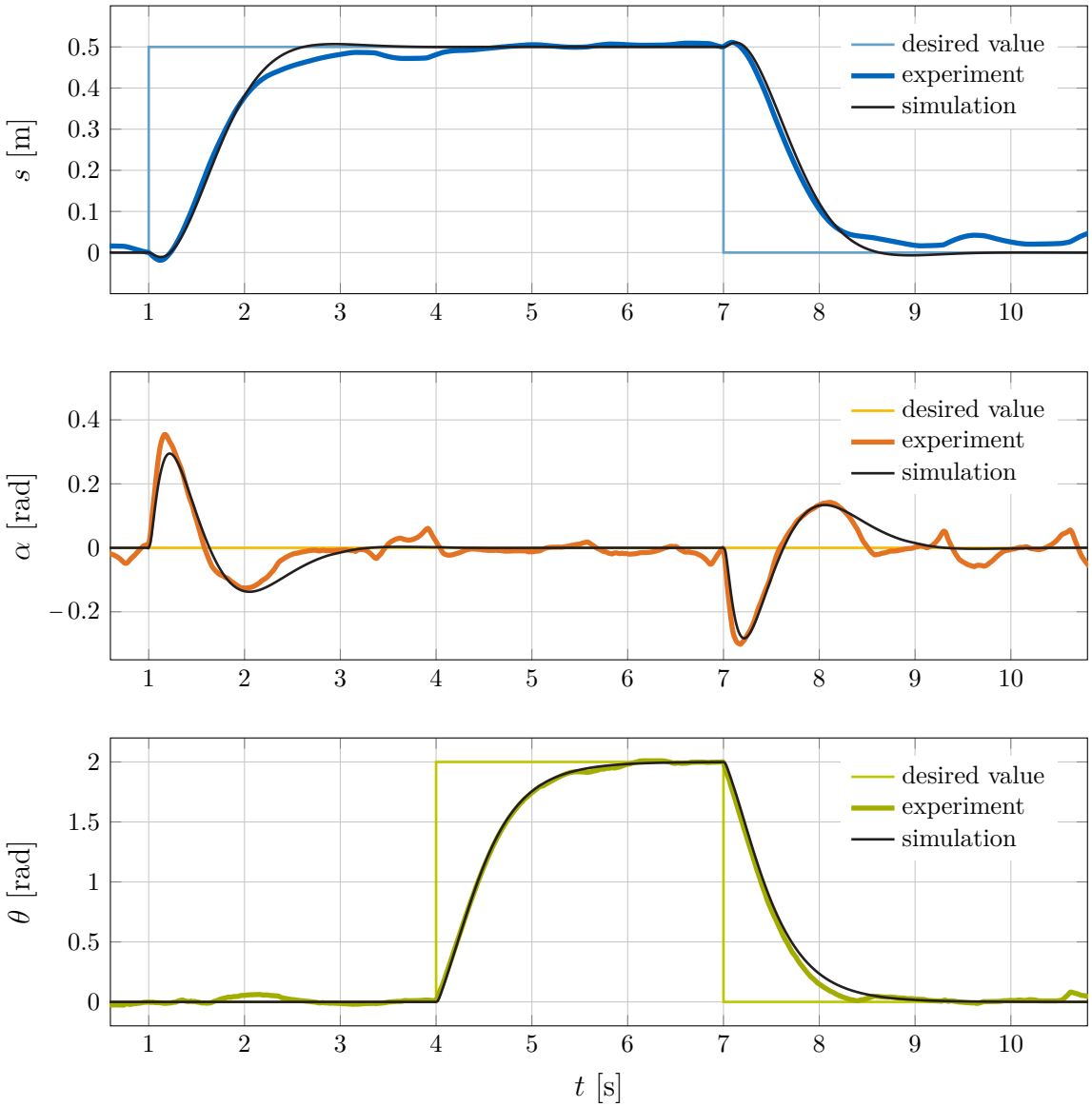

Figure 8.6: Position control of the WIP in reduced coordinates.

Set point changes in reduced space. The first scenario corresponds to the position stabilizing controller in reduced space. Specifically, the idea is to asymptotically stabilize different admissible equilibrium points $\boldsymbol{\xi}^*$. In reduced coordinates $\boldsymbol{\xi} \in \mathcal{Q}_{\mathrm{R}}$, the system evolves unconstrained, such that the control problem resembles the classical stabilization problem for holonomic systems. One can, thus, asymptotically stabilize a desired equilibrium $\boldsymbol{\xi}^*$ employing the smooth control law that arises from the energy shaping procedure. Figure 8.6 shows the results from the stabilizing controller. Before the start of the experiment, the system is stabilized at the equilibrium point given by $\boldsymbol{\xi}^* = \mathbf{0}$. At $t = 1\,\mathrm{s}$, the set point s^* changes from $s^* = 0\,\mathrm{m}$ to $s^* = 0.5\,\mathrm{m}$; at $t = 4\,\mathrm{s}$, the

set point θ^* changes from $\theta^* = 0\,\mathrm{m}$ to $\theta^* = 2\,\mathrm{rad}$. From $t = 7\,\mathrm{s}$ on, the origin is again stabilized. Clearly, the experimental results correspond well to the simulation.

Stabilization of a point in the horizontal plane. Let us now consider the constrained space $\mathcal{Q}_\mathrm{C}$ parametrized by $\boldsymbol{\eta} = (x,\, y,\, \theta, \alpha)$. The goal of this approach is to stabilize the point in the horizontal plane given by $x = 0$, and $y = 0$, starting from different initial positions, while maintaining stable pitch dynamics. Point stabilization cannot be achieved using smooth or continuous controllers [39], although the system is proven to be controllable [145]. Steering via Lie bracket motion (cf. Chow's Theorem [142]), or discontinuous controllers have proven to show slow convergence, and—in the case of controllers that require infinite switching, like sliding mode approaches—undesired chattering effects occur. However, often the goal is for the system to reach a certain position in the Euclidean space. For the WIP in $\mathcal{Q}_\mathrm{C}$, this is equivalent to stabilizing a specific position $\mathbf{r}^* = (x^*,\, y^*)$, maintaining stable pitch dynamics (cf. [138, 161]). The orientation θ at $\mathbf{r}^*$ is not of interest. Let us consider the dynamics of the WIP on $\mathcal{Q}_\mathrm{C}$, and let us assume, without loss of generality, that $\mathbf{r}^* = \mathbf{0}$. According to Theorem 6.2, the potential energy

$$\tilde{V}_\mathrm{c}(\boldsymbol{\eta}) = V_\mathrm{c}(\boldsymbol{\xi} = \boldsymbol{\vartheta}(\boldsymbol{\eta})), \tag{8.22}$$

with

$$\boldsymbol{\vartheta} = (\mathbf{S}_{\boldsymbol{\eta}}^\mathrm{T}\mathbf{S}_{\boldsymbol{\eta}})^{-1}\mathbf{S}_{\boldsymbol{\eta}}^\mathrm{T}\boldsymbol{\eta} = \begin{bmatrix} x\cos\theta + y\sin\theta \\ \alpha \\ \theta - \hat{\theta} \end{bmatrix}, \tag{8.23}$$

represents a solution to the matching problem in the constrained space $\mathcal{Q}_\mathrm{C}$. The corresponding closed-loop dynamics

$$\mathbf{M}_\mathrm{c}\dot{\boldsymbol{\nu}} + \mathbf{C}_\mathrm{c}\boldsymbol{\nu} + \mathbf{S}_{\boldsymbol{\eta}}^\mathrm{T}\nabla_{\mathbf{q}}\tilde{V}_\mathrm{c} = (\mathbf{J}_\mathrm{c} - \mathbf{R}_\mathrm{c})\boldsymbol{\nu} \tag{8.24}$$

asymptotically stabilize the set

$$\mathcal{X} = \left\{(\boldsymbol{\eta},\, \boldsymbol{\nu}) \in \mathsf{T}\mathcal{Q}_\mathrm{C} \mid \mathbf{S}_{\boldsymbol{\eta}}^\mathrm{T}\nabla_{\mathbf{q}}\tilde{V}_\mathrm{c} = \mathbf{0}\right\} \tag{8.25}$$

according to Theorem 2.4. The set $\mathcal{X}$ corresponds to

$$\begin{aligned} x\cos\theta + y\sin\theta &= 0 \\ \alpha &= 0 \\ \theta &= \hat{\theta}. \end{aligned}$$

Note that the yaw dynamics (8.20) are almost global asymptotically stable (up to a set of Lebesgue measure 0). This implies that the yaw dynamics (8.20) are globally ISS with respect to the *input disturbance* $\hat{\theta}$. Hence, the system's response to changes in $\hat{\theta}$ remains bounded. If $\hat{\theta}$ is constant, then also θ converges towards $\hat{\theta}$. This reflection gives rise to apply a control strategy that continuously changes the value of $\hat{\theta}$ such that x and y converge towards the origin. We apply the following strategy

$$\hat{\theta} = \begin{cases} \arctan\left(\frac{y}{x}\right), & \text{for } x\cos\theta + y\sin\theta \geq 0 \\ \arctan\left(\frac{y}{x}\right) \pm \pi, & \text{for } x\cos\theta + y\sin\theta < 0. \end{cases} \tag{8.26}$$

Figure 8.7 shows the response of the distance $\rho = \sqrt{x^2 + y^2}$ to the origin, and the path on the xy-plane taken by the WIP for four different initial positions $\mathbf{r}_0$. The initial orientation is in all cases $\theta_0 = 0$. The simulations and experiments illustrate the applicability of the approach. The system remains stable and converges towards $\mathbf{r}^* = \mathbf{0}$.

Remark 8.4.1. To avoid input saturation, or even instability of the plant, for the stabilization of a distant point in the xy-plane, a path following strategy can be first pursued to get closer to the origin $\mathbf{r}^* = \mathbf{0}$ (cf. Section 8.4.3). Once the WIP enters the stability boundaries of the position controller, it is possible to safely switch to the stabilizing controller presented in this section, as a onetime switching between two stabilizing controllers remains stable [129]. By doing so, the position stabilizing controller is only active in a small region surrounding the desired position.

8.4.2 Tracking

In this section, we consider the tracking problem from Section 7.2 for two different scenarios. The first scenario corresponds to the hybrid position and velocity controller in reduced space as presented in Section 7.2.3. The second scenario represents the tracking problem in the constrained space as a combination of tracking for non-admissible trajectories in reduced space together with an orientation control law to compensate

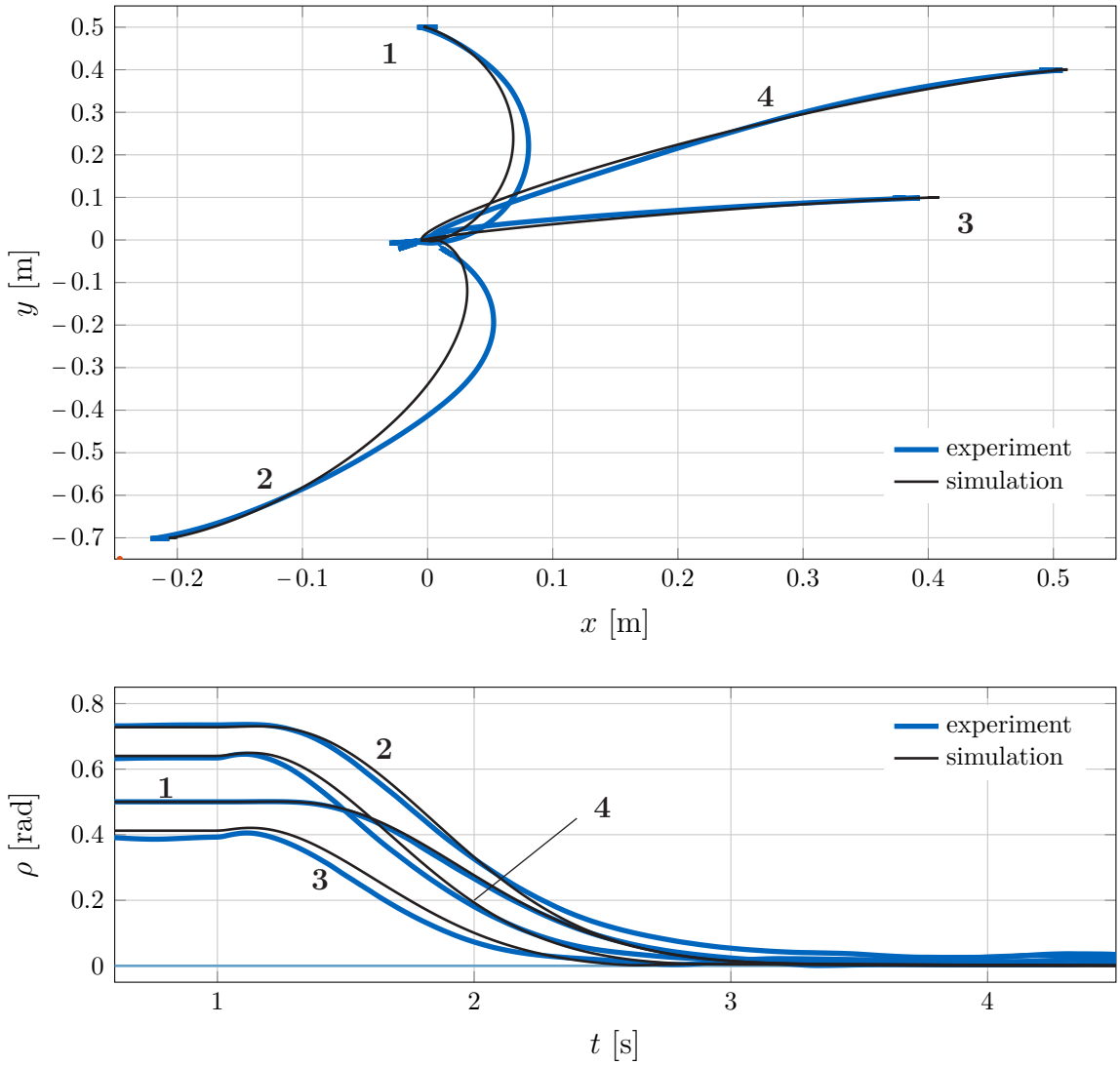

Figure 8.7: Stabilization of the WIP at a position in the xy-plane.

for the error in the xy-plane.

Hybrid position and speed stabilizing controller. This controller is based on Corollary 7.1. The goal is to stabilize a constant velocity v^*, and, at the same time, the corresponding time-varying path length $\hat{s} = v^* t + \hat{s}_0$, for some constant s_0. In this particular case, we additionally demand a constant yaw rate θ^*. Prior to the beginning of the experiment, the system is stabilized at the equilibrium $\boldsymbol{\xi}^* = \mathbf{0}$. At $t = 1\,\mathrm{s}$, the set point v^* changes from $v^* = 0\,\mathrm{m/s}$ to $v^* = 0.6\,\mathrm{m/s}$, the corresponding desired position is defined as $\hat{s}(t) = v^*(t-1) + \hat{s}_0$, with $\hat{s}_0 = 0.1\,\mathrm{m}$. Since $\mathbf{G}_\perp (\mathbf{C} - \mathbf{J})\hat{\boldsymbol{\nu}} = 0$, the system asymptotically converges towards the desired values according to Corollary 7.1. As per the results shown in Figure 8.8, the error regulation is concluded after approximately

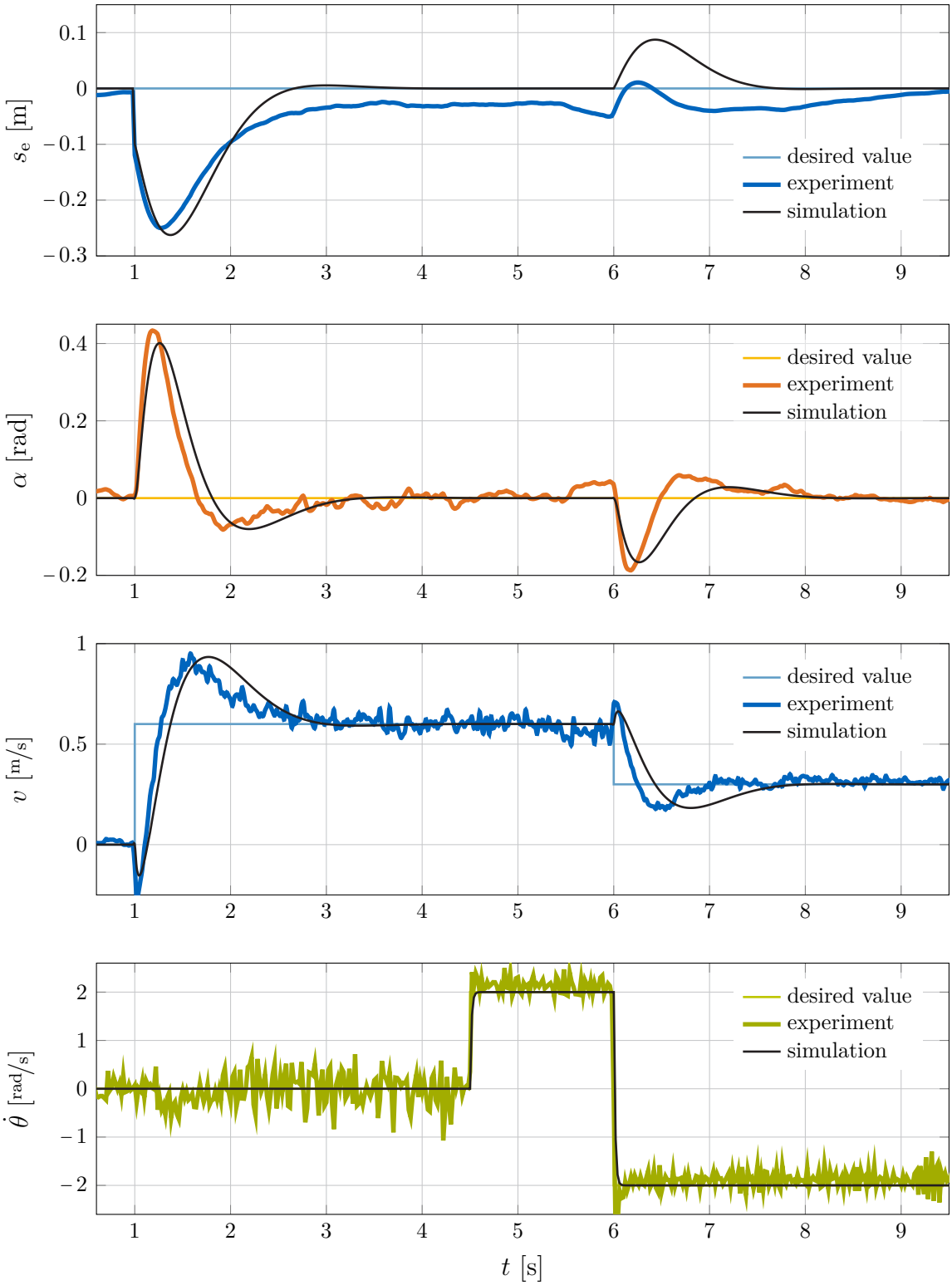

Figure 8.8: Hybrid position and speed control for the WIP.

2 seconds $t = 3\,\mathrm{s}$. At $t = 4.5\,\mathrm{s}$, a pure velocity controller (i. e., $\hat{\theta} = \theta$) is used for the regulation of the yawing angular velocity $\dot{\theta}^* = 2\,{}^{\mathrm{rad}}/_{\mathrm{s}}$. At $t = 6\,\mathrm{s}$, the set point $\dot{\theta}^*$ changes to $\dot{\theta}^* = -2\,{}^{\mathrm{rad}}/_{\mathrm{s}}$, and, at the same time, the desired forward velocity is reduced to $v^* = 0.3\,{}^{\mathrm{m}}/_{\mathrm{s}}$. We can see from Figure 8.8 that the hybrid position and speed controller stabilizes both the error in the velocity v and the error in the position s. The pure speed controller used for the yawing velocity assumes no error in the yaw angle θ and regulates the desired yawing velocity within fractions of seconds.

Tracking non-admissible reference trajectories in the constrained space $\mathcal{Q}_{\mathrm{C}}$. This scenario consists in (approximately) tracking a non-admissible trajectory defined as follows: The x-coordinate evolves in time according to

$$\hat{x}(t) = \frac{21}{40}\,t - \frac{3t_e}{40\pi}\sin\left(\frac{2\pi}{t_e}\,t\right) - \frac{3t_e}{32\pi}\sin\left(\frac{4\pi}{t_e}\,t\right). \tag{8.27}$$

The y-coordinate is defined as

$$\hat{y}(t) = \sin\hat{x}(t), \quad \Rightarrow \quad \dot{\hat{y}}(t) = \dot{\hat{x}}(t)\cos\hat{x}(t). \tag{8.28}$$

The orientation along the trajectory θ_{t} is given by

$$\theta_{\mathrm{t}} = \arctan\left(\frac{\dot{\hat{y}}}{\dot{\hat{x}}}\right) = \arctan\left(\cos\hat{x}\right). \tag{8.29}$$

To account for initial errors, the desired value $\hat{\boldsymbol{\xi}}(t)$ is defined as

$$\hat{\boldsymbol{\xi}} = \begin{bmatrix} s - (x - \hat{x})\cos\theta - (y - \hat{y})\sin\theta \\ 0 \\ \theta_{\mathrm{t}} - \arctan\left(k(y - \hat{y})\right) \end{bmatrix}, \tag{8.30}$$

where the transition factor is chosen as $k = 5$. The particular choice of $\hat{\boldsymbol{\xi}}(t)$ emerges on the one hand from the stabilization of a point in the horizontal plane, and on the other hand, from path following: For the computation of the desired path length $\hat{s}$, we employ the coordinates of the constrained space $\mathcal{Q}_{\mathrm{C}}$; the desired orientation $\hat{\theta}$ resembles path following. The desired values $\hat{\boldsymbol{\nu}}(t)$ and $\dot{\hat{\boldsymbol{\nu}}}(t)$ can then be computed as

$$\hat{\boldsymbol{\nu}} = \begin{bmatrix} \frac{\dot{\hat{x}}}{\cos\theta_{\mathrm{p}}} \\ 0 \\ \dot{\hat{\theta}} \end{bmatrix}, \qquad \dot{\hat{\boldsymbol{\nu}}} = \begin{bmatrix} \frac{\ddot{\hat{x}}}{\cos\theta_{\mathrm{p}}} + \frac{\dot{\hat{x}}\dot{\theta}_{\mathrm{p}}\sin\theta_{\mathrm{p}}}{\cos^2\theta_{\mathrm{p}}} \\ 0 \\ \ddot{\hat{\theta}} \end{bmatrix}. \tag{8.31}$$

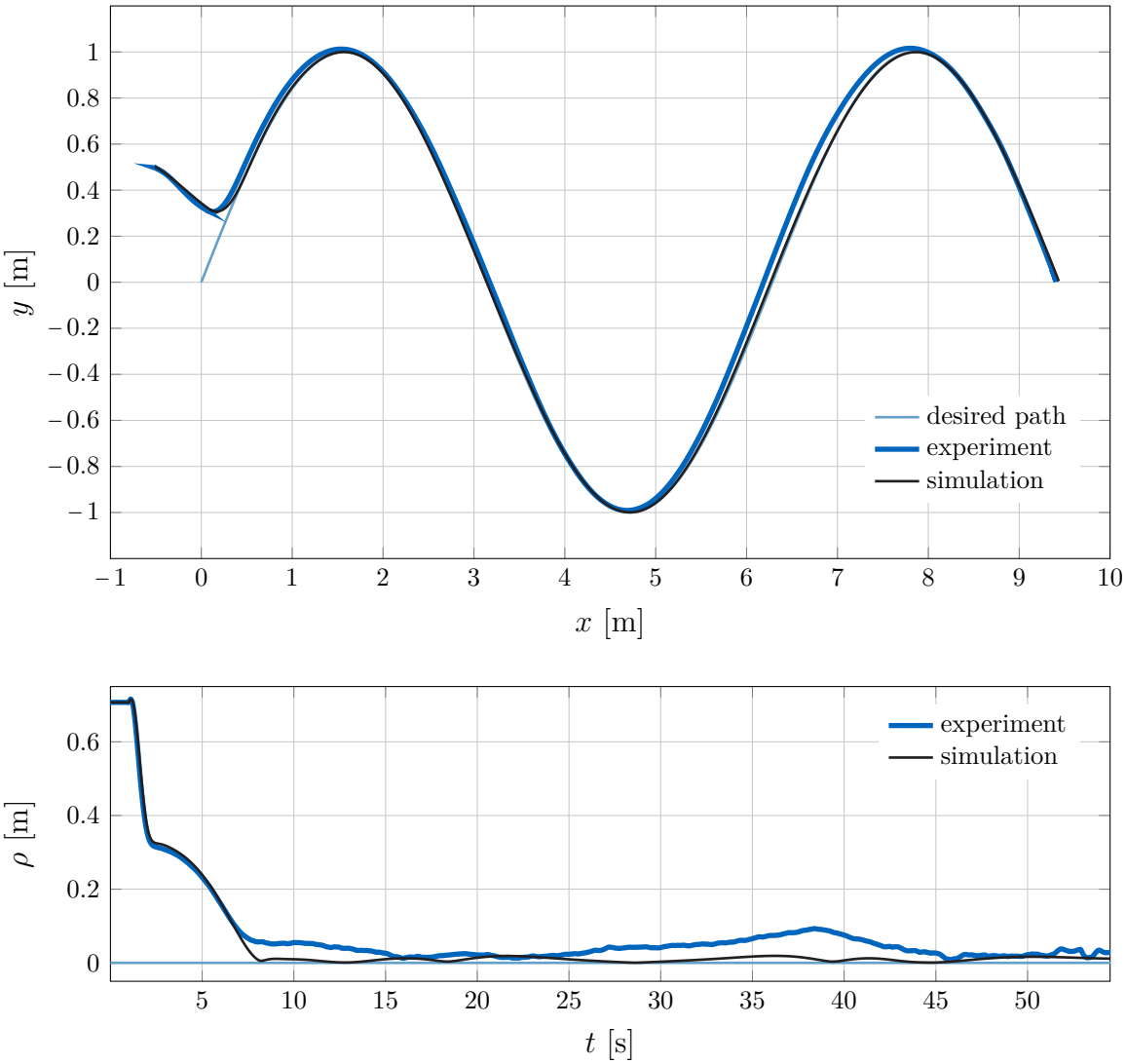

Figure 8.9: Tracking control for the WIP. Position in the plane and distance error.

Clearly, the defined *trajectory* is not compatible with the system's dynamics, as it is not possible to accelerate and decelerate the WIP without affecting the pitch angle α.

Figure 8.9 shows the system's response for an initial position given by $x_0 = -0.5\,\text{m}$, and $y_0 = 0.5\,\text{m}$. The first plot shows the driven path in the xy-plane. The second graph shows the evolution of the error $\rho = \sqrt{(x-\hat{x})^2 + (y-\hat{y})^2}$. Figure 8.10 shows the velocity profile, the pitch angle, and the yaw angle in comparison with the desired values. The results clearly show that the WIP converges towards the reference trajectory and stay within a small region around the desired values. As the trajectory is non-admissible, the errors do not converge towards the origin.

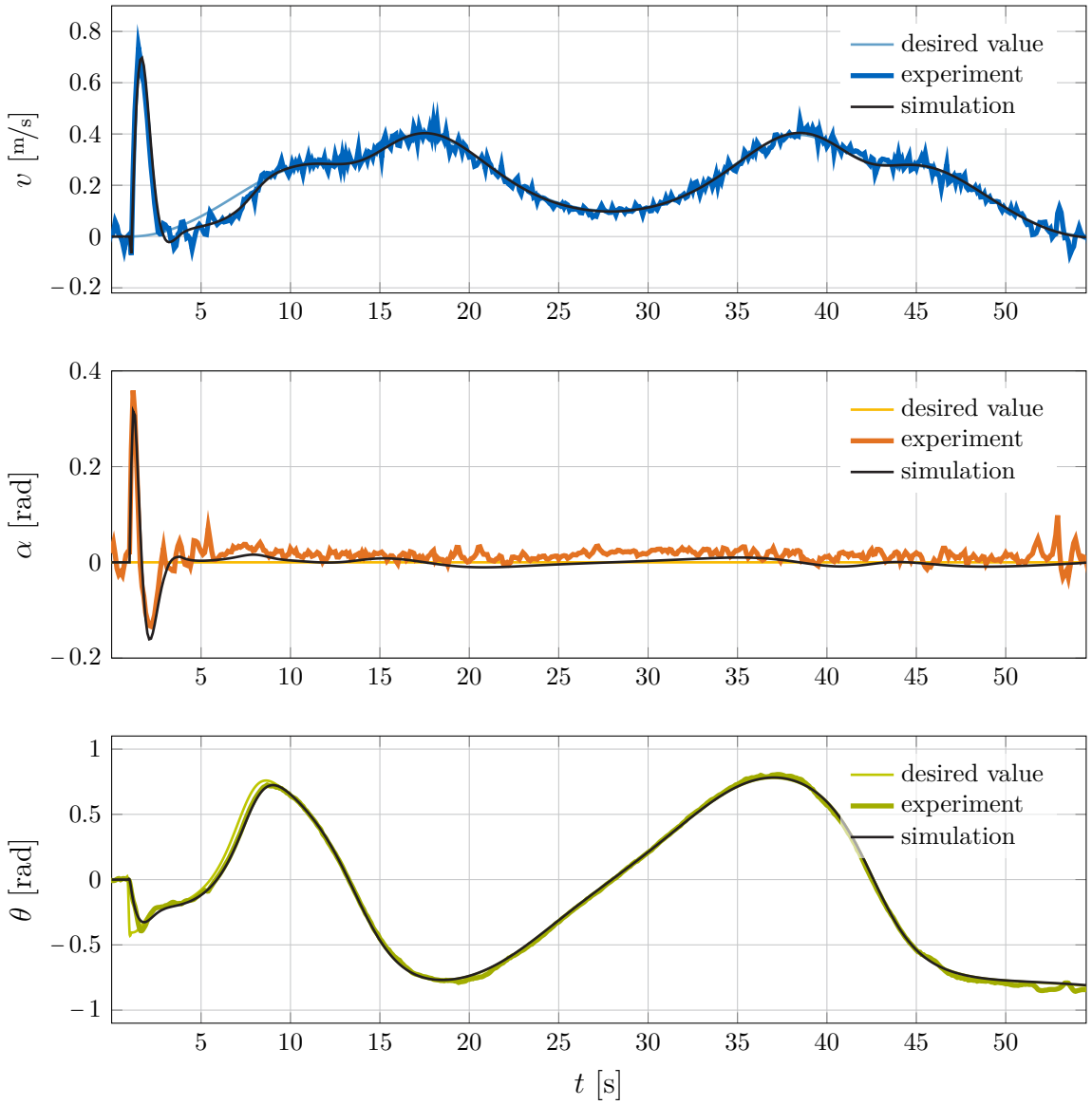

Figure 8.10: Tracking control for the WIP. Forward velocity, pitch and yaw angle for a non-admissible trajectory.

8.4.3 Path following

In this section, we present the results for two different path following strategies for the same scenario. The first strategy corresponds to the classical path following from Theorem 7.3, where we command a desired orientation angle $\hat{\theta}$ depending on the actual position with respect to the path. In the second strategy, the desired yawing velocity $\dot{\theta}_{\mathbf{p}}$ is included in the speed stabilization to achieve a better convergence to path segments that are not necessarily a straight line. That is, the steering of the WIP does not only depend on its position with respect to the path, but also on its forward velocity

and yawing rate with respect to the desired values along the path. The path consists of two parallel lines of length 1.2 m separated by a distance of 0.4 m, and two circle segments of radius $R = 0.2\,\mathrm{m}$ at both ends to create a closed circuit. The goal is for the WIP to approach and stay on the path, and to travel along the path (in a mathematically positive direction) with a constant forward velocity $v^* = 0.3\,\mathrm{m/s}$. To illustrate the differences of the approaches, both experiments are started with the same initial error $\rho_0 = 0.2\,\mathrm{m}$ above the path, the initial orientation is $\theta_0 = 0\,\mathrm{rad}$, which corresponds to the WIP facing the wrong travel direction.

Path following without yaw rate reference. Due to the nonholonomic constraints of the WIP, the position error with respect to the desired path $\mathcal{P}$ can only be reduced with the aid of appropriate steering commands $\hat{\theta}$ as the WIP moves forward. As the shape of the desired path is simple, the point $\mathbf{p} \in \mathbb{R}^2$, which characterizes the closest point of the path with respect to the actual position (x, y), can be easily computed. The distance ρ is defined as a positive quantity for points lying outside the path, and it takes negative values for all points inside the path. With this particular way of defining ρ, the vector field that defines the desired orientation commands is given as

$$\hat{\theta} = \theta_{\mathbf{p}} + \arctan(k\rho), \tag{8.32}$$

where the convergence parameter is chosen as $k = 36$. The orientation $\theta_{\mathbf{p}}$ at $\mathbf{p}$ is equal to 0 or $\pi/-\pi$ for the line segments, and given by the tangent line to the path for the circular segments. Figure 8.11 shows the results of the first path following strategy. The system clearly approaches and stays on the path for the linear segments. However, the error increases for the circular path segments, since a constant yawing velocity would be required for the system to stay on the path.

Path following with yaw rate reference. The aforementioned drawback of the first path following strategy is overcome by augmenting the vector-field-based orientation commands (8.32) by the desired orientation angular velocity $\dot{\hat{\theta}} = \dot{\theta}_{\mathbf{p}}$, where $\dot{\theta}_{\mathbf{p}}$ is equal to zero for the linear segments, and take the values $\dot{\theta}_{\mathbf{p}} = \kappa_{\mathbf{p}} v^*$ for the curved sections, where $\kappa_{\mathbf{p}}$ represents the curvature of the path at $\mathbf{p}$. Figure 8.12 shows the results of the second path following strategy. In contrast to the first strategy, the integration of the angular velocity information for path following strategies significantly increases the performance by means of a faster convergence and smaller errors to the path.

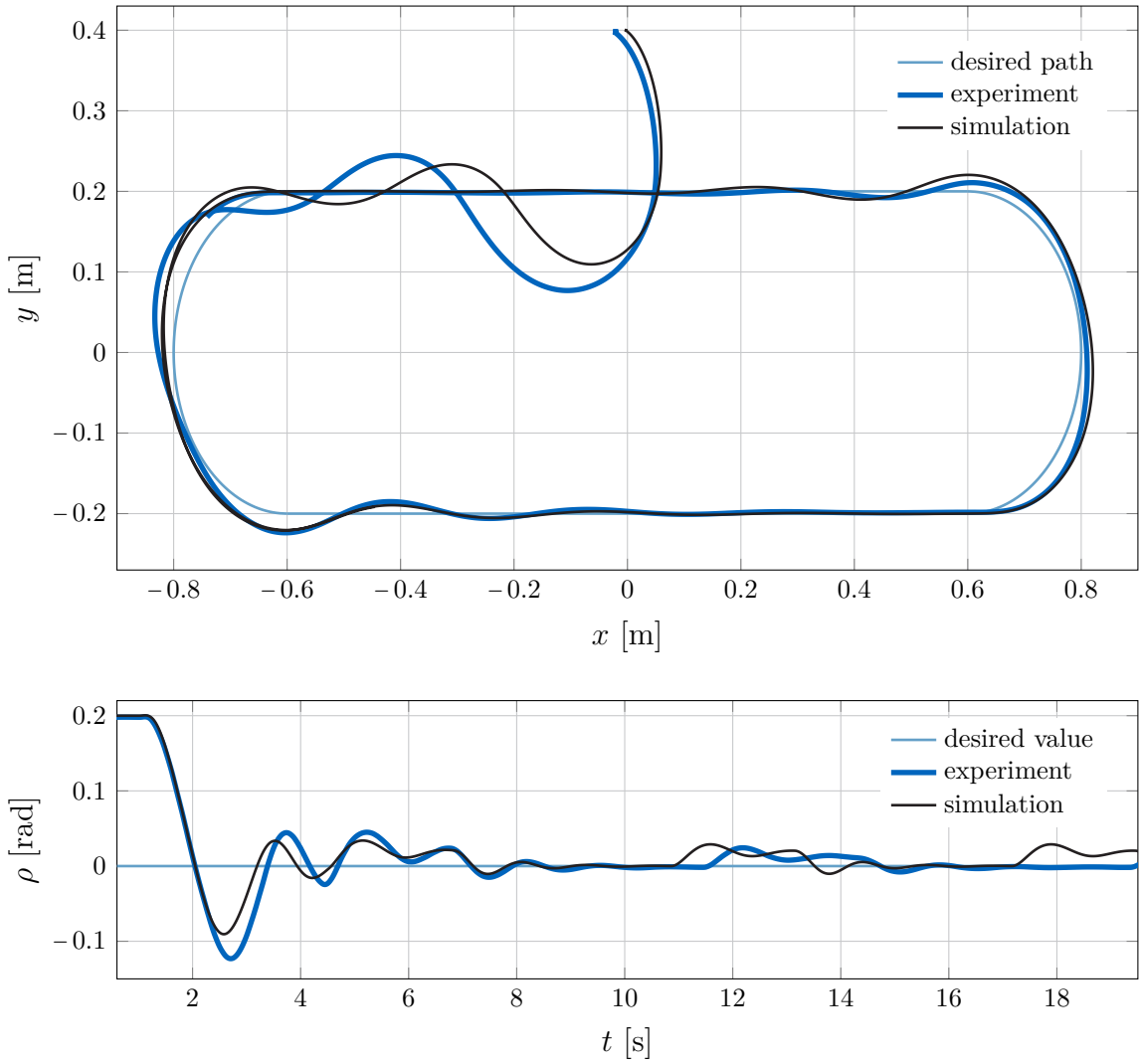

Figure 8.11: Path following control for the WIP.

8.5 Concluding remarks

In this chapter, we systematically designed and parametrized smooth control strategies for the WIP, based upon the results from Chapter 6 and Chapter 7. The design procedure results in an asymptotically stable closed-loop system with desired local dynamics and a large domain of attraction.

The key advantage of the energy shaping control for the WIP relies on the unified framework that is employed to tackle the different tasks: stabilization, tracking, and path following. While the feedback controller remains essentially equal for all different tasks, only the definition and computation of the desired values $\hat{\boldsymbol{\xi}}$ and $\hat{\boldsymbol{\nu}}$ differs.

Even though we restrict the analysis to a reduced (unconstrained) space $\mathcal{Q}_{\mathrm{R}}$, we can

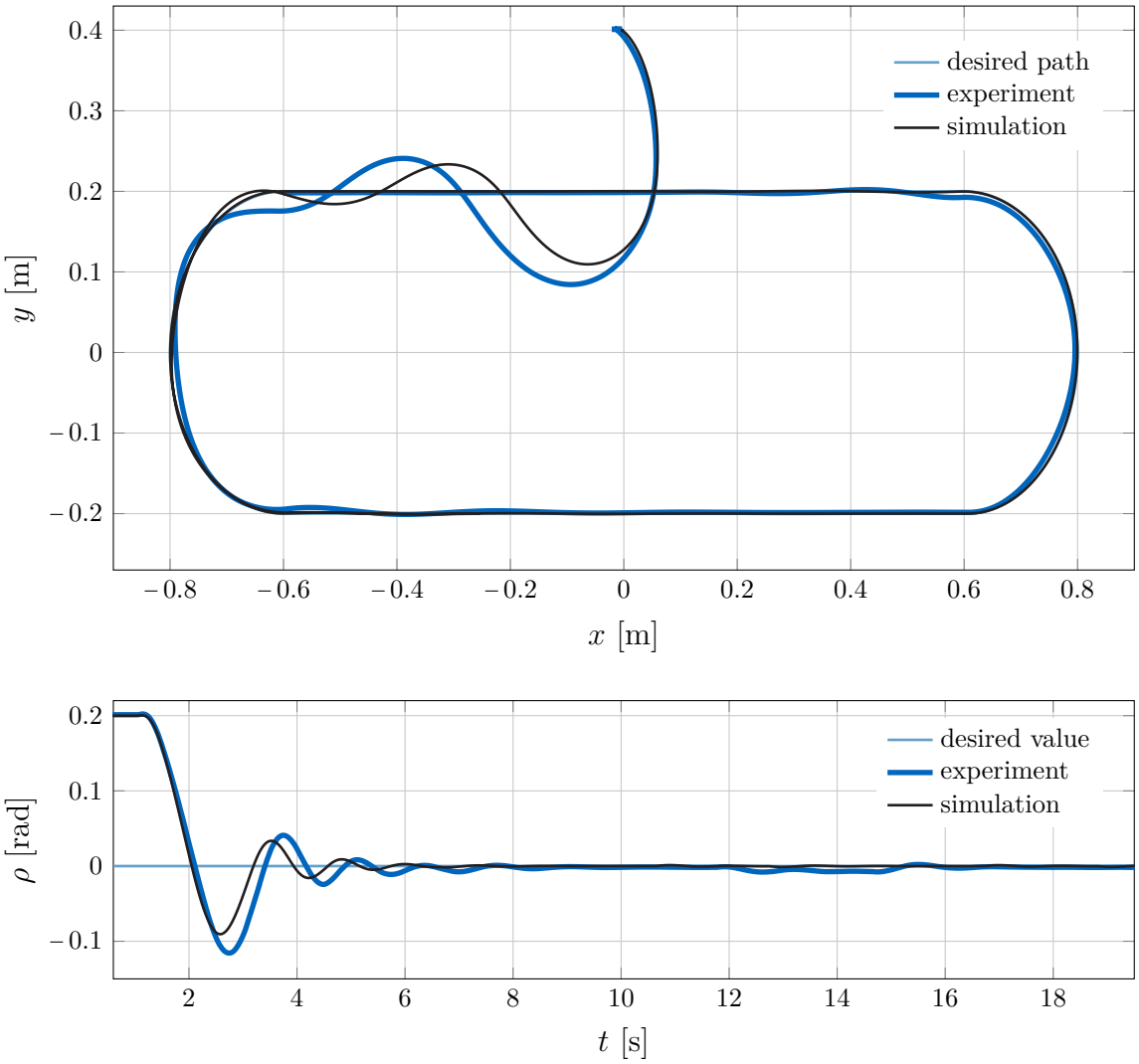

Figure 8.12: Path following control WIP including yaw rate reference.

still employ smooth control laws to tackle stabilization, tracking and path following problems that require the absolute position of the WIP in the horizontal plane given by the coordinates x and y. The ISS property allows us to continuously change the desired position and/or velocity for the completion of a variety of tasks without compromising the stability of the WIP. This feature has been extensively exploited in this chapter.

In particular, this chapter presented the systematic and integrated design of a stabilizing, tracking and path following controllers for the wheeled inverted pendulum system in a single, energy-based framework. The advantage is clear compared to other existing methods, as it exploits the mechanical structure of the system, is inherently robust, and the controller design and its parametrization are transparent and physically motivated. The applicability and the performance of the proposed controllers was demonstrated

with a series of simulations and experimental results.

The controllers were implemented in *Simulink*[7] as continuous-time control laws. The discrete-time code for the micro-controller was automatically generated by the software.

[7] ©2015 The MathWorks, Inc. MATLAB and Simulink are registered trademarks of The MathWorks, Inc. See www.mathworks.com/trademarks for a list of additional trademarks. Other product or brand names may be trademarks or registered trademarks of their respective holders.

IV

Conclusion

9 Final remarks

To satisfy the demand for increasing performance and robustness for mechanical control systems, it is indispensable to employ model-based approaches for the controller design. Total energy shaping control methods exploit the inherent properties of the mechanical systems, as they integrate the nonlinear structure into the design procedure. Additionally, these techniques are intuitive and physically motivated, and provide intrinsically robust controllers.

In this work, we presented energy shaping from a practicable point of view for both holonomic and nonholonomic mechanical systems. The first part of the thesis was devoted to a known obstacle in passivity based-control for underactuated mechanical systems, namely, the dissipation in unactuated coordinates, which may impede the passivation of the closed-loop system [74]. Since it is necessary to break the mechanical structure of the closed-loop Hamiltonian in order to bypass the dissipation condition, we proposed in this thesis the introduction of a non-physical cross term between configuration variables and generalized momenta into the closed-loop energy. By doing so, we break the mechanical structure as desired, but retain some structural properties by not leaving the closed-loop Hamiltonian completely free. All in all, we developed a framework that

i) allows for a systematic design of stabilizing controllers for underactuated mechanical systems

ii) guarantees passivity and, based thereon, asymptotic stability of the closed-loop system in spite of physical dissipation in unactuated coordinates,

iii) does not require the solution of partial differential equations,

iv) is transparent to parametrize via local linear dynamics assignment,

v) directly provides a Lyapunov function, which can be employed for the stability analysis.

This is a strong result, as this theory copes with three of the fundamental difficulties of energy-based approaches. On the one hand, the solution of complicated PDEs is obviated, as we only require the solution to some algebraic equations, and to one Lyapunov

equation. On the other hand, we are able to render the closed-loop system passive regardless of the dissipation condition, and, finally, the controller parametrization can be easily performed via LLDA by assigning desired local behavior by means of the eigenvalues of the linearized closed-loop system.

The second part of the manuscript was devoted to total energy shaping for underactuated nonholonomic systems. In particular, the developed theory was applied to the speed and velocity stabilization as well as to tracking and path following for the wheeled inverted pendulum (WIP)—commercially known as *Segway* [186]. The fast development and commercialization of two-wheeled transportation devices and robots has lead to a growing demand for controllers that fully exploit the performance potential of the plant, but that also remain manageable in their complexity. Based on a solid mathematical foundation, we developed a unified framework that

i) tackles a variety of practical problems,

ii) is physically motivated and intuitive,

iii) imparts controllers that are transparent to parametrize either via local linear dynamics assignment, or by tuning the mechanical parameters of the closed-loop system,

iv) provides inherently robust control systems,

v) takes into account nonlinear effects, actuator dynamics, and input disturbances.

From a practical point of view, we believe that energy shaping as a physically motivated approach, constitutes a good trade-off between required controller complexity and intuitive parametrization. Linear control systems are limited to a specific operating point and, thus, do not provide the required flexibility and performance that the increasing complexity and nonlinear behavior of mechanical systems demand. On the other hand, current non-linear approaches are often unintuitive in their computation and parametrization, as diverse task specifications usually lead to completely different control approaches. We can hardly overestimate the physical insight energy-based approaches are likely to provide.

However, this research also gives rise to further questions. Motivated by the results of the thesis, the following topics are of interest for further study.

Augmented design in the Lagrangian framework. In Chapter 3, we developed a theory for the passivity-based control of mechanical systems that considers physical dissipation from the very beginning of the controller design. The approach relies on the augmentation of the closed-loop Hamiltonian (energy function) by a non-physical

term. It would be interesting to investigate the meaning and interpretation of the new structure, for instance, in the Lagrangian framework. In Section 3.4, we introduced the Lagrangian formulation (3.41) of the closed-loop dynamics. The coupling of position and velocity terms in the pseudo-velocities $\mathbf{y}$ gives rise to forces that depend on the configuration, but which are not stemming from a potential field. Such forces are known from circulatory systems [41, 122, 201]. The relationship between the formulation (3.41) and circulatory systems is still an open question. Additionally, the approach breaks the classical mechanical formulation, as it augments the energy function by a non-mechanical cross term. It would be interesting to study whether the system (3.41) admits a mechanical structure based on [171] nonetheless.

Exploiting the huge amount of degrees of freedom. In Chapter 4, we presented a framework of five simple steps to systematically compute stabilizing controllers with the augmented IDA-PBC methodology for mechanical systems. In Chapter 5, we applied the theory to three benchmark systems, and, to keep the procedure manageable, we made a number of simplifications along the way. Nonetheless, the tuning freedom has been shown to still be massive. The large number of free design parameters and functions inevitably demands the embedding of the controller design procedure into an optimization process. Additionally, it would be interesting to consider non-quadratic energy functions, and to allow for non-constant scalar and matrix-valued free functions to fully exploit the potential of the approach.

Non-smooth potential functions in total energy shaping for nonholonomic systems. For nonholonomic mechanical systems, the asymptotic stabilization of a desired configuration $\mathbf{q} \in \mathcal{Q}$ requires discontinuous or time-varying control laws [14, 39]. In the context of energy shaping, this can be achieved by assigning non-smooth potential functions as shown in [66] for fully actuated systems. It would be interesting to study the applicability of the approach to underactuated systems, for which the matching equation for the potential energy needs to be satisfied. We have seen that finding the solution to the matching PDEs constitutes the main obstacle of energy shaping. Allowing for non-smooth functions—or smooth functions in non-smooth coordinates—would, thus, establish new research directions in the field of energy shaping for underactuated nonholonomic systems.

Input saturation. In real applications, we cannot ignore the saturation of the actuators. In this thesis, we assumed that the motors are capable of supplying the necessary input. However, it is of practical interest to explicitly include input saturation in the controller design procedure, for example, employing a Lyapunov-based set point gen-

erator for stabilization and/or waypoint tracking [40, 55]. As energy shaping relies on Lyapunov theory for the stabilization of the plant, it should be possible to embed the Lyapunov-based set point generator in the approach developed in this thesis. The original strategy presented in [40] requires a quadratic function for the explicit incorporation of input saturation. A possible method to include this strategy in our energy shaping approach is employing a quadratic estimate of the closed-loop energy function. By doing so, it is possible to make use of Lyapunov-based set point generator to analytically incorporate input saturation into the energy shaping methodology.

V

Appendix

Appendix A

Technical Proofs

A.1 Proof of Proposition 3.1

As Assumption 3.1 and Assumption 3.2 hold, (3.24a) can be given as

$$2\,\mathbf{G}_{\perp}\mathbf{Z}_1\mathbf{M}_{\mathrm{d}*}^{-1}\mathbf{p} + \mathbf{G}_{\perp}\nabla_{\mathbf{q}}\left(\mathbf{p}^{\mathrm{T}}\mathbf{M}^{-1}\mathbf{p}\right) = 0. \tag{A.1}$$

For an equivalent formulation of the term $\mathbf{G}_{\perp}\mathbf{Z}_1$, we use the following lemma:

Lemma A.1 (see, e., g., [5])**.** *Any skew-symmetric matrix* $\mathbf{Z}_1(\mathbf{q},\mathbf{p})$ *linear in* $\mathbf{p}$ *can be expressed as:*

$$\mathbf{Z}_1 = \sum_{i=1}^{N} \mathbf{p}^{\mathrm{T}}\mathbf{f}_i(\mathbf{q})\,\boldsymbol{\mathcal{J}}_i, \tag{A.2}$$

where the vector-values functions $\mathbf{f}_i(\mathbf{q}) \in \mathbb{R}^n$, $i = 1,\ldots,N$, $N = \frac{n^2-n}{2}$, *are free parameters, and the matrices* $\boldsymbol{\mathcal{J}}_i$ *constitute a basis for the space of skew-symmetric matrices defined as follows. Let us first define the set*[1]

$$\mathcal{Z} = \left\{\boldsymbol{\mathcal{W}}_{ij} \in \mathbb{R}^{n\times n} \mid 1 \le i < j \le n,\, \mathcal{W}_{ij} = 1,\, \mathcal{W}_{ji} = -1\right\}. \tag{A.3}$$

In particular, for $n = 2$ *the set (A.3) corresponds to the matrix*

$$\boldsymbol{\mathcal{W}}_{12} = \begin{bmatrix} 0 & 1 \\ -1 & 0 \end{bmatrix}, \tag{A.4}$$

[1] $\mathcal{W}_{ij}$ refers to the (i,j)-th element of the matrix $\boldsymbol{\mathcal{W}}_{ij}$.

and for $n = 3$ the set (A.3) is composed by

$$\boldsymbol{\mathcal{W}}_{12} = \begin{bmatrix} 0 & 1 & 0 \\ -1 & 0 & 0 \\ 0 & 0 & 0 \end{bmatrix}, \quad \boldsymbol{\mathcal{W}}_{13} = \begin{bmatrix} 0 & 0 & 1 \\ 0 & 0 & 0 \\ -1 & 0 & 0 \end{bmatrix}, \quad \boldsymbol{\mathcal{W}}_{23} = \begin{bmatrix} 0 & 0 & 0 \\ 0 & 0 & 1 \\ 0 & -1 & 0 \end{bmatrix}. \tag{A.5}$$

As the set (A.3) consists of N different matrices, we define

$$\boldsymbol{\mathcal{J}}_1 = \boldsymbol{\mathcal{W}}_{12}, \ldots, \boldsymbol{\mathcal{J}}_{n-1} = \boldsymbol{\mathcal{W}}_{1n}, \boldsymbol{\mathcal{J}}_n = \boldsymbol{\mathcal{W}}_{23}, \ldots, \boldsymbol{\mathcal{J}}_N = \boldsymbol{\mathcal{W}}_{(n-1)n}.$$

With the help of Lemma A.1, $\mathbf{G}_\perp \mathbf{Z}_1$ can be rewritten as

$$\begin{aligned} \mathbf{G}_\perp \mathbf{Z}_1 &= \mathbf{G}_\perp \sum_{i=1}^{N} \mathbf{p}^{\mathrm{T}} \mathbf{f}_i(\mathbf{q})\, \boldsymbol{\mathcal{J}}_i \\ &= \sum_{i=1}^{N} \mathbf{p}^{\mathrm{T}} \mathbf{f}_i(\mathbf{q})\, \mathbf{G}_\perp \boldsymbol{\mathcal{J}}_i \\ &= \mathbf{p}^{\mathrm{T}} \underbrace{\sum_{i=1}^{N} \mathbf{f}_i(\mathbf{q})\, \mathbf{G}_\perp \boldsymbol{\mathcal{J}}_i}_{\boldsymbol{\Gamma}} = \mathbf{p}^{\mathrm{T}} \boldsymbol{\Gamma}. \end{aligned} \tag{A.6}$$

For an equivalent formulation of the term $\mathbf{G}_\perp \nabla_{\mathbf{q}} \left(\mathbf{p}^{\mathrm{T}} \mathbf{M}^{-1} \mathbf{p} \right)$, note that, as $\mathbf{G}_\perp$ is a row vector of dimension n (according to Assumption 3.1), the following relationship holds

$$\mathbf{G}_\perp \nabla_{\mathbf{q}} \left(\mathbf{p}^{\mathrm{T}} \mathbf{M}^{-1} \mathbf{p} \right) = \mathbf{p}^{\mathrm{T}} \left(\sum_{j=1}^{n} G_{\perp j} (\partial_{q_j} \mathbf{M}^{-1}) \right) \mathbf{p}, \tag{A.7}$$

where $G_{\perp j}$ is the j-th coefficient of $\mathbf{G}_\perp$, and $\partial_{q_j} \mathbf{M}^{-1}$ denotes the element-wise derivative of the matrix $\mathbf{M}^{-1}$ with respect to the configuration variable q_j. The relations (A.6) and (A.7) imply that (A.1) equals

$$2\, \mathbf{p}^{\mathrm{T}} \boldsymbol{\Gamma} \mathbf{M}_{\mathrm{d}*}^{-1} \mathbf{p} + \mathbf{p}^{\mathrm{T}} \left(\sum_{j=1}^{n} G_{\perp j} (\partial_{q_j} \mathbf{M}^{-1}) \right) \mathbf{p} = 0, \tag{A.8}$$

which, for all values of $\mathbf{p}$, is equivalent to

$$\boldsymbol{\Gamma} \mathbf{M}_{\mathrm{d}*}^{-1} + \mathbf{M}_{\mathrm{d}*}^{-1} \boldsymbol{\Gamma}^{\mathrm{T}} + \sum_{j=1}^{n} G_{\perp j} (\partial_{q_j} \mathbf{M}^{-1}) = \mathbf{0}.$$

A.2 Proof of Proposition 6.3

To prove necessity and sufficiency of the condition, let us consider the function

$$E_{\mathrm{c}} = \frac{1}{2}\boldsymbol{\nu}^{\mathrm{T}}\mathbf{M}_{\mathrm{c}}\boldsymbol{\nu} + V_{\mathrm{c}}, \tag{A.9}$$

where $\mathbf{M}_{\mathrm{c}} > \mathbf{0}$, and V_{c} is positive semidefinite. Its rate of change along the solutions of the closed-loop system

$$\mathbf{M}_{\mathrm{c}}\dot{\boldsymbol{\nu}} + \mathbf{C}_{\mathrm{c}}\boldsymbol{\nu} + \nabla_{\boldsymbol{\xi}}V_{\mathrm{c}} = (\mathbf{J}_{\mathrm{c}} - \mathbf{R}_{\mathrm{c}})\boldsymbol{\nu} \tag{A.10}$$

is given by

$$\dot{E}_{\mathrm{c}} = -\boldsymbol{\nu}^{\mathrm{T}}\mathbf{R}_{\mathrm{c}}\boldsymbol{\nu} = -\mathbf{y}^{\mathrm{T}}\mathbf{K}_{\mathrm{di}}\mathbf{y}, \qquad \mathbf{K}_{\mathrm{di}} > \mathbf{0}. \tag{A.11}$$

As per Theorem 2.4, the system (A.10) converges towards the set $\mathbf{y} = \mathbf{G}^{\mathrm{T}}\mathbf{M}\mathbf{M}_{\mathrm{c}}^{-1}\boldsymbol{\nu} = \mathbf{0}$, which is characterized by

$$\boldsymbol{\nu} = \beta\mathbf{M}_{\mathrm{c}}^{-1}\mathbf{M}\mathbf{G}_{\perp}^{\mathrm{T}}, \tag{A.12}$$

where $\beta(\boldsymbol{\xi}, \boldsymbol{\nu}, t)$ is an arbitrary scalar function. The dynamics of (A.10) constrained to the set

$$\mathcal{X}_{\mathbf{0}}^{\mathbf{y}} = \{(\boldsymbol{\xi}\ \boldsymbol{\nu}) \in \mathsf{T}\mathcal{Q}_{\mathrm{R}} \mid \mathbf{y} = \mathbf{0}\} \tag{A.13}$$

are then represented by

$$\beta\mathbf{M}_{\mathrm{c}}\dot{\bar{\mathbf{M}}}_{\mathrm{c}}\mathbf{M}\mathbf{G}_{\perp}^{\mathrm{T}} + \beta\dot{\mathbf{M}}\mathbf{G}_{\perp}^{\mathrm{T}} + \dot{\beta}\mathbf{M}\mathbf{G}_{\perp}^{\mathrm{T}} + \beta\mathbf{C}_{\mathrm{c}}\mathbf{M}_{\mathrm{c}}^{-1}\mathbf{M}\mathbf{G}_{\perp}^{\mathrm{T}} + \nabla_{\boldsymbol{\xi}}V_{\mathrm{c}} = \beta\mathbf{J}_{\mathrm{c}}\mathbf{M}_{\mathrm{c}}^{-1}\mathbf{M}\mathbf{G}_{\perp}^{\mathrm{T}}. \tag{A.14}$$

The fact that $\dot{\mathbf{M}}_{\mathrm{c}} = \mathbf{C}_{\mathrm{c}} + \mathbf{C}_{\mathrm{c}}^{\mathrm{T}}$ implies

$$\dot{\bar{\mathbf{M}}}_{\mathrm{c}} = -\mathbf{M}_{\mathrm{c}}^{-1}\left(\mathbf{C}_{\mathrm{c}} + \mathbf{C}_{\mathrm{c}}^{\mathrm{T}}\right)\mathbf{M}_{\mathrm{c}}^{-1}, \tag{A.15}$$

where $\bar{\mathbf{M}}_{\mathrm{c}} = \mathbf{M}_{\mathrm{c}}^{-1}$. And since $\dot{\mathbf{M}} = \mathbf{C} + \mathbf{C}^{\mathrm{T}}$, the constrained dynamics (A.14) become

$$\begin{aligned} &-\beta\left(\mathbf{C}_{\mathrm{c}} + \mathbf{C}_{\mathrm{c}}^{\mathrm{T}}\right)\mathbf{M}_{\mathrm{c}}^{-1}\mathbf{M}\mathbf{G}_{\perp}^{\mathrm{T}} + \beta\left(\mathbf{C} + \mathbf{C}^{\mathrm{T}}\right)\mathbf{G}_{\perp}^{\mathrm{T}} + \dot{\beta}\mathbf{M}\mathbf{G}_{\perp}^{\mathrm{T}} + \beta\mathbf{C}_{\mathrm{c}}\mathbf{M}_{\mathrm{c}}^{-1}\mathbf{M}\mathbf{G}_{\perp}^{\mathrm{T}} + \nabla_{\boldsymbol{\xi}}V_{\mathrm{c}} \\ &\quad = \beta\mathbf{J}_{\mathrm{c}}\mathbf{M}_{\mathrm{c}}^{-1}\mathbf{M}\mathbf{G}_{\perp}^{\mathrm{T}}. \end{aligned} \tag{A.16}$$

From the solution of the matching equation for the kinetic energy (6.27a), and knowing that $\mathbf{J}$ and $\mathbf{J}_\mathrm{c}$ are skew-symmetric matrices, we have the following relation

$$\begin{aligned} &\mathbf{G}_\perp \mathbf{M}\mathbf{M}_\mathrm{c}^{-1}\left(\mathbf{J}_\mathrm{c}-\mathbf{C}_\mathrm{c}\right)=\mathbf{G}_\perp\left(\mathbf{J}-\mathbf{C}\right) \\ \Rightarrow\quad &\left(\mathbf{J}_\mathrm{c}+\mathbf{C}_\mathrm{c}^\mathrm{T}\right)\mathbf{M}_\mathrm{c}^{-1}\mathbf{M}\mathbf{G}_\perp^\mathrm{T}=\left(\mathbf{J}+\mathbf{C}^\mathrm{T}\right)\mathbf{G}_\perp^\mathrm{T}, \end{aligned} \tag{A.17}$$

such that (A.16) can be rewritten as

$$\dot{\beta}\mathbf{M}\mathbf{G}_\perp^\mathrm{T}+\beta\left(\mathbf{C}-\mathbf{J}\right)\mathbf{G}_\perp^\mathrm{T}+\nabla_{\boldsymbol{\xi}}V_\mathrm{c}=\mathbf{0}. \tag{A.18}$$

Necessity. (*The damping is pervasive* $\Rightarrow$ $\beta=0$ *is the only solution to (A.18)*) According to the definition, the damping is called pervasive if every trajectory elicits energy dissipation. In turn, the system cannot move infinitely and will eventually come to rest. Therefore, pervasive damping implies that $\beta=0$, and the dynamics of (A.10) constrained to the set $\mathcal{X}_\mathbf{0}^\mathbf{y}$—which are given by (A.18)—are restricted to $\nabla_{\boldsymbol{\xi}}V_\mathrm{c}=\mathbf{0}$.

Sufficiency. ($\beta=0$ *is the only solution to (A.18)* $\Rightarrow$ *the damping is pervasive*) Suppose that (A.18) only admits the solution $\beta=0$. Then, $\mathbf{y}=0$ implies $\boldsymbol{\nu}=\mathbf{0}$, such that $\dot{E}_\mathrm{c}=0$ is only satisfied in the set

$$\mathcal{X}_\mathbf{0}^{\boldsymbol{\nu}}=\{(\boldsymbol{\xi}\ \boldsymbol{\nu})\in\mathsf{T}\mathcal{Q}_\mathrm{R}\mid\boldsymbol{\nu}=\mathbf{0},\ \nabla_{\boldsymbol{\xi}}V_\mathrm{c}=\mathbf{0}\}.$$

Consequently, the system asymptotically converges towards $\mathcal{X}_\mathbf{0}^{\boldsymbol{\nu}}$, which implies that it will come to rest. If V_c is positive definite, then $\mathcal{X}_\mathbf{0}^{\boldsymbol{\nu}}=\boldsymbol{\xi}^*$ (as $\boldsymbol{\xi}^*=\arg\min V_\mathrm{c}$), and $\beta\equiv0$ is the only possible solution to (A.18)—which represents the dynamics for $\mathbf{y}=\mathbf{0}$—then the output $\mathbf{y}=\mathbf{G}^\mathrm{T}\mathbf{M}\mathbf{M}_\mathrm{c}^{-1}\boldsymbol{\nu}$ is zero-state observable, i. e., $\mathbf{y}=\mathbf{0}$ implies $\boldsymbol{\nu}=\mathbf{0}$ and $\boldsymbol{\xi}=\boldsymbol{\xi}^*$. Ergo, the damping is pervasive and the equilibrium $\boldsymbol{\xi}=\boldsymbol{\xi}^*$ is asymptotically stable.

A.3 Proof of Proposition 8.1

To proof pervasive damping of the WIP, we need to check whether (A.18) accepts solutions for $\beta\neq0$. Let us begin by writing (A.18) for the WIP. Without loss of generality, we assume $\boldsymbol{\xi}^*=\mathbf{0}$, (and $\hat{\boldsymbol{\nu}}=\mathbf{0}$), such that for the WIP, the closed-loop potential energy (8.15) can be given in the general form

$$V_\mathrm{c}=f_1(\alpha)+\frac{1}{2}\mu\left(s+f_2(\alpha)\right)^2+k_\mathrm{p}\left(1-\cos\theta\right),$$

where the functions $f_i(\alpha)$ satisfy $f_1(0) = f_1'(0) = f_2(0) = 0$. Thus, (6.39) (or, equivalently, (A.18)) can be explicitly given as

$$\begin{bmatrix} \psi_1 \\ \psi_2 \\ 0 \end{bmatrix} \dot{\beta} + \begin{bmatrix} -\dot{\alpha} c_2 \sin\alpha \\ 0 \\ (c_2 r + c_5 \cos\alpha)\, \dot{\theta} \sin\alpha \end{bmatrix} \beta + \begin{bmatrix} \mu\,(s + f_2(\alpha)) \\ f_1'(\alpha) + \mu\,(s + f_2(\alpha))\, f_2'(\alpha) \\ k_{\mathrm{p}} \sin\theta \end{bmatrix} = \mathbf{0}, \quad \text{(A.19)}$$

where[2] $\psi_1(\alpha) = c_1 r + c_2 \cos\alpha - c_3$, and $\psi_2(\alpha) = c_4 + r\,(c_2 \cos\alpha - c_3)$. According to (A.12), the velocities in the set $\mathcal{X}_{\mathbf{0}}^{\mathbf{y}}$ take the following form

$$\boldsymbol{\nu} = \beta \mathbf{M}_{\mathrm{c}}^{-1} \mathbf{M} \mathbf{G}_{\perp}^{\mathrm{T}} = \beta \begin{bmatrix} \psi_1\,(k_1 - k_3) - \frac{g}{\gamma} \\ -\frac{g\psi_1}{\gamma\psi_2} \\ 0 \end{bmatrix}, \quad \text{(A.20)}$$

which implies that $\dot{\theta} = 0$, and

$$\beta = \dot{s}\, \frac{1}{\psi_1\,(k_1 - k_3) - \frac{g}{\gamma}} = -\dot{\alpha}\, \frac{\gamma\psi_2}{g\psi_1}.$$

Consequently, its time derivative is given as

$$\dot{\beta} = -\ddot{\alpha}\, \frac{\gamma\psi_2}{g\psi_1} + \dot{\alpha}^2\, \frac{\gamma}{g}\, \frac{r\psi_1 - \psi_2}{\psi_1^2}\, c_2 \sin\alpha.$$

As β is a free function, the following relation holds

$$\dot{s} = -\dot{\alpha}\, \frac{\gamma\psi_2}{g\psi_1} \left(\psi_1\,(k_1 - k_3) - \frac{g}{\gamma} \right). \quad \text{(A.21)}$$

Replacing $\dot{\theta} = 0$, β, and $\dot{\beta}$ into (A.19), and making some simple calculations yields

$$\ddot{\alpha}\psi_2 - \dot{\alpha}^2 r c_2 \sin\alpha = \frac{g\mu}{\gamma}\,(s + f_2) \quad \text{(A.22)}$$

$$\ddot{\alpha}\psi_2 + \dot{\alpha}^2\, \frac{\psi_2 - r\psi_1}{\psi_1}\, c_2 \sin\alpha - \frac{g\psi_1}{\gamma\psi_2}\,(f_1' + \mu\,(s + f_2)\, f_2') = 0 \quad \text{(A.23)}$$

$$k_{\mathrm{p}} \sin\theta = 0 \quad \text{(A.24)}$$

[2] The functions $\psi_1(\alpha)$ and $\psi_2(\alpha)$ are strictly positive in the physically relevant domain $-\pi/2 < \alpha < \pi/2$.

The third equation shows that θ converges towards the set given by $\sin\theta = 0$. Equation (A.23). Let us now derive (A.22) with respect to time. It results in the ODE

$$\dddot{\alpha}\psi_2 - 3\dot{\alpha}\ddot{\alpha}rc_2 \sin\alpha - \dot{\alpha}^3 rc_2 \cos\alpha = \frac{g\mu}{\gamma}\left(\dot{s} + f_2'\dot{\alpha}\right). \tag{A.25}$$

We can eliminate the variable s from the equations by replacing (A.21) into (A.25), and (A.22) into (A.23). By doing so, we get two conditions for pervasive damping

$$\dddot{\alpha}\psi_2 - 3\dot{\alpha}\ddot{\alpha}rc_2 \sin\alpha - \dot{\alpha}^3 rc_2 \cos\alpha - \dot{\alpha}\frac{g\mu}{\gamma}\left(f_2' - \frac{\gamma}{g}\psi_2\left(k_1 - k_3\right) + \frac{\psi_2}{\psi_1}\right) = 0, \tag{A.26}$$

$$\ddot{\alpha}\left(\psi_2 - \psi_1 f_2'\right) + \dot{\alpha}^2\left(\frac{\psi_2}{\psi_1} - r + \frac{\psi_1}{\psi_2} r f_2'\right) c_2 \sin\alpha - \frac{g\psi_1}{\gamma\psi_2} f_1' = 0, \tag{A.27}$$

by means of the pitch angle α. Hence, we are looking for a solution $\alpha(t)$ to both (A.26) and (A.27) simultaneously. As the ODEs (A.26) and (A.27) are not equivalent, the only possible solution to (A.26) and (A.27) is the trivial solution given by

$$\dddot{\alpha} = \ddot{\alpha} = \dot{\alpha} = \alpha = 0.$$

This implies that also $\beta \equiv 0$ is the only solution to (A.19). Thus, the damping injection term (8.19) with $\mathbf{K}_{\mathrm{di}} > \mathbf{0}$ guarantees pervasive damping.

Appendix B

Dynamical Model of the WIP

In Chapter 8, we use the equations of motion (8.3) for the controller design. In the following, we show how to derive the dynamical model for the WIP. After presenting the actuator dynamics, we compute the Lagrangian and the non-conservative forces acting on the WIP to derive the complete mathematical model that we use for the simulations. The derivation of the equations of motion for the WIP excluding the motor dynamics has been carried out in the conference paper [51]. However, since the dynamics of the system slightly differ by including the effect of the actuator and internal friction forces, in this chapter, we present the main steps for the derivation of the equations of motion for the complete model.

Figure B.1 shows a sketch of the WIP. It consists of three different bodies: the pendulum, and the left and right wheel. The set of generalized coordinates describing the WIP consists of

- the coordinates of the midpoint P of the wheel axis in the horizontal plane ($(x, y) \in \mathbb{R}^2$),
- the heading angle around the vertical axis ($\theta \in \mathbb{S}^1$),
- the tilting angle around the wheel axis ($\alpha \in \mathbb{S}^1$), and
- the absolute rotation angle of the right and left wheel around the wheel axis ($\varphi_\mathrm{r} \in \mathbb{S}^1$ and $\varphi_\mathrm{l} \in \mathbb{S}^1$). The relative angle of rotation of the wheels with respect to the body is denoted by ϕ_r and ϕ_l. The relations $\varphi_\mathrm{r} = \phi_\mathrm{r} + \alpha$ and $\varphi_\mathrm{l} = \phi_\mathrm{l} + \alpha$ hold.

Thus, the six-dimensional configuration space is $\mathcal{Q} = \mathbb{R}^2 \times \mathcal{S}^1 \times \mathcal{S}^1 \times \mathcal{S}^1 \times \mathcal{S}^1$. As the system is subject to nonholonomic constraints

$$\mathbf{A}^\mathrm{T}\dot{\mathbf{q}} = \begin{bmatrix} -\sin\theta & \cos\theta & 0 & 0 & 0 & 0 \\ \cos\theta & \sin\theta & d & 0 & -r & 0 \\ \cos\theta & \sin\theta & -d & 0 & 0 & -r \end{bmatrix} \dot{\mathbf{q}} = \mathbf{0}, \tag{B.1}$$

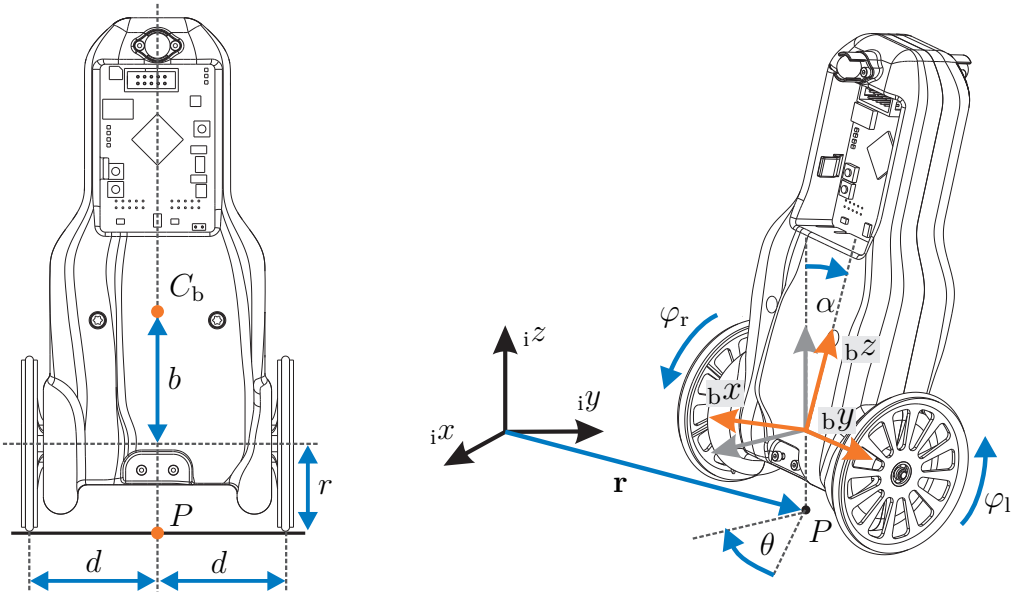

Figure B.1: Configuration variables and measurements of the WIP. The configuration space is parametrized by the coordinates of the midpoint P of the wheel axis in the horizontal plane, given by (x, y), the yaw angle θ, the pitch angle α, and the right (φ_r) and left (φ_l) wheel's total angle of rotation ($\varphi_r = \phi_r + \alpha$, and $\varphi_l = \phi_l + \alpha$). The wheel radius is denoted by r, the distance between the wheel axis and the body's center of mass C_b is denoted by b, and d is the value of half the wheel distance.

the velocity space is of dimension three. Let us choose the coordinates $\boldsymbol{\nu} = (v, \dot{\alpha}, \dot{\theta})$ to parametrize the velocity space, where v is the forward velocity of the WIP. For this particular choice, the matrix $\mathbf{S}$ required for the reconstruction equation (8.2) becomes

$$\mathbf{S} = \begin{bmatrix} \cos\theta & 0 & 0 \\ \sin\theta & 0 & 0 \\ 0 & 0 & 1 \\ 0 & 1 & 0 \\ \frac{1}{r} & 0 & \frac{d}{r} \\ \frac{1}{r} & 0 & -\frac{d}{r} \end{bmatrix}. \tag{B.2}$$

B.1 Motor dynamics

Each wheel of the WIP is independently actuated by a DC motor placed in the main body. The equivalent circuit model for the DC motor, shown in Figure B.2, can be

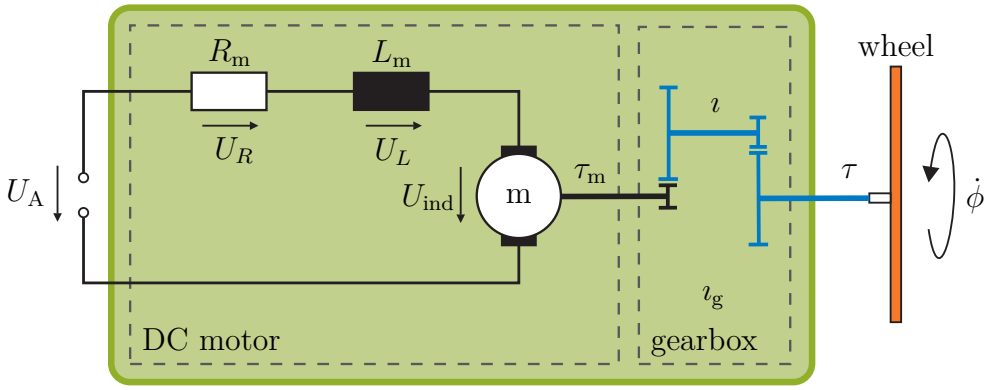

Figure B.2: Circuit diagram for the DC motor.

represented as

$$U_\mathrm{A} = R_\mathrm{m} i + L_\mathrm{m} \frac{\mathrm{d}}{\mathrm{d}t} i + U_\mathrm{ind}, \tag{B.3}$$

where the induction voltage is proportional to the rotor velocity, expressed by $U_\mathrm{ind} = k_\mathrm{v} \omega_\mathrm{m}$. As for the resulting motor torque $\tau_\mathrm{m} = k_\mathrm{m} i$, the relation is given by the differential equation

$$L_\mathrm{m} \dot{\tau}_\mathrm{m} = -R_\mathrm{m} \tau_\mathrm{m} - k_\mathrm{v} k_\mathrm{m} \omega_\mathrm{m} + k_\mathrm{m} U_\mathrm{A}. \tag{B.4}$$

By considering the gearbox' transmission ratio $\imath_\mathrm{g}$, we get the relationships

$$\tau = \imath_\mathrm{g} \tau_\mathrm{m}, \qquad \text{and} \qquad \dot{\phi} = \frac{1}{\imath_\mathrm{g}} \omega_\mathrm{m} \tag{B.5}$$

for the torque τ acting on the wheel, and the wheel's angular velocity $\dot{\phi}$. Since the current dynamics are significantly faster than the wheel dynamics, the static model for the DC motor (neglecting the current dynamics)

$$0 = -\frac{R_\mathrm{m}}{\imath_\mathrm{g}} \tau - k_\mathrm{v} k_\mathrm{m} \imath_\mathrm{g} \dot{\phi} + k_\mathrm{m} U_\mathrm{A}, \tag{B.6}$$

gives an accurate relation between the armature voltage U_A and the motor torque τ_m.

B.2 Lagrangian

To derive the equations of motion as presented in Section 6.2.1, we require the Lagrangian L, which is defined as kinetic energy minus potential energy. The potential

energy V is only defined by the gravity field and is given as

$$V = m_\mathrm{b} g b \cos\alpha, \tag{B.7}$$

where m_b is the mass of the main body (including the shell, the motors and gearboxes, the battery, and all other components), g denotes the gravitational acceleration, and b represents the distance from the wheel rotation axis to the body's center of mass C_b. To compute the kinetic energy T, we independently calculate the translational and rotational terms for each of the bodies. For a detailed calculation of each of the expressions, the reader is referred to the conference paper [51]. The kinetic energy of the main body is given as

$$T_\mathrm{b} = \frac{1}{2} m_\mathrm{b} \mathbf{v}_\mathrm{b}^\mathrm{T} \mathbf{v}_\mathrm{b} + \frac{1}{2} \boldsymbol{\omega}_\mathrm{b}^\mathrm{T} \mathbf{I}_\mathrm{b} \boldsymbol{\omega}_\mathrm{b}, \tag{B.8}$$

where $\mathbf{I}_\mathrm{b} = \mathrm{diag}(I_{\mathrm{b}_{xx}}, I_{\mathrm{b}_{yy}}, I_{\mathrm{b}_{zz}})$ is the moment of inertia of the main body (again, as a rigid body including all its components) with respect to its center of mass C_b, and given in body-fixed representation. The translational velocity of the point C_b, and the total body's angular velocity are

$$\mathbf{v}_\mathrm{b} = \begin{bmatrix} \dot{x} + \dot{\alpha} b \cos\alpha \cos\theta - \dot{\theta} b \sin\alpha \sin\theta \\ \dot{y} + \dot{\alpha} b \cos\alpha \sin\theta + \dot{\theta} b \sin\alpha \cos\theta \\ -\dot{\alpha} b \sin\alpha \end{bmatrix}, \quad \text{and} \quad \boldsymbol{\omega}_\mathrm{b} = \begin{bmatrix} -\dot{\theta} \sin\alpha \\ \dot{\alpha} \\ \dot{\theta} \cos\alpha \end{bmatrix}, \tag{B.9}$$

respectively. Note that $\mathbf{v}_\mathrm{b}$ is given in inertial coordinates, and $\boldsymbol{\omega}_\mathrm{b}$ is given with respect to a body-fixed coordinate frame. Analogously, the kinetic energy of each single wheel is

$$T_\mathrm{w} = \frac{1}{2} m_\mathrm{w} \mathbf{v}_\mathrm{w}^\mathrm{T} \mathbf{v}_\mathrm{w} + \frac{1}{2} \boldsymbol{\omega}_\mathrm{w}^\mathrm{T} \mathbf{I}_\mathrm{w} \boldsymbol{\omega}_\mathrm{w}, \tag{B.10}$$

where m_w denotes the mass of the wheel, and $\mathbf{I}_\mathrm{w} = \mathrm{diag}(I_{\mathrm{w}_{xx}}, I_{\mathrm{w}_{yy}}, I_{\mathrm{w}_{zz}})$ denotes the wheel's moment of inertia with respect to the center of the wheel, given in body-fixed coordinates. The translational velocity of the left and right wheel's center point is given as

$$\mathbf{v}_\mathrm{w,l} = \begin{bmatrix} \dot{x} - \dot{\theta} d \cos\theta \\ \dot{y} - \dot{\theta} d \sin\theta \\ 0 \end{bmatrix}, \quad \text{and} \quad \mathbf{v}_\mathrm{w,r} = \begin{bmatrix} \dot{x} + \dot{\theta} d \cos\theta \\ \dot{y} + \dot{\theta} d \sin\theta \\ 0 \end{bmatrix}, \tag{B.11}$$

respectively. The angular velocities of the wheels are

$$\boldsymbol{\omega}_{\mathrm{w,l}} = \begin{bmatrix} 0 \\ \dot{\varphi}_{\mathrm{l}} \\ \dot{\theta} \end{bmatrix}, \quad \text{and} \quad \boldsymbol{\omega}_{\mathrm{w,r}} = \begin{bmatrix} 0 \\ \dot{\varphi}_{\mathrm{r}} \\ \dot{\theta} \end{bmatrix}. \tag{B.12}$$

As both the motor and the gearbox rotate at a different angular velocity than the wheels, the rotational energy stemming from their relative rotation with respect to the body needs to be additionally calculated. Take, for instance, the right motor and gearbox. Their angular velocity with respect to the body-fixed frame is given as

$$\boldsymbol{\omega}_{\mathrm{m,r}} = \begin{bmatrix} -\dot{\theta}\sin\alpha \\ \dot{\alpha} + \omega_{\mathrm{m,r}} \\ \dot{\theta}\cos\alpha \end{bmatrix}, \quad \text{and} \quad \boldsymbol{\omega}_{\mathrm{g,r}} = \begin{bmatrix} -\dot{\theta}\sin\alpha \\ \dot{\alpha} + \omega_{\mathrm{g,r}} \\ \dot{\theta}\cos\alpha \end{bmatrix}. \tag{B.13}$$

The moment of inertia of the motor is $\mathbf{I}_{\mathrm{m}} = \mathrm{diag}(I_{\mathrm{m}_{xx}}, I_{\mathrm{m}_{yy}}, I_{\mathrm{m}_{zz}})$, and the one of the gearbox is $\mathbf{I}_{\mathrm{g}} = \mathrm{diag}(I_{\mathrm{g}_{xx}}, I_{\mathrm{g}_{yy}}, I_{\mathrm{g}_{zz}})$. As most of the energy terms arising from the motor and the gearbox have been considered in (B.7) and (B.8), we are only concerned with the kinetic energy term resulting from the relative rotation $\omega_{\mathrm{m,r}}$ (or $\omega_{\mathrm{g,r}}$) with respect to the body. The extra terms are given as

$$\begin{aligned} T_{\mathrm{m,r}} &= \frac{1}{2} I_{\mathrm{m}} \imath_{\mathrm{g}}^2 \dot{\phi}_{\mathrm{r}}^2 + I_{\mathrm{m}} \imath_{\mathrm{g}} \dot{\alpha} \dot{\phi}_{\mathrm{r}}, \qquad \text{and} \\ T_{\mathrm{g,r}} &= \frac{1}{2} I_{\mathrm{g}} \imath^2 \dot{\phi}_{\mathrm{r}}^2 + I_{\mathrm{m}} \imath_{\mathrm{g}} \dot{\alpha} \dot{\phi}_{\mathrm{r}}, \end{aligned}$$

where $I_{\mathrm{m}} = I_{\mathrm{m}_{yy}}$ and $I_{\mathrm{g}} = I_{\mathrm{g}_{yy}}$ denote the moment of inertia of the rotor and the gears about the rotor axis, respectively, $\imath$ is the transmission ratio of a single stage, and $\imath_{\mathrm{g}}$ is the total transmission ratio of the gearbox. The Lagrangian of the WIP is then given as

$$L = T_{\mathrm{b}} + T_{\mathrm{w,r}} + T_{\mathrm{w,l}} + T_{\mathrm{m,r}} + T_{\mathrm{m,l}} + T_{\mathrm{g,r}} + T_{\mathrm{g,l}} - V. \tag{B.14}$$

The derivation of the equations of motion for the WIP according to Section 6.2.1 yields

$$\mathbf{M}\dot{\boldsymbol{\nu}} + \mathbf{C}\boldsymbol{\nu} + \mathbf{S}^{\mathrm{T}} \nabla_{\mathbf{q}} V = \mathbf{J}\boldsymbol{\nu} + \mathbf{F}_{\mathrm{nc}}, \tag{B.15}$$

where $\mathbf{F}_{\mathrm{nc}} = \mathbf{G}\mathbf{u} + \boldsymbol{\tau}_{\mathrm{fr}}$ represents the non-conservative forces acting on the WIP (cf. Section B.3), which are composed of the input $\mathbf{u}$, and the generalized friction forces/torques $\boldsymbol{\tau}_{\mathrm{fr}}$. The matrix S is given by (B.2), and the remaining dynamical parameters are given

as

$$\mathbf{M} = \begin{bmatrix} c_1 & c_2\cos\alpha - c_3 & 0 \\ c_2\cos\alpha - c_3 & c_4 & 0 \\ 0 & 0 & \Theta(\alpha) \end{bmatrix}, \qquad \mathbf{J} = \begin{bmatrix} 0 & 0 & c_2\dot{\theta}\sin\alpha \\ 0 & 0 & 0 \\ -c_2\dot{\theta}\sin\alpha & 0 & 0 \end{bmatrix},$$

$$\mathbf{C} = \begin{bmatrix} 0 & -c_2\dot{\alpha}\sin\alpha & 0 \\ 0 & 0 & -c_5\dot{\theta}\sin\alpha\cos\alpha \\ 0 & c_5\dot{\theta}\sin\alpha\cos\alpha & c_5\dot{\alpha}\sin\alpha\cos\alpha \end{bmatrix}, \qquad \mathbf{G} = \begin{bmatrix} \frac{1}{r} & 0 \\ -1 & 0 \\ 0 & 1 \end{bmatrix}, \tag{B.16}$$

where $\Theta = c_5\sin^2\alpha + c_6$, and for constant parameters

$$c_1 = m_\mathrm{b} + 2m_\mathrm{w} + 2\,\frac{I_{\mathrm{w}_{yy}} + I_\mathrm{m}\imath_\mathrm{g}^2 + I_\mathrm{g}\imath^2}{r^2}, \quad c_2 = m_\mathrm{b}b,$$
$$c_3 = 2\,\frac{I_\mathrm{m}\imath_\mathrm{g}^2 + I_\mathrm{g}\imath^2}{r} - 2\,\frac{I_\mathrm{m}\imath_\mathrm{g} + I_\mathrm{g}\imath}{r}, \quad c_4 = m_\mathrm{b}b^2 + I_{\mathrm{b}_{yy}} + 2\left(I_\mathrm{m}\imath_\mathrm{g}^2 + I_\mathrm{g}\imath^2\right) - 4\left(I_\mathrm{m}\imath_\mathrm{g} + I_\mathrm{g}\imath\right),$$
$$c_5 = I_{\mathrm{b}_{xx}} + m_\mathrm{b}b^2 - I_{\mathrm{b}_{zz}}, \quad c_6 = I_{\mathrm{b}_{zz}} + 2\,\frac{I_{\mathrm{w}_{yy}}d^2}{r^2} + 2m_\mathrm{w}d^2 + 2I_{\mathrm{w}_{zz}} + 2\,\frac{\left(I_\mathrm{m}\imath_\mathrm{g}^2 + I_\mathrm{g}\imath^2\right)d^2}{r^2}.$$

B.3 Non-conservative forces

The generalized non-conservative forces $\mathbf{F}_\mathrm{nc}$ that act on the mechanical system are composed of the input torques $\boldsymbol{\tau} = (\tau_\mathrm{l},\, \tau_\mathrm{r})$ steering the left and right wheel, and friction torques $\boldsymbol{\tau}_\mathrm{fr}$, mainly in the gearbox, that emerge from the relative rotation of the wheel with respect to the body.

Let us begin with the input and assume that we can directly control the torques $\boldsymbol{\tau}$. Projecting $\boldsymbol{\tau}$ on the admissible space results in the generalized input forces

$$\mathbf{G}_{\boldsymbol{\tau}}\boldsymbol{\tau} = \begin{bmatrix} \frac{1}{r} & \frac{1}{r} \\ -1 & -1 \\ -\frac{d}{r} & \frac{d}{r} \end{bmatrix} \begin{bmatrix} \tau_\mathrm{l} \\ \\ \tau_\mathrm{r} \end{bmatrix}. \tag{B.17}$$

These inputs can, however, be transformed into more natural quantities for the control of the WIP. Employing the input transformation

$$u_1 = \tau_\mathrm{r} + \tau_\mathrm{l}, \quad u_2 = \frac{d}{r}(\tau_\mathrm{r} - \tau_\mathrm{l}), \tag{B.18}$$

or, equivalently

$$\boldsymbol{\tau} = \mathbf{T}_\mathbf{u}\mathbf{u} = \begin{bmatrix} \frac{1}{2} & \frac{r}{2d} \\ \frac{1}{2} & -\frac{r}{2d} \end{bmatrix} \begin{bmatrix} u_1 \\ u_2 \end{bmatrix}, \tag{B.19}$$

the inputs u_1 and u_2 represent the resulting torque for the forward and the turning motion, respectively, and the system's input becomes

$$\mathbf{G}_\tau\boldsymbol{\tau} = \mathbf{G}_\tau\mathbf{T}_\mathbf{u}\mathbf{u} = \begin{bmatrix} \frac{1}{r} & 0 \\ -1 & 0 \\ 0 & 1 \end{bmatrix} \begin{bmatrix} u_1 \\ u_2 \end{bmatrix} = \mathbf{G}\mathbf{u}. \tag{B.20}$$

Now, as we cannot directly control the torques $\boldsymbol{\tau}$ (or $\mathbf{u}$), the static model for the DC motor (B.6) provides the required relation

$$\mathbf{u}_\mathrm{A} = \frac{R_\mathrm{m}}{k_\mathrm{m}\imath_\mathrm{g}}\mathbf{T}_\mathbf{u}\mathbf{u} + k_\mathrm{v}\imath_\mathrm{g}\mathbf{T}_{\boldsymbol{\nu}}\boldsymbol{\nu}, \tag{B.21}$$

between the armature voltage of the right and left motor ($\mathbf{u}_\mathrm{A} = (U_\mathrm{A,l}, U_\mathrm{A,r})$), and the input $\mathbf{u}$. Note that for the angular velocity of the wheels, we have used the relation

$$\begin{bmatrix} \dot{\phi}_\mathrm{r} \\ \dot{\phi}_\mathrm{l} \end{bmatrix} = \begin{bmatrix} \frac{1}{r} & -1 & \frac{d}{r} \\ \frac{1}{r} & -1 & -\frac{d}{r} \end{bmatrix} \begin{bmatrix} v \\ \dot{\alpha} \\ \dot{\theta} \end{bmatrix} = \mathbf{T}_{\boldsymbol{\nu}}\boldsymbol{\nu}. \tag{B.22}$$

For the friction torques $\boldsymbol{\tau}_\mathrm{fr}$, we use a smooth friction model that captures the effect of both the Coulomb and the viscous damping. The friction torques acting on the body—and which arise from the relative velocity $\dot{\phi}$ between wheel and body—are given as

$$\tau_\mathrm{b} = d_\mathrm{v}\dot{\phi} + d_\mathrm{c}\tanh(d_0\dot{\phi}), \tag{B.23}$$

with viscous damping coefficient d_v, and Coulomb friction d_c. The constant d_0 characterizes the steepness of τ_b around the equilibrium point (cf. Figure B.3). The friction forces acting on the right and left part of the body are given as

$$\tau_\mathrm{b,l} = d_\mathrm{v}\dot{\phi}_\mathrm{l} + d_\mathrm{c}\tanh(d_0\dot{\phi}_\mathrm{l}), \tag{B.24}$$

$$\tau_\mathrm{b,r} = d_\mathrm{v}\dot{\phi}_\mathrm{r} + d_\mathrm{c}\tanh(d_0\dot{\phi}_\mathrm{r}), \tag{B.25}$$

where $\dot{\phi}_\mathrm{r}$ and $\dot{\phi}_\mathrm{l}$ are computed according to (B.22). Note that, since the friction torques

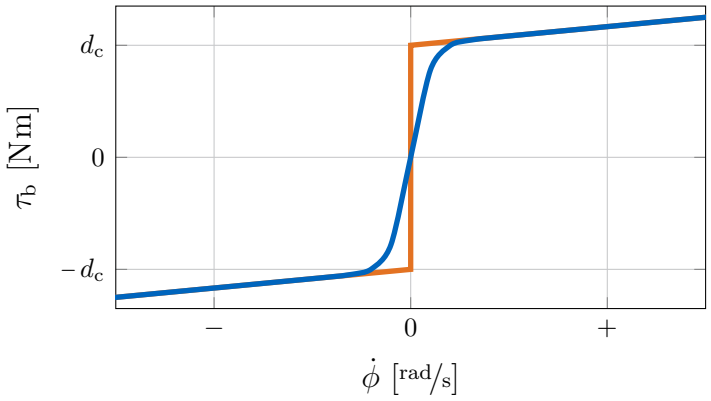

Figure B.3: Smooth and ideal friction models.

are *internal* torques, the reaction torques acting on the wheels $\tau_{w,l} = -\tau_{b,l}$ and $\tau_{w,r} = -\tau_{b,r}$ need to be taken into account as well. Projecting these friction torques on the admissible coordinates $\boldsymbol{\nu}$ yields

$$\boldsymbol{\tau}_b = \begin{bmatrix} 0 \\ 2d_v\left(\frac{v}{r} - \dot{\alpha}\right) + d_c\left(\tanh(d_0\dot{\phi}_l) + \tanh(d_0\dot{\phi}_r)\right) \\ 0 \end{bmatrix}, \tag{B.26}$$

$$\boldsymbol{\tau}_{w,l} = \begin{bmatrix} -\frac{1}{r}\left(d_v\left(\frac{v}{r} - \dot{\alpha} - \frac{d}{r}\dot{\theta}\right) + d_c\tanh(d_0\dot{\phi}_l)\right) \\ 0 \\ \frac{d}{r}\left(d_v\left(\frac{v}{r} - \dot{\alpha} - \frac{d}{r}\dot{\theta}\right) + d_c\tanh(d_0\dot{\phi}_l)\right) \end{bmatrix}, \tag{B.27}$$

$$\boldsymbol{\tau}_{w,r} = \begin{bmatrix} -\frac{1}{r}\left(d_v\left(\frac{v}{r} - \dot{\alpha} + \frac{d}{r}\dot{\theta}\right) + d_c\tanh(d_0\dot{\phi}_r)\right) \\ 0 \\ -\frac{d}{r}\left(d_v\left(\frac{v}{r} - \dot{\alpha} + \frac{d}{r}\dot{\theta}\right) + d_c\tanh(d_0\dot{\phi}_r)\right) \end{bmatrix}. \tag{B.28}$$

Hence, the friction torque takes the form

$$\boldsymbol{\tau}_{fr} = \boldsymbol{\tau}_b + \boldsymbol{\tau}_{w,l} + \boldsymbol{\tau}_{w,r}. \tag{B.29}$$

The non-conservative forces are, thus, given as

$$\mathbf{F}_{nc} = \mathbf{G}\mathbf{u} + \boldsymbol{\tau}_{fr}. \tag{B.30}$$

Since $\mathbf{G}_\perp\boldsymbol{\tau}_{fr} = 0$ holds true—the friction torques $\boldsymbol{\tau}_{fr}$ act on the actuated coordinates—

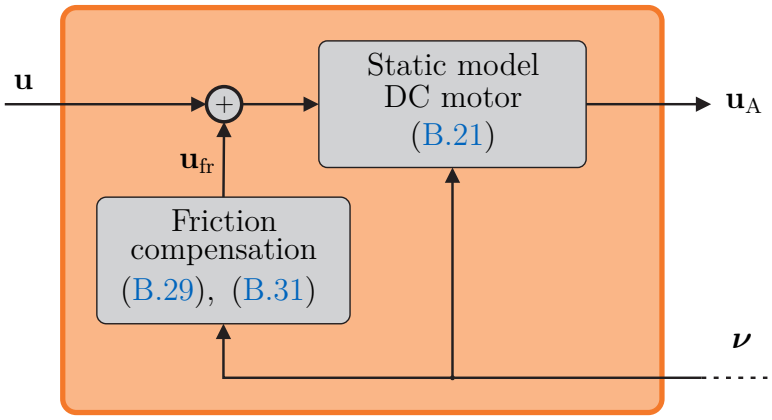

Figure B.4: Input transformation and friction compensation.

the effect of the friction can be fully compensated by the input

$$\mathbf{u}_{\mathrm{fr}} = -(\mathbf{G}^{\mathrm{T}}\mathbf{G})^{-1}\mathbf{G}^{\mathrm{T}}\boldsymbol{\tau}_{\mathrm{fr}}. \tag{B.31}$$

Figure B.4 illustrates the relation between the input $\mathbf{u}$, which is used for the controller design in Chapter 8, and the real system's input $\mathbf{u}_{\mathrm{A}}$.

B.4 Reduced coordinates

Finally, as the conditions of Proposition 6.2 are satisfied, we define reduced coordinates $\boldsymbol{\xi} = (s, \alpha, \theta) \in \mathcal{Q}_{\mathrm{R}} \subset \mathcal{Q}$, such that $\dot{\boldsymbol{\xi}} = \boldsymbol{\nu}$, and restrict the analysis to $\mathcal{Q}_{\mathrm{R}}$ by replacing $\mathbf{S}^{\mathrm{T}}\nabla_{\mathbf{q}}V$ in (B.15) by

$$\nabla_{\boldsymbol{\xi}}V = \begin{bmatrix} 0 \\ -c_2 g \sin\alpha \\ 0 \end{bmatrix}. \tag{B.32}$$

The control system for the wheeled inverted pendulum is shown in Figure B.5. The blue box with input $\mathbf{u}$ and output $\mathbf{q}$, $\boldsymbol{\xi}$, and $\boldsymbol{\nu}$ represents the WIP model (8.3) with the corresponding reconstruction equation (8.2) used for controller design in Chapter 8. The system's parameters are taken from [10, 98], and are listed in Table B.1.

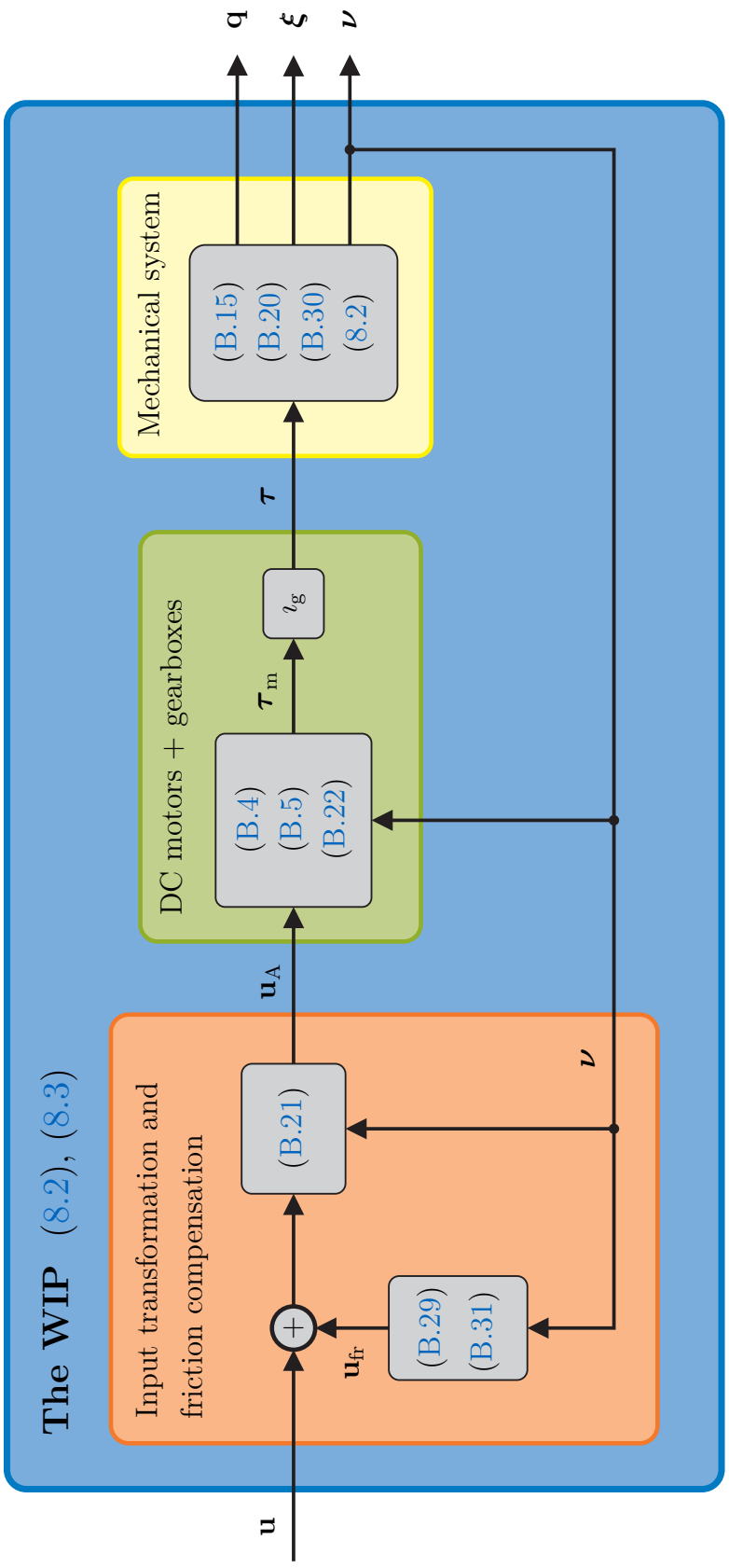

Figure B.5: Scheme of the full model for the WIP.

Table B.1: System parameters for the wheeled inverted pendulum.

Model parameter	Symbol	Value	Unit
Body mass	m_b	0.277	kg
Distance from the wheel axis to the body's center of gravity	b	$48.67 \cdot 10^{-3}$	m
Gravitational acceleration	g	9.81	m/s^2
Wheel mass	m_w	0.028	kg
Half of the wheel distance	d	$49 \cdot 10^{-3}$	m
Wheel radius	r	$33.1 \cdot 10^{-3}$	m
Body's moment of inertia	$\mathbf{I}_\mathrm{b}$		
around x-axis	$I_{\mathrm{b}_{xx}}$	$543.108 \cdot 10^{-6}$	$\mathrm{kg\,m}^2$
around y-axis	$I_{\mathrm{b}_{yy}}$	$481.457 \cdot 10^{-6}$	$\mathrm{kg\,m}^2$
around z-axis	$I_{\mathrm{b}_{zz}}$	$153.951 \cdot 10^{-6}$	$\mathrm{kg\,m}^2$
Wheel's moment of inertia	$\mathbf{I}_\mathrm{w}$		
around y-axis (rotation axis)	$I_{\mathrm{w}_{yy}}$	$7.411 \cdot 10^{-6}$	$\mathrm{kg\,m}^2$
around z-axis	$I_{\mathrm{w}_{zz}}$	$4.957 \cdot 10^{-6}$	$\mathrm{kg\,m}^2$
Viscous damping coefficient	d_v	$1.532 \cdot 10^{-3}$	$\mathrm{N\,m\,s}/\mathrm{rad}$
Coulomb friction coefficient	d_c	$32.6 \cdot 10^{-3}$	$\mathrm{N\,m}$
Steepness friction coefficient	d_0	8	–
Single stage transmission rate	$\imath$	7.091	–
Gearbox' transmission rate	$\imath_\mathrm{g}$	50.281	–
Gearbox' moment of inertia around the rotation axis	I_g	$1.807 \cdot 10^{-6}$	$\mathrm{kg\,m}^2$
Motor's moment of inertia around the rotation axis	I_m	$0.269 \cdot 10^{-6}$	$\mathrm{kg\,m}^2$
Motor inductance	L_m	$400 \cdot 10^{-6}$	H
Motor electric resistance	R_m	1.5	Ohm
Motor torque constant	k_m	$3.76 \cdot 10^{-3}$	$\mathrm{M\,m}/\mathrm{A}$
Motor voltage constant	k_v	$3.76 \cdot 10^{-3}$	$\mathrm{V\,s}/\mathrm{rad}$

List of Figures

List of Tables

References

[1] J. A. Acosta and M. López-Martínez. Constructive feedback linearization of underactuated mechanical systems with 2-DOF. In: *Proceedings of the 44th IEEE Conference on Decision and Control, held jointly with the European Control Conference*. 2005, 4909–4914 (cf. p. 9).

[2] J. A. Acosta, R. Ortega, and A. Astolfi. Interconnection and damping assignment passivity-based control of mechanical systems with underactuation degree one. In: *Proceedings of the American Control Conference*. Vol. 4. 2004, 3029–3034 (cf. pp. 7, 79).

[3] J. Á. Acosta, R. Ortega, A. Astolfi, and I. Sarras. A constructive solution for stabilization via immersion and invariance: the cart and pendulum system. *Automatica,* 44.9 (2008), 2352–2357 (cf. p. 79).

[4] J. A. Acosta and A. Astolfi. On the PDEs arising in IDA-PBC. In: *Proceedings of the 48th IEEE Conference on Decision and Control, held jointly with the 28th Chinese Control Conference*. 2009, 2132–2137 (cf. p. 8).

[5] J. A. Acosta, R. Ortega, A. Astolfi, and A. D. Mahindrakar. Interconnection and damping assignment passivity-based control of mechanical systems with underactuation degree one. *IEEE Transactions on Automatic Control,* 50.12 (2005), 1936–1955 (cf. pp. 7, 58, 82, 83, 163).

[6] A. Albu-Schäffer, C. Ott, and G. Hirzinger. Constructive energy shaping based impedance control for a class of underactuated Euler-Lagrange systems. In: *Proceedings of the IEEE International Conference on Robotics and Automation*. 2005, 1387–1393 (cf. p. 6).

[7] A. Albu-Schäffer, C. Ott, and F. Petit. Energy shaping control for a class of underactuated Euler-Lagrange systems. In: *Proceedings of the 10th International IFAC Symposium on Robot Control*. 2012, 567–575 (cf. pp. 3, 6).

[8] C. W. Anderson. Learning to control an inverted pendulum using neural networks. *IEEE Control Systems Magazine,* 9.3 (1989), 31–37 (cf. p. 80).

[9] D. Angeli, E. D. Sontag, and Y. Wang. A characterization of integral input-to-state stability. *IEEE Transactions on Automatic Control,* 45.6 (2000), 1082–1097 (cf. p. 39).

[10] F. Anhalt. *Zeitdiskreter Regler- und Führungsfilterentwurf für ein zweirädriges inverses Pendel*. Master's thesis. Technische Universität München. 2016 (cf. pp. 139, 177).

[11] S. Arimoto and M. Takegaki. A new feedback method for dynamic control of manipulators. *Journal of Dynamical Systems, Measurement, and Control,* 102 (1981), 119–125 (cf. pp. 6, 40, 41).

[12] V. I. Arnold. *Mathematical Methods of Classical Mechanics*. Vol. 60. Springer, 1989 (cf. pp. 28, 29).

[13] A. Astolfi. On the stabilization of nonholonomic systems. In: *Proceedings of the 33rd IEEE Conference on Decision and Control*. Vol. 4. 1994, 3481–3486 vol.4 (cf. p. 90).

[14] A. Astolfi. Discontinuous control of nonholonomic systems. *Systems & Control Letters,* 27.1 (1996), 37–45 (cf. pp. 8, 90, 159).

[15] D. Auckly and L. Kapitanski. On the λ-equations for matching control laws. *SIAM Journal on Control and Optimization,* 41.5 (2002), 1372–1388 (cf. p. 8).

[16] D. Auckly, L. Kapitanski, and W. White. Control of nonlinear underactuated systems. *Communications on Pure and Applied Mathematics,* 53 (2000), 0354–0369 (cf. p. 8).

[17] M. Baloh and M. Parent. Modeling and model verification of an intelligent self-balancing two-wheeled vehicle for an autonomous urban transportation system. In: *Proceedings of the Conference on Computational Intelligence, Robotics, and Autonomous Systems*. 2003, 1–7 (cf. p. 131).

[18] I. Barkana. Defending the beauty of the invariance principle. *International Journal of Control,* 87.1 (2014), 186–206 (cf. p. 38).

[19] R. Bayadi, R. N. Banavar, and D. E. Chang. Characterizing the reachable set for a spacecraft with two rotors. *Systems & Control Letters,* 62.6 (2013), 453–460 (cf. p. 6).

[20] C. Belta and V. Kumar. Trajectory design for formations of robots by kinetic energy shaping. In: *Proceedings of the IEEE International Conference on Robotics and Automation*. Vol. 3. 2002, 2593–2598 (cf. p. 7).

[21] G. Blankenstein. Matching and stabilization of constrained systems. In: *Proceedings of the 15th International Symposium on Mathematical Theory of Networks and Systems*. 2002 (cf. pp. 8, 91, 94).

[22] G. Blankenstein. Matching in the method of controlled Langrangians and IDA-passivity based control. *Nonlinear and Adaptive Control: Tools and Algorithms for the User,* CHAP (2006), 79–114 (cf. pp. 7, 40, 62).

[23] G. Blankenstein, R. Ortega, and A. J. van Der Schaft. The matching conditions of controlled Lagrangians and IDA-passivity based control. *International Journal of Control,* 75.9 (2002), 645–665 (cf. p. 98).

[24] A. M. Bloch. *Nonholonomic Mechanics and Control*. Vol. 24. Springer, 2003 (cf. pp. 23, 28–31, 90, 92, 93).

[25] A. M. Bloch, D. E. Chang, N. E. Leonard, and J. E. Marsden. Controlled Lagrangians and the stabilization of mechanical systems ii: potential shaping. *IEEE Transactions on Automatic Control,* 46.10 (2001), 1556–1571 (cf. p. 7).

[26] A. M. Bloch, P. S. Krishnaprasad, J. E. Marsden, and G. S. De Alvarez. Stabilization of rigid body dynamics by internal and external torques. *Automatica,* 28.4 (1992), 745–756 (cf. p. 7).

[27] A. M. Bloch, P. Krishnaprasad, J. E. Marsden, and R. M. Murray. Nonholonomic mechanical systems with symmetry. *Archive for Rational Mechanics and Analysis,* 136.1 (1996), 21–99 (cf. pp. 31, 92).

[28] A. M. Bloch, N. E. Leonard, and J. E. Marsden. Stabilization of mechanical systems using controlled Lagrangians. In: *Proceedings of the 36th IEEE Conference on Decision and Control*. Vol. 3. 1997, 2356–2361 (cf. p. 7).

[29] A. M. Bloch, N. E. Leonard, and J. E. Marsden. Matching and stabilization by the method of controlled Lagrangians. In: *Proceedings of the 37th IEEE Conference on Decision and Control*. Vol. 2. 1998, 1446–1451 (cf. p. 7).

[30] A. M. Bloch, N. E. Leonard, and J. E. Marsden. Potential shaping and the method of controlled Lagrangians. In: *Proceedings of the 38th IEEE Conference on Decision and Control*. Vol. 2. 1999, 1652–1657 (cf. p. 7).

[31] A. M. Bloch, N. E. Leonard, and J. E. Marsden. Stabilization of the pendulum on a rotor arm by the method of controlled Lagrangians. In: *Proceedings of the IEEE International Conference on Robotics and Automation*. Vol. 1. 1999, 500–505 (cf. p. 7).

[32] A. M. Bloch, N. E. Leonard, and J. E. Marsden. Controlled Lagrangians and the stabilization of mechanical systems i: the first matching theorem. *IEEE Transactions on Automatic Control,* 45.12 (2000), 2253–2270 (cf. pp. 7, 79).

[33] A. M. Bloch, J. E. Marsden, and D. V. Zenkov. Quasivelocities and stabilization of relative equilibria of underactuated nonholonomic systems. In: *Proceedings of the 48th IEEE Conference on Decision and Control*. 2009, 3335–3340 (cf. pp. 8, 90).

[34] A. M. Bloch, J. E. Marsden, and D. V. Zenkov. Quasivelocities and symmetries in non-holonomic systems. *Dynamical Systems,* 24.2 (2009), 187–222 (cf. pp. 93, 96).

[35] A. M. Bloch, M. Reyhanoglu, and N. H. McClamroch. Control and stabilization of nonholonomic dynamic systems. *IEEE Transactions on Automatic Control,* 37.11 (1992), 1746–1757 (cf. p. 90).

[36] D. J. Block, K. J. Åström, and M. W. Spong. The reaction wheel pendulum. *Synthesis Lectures on Controls and Mechatronics,* 1.1 (2007), 1–105 (cf. p. 75).

[37] N. M. Bou-Rabee, J. E. Marsden, and L. A. Romero. Tippe top inversion as a dissipation-induced instability. *SIAM Journal on Applied Dynamical Systems,* 3.3 (2004), 352–377 (cf. p. 10).

[38] S. P. Boyd, L. El Ghaoui, E. Feron, and V. Balakrishnan. *Linear Matrix Inequalities in System and Control Theory*. Vol. 15. SIAM, 1994 (cf. p. 64).

[39] R. W. Brockett. Asymptotic stability and feedback stabilization. In: *Differential Geometric Control Theory*. Ed. by R. S. M. R. W. Brockett and H. J. Sussmann. Boston: Birkhauser, 1983, 181–191 (cf. pp. 31, 90, 144, 159).

[40] M. Buhl and B. Lohmann. Lyapunov-Funktionen-basiertes Führungsfilter (Lyapunov function based set point generator). *at-Automatisierungstechnik,* 57.10 (2009), 499–504 (cf. pp. 14, 160).

[41] R. M. Bulatovic. On the stability of linear circulatory systems. *Zeitschrift für angewandte Mathematik und Physik,* 50.4 (1999), 669–674 (cf. p. 159).

[42] F. Bullo and A. D. Lewis. *Geometric Control of Mechanical Systems.* Vol. 49. Springer, 2005 (cf. pp. 11, 22, 23, 28, 116, 118).

[43] J. C. M. van der Burg, R. Ortega, J. M. A. Scherpen, J. A. Acosta, and H. B. Siguerdidjane. An experimental application of total energy shaping control: stabilization of the inverted pendulum on a cart in the presence of friction. In: *Proceedings of the European Control Conference.* 2007, 2–5 (cf. pp. 10, 53, 79).

[44] C. I. Byrnes, A. Isidori, and J. C. Willems. Passivity, feedback equivalence, and the global stabilization of minimum phase nonlinear systems. *IEEE Transactions on Automatic Control,* 36.11 (1991), 1228–1240 (cf. p. 40).

[45] A. Chaillet, D. Angeli, and H. Ito. Combining iISS and ISS with respect to small inputs: the strong iISS property. *IEEE Transactions on Automatic Control,* 59.9 (2014), 2518–2524 (cf. p. 40).

[46] R. P. M. Chan, K. A. Stol, and C. R. Halkyard. Review of modelling and control of two-wheeled robots. *Annual Reviews in Control,* 37.1 (2013), 89–103 (cf. p. 133).

[47] D. E. Chang, A. M. Bloch, N. E. Leonard, J. E. Marsden, and C. A. Woolsey. The equivalence of controlled Lagrangian and controlled Hamiltonian systems. *ESAIM: Control, Optimisation and Calculus of Variations,* 8 (2002), 393–422 (cf. pp. 7, 40, 98).

[48] C.-H. Chiu, Y.-F. Peng, and Y.-W. Lin. Intelligent backstepping control for wheeled inverted pendulum. *Expert Systems with Applications,* 38.4 (2011), 3364–3371 (cf. p. 133).

[49] D. Chwa. Sliding-mode tracking control of nonholonomic wheeled mobile robots in polar coordinates. *IEEE Transactions on Control Systems Technology,* 12.4 (2004), 637–644 (cf. p. 13).

[50] S. Delgado and P. Kotyczka. Energy shaping for the robust stabilization of a wheeled inverted pendulum. In: *Proceedings of the 5th IFAC Workshop on Lagrangian and Hamiltonian Methods for Non Linear Control.* 2015 (cf. pp. 92, 132).

[51] S. Delgado, S. Gajbhiye, and R. N. Banavar. Reduced equations of motion for a wheeled inverted pendulum. In: *Proceedings of the 8th Vienna International Conference on Mathematical Modelling.* 2015 (cf. pp. 93, 134, 169, 172).

[52] S. Delgado and P. Kotyczka. Overcoming the dissipation condition in passivity-based control for a class of mechanical systems. In: *Proceedings of the 19th IFAC World Congress.* Vol. 19. 1. 2014, 11189–11194 (cf. pp. 58, 81).

[53] S. Delgado and P. Kotyczka. Energy shaping for the position and speed control of a wheeled inverted pendulum. *Automatica (submitted),* (2016) (cf. pp. 92, 132).

[54] S. Devasia, D. Chen, and B. Paden. Nonlinear inversion-based output tracking. *IEEE Transactions on Automatic Control,* 41.7 (1996), 930–942 (cf. pp. 12, 17, 116).

[55] K. J. Diepold and S. J. Pieczona. Tracking control with adaptively allocated maximum input amplitudes and enlarged domain of attraction for linear systems. In: *Proceedings of the 52nd IEEE Conference on Decision and Control*. 2013, 2090–2096 (cf. pp. 14, 160).

[56] D. Dirksz and J. M. A. Scherpen. Passivity-based tracking control of port-Hamiltonian mechanical systems with only position measurements. In: *Proceedings of the European Control Conference*. 2009 (cf. p. 11).

[57] A. W. Divelbiss and J. T. Wen. Trajectory tracking control of a car-trailer system. *IEEE Transactions on Control Systems Technology,* 5.3 (1997), 269–278 (cf. pp. 12, 115).

[58] A. Donaire. Shaping the energy of mechanical systems without solving partial differential equations. *IEEE Transactions on Automatic Control,* (2015) (cf. p. 9).

[59] V. Duindam, A. Macchelli, S. Stramigioli, and H. Bruyninckx. *Modeling and Control of Complex Physical Systems*. Springer, 2009 (cf. p. 42).

[60] V. Duindam and S. Stramigioli. Passive asymptotic curve tracking. In: *Proceedings of the 1st IFAC Workshop on Lagrangian and Hamiltonian Methods for Nonlinear Control*. IEEE, 2003, 199 (cf. p. 13).

[61] P. Encarnaçao and A. Pascoal. Combined trajectory tracking and path following: an application to the coordinated control of autonomous marine craft. In: *Proceedings of the 40th IEEE Conference on Decision and Control*. Vol. 1. 2001, 964–969 (cf. p. 11).

[62] M. Fliess, J. Lévine, P. Martin, and P. Rouchon. Flatness and defect of non-linear systems: introductory theory and examples. *International Journal of Control,* 61.6 (1995), 1327–1361 (cf. p. 12).

[63] T. Frankel. *The Geometry of Physics: An Introduction*. 3rd Ed. Cambridge University Press, 2011 (cf. pp. 23, 26).

[64] O. Fritsch, B. Henze, and B. Lohmann. Fast and saturating thrust direction control for a quadrotor helicopter. *at-Automatisierungstechnik,* 61.3 (2013), 172–182 (cf. p. 7).

[65] O. Fritsch, D. Tromba, and B. Lohmann. Cascaded energy based trajectory tracking control of a quadrotor. *at-Automatisierungstechnik,* 62.6 (2014), 408–422 (cf. p. 11).

[66] K. Fujimoto, S. Sakai, and T. Sugie. Passivity based control of a class of Hamiltonian systems with nonholonomic constraints. *Automatica,* 48.12 (2012), 3054–3063 (cf. pp. 8, 90, 94, 159).

[67] K. Fujimoto, K. Sakurama, and T. Sugie. Trajectory tracking control of port-controlled Hamiltonian systems via generalized canonical transformations. *Automatica,* 39.12 (2003), 2059–2069 (cf. p. 11).

[68] K. Fujimoto and T. Sugie. Canonical transformation and stabilization of generalized Hamiltonian systems. *Systems & Control Letters,* 42.3 (2001), 217–227 (cf. p. 7).

[69] K. Fujimoto and T. Sugie. Stabilization of Hamiltonian systems with nonholonomic constraints based on time-varying generalized canonical transformations. *Systems & Control Letters,* 44.4 (2001), 309–319 (cf. p. 8).

[70] K. Fujimoto and M. Taniguchi. Passive path following control for port-Hamiltonian systems. In: *Proceedings of the 47th IEEE Conference on Decision and Control*. 2008, 1285–1290 (cf. pp. 13, 125).

[71] T. Fukao, H. Nakagawa, and N. Adachi. Adaptive tracking control of a nonholonomic mobile robot. *IEEE Transactions on Robotics and Automation,* 16.5 (2000), 609–615 (cf. p. 13).

[72] B. Garabédian, M. Benoit, and S. Krut. A futuristic monorail tramway stabilized by an inertia wheel. In: *Proceedings of the IEEE International Conference on Control and Automation*. 2007, 1581–1586 (cf. p. 69).

[73] F. Gómez-Estern, A. J. van der Schaft, and J. A. Acosta. Passivation of underactuated systems with physical damping. In: *Proceedings of the 15th IFAC Symposium on Nonlinear Control Systems*. 2004 (cf. pp. 10, 56).

[74] F. Gómez-Estern and A. J. van der Schaft. Physical damping in IDA-PBC controlled underactuated mechanical systems. *European Journal of Control,* 10.5 (2004), 451–468 (cf. pp. 5, 10, 14, 51, 53, 157).

[75] A. Goswami, B. Espiau, and A. Keramane. Limit cycles and their stability in a passive bipedal gait. In: *Proceedings of the IEEE International Conference on Robotics and Automation*. Vol. 1. 1996, 246–251 (cf. p. 69).

[76] K. Graichen and M. Zeitz. Inversionsbasierter Vorsteuerungsentwurf mit Ein- und Ausgangsbeschränkungen (Inversion-based feedforward control design under input and output constraints). *at-Automatisierungstechnik,* 54.4/2006 (2006), 187–199 (cf. pp. 12, 17, 116).

[77] F. Grasser, A. D'Arrigo, S. Colombi, and A. C. Rufer. JOE: a mobile, inverted pendulum. *IEEE Transactions on Industrial Electronics,* 49.1 (2002), 107–114 (cf. pp. 131, 133).

[78] Y.-S. Ha and S. Yuta. Trajectory tracking control for navigation of the inverse pendulum type self-contained mobile robot. *Robotics and Autonomous Systems,* 17.1 (1996), 65–80 (cf. pp. 14, 131, 133).

[79] Y. Ha and S. Yuta. Trajectory tracking control for navigation of self-contained mobile inverse pendulum. In: *Proceedings of the IEEE/RSJ International Conference on Intelligent Robots and Systems*. Vol. 3. 1994, 1875–1882 (cf. p. 133).

[80] N. K. Haddad, A. Chemori, and S. Belghith. External disturbance rejection in IDA-PBC controller for underactuated mechanical systems: from theory to real time experiments. In: *Proceedings of the IEEE International Conference on Control Applications*. 2014, 1747–1752 (cf. p. 75).

[81] W. Hahn. *Stability of motion*. Vol. 422. Springer, 1967 (cf. p. 38).

[82] J. Hamberg. Simplified conditions for matching and for generalized matching in the theory of controlled Lagrangians. In: *Proceedings of the American Control Conference*. Vol. 6. 2000, 3918–3923 (cf. p. 91).

[83] O. Hamdous. Feedback stabilization of the inverted pendulum system via interconnection and damping assignment-passivity based control. In: *Proceedings of the 3rd International Conference on Systems and Control*. 2013, 774–779 (cf. p. 79).

[84] J. Hauser and R. M. Murray. Nonlinear controllers for non-integrable systems: the acrobot example. In: *Proceedings of the American Control Conference*. 1990, 669–671 (cf. p. 70).

[85] R. Hermann and A. J. Krener. Nonlinear controllability and observability. *IEEE Transactions on Automatic Control,* 22.5 (1977), 728–740 (cf. p. 31).

[86] H. Hertz. *Die Prinzipien der Mechanik in neuem Zusammenhaenge dargestellt (Leipzig: JA Barth, 1894); translated as The Principles of Mechanics Presented in a New Form*. New York: Dover, 1956 (cf. p. 22).

[87] J. P. Hespanha et al. Trajectory-tracking and path-following of underactuated autonomous vehicles with parametric modeling uncertainty. *IEEE Transactions on Automatic Control,* 52.8 (2007), 1362–1379 (cf. pp. 11, 17).

[88] D. Hill and P. Moylan. The stability of nonlinear dissipative systems. *IEEE Transactions on Automatic Control,* 21.5 (1976), 708–711 (cf. p. 41).

[89] R. Hollis. Ballbots. *Scientific American,* 295.4 (2006), 72–77 (cf. p. 131).

[90] D. D. Holm. *Geometric Mechanics Part I: Dynamics and Symmetry*. 2nd Edition. Imperial College Press, 2011 (cf. p. 29).

[91] D. D. Holm. *Geometric Mechanics Part II: Rotating, Translating and Rolling*. 2nd Edition. Imperial College Press, 2011 (cf. p. 30).

[92] J. K. Holm and M. W. Spong. Kinetic energy shaping for gait regulation of underactuated bipeds. In: *Proceedings of the IEEE International Conference on Control Applications*. 2008, 1232–1238 (cf. p. 7).

[93] J. Huang, Z.-H. Guan, T. Matsuno, T. Fukuda, and K. Sekiyama. Sliding-mode velocity control of mobile-wheeled inverted-pendulum systems. *IEEE Transactions on Robotics,* 26.4 (2010), 750–758 (cf. p. 133).

[94] A. Isidori. *Nonlinear Control Systems*. 3rd Edition. Vol. 1. Springer, 1995 (cf. pp. 12, 23).

[95] Z.-P. Jiang and H. Nijmeijer. A recursive technique for tracking control of nonholonomic systems in chained form. *IEEE Transactions on Automatic Control,* 44.2 (1999), 265–279 (cf. p. 13).

[96] S. Jung and S. S. Kim. Control experiment of a wheel-driven mobile inverted pendulum using neural network. *IEEE Transactions on Control Systems Technology,* 16.2 (2008), 297–303 (cf. p. 133).

[97] Y. Kanayama, Y. Kimura, F. Miyazaki, and T. Noguchi. A stable tracking control method for a non-holonomic mobile robot. In: *Proceedings of the IEEE/RSJ International Conference on Intelligent Robots and Systems*. 1991, 1236–1241 (cf. p. 115).

[98] F. Kaufmann. *Implementierung und Evaluation verschiedener Regelungskonzepte auf einem zweirädrigen inversen Pendel*. Master's thesis. Technische Universität München. 2015 (cf. pp. 136, 177).

[99] Z. Kausar, K. Stol, and N. Patel. Stability region estimation of statically unstable two wheeled mobile robots. In: *Proceedings of the IEEE International Conference on Robotics and Biomimetics*. 2011, 1379–1384 (cf. p. 133).

[100] Z. Kausar, K. Stol, and N. Patel. Nonlinear control design using Lyapunov function for two-wheeled mobile robots. In: *Proceedings of the 19th International Conference on Mechatronics and Machine Vision in Practice*. 2012, 123–128 (cf. p. 133).

[101] R. Kelly, V. S. Davila, and A. Loría. *Control of Robot Manipulators in Joint Space*. Springer, 2005 (cf. p. 28).

[102] H. K. Khalil. *Nonlinear Systems*. Vol. 3. Prentice Hall, 2002 (cf. pp. 32, 38, 39).

[103] D. E. Kirk. *Optimal Control Theory: An Introduction*. Courier Dover Publications, 2004 (cf. p. 64).

[104] T. Kloiber and P. Kotyczka. Estimating and enlarging the domain of attraction in IDA-PBC. In: *Proceedings of the 51st IEEE Conference on Decision and Control*. 2012, 1852–1858 (cf. pp. 66–68, 140).

[105] P. V. Kokotovic. The joy of feedback: nonlinear and adaptive. *IEEE Control Systems,* 12.3 (1992), 7–17 (cf. p. 112).

[106] I. Kolmanovsky and N. H. McClamroch. Developments in nonholonomic control problems. *IEEE Control Systems,* 15.6 (1995), 20–36 (cf. pp. 89, 90).

[107] J. Koopman, D. Jeltsema, and M. Verhaegen. Port-Hamiltonian description and analysis of the LuGre friction model. *Simulation Modelling Practice and Theory,* 19.3 (2011), 959–968 (cf. p. 10).

[108] P. Kotyczka. Transparente Dynamikvorgabe bei der nichtlinearen passivitätsbasierten Zustandsregelung. PhD thesis. Technische Universität München, 2010 (cf. p. 9).

[109] P. Kotyczka. Local linear dynamics assignment in IDA-PBC for underactuated mechanical systems. In: *Proceedings of the 50th IEEE Conference on Decision and Control and European Control Conference*. 2011, 6534–6539 (cf. pp. 15, 64, 72).

[110] P. Kotyczka. Local linear dynamics assignment in IDA-PBC. *Automatica,* 49.4 (2013), 1037–1044 (cf. pp. 9, 64).

[111] P. Kotyczka and S. Delgado. Passivity based stabilization of linear mechanical systems with dissipation in unactuated degrees of freedom. *Proceedings in Applied Mathematics and Mechanics,* 12.1 (2012), 707–708 (cf. p. 56).

[112] P. Kotyczka and S. Delgado-Londoño. On a generalized port-Hamiltonian representation for the control of damped underactuated mechanical systems. In: *Proceedings of the 4th IFAC Workshop on Lagrangian and Hamiltonian Methods for Non Linear Control*. Vol. 4. 1. 2012, 149–154 (cf. pp. 10, 56, 58, 59).

[113] P. Kotyczka and B. Lohmann. Parametrization of IDA-PBC by assignment of local linear dynamics. In: *Proceedings of the European Control Conference*. 2009, 4721–4726 (cf. p. 63).

[114] P. Kotyczka, A. Volf, and B. Lohmann. Passivity based trajectory tracking control with predefined local linear error dynamics. In: *Proceedings of the American Control Conference*. 2010, 3429–3434 (cf. pp. 11, 64).

[115] R. Krechetnikov and J. Marsden. Dissipation-induced instabilities in finite dimensions. *Reviews of Modern Physics,* 79.2 (2007), 519 (cf. p. 10).

[116] J. Lee. *Introduction to Smooth Manifolds*. Vol. 218. Springer, 2012 (cf. p. 23).

[117] S. Lee and S. Jung. Novel design and control of a home service mobile robot for korean floor-living life style: KOBOKER. In: *Proceedings of the 8th International Conference on Ubiquitous Robots and Ambient Intelligence*. 2011, 863–867 (cf. p. 131).

[118] J. Lévine. *Analysis and Control of Nonlinear Systems: A Flatness-Based Approach*. Springer, 2009 (cf. pp. 12, 23, 116).

[119] A. D. Lewis. Is it worth learning differential geometric methods for modeling and control of mechanical systems? *Robotica,* 25.06 (2007), 765–777 (cf. p. 92).

[120] E. V. Lewis. Principles of naval architecture (second revision). *Society of Naval Architects and Marine Engineers (SNAME),* Volume III - Motions in Waves and Controllability (1989) (cf. p. 69).

[121] C. Li, X. Gao, Q. Huang, F. Dai, J. Shao, Y. Bai, and K. Li. A coaxial couple wheeled robot with TS fuzzy equilibrium control. *Industrial Robot: An International Journal,* 38.3 (2011), 292–300 (cf. p. 133).

[122] J. Li. On the stability of dissipative mechanical systems with circulatory forces. *Zeitschrift für angewandte Mathematik und Physik,* 48.1 (1997), 161–164 (cf. p. 159).

[123] P. Y. Li and R. Horowitz. On velocity field control of mechanical systems. In: *Proceedings of the 32nd Conference on Decision and Control*. 1993 (cf. pp. 13, 117).

[124] P. Y. Li and R. Horowitz. Passive velocity field control of mechanical manipulators. *IEEE Transactions on Robotics and Automation,* 15.4 (1999), 751–763 (cf. p. 13).

[125] P. Y. Li and R. Horowitz. Passive velocity field control (PVFC) - part i: geometry and robustness. *IEEE Transactions on Automatic Control,* 46.9 (2001), 1346–1359 (cf. p. 13).

[126] P. Y. Li and R. Horowitz. Passive velocity field control (PVFC) - part ii: application to contour following. *IEEE Transactions on Automatic Control,* 46.9 (2001), 1360–1371 (cf. pp. 13, 117).

[127] X. Li. *Augmented passivity-based control for underactuated mechanical systems: examples and interpretation*. Semesterarbeit. Technische Universität München. Supervisor: Sergio Delgado. 2015 (cf. p. 62).

[128] Z. Li, C. Yang, and L. Fan. *Advanced Control of Wheeled Inverted Pendulum Systems*. Springer, 2013 (cf. pp. 5, 69, 131, 133).

[129] D. Liberzon. *Switching in Systems and Control*. Springer Science & Business Media, 2003 (cf. p. 145).

[130] L. Magni, R. Scattolini, and K. J. Åström. Global stabilization of the inverted pendulum using model predictive control. In: *Proceedings of the 15th IFAC World Congress*. 2002, 1554 (cf. p. 80).

[131] A. D. Mahindrakar, A. Astolfi, R. Ortega, and G. Viola. Further constructive results on interconnection and damping assignment control of mechanical systems: the acrobot example. *International Journal of Robust and Nonlinear Control,* 16.14 (2006), 671–685 (cf. pp. 70, 72, 74).

[132] J. E. Marsden. *Lectures on Mechanics*. Vol. 174. Cambridge University Press, 1992 (cf. p. 23).

[133] J. E. Marsden and T. S. Ratiu. *Introduction to Mechanics and Symmetry: A Basic Exposition of Classical Mechanical Systems*. 2nd. Springer, 1999 (cf. pp. 23, 28).

[134] B. M. Maschke and A. J. van der Schaft. A Hamiltonian approach to stabilization of nonholonomic mechanical systems. In: *Proceedings of the 33rd IEEE Conference on Decision and Control*. Vol. 3. 1994, 2950–2950 (cf. pp. 8, 91).

[135] D. R. Merkin. *Introduction to the Theory of Stability*. Vol. 24. Springer Science & Business Media, 1997 (cf. p. 9).

[136] mObi. *[online]: http://www.bnrobotics.com/* (cf. p. 131).

[137] A. Morro, A. Sgorbissa, and R. Zaccaria. Path following for unicycle robots with an arbitrary path curvature. *IEEE Transactions on Robotics,* 27.5 (2011), 1016–1023 (cf. pp. 12, 115).

[138] V. Muralidharan and A. D. Mahindrakar. Position stabilization and waypoint tracking control of mobile inverted pendulum robot. *IEEE Transactions on Control Systems Technology,* 22.6 (2014), 2360–2367 (cf. pp. 14, 133, 144).

[139] V. Muralidharan, M. T. Ravichandran, and A. D. Mahindrakar. Extending interconnection and damping assignment passivity-based control (IDA-PBC) to underactuated mechanical systems with nonholonomic Pfaffian constraints: the mobile inverted pendulum robot. In: *Proceedings of the 48th IEEE Conference on Decision and Control, held jointly with the 28th Chinese Control Conference.* 2009, 6305–6310 (cf. pp. 96, 133).

[140] R. M. Murray and J. E. Hauser. *A case study in approximate linearization: The acrobot example.* Electronics Research Laboratory, College of Engineering, University of California, 1991 (cf. p. 70).

[141] R. M. Murray, Z. Li, and S. S. Sastry. *A Mathematical Introduction to Robotic Manipulation.* CRC press, 1994 (cf. pp. 3, 6, 21, 28, 70, 116, 120).

[142] R. M. Murray and S. S. Sastry. Nonholonomic motion planning: steering using sinusoids. *IEEE Transactions on Automatic Control,* 38.5 (1993), 700–716 (cf. pp. 12, 90, 144).

[143] U. Nagarajan, G. Kantor, and R. L. Hollis. Trajectory planning and control of an underactuated dynamically stable single spherical wheeled mobile robot. In: *Proceedings of the IEEE International Conference on Robotics and Automation.* 2009, 3743–3748 (cf. p. 131).

[144] D. S. Nasrallah, J. Angeles, and H. Michalska. Velocity and orientation control of an anti-tilting mobile robot moving on an inclined plane. In: *Proceedings of the IEEE International Conference on Robotics and Automation.* 2006, 3717–3723 (cf. p. 92).

[145] D. S. Nasrallah, H. Michalska, and J. Angeles. Controllability and posture control of a wheeled pendulum moving on an inclined plane. *IEEE Transactions on Robotics,* 23.3 (2007), 564–577 (cf. pp. 131, 133, 144).

[146] D. R. Nelson, D. B. Barber, T. W. McLain, and R. W. Beard. Vector field path following for miniature air vehicles. *IEEE Transactions on Robotics,* 23.3 (2007), 519–529 (cf. pp. 13, 117, 125).

[147] H. Nijmeijer and A. J. van der Schaft. *Nonlinear Dynamical Control Systems.* Springer, 1990 (cf. pp. 23, 116).

[148] K. Nunna, M. Sassano, and A. Astolfi. Constructive interconnection and damping assignment for port-controlled Hamiltonian systems. *IEEE Transactions on Automatic Control,* 60.9 (2015), 2350–2361 (cf. p. 9).

[149] R. Olfati-Saber. Fixed point controllers and stabilization of the cart-pole system and the rotating pendulum. In: *Proceedings of the 38th IEEE Conference on Decision and Control.* Vol. 2. 1999, 1174–1181 (cf. p. 79).

[150] R. Olfati-Saber. Nonlinear Control of Underactuated Mechanical Systems with Application to Robotics and Aerospace Vehicles. PhD thesis. Massachusetts Institute of Technology, 2001 (cf. p. 70).

[151] R. Ortega and E. García-Canseco. Interconnection and damping assignment passivity-based control: a survey. *European Journal of Control,* 10.5 (2004), 432–450 (cf. pp. 7, 9, 40, 42, 58).

[152] R. Ortega, Z. Liu, and H. Su. Control via interconnection and damping assignment of linear time-invariant systems: a tutorial. *International Journal of Control,* 85.5 (2012), 603–611 (cf. pp. 54, 56).

[153] R. Ortega, A. Loria, P. J. Nicklasson, and H. Sira-Ramirez. *Passivity-Based Control of Euler-Lagrange Systems: Mechanical, Electrical and Electromechanical Applications.* Ed. by R. Ortega. Springer, 1998 (cf. pp. 6, 40).

[154] R. Ortega, A. J. van der Schaft, F. Castaños, and A. Astolfi. Control by interconnection and standard passivity-based control of port-Hamiltonian systems. *IEEE Transactions on Automatic Control,* 53.11 (2008), 2527–2542 (cf. pp. 40, 43).

[155] R. Ortega, A. J. van der Schaft, I. Mareels, and B. Maschke. Putting energy back in control. *IEEE Control Systems,* 21.2 (2001), 18–33 (cf. pp. 4, 7, 8, 15, 53).

[156] R. Ortega, A. J. van der Schaft, B. Maschke, and G. Escobar. Interconnection and damping assignment passivity-based control of port-controlled Hamiltonian systems. *Automatica,* 38.4 (2002), 585–596 (cf. pp. 7, 42).

[157] R. Ortega and M. W. Spong. Adaptive motion control of rigid robots: a tutorial. *Automatica,* 25.6 (1989), 877–888 (cf. pp. 40, 41).

[158] R. Ortega, M. W. Spong, F. Gómez-Estern, and G. Blankenstein. Stabilization of a class of underactuated mechanical systems via interconnection and damping assignment. *IEEE Transactions on Automatic Control,* 47.8 (2002), 1218–1233 (cf. pp. 7, 42, 44, 58, 75, 76, 78, 79).

[159] J. P. Ostrowski. Computing reduced equations for robotic systems with constraints and symmetries. *IEEE Transactions on Robotics and Automation,* 15.1 (1999), 111–123 (cf. pp. 31, 92).

[160] K. Pathak and S. K. Agrawal. An integrated path-planning and control approach for nonholonomic unicycles using switched local potentials. *IEEE Transactions on Robotics,* 21.6 (2005), 1201–1208 (cf. p. 13).

[161] K. Pathak, J. Franch, and S. K. Agrawal. Velocity and position control of a wheeled inverted pendulum by partial feedback linearization. *IEEE Transactions on Robotics,* 21.3 (2005), 505–513 (cf. pp. 92, 133, 144).

[162] S. Prajna, A. J. van der Schaft, and G. Meinsma. An LMI approach to stabilization of linear port-controlled Hamiltonian systems. *Systems & Control Letters,* 45.5 (2002), 371–385 (cf. pp. 54, 56).

[163] PUMA. *[online]. http://www.segway.com/puma* (cf. p. 131).

[164] Y. Qin, Y. Liu, X. Zang, et al. Balance control of two-wheeled self-balancing mobile robot based on TS fuzzy model. In: *Proceedings of the 6th International Forum on Strategic Technology*. Vol. 1. 2011, 406–409 (cf. p. 133).

[165] F. H. Ramírez-Leyva, E. Peralta-Sánchez, J. J. Vásquez-Sanjuan, and F. Trujillo-Romero. Passivity-based speed control for permanent magnet motors. *Procedia Technology,* 7 (2013), 215–222 (cf. p. 92).

[166] M. T. Ravichandran and A. D. Mahindrakar. Robust stabilization of a class of underactuated mechanical systems using time scaling and Lyapunov redesign. *IEEE Transactions on Industrial Electronics,* 58.9 (2011), 4299–4313 (cf. p. 133).

[167] C. K. Reddy, W. W. Whitacre, and C. A. Woolsey. Controlled Lagrangians with gyroscopic forcing: an experimental application. In: *Proceedings of the American Control Conference*. Vol. 1. 2004, 511–516 (cf. pp. 9, 11, 53).

[168] C. K. Reddy. Practical Challenges in the Method of Controlled Lagrangians. PhD thesis. Virginia Polytechnic Institute and State University, 2005 (cf. pp. 11, 53).

[169] R. Reichart. *Passivity-based trajectory control for a wheeled inverted pendulum.* Term paper (Semesterarbeit). Technische Universität München. 2015 (cf. p. 142).

[170] T.-J. Ren, T.-C. Chen, and C.-J. Chen. Motion control for a two-wheeled vehicle using a self-tuning PID controller. *Control Engineering Practice,* 16.3 (2008), 365–375 (cf. p. 133).

[171] S. Ricardo and W. Respondek. Control systems that admit a mechanical structure. In: *Proceedings of the 8th International IFAC Symposium on Nonlinear Control Systems*. 2010, 102–107 (cf. p. 159).

[172] R. Rothfuß, J. Rudolph, and M. Zeitz. Flachheit: ein neuer Zugang zur Steuerung und Regelung nichtlinearer Systeme. *at-Automatisierungstechnik,* 45.11 (1997), 517–525 (cf. p. 12).

[173] M. Ryalat and D. S. Laila. IDA-PBC for a class of underactuated mechanical systems with application to a rotary inverted pendulum. In: *Proceedings of the 52nd IEEE Conference on Decision and Control*. 2013, 5240–5245 (cf. p. 9).

[174] S. Sakai and K. Fujimoto. Dynamic output feedback stabilization of a class of nonholonomic Hamiltonian systems. In: *Proceedings of the 16th IFAC World Congress*. 2005, 1967–1970 (cf. p. 90).

[175] A. Salerno and J. Ángeles. A new family of two-wheeled mobile robots: modeling and controllability. *IEEE Transactions on Robotics,* 23.1 (2007), 169–173 (cf. p. 133).

[176] C. Samson. Velocity and torque feedback control of a nonholonomic cart. In: *Advanced Robot Control*. Ed. by C. Canudas de Wit. Vol. 162. Lecture Notes in Control and Information Sciences. Springer Berlin Heidelberg, 1991, 125–151 (cf. p. 92).

[177] C. Samson. Control of chained systems application to path following and time-varying point-stabilization of mobile robots. *IEEE Transactions on Automatic Control,* 40.1 (1995), 64–77 (cf. pp. 12, 90).

[178] J. Sandoval, R. Kelly, and V. Santibáñez. Interconnection and damping assignment passivity-based control of a class of underactuated mechanical systems with dynamic friction. *International Journal of Robust and Nonlinear Control,* 21.7 (2011), 738–751 (cf. p. 10).

[179] S. Sastry. *Nonlinear Systems: Analysis, Stability, and Control*. Vol. 10. Springer, 1999 (cf. p. 32).

[180] A. J. van der Schaft. Stabilization of Hamiltonian systems. *Nonlinear Analysis: Theory, Methods & Applications,* 10.10 (1986), 1021–1035 (cf. p. 6).

[181] A. J. van der Schaft. *L2-Gain and Passivity in Nonlinear Control*. Springer, 1999 (cf. pp. 40, 41).

[182] A. J. van der Schaft. Port-controlled Hamiltonian systems: towards a theory for control and design of nonlinear physical systems. *Journal of the Society of Instrument and Control Engineers,* 39.2 (2000), 91–98 (cf. p. 42).

[183] A. J. van der Schaft. *Port-Hamiltonian Systems: Network Modeling and Control of Nonlinear Physical Systems*. Springer, 2004 (cf. p. 42).

[184] A. J. van der Schaft. Port-Hamiltonian systems: an introductory survey. In: *Proceedings of the International Congress of Mathematicians*. European Mathematical Society Publishing House (EMS Ph), 2006 (cf. p. 42).

[185] A. J. van der Schaft and B. M. Maschke. On the Hamiltonian formulation of nonholonomic mechanical systems. *Reports on Mathematical Physics,* 34.2 (1994), 225–233 (cf. pp. 8, 31, 32, 92–95).

[186] Segway. *[online]. http://www.segway.com* (cf. pp. 69, 131, 158).

[187] R. Sepulchre, M. Jankovic, and P. Kokotovic. *Constructive Nonlinear Control*. Springer, 1997 (cf. p. 40).

[188] J.-J. E. Slotine. Putting physics in control—the example of robotics. *IEEE Control Systems Magazine,* 8.6 (1988), 12–18 (cf. pp. 4, 5).

[189] J.-J. E. Slotine, W. Li, et al. *Applied Nonlinear Control*. Vol. 199. 1. Prentice Hall, 1991 (cf. pp. 6, 11, 32, 38, 116).

[190] E. D. Sontag. Smooth stabilization implies coprime factorization. *IEEE Transactions on Automatic Control,* 34.4 (1989), 435–443 (cf. p. 38).

[191] E. D. Sontag. Input to state stability: basic concepts and results. In: *Nonlinear and Optimal Control Theory*. Springer, 2008, 163–220 (cf. pp. 39, 40).

[192] E. D. Sontag and Y. Wang. On characterizations of the input-to-state stability property. *Systems & Control Letters,* 24.5 (1995), 351–359 (cf. p. 39).

[193] M. D. Spivak. *A Comprehensive Introduction to Differential Geometry.* Publish or Perish, 1970 (cf. p. 23).

[194] M. W. Spong. Partial feedback linearization of underactuated mechanical systems. In: *Proceedings of the IEEE/RSJ International Conference on Intelligent Robots and Systems.* Vol. 1. 1994, 314–321 (cf. pp. 70, 79, 80).

[195] M. W. Spong. The swing up control problem for the acrobot. *IEEE Control Systems,* 15.1 (1995), 49–55 (cf. pp. 69–71).

[196] M. W. Spong. Underactuated mechanical systems. In: *Control Problems in Robotics and Automation.* Ed. by K. P. Siciliano Bruno abd Valavanis. Springer, 1998, 135–150 (cf. pp. 4, 22, 70).

[197] M. W. Spong, P. Corke, and R. Lozano. Nonlinear control of the reaction wheel pendulum. *Automatica,* 37.11 (2001), 1845–1851 (cf. p. 75).

[198] M. W. Spong, S. Hutchinson, and M. Vidyasagar. *Robot Modeling and Control.* Vol. 3. Wiley, 2006 (cf. pp. 13, 28, 70).

[199] R. Stadlmayr, M. Schoberl, and K. Schlacher. A combination of feedforward and feedback for the control of the nonlinear benchmark inertia wheel pendulum. In: *Proceedings of the European Control Conference.* 2007, 5802–5808 (cf. pp. 11, 75).

[200] M. Taniguchi and K. Fujimoto. Time-varying path following control for port-Hamiltonian systems. In: *Proceedings of the 48th IEEE Conference on Decision and Control, held jointly with the 28th Chinese Control Conference.* 2009, 3323–3328 (cf. p. 13).

[201] H. Tasso. On the stability of dissipative systems with circulatory forces. *Zeitschrift für angewandte Mathematik und Physik,* 31.4 (1980), 536–537 (cf. p. 159).

[202] R. Tedrake. Underactuated robotics: learning, planning, and control for efficient and agile machines course notes for mit 6.832. *Working draft edition,* (2009) (cf. pp. 3, 22).

[203] V. Utkin, J. Guldner, and J. Shi. *Sliding mode control in electro-mechanical systems.* Vol. 34. CRC press, 2009 (cf. p. 80).

[204] En-V. *[online]: http://media.gm.com/autoshows/shanghai/2010/public/cn/...en/env/news.html* (cf. pp. 5, 131).

[205] G. Viola, R. N. Banavar, J. A. Acosta, and A. Astolfi. Some remarks on interconnection and damping assignment passivity-based control of mechanical systems. *Taming Heterogeneity and Complexity of Embedded Control,* - (2006), 721–735 (cf. p. 79).

[206] G. Viola, R. Ortega, R. N. Banavar, J. Á. Acosta, and A. Astolfi. Total energy shaping control of mechanical systems: simplifying the matching equations via coordinate changes. *IEEE Transactions on Automatic Control,* 52.6 (2007), 1093–1099 (cf. p. 8).

[207] J. C. Willems. Dissipative dynamical systems part i: general theory. *Archive for Rational Mechanics and Analysis,* 45.5 (1972), 321–351 (cf. p. 40).

[208] R. K. Williamson. *Pervasive Damping and Stability with Application to a Gravitationally Stabilized Satellite Augmented by a Constant Speed Rotor.* Tech. rep. DTIC Document, 1969 (cf. p. 35).

[209] C. Woolsey, C. K. Reddy, A. M. Bloch, D. E. Chang, N. E. Leonard, and J. E. Marsden. Controlled Lagrangian systems with gyroscopic forcing and dissipation. *European Journal of Control,* 10.5 (2004), 478–496 (cf. pp. 8, 10, 11, 53, 100).

[210] X. Xin. On the energy based control for underactuated mechanical systems. In: *Proceedings of the ICROS-SICE International Joint Conference,* 2009 (cf. p. 71).

[211] X. Xin and M. Kaneda. The swing up control for the acrobot based on energy control approach. In: *Proceedings of the 41st IEEE Conference on Decision and Control.* Vol. 3. 2002, 3261–3266 (cf. p. 71).

[212] C. Yang, Z. Li, and J. Li. Trajectory planning and optimized adaptive control for a class of wheeled inverted pendulum vehicle models. *IEEE Transactions on Cybernetics,* 43.1 (2013), 24–36 (cf. p. 133).

[213] J.-M. Yang and J.-H. Kim. Sliding mode control for trajectory tracking of nonholonomic wheeled mobile robots. *IEEE Transactions on Robotics and Automation,* 15.3 (1999), 578–587 (cf. pp. 13, 90).

[214] K. Yokoyama and M. Takahashi. Stabilization of a cart-inverted pendulum with interconnection and damping assignment passivity-based control focusing on the kinetic energy shaping. *Journal of System Design and Dynamics,* 4.5 (2010), 698–711 (cf. p. 79).

[215] K. Yokoyama and M. Takahashi. Stabilization of a mobile inverted pendulum with IDA-PBC and experimental verification. *Journal of System Design and Dynamics,* 5.8 (2011), 1605–1623 (cf. p. 133).

[216] M. Yue, P. Hu, and W. Sun. Path following of a class of non-holonomic mobile robot with underactuated vehicle body. *IET Control Theory & Applications,* 4.10 (2010), 1898–1904 (cf. p. 14).

[217] J. Zabczyk. Some comments on stabilizability. *Applied Mathematics and Optimization,* 19.1 (1989), 1–9 (cf. p. 31).

[218] D. V. Zenkov, A. M. Bloch, and J. E. Marsden. Flat nonholonomic matching. In: *Proceedings of the American Control Conference.* Vol. 4. 2002, 2812–2817 (cf. p. 90).

[219] D. V. Zenkov. Matching and stabilization of linear mechanical systems. In: *Proceedings of the 15th International Symposium on Mathematical Theory of Networks and Systems.* 2002 (cf. pp. 54, 56).

[220] D. V. Zenkov, A. M. Bloch, N. E. Leonard, and J. E. Marsden. Matching and stabilization of low-dimensional nonholonomic systems. In: *Proceedings of the 39th IEEE Conference on Decision and Control*. Vol. 39. 2000, 1289–1295 (cf. p. 91).

[221] H. Ziegler. Die Stabilitätskriterien der Elastomechanik. *Archive of Applied Mechanics,* 20.1 (1952), 49–56 (cf. p. 9).

Index